PREPARATION AND CHARACTERIZATION OF NATURAL RUBBER-MONTMORILLONITE CLAY NANOCOMPOSITES AND THEIR VULCANIZATES

SUDARSHANA GERARD JAYARAJ PERERA

(148014X)

Degree of Doctor of Philosophy in Chemical and Process Engineering

Department of Chemical and Process Engineering

University of Moratuwa

Sri Lanka

May 2019

DECLARATION

I declare that this is my own work and this dissertation does not incorporate without acknowledgement any material previously submitted for a degree or diploma in any other university or institute of higher learning and to the best of my knowledge and belief it does not contain any material previously published or written by another person except where the acknowledgement is made in the text.

Also, I hereby grant to University of Moratuwa the non-exclusive right to reproduce and distribute my dissertation, in whole or in part in print, electronic or other medium. I retain the right to use this content in whole or part in future works.

Signature of the Candidate Date

The above candidate has carried out research for the PhD dissertation under my supervision.

Signature of the Supervisor Date

Signature of the Supervisor Date

DEDICATION

To,

My ever loving...

Parents,

Wife

&

Son

ACKNOWLEDGEMENT

I wish to express my most sincere gratitude and appreciation to my principal supervisor – Dr. Mrs. SM Egodage, Senior Lecturer of University of Moratuwa Sri Lanka, who provided me with the most valuable and wonderful opportunity to read for a PhD. research degree under her guidance in the field of rubber nanocomposites. It is difficult to express in words for her invaluable guidance, encouragement, and support on me throughout the study. Her thoughtfulness deeply inspired me to take the correct decision at a crucial stage in the study.

Prof. S Walpalage, the Head of the Department of Chemical Process and Engineering, University of Moratuwa, and the co-supervisor of the research, with his vast experience and professional knowledge in this specialist field of research kept me on track with his guidance, supervision, and support throughout the research period. Many thanks are extended to my both supervisors for their valuable advices and constructive comments on my research.

I am indebted and immensely thankful to the Senate Research Grant Committee, University of Moratuwa for providing me with a research grant (SRC/CAP/14/05) to realize this research project.

Prof. PG Rathnasiri the present research coordinator and Dr. Ms. MY Gunasekara the former research coordinator of the Department of Chemical and Process Engineering of the University of Moratuwa also provided me with several useful inputs, and stimulating discussions during my research project. I am also deeply grateful to the former Heads of the Department of Chemical and Process Engineering, University of Moratuwa, Prof. PG Rathnasiri and Dr. Mrs. SHP Gunawardena enabled me to complete this research by providing me constant administrative support in accomplishing this task, and I am also deeply indebted for their assistance and support.

I would like to acknowledge Dr. S Siriwardena, the Deputy Director and Dr. Mrs. DG Edirisinghe, the Head of the Rubber Technology and Development department, at the Rubber Research Institute of Sri Lanka, and Prof. SU Adikary and Mr. VSC Weragoda, the former Heads of the Department of Material Science and Engineering of the University of Moratuwa for permitting me to use their laboratory premises with great guidance.

I wish to thank Mrs. WSMD Silva, the technical officer of the Department of Chemical Process and Engineering, University of Moratuwa, for her help to conduct most of my experimental works in the laboratory premises. I also wish to place on record the valuable support and assistance on practical aspects received during the entire research project from Mrs. HBR Sajeewani, Mr. CL Gunaratne the technical officers, Mr. DS Dayananda and Mr. SMRN Dhammika the laboratory assistants at the Department of Chemical Process and Engineering, Mr. MAPC Gunawardena, DF Ranasinghe and MTMR Jayaweera the technical officers and Mr. RRP Perera the laboratory assistant at the Department of Material Science and Engineering, University of Moratuwa, Mr. AMKSP Adikari, Mr WDM Sampath, the research officers and Mr. V.G.M.J Abeywardena, the technical officer at the Rubber Research Institute of Sri Lanka.

Last but not least, I would like to thank my wife Jeewani, son Dulnith and both our parents for their care, love, and sacrifice, and also for understanding, encouragement, and assistance throughout the completion of the research.

ABSTRACT

Preparation and characterization of Natural rubber-montmorillonite clay nanocomposites and their vulcanizates

Rubber-clay nanocomposites at low nanoclay loadings are generally prepared using mechanical mixing method as similar to mixing of conventional fillers with rubber. However, the resultant properties prepared with mixing method were reported as not high as expected and the main challenge was the retaining of exfoliated clay structures in the final product after vulcanization. This study focuses on the development of nanocomposites with superior properties from Natural rubber (NR) and Montmorillonite clay (MMT), through development of suitable clay structures, by incorporating of nanoclay into rubber at the latex stage. Twelve series of nanocomposites were prepared to study the effect of processing method (acid co-coagulation named ACC method and acid free co-coagulation named AFCC method using latex, and mechanical mixing method with pale crepe); gelling agents (sodium silicofluoride-G1, cetyl trimethyl ammonium bromide (CTAB)-G2 and combination of CTAB and sodium dodycyl sulphate (SDS)-G3); type of natural rubber latex (field NRL and centrifuged NRL); modifications of MMT and NRL. MMT was organically modified with a cationic surfactant of CTAB to enhance interactions with NR. The modified MMT (OMMT) was further treated with bis(triethoxysilylpropyl) tetrasulfide to facilitate separation of clay layers in the clay stacks, and the treated clay was designated as OMMT-S. The NRL was grafted with succinimide to enhance the compatibility with OMMT-S. The incorporation of OMMT-S into Succinimide grafted NRL was the novelty of the study. These nanocomposites prepared were compounded with the curing and other compounding ingredients to prepare nanocomposite vulcanizates. The clay dispersions, nanocomposites, nanocomposite compounds were characterized by XRD, SEM, FTIR, TGA and the mechanical and thermal properties of the nanocomposite vulcanizates were determined as per the international standards.

Tensile strength, elongation at break, mod 300% and hardness of the nanocomposite vulcanizates prepared using AFCC and ACC methods initially increased and then decreased with the increase of MMT loading while tear strength remained unchanged. The nanocomposite vulcanizates prepared using AFCC method showed higher mechanical properties compared to the nanocomposite vulcanizates prepared using ACC method. However, AFCC method exhibited slow drying characteristics. The optimum MMT loadings for nanocomposites prepared using AFCC method and ACC method were recorded at 8 phr and 12 phr, respectively, due to formation of aggregated clay structures at higher loadings, as evident by SEM images. Addition of a gelling agent successfully solved the slow drying problem associated with the AFCC method, however, G1 and G2 gelling agents exhibited significant changes to the properties of the vulcanizates. G3 gelling agent functioned effectively by facilitating quick gel formation, and by exhibiting better mechanical properties of the nanocomposite vulcanizates.

Replacement of MMT by OMMT in nanocomposite vulcanizates prepared using AFCC method without a gelling agent showed enhanced mechanical properties at a lower loading of 2 phr. The mechanical properties were further enhanced with the addition of the G3 gelling agent to the nanocomposites with OMMT and is associated with greater interactions between OMMT and NR. The optimum loading was recorded at 5 phr. Replacement of OMMT by OMMT-S in nanocomposite vulcanizate prepared with G3 gelling agent exhibited greater tensile strength and elongation at break at 2 phr loading, and greater mod 300%, tear strength and hardness at 5 phr. XRD analysis and SEM images of nanocomposite vulcanizates revealed that the addition of OMMT-S promotes existences of separated clay layers and fine morphology in the vulcanizates. The nanocomposite vulcanizates prepared using mechanical mixing method incorporating OMMT and OMMT-S into pale crepe gave comparatively lower mechanical properties due to presence of clay aggregates.

The novel nanocomposite vulcanizates prepared with grafted NRL and OMMT-S with the G3 gelling agent showed overall remarkable mechanical properties at 5 phr. The X-ray diffractograms of the nanocomposite vulcanizates showed exfoliated clay structures and fine morphology. The remarkable properties obtained due to fine morphology developed through exfoliated clay structures as a result of rubber filler interactions are tensile strength of 41 MPa, mod 300% of 6 MPa, elongation at break of 620%, tear strength of 49 N/mm, hardness of 55 IRHD, and abrasion loss of 190 mm^3.

Keywords

Nanocomposite, Organoclay**,** Acid-free Co-coagulation, Modified natural rubber, Exfoliated clay

TABLE OF CONTENTS

LIST OF FIGURES

LIST OF TABLES

LIST OF ABBREVIATIONS

ACC	-	Acid Co-Coagulation
AFCC	-	Acid Free Co-Coagulation
AFCC-G1	-	AFCC used with gelling agent SSF
AFCC-G2	-	AFCC used with gelling agent CTAB
AFCC-G3	-	AFCC used with gelling agent CTAB and SDS
CEC	-	Cation Exchange Capasity
CRI	-	Cure Rate Index
CTAB	-	Cetyl Trimethyl Ammonium bromide
DMTA	-	Dynamic Mechanical Thermal Analysis
DRC	-	Dry Rubber Content
DSC	-	Differential Scanning Calorimetry
FTIR	-	Fourier Transform Infrared
HCl	-	Hydrochloric Acid
IRHD	-	International Rubber Hardness Degrees
KOH	-	Potassium Hydroxide
NR	-	Natural Rubber
NRL	-	Natural Rubber Latex
MA	-	Maleamic Acid
MAH	-	Maleic Anhydride
MBTS	-	Mercaptobenzothiazole Sulphanamide
M_H	-	Maximum Torque
M_L	-	Minimum Torque
MMT	-	Montmorillonite
mod 300%	-	Modulus at 300% elongation
OMMT	-	MMT Clay modified by CTAB
OMMT-S	-	OMMT clay modified by TESPT
PRV	-	Property retention value

RSS	-	Ribbed Smoke Sheet
SA	-	Succinamic acid
SBR	-	Styrene Buitadiene Rubber
SDS	-	Sodium Dodecyl Sulfate
SEM	-	Scanning Electron Microscopy
SI	-	Succinimide
SSF	-	Sodium Silicofluoride
TEPA	-	Tetraethylenepentamine
TESPT	-	Bis(Triethoxysilylpropyl) Tetrasulfide
T_g	-	Glass Transition Temperature
TMTD	-	Tetramethyl Thiurium Disulfide
XRD	-	X-ray Diffraction
ZnO	-	Zinc Oxide

LIST OF APPENDICES

CHAPTER 1

INTRODUCTION

1.1 Natural Rubber

Natural rubber (NR), both in latex and dry rubber forms, is used to manufacture different rubber products. Sri Lanka, being one of the leaders in natural rubber producers in the world, manufactures high-quality natural rubber products mainly solid tires, shoe soles, and surgical gloves for the global market. In recent times, the income of the export of rubber and rubber-based products in Sri Lanka was approximately 7% of total annual gross turnover, and a higher percentage of it was contributed by the tire industry. The annual gross turnover of the Sri Lankan rubber industry currently stands at approximately US$ 1 billion. It was estimated based on the recorded rubber products export worth US$ 855 million in 2017 that the year-on-year growth of annual turnover is approximately 11% and the target on achieving an annual gross industry turnover of US$ 4.4 billion by 2025 (AGM SLAMERP, 2019)

The NR based products are highly demanded due to the remarkable properties of NR not shared in other materials. The non-rubber substances such as proteins and phospholipids presence in NR form a naturally occurring network, which play a significant role in the orientation of isoprene molecules during deformation, and enhance strain-induced crystallinity of NR and corresponding mechanical property (Amnuaypornsri et al., 2008; Tosaka et al., 2009). The unique properties of NR could be modified with the addition of fillers, vulcanizing agent/system, and other specialty chemicals as per the requirement for a specific application.

Fillers like carbon black, silica, calcium carbonate, kaolin, clay, and mica are incorporated into NR to obtain improved physico-mechanical properties such as strength, modulus, hardness, and abrasion resistance. Carbon black is the frequently used and highly consumed reinforcing filler in the rubber industry, however, its usage at loadings above 40 phr reduces mechanical properties of the rubber vulcanizates. The appearance of black color in the product, and environmental pollution are the main limitations for the use of carbon black as filler in the rubber products. The use of silica could overcome the said limitations, however, its incompatibility to NR explains the

need of an additional chemical ingredient like coupling agent to provide reinforcement. In general, carbon black-reinforced NR exhibits higher modulus than silica-reinforced NR at the same filler loading (Kojima et al., 1993). However, silica provides a unique combination of tear strength and ageing resistance to the NR vulcanizate. Though the inexpensive calcium carbonate, kaolin and bentonite clays are available to use as fillers in NR, they do not reinforce the rubber, but reduce the compound cost. Hence, finding an inexpensive and environment friendly reinforcing filler, as an alternative to carbon black, is a timely needed investigation. Reduction in consumption of expensive and environmentally harmful carbon black especially in the tire industry would be beneficial for the economy of the country. In recent years, nano-fillers like nanoclay, nano-silica have attracted attention due to their ability to enhance mechanical properties of rubber vulcanizates with low filler loadings of less than 10 phr (Rezende et al., 2010; Thomas et al., 2010). The light weight gained through the low filler loading in the nanocomposite and the improved mechanical properties obtained through the increased interfacial area between rubber and filler are the significant advantages of the rubber nanocomposites over the conventional rubber vulcanizates.

1.2 Nanoclay structures and rubber-clay nanocomposites

Montmorillonite (MMT) has layered clay structures and is widely used in the preparation of nanocomposites due to its availability, intercalation /exfoliation chemistry, higher surface area with improved surface activity, and excellent swelling behavior over the other clay types such as kaolin (Pinnvaia et al., 2001). Since MMT is in hydrophilic nature and is incompatible with rubber, it is difficult to incorporate into rubber in the solid-state, and therefore organically modified MMT called organoclay is used in common as filler in dry rubber applications. MMT is modified using various techniques to increase its interlayer-gallery spaces when in rubber-clay nanocomposites (Bottcher et al., 2002; Chou et al., 2004; Lin et al., 2004; Guegan et al., 2010; Liao et al., 2010; Finocchio et al., 2011). MMT could be incorporated into the natural rubber latex (NRL) due to its hydrophilic nature, however, the clay layers are separated and are dispersed in the rubber matrix as aggregated clay structures. The commercially available organoclays are difficult to incorporate into the NRL due to its

poor solubility in the aqueous medium (Fox et al., 2007). Hence, the development of a suitable method to disperse of organoclay in NRL is important.

A dry rubber compounding technique based on melt mixing is the main industrial method practiced in the preparation of rubber-clay nanocomposites, at present. However, shear strains generated in conventional processing equipment is not sufficient to disperse nanoclay in the rubber matrix to develop fully exfoliated structures and thereby to obtain good mechanical properties of nanocomposite vulcanizates (Hwang et al., 2004). The higher viscosity of solid rubber would be the reason for the difficulty in producing well-dispersed clay structures. Instead, aggregated clay structures are formed in the rubber-clay nanocomposite vulcanizates without separating clay layers from the clay stacks (Rezende et al., 2010). In order to prevent clay aggregation in the rubber matrix, nanoclay can be first incorporated into NRL, and then clay incorporated dry rubber could be prepared upon destabilization of NRL. Incorporation of nanoclay into NRL was studied extensively in order to develop latex-based casting products with enhanced mechanical properties (Bala et al., 2004; Vargese et al 2003; Valdares et al 2006). Incorporation of nanoclay into dry rubber with modifications of rubber and/or clay was also studied (Teh et al., 2005; Carretero-Gonzalez et al., 2008; Yahaya et al., 2009), however, the mechanical properties of the nanocomposite vulcanizates were not exhibited as increase as expected. Difficulty in obtaining and retaining of the exfoliated structures in the vulcanizates was the main reason for not enhancing the properties in many studies, and is the major challenge that the researchers currently faced.

Co-coagulation is another destabilization method used to prepare rubber-clay nanocomposites and it is still in the developing stage (Wang et al., 2005; Wu et al., 2005; Duy et al., 2009; Gu et al 2009; Alex et al., 2006; Abdhollahi et al., 2008; Rattanasom et al., 2009; Bhowmick et al., 2010; Lee et al, 2011; Tan et al., 2012; Tan et al., 2016). It is similar to the RSS manufacturing method, however, in the co-coagulation method both NRL and clay are destabilized together in the presence of a co-coagulating agent like formic acid, acetic acids, and organic/inorganic salts, etc. The exfoliated clay structures are developed in the clay-NRL mix during mixing; however, these structures are disappeared when a co-coagulating agent is added. At the destabilization stage, the clay layers may stack together with the transfer of

hydrogen ions in the co-coagulating agent into interlayer-gallery spaces and prevent the formation of exfoliated clay structures. The clay stacks or the aggregated clay structures will not be fully delaminated even when the high shear forces applied at the dry rubber compounding stages. This results in inferior mechanical and barrier properties to the nanocomposite vulcanizates. The clay aggregation and the possible delays in vulcanization under acidic medium are the main drawbacks of the co-coagulation method (Abdollahi et al., 2008). However, nanocomposite vulcanizates prepared by the co-coagulation method exhibited better properties than those prepared by the conventional melt mixing method (Wang et al., 2005). The shortcomings of the co-coagulation method could be partly overcome by addition of a compatibilizing agent or a surfactant, and by modification of the rubber phase with a grafting agent (Hwang et al., 2004). In-situ polymerization and in-situ template synthesis (Pinnavaia, 2001) could also be to prepare nanocomposites, even though they are not widely applied yet to prepare rubber-clay nanocomposites.

The co-coagulation method in absence of a co-coagulating agent like acid would be an alternative method to prepare NR-clay nanocomposites with retention of exfoliated clay structures during the destabilization of both clay and rubber. In this method, destabilization would occur during oven drying, and therefore only water will be removed by evaporation without removing non-rubber substances. Modification of MMT with a long-chain cationic surfactant would facilitate further retention of exfoliated clay structures in the rubber phase and the superior mechanical and barrier properties would be expected. Using different strategies, many successful attempts were taken by the researchers to develop NR-clay nanocomposite vulcanizates with enhanced mechanical properties (Ghari et al., 2016; Rahim et al., 2016; Tan et al., 2016; Zhang et al., 2018). However, none of the studies were able to produce nanocomposite vulcanizates with enhancements in every important mechanical property.

Therefore, this study aims to prepare NR-clay nanocomposite vulcanizates with retention of exfoliated clay structures using a novel acid-free co-coagulation method followed by conventional dry rubber processing techniques. In this study, modified MMT is used to retain exfoliated clay structures and thereby to improve combined mechanical properties of the resultant nanocomposite vulcanizates. The

introduction of this developed nanocomposite vulcanizates and the novel method of producing NR-clay nanocomposite vulcanizates to the dry rubber products manufacturing industry will be the scope of the study. Further, the introduction of an environmentally friendly filler like nanoclay or organoclay to the rubber industry, and its usage at low loadings as a reinforcing filler to achieve enhancements in combined mechanical properties would bring economic advantages to the dry rubber industry in Sri Lanka.

The objectives of this study are given as follows.

- Study the effect of coagulant, and incorporation of a surfactant/modifier, on retaining the exfoliated structures during coagulation.
- Investigate the effect of conventional dry rubber processing techniques on further retaining of exfoliated structures.
- Study the effect of nanoclay loading on mechanical properties of the NR-clay nanocomposite vulcanizates preparing using different types of nanocomposites and to identify the optimum nanoclay loading.
- Propose a suitable mechanism for the development of rubber clay interactions

CHAPTER 2

2. LITERATURE REVIEW

2.1 Natural rubber

Natural Rubber Latex (NRL) is obtained by tapping the trees of *Hevea brasiliensis* of the family Euphorbiaceae. Freshly-tapped NRL is a white fluid with a density approximately 0.975 and 0.980 gml^{-1} and pH between 6.5 and 7.0. It exists as a stable colloidal dispersion of rubber particles in water. The chemical structure of the natural rubber (NR) is cis-1,4 polyisoprene with 4% trans-structures in the rubber backbone. The molecular weight of NR is in the range 200,000-600,000, with a relatively broad molecular weight distribution (Blackley, 1997a).

NR is used in different applications as latex and dry rubber-based products. NR vulcanizates have high tensile strength over a wide hardness range due to its strain-induced crystallization (Ratnayake, 2014). It has the higher resilience, which is responsible for its low heat buildup. It shows low compression set and stress relaxation, good electrical insulation, and good resistance to abrasion tear and fatigue with compared to other materials but those properties must be further improved to obtain more quality products with higher durability. The said properties of NR above could be further enhanced by adding various fillers, blending with other materials, and compounding with special chemicals. Development of NR-clay nanocomposites is the trend in academic research over several decades, mainly to produce high-performance rubber products with superior properties. However, the application of such research findings in the industrial premises as a large scale production is a challenge.

2.1.1 Natural rubber latex

Natural rubber latex is commonly available as field NRL and centrifuged NRL. A variety of products are made with the use of both latex in many industrial applications. Dry raw rubber sheets produced by coagulation and drying of field natural rubber latexes are mainly used in the dry rubber industry for the preparation of various dry rubber products whereas centrifuged latex is widely used for

manufacturing the latex based products in latex blending, casting, and foam rubber industry.

2.1.1.1 Field natural rubber latex

Field NRL is consists of three main phases namely rubber phase 35% (w/w), aqueous phase 55% (w/w), and lutoid phase 10% (w/w) of the whole latex. In the rubber phase, rubber particles are mainly spherical, and the diameter of particles are basically in the range of 20-2,000 nm. The trace metals such as magnesium, potassium, and copper are also found in the rubber phase at the level of approximately 0.05% (w/w).

The sol fraction has a number average molecular weight of 300,000 and a degree of polymerization of 5000. The contents of protein and lipid, which play an important role in the change of mechanical properties, are 1–1.5% and 1–2.5% from the total weight of the latex, respectively. The protein component of the rubber particles occurs entirely as an adsorbed layer that surrounds the external surface of the particles. The major component of the adsorbed proteins is most likely the same with α-globulin, which is dissolved in the serum. The adsorbed layer of a protein determines the charge on the rubber particle, its electrophoretic characteristics, and its coacervation behavior. The lipids such as sterols, sterol esters are probably dissolved in rubber hydrocarbon, and phospholipids are strongly adsorbed on to rubber particles.

The principal phospholipids of the *Hevea* latex particles are of the lecithin type. The presence of hydrocarbon radicals in molecules, which also contains a remote permanent ionized site, is responsible for strong adsorption of these substances at the rubber-serum interface. The adhesion between the protein and lecithin is probably to be accounted for fresh NRL. The lipid layer carries slight overall positives, whereas the proteins, being on the alkaline side of their isoelectric points, are negatively charged.

The aqueous phase of fresh NRL consists of a dilute aqueous solution of density 1.02 gml^{-1} and contains many chemical species. Quebrachitol is the main carbohydrate present in the aqueous phase which accounts for about 1% (w/w) of the whole latex. Such carbohydrates are microbiologically oxidized to simple volatile fatty acids such as formic, acetic, and propionic acids if proper preservation is not carried

out. The aqueous phase also contains various proteins, among them α-globulin and hevein are the most abundant. This aqueous phase is known as serum also includes enzymes, inorganic ions, especially phosphates, carbonate and metallic ions including K, Mg, Fe, Na, Cu and Organic acid (Blackley, 1997a).

Synthetic polyisoprene latex is very different from its natural counterpart. In many properties in the latex and dry state, raw or vulcanized, the synthetic latex shows inferior properties to that of NRL. The unique combination of the polyisoprene rubber phase and the stabilizing system of protein/fatty acid soap in NRL concentrate shows comparatively higher mechanical properties in their final vulcanizates than those made up from synthetic polyisoprene latex (Duy & Bitch ., 2009) .

Two models are used to explain the membrane structure of a rubber particle in latex. In the most accepted model, the rubber particle core, which is the polyisoprene chain, is surrounded by a lipid monolayer. The outermost layer facing the aqueous medium is the protein monolayer in Figure 2.1 (Tanaka et al., 1990; Cornish et al., 1999) and in the second model, the rubber particle membrane is a mixed layer of lipids and proteins without any spatial separation and is given in Figure 2.2 (Wren., 1942; Ho et al., 1996)

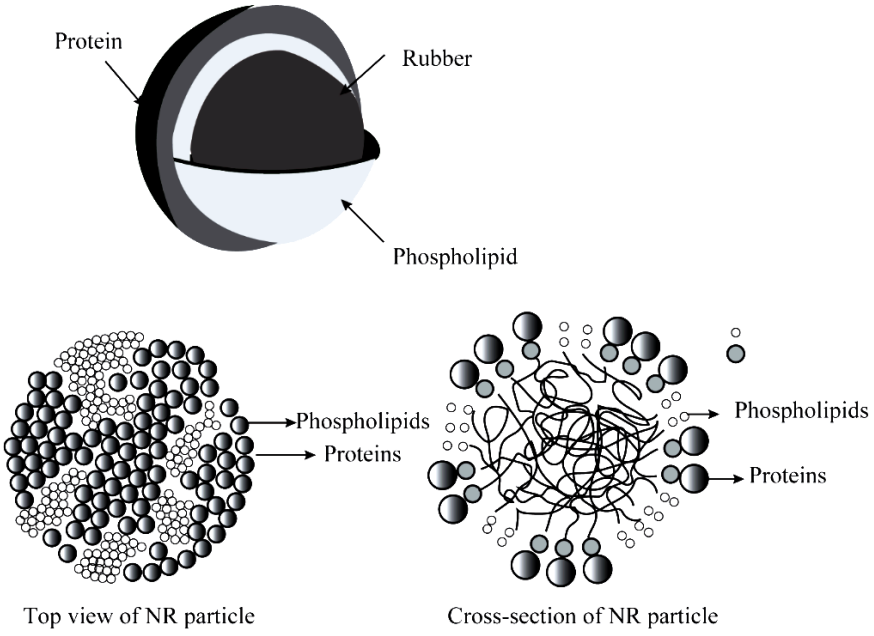

Figure 2. 1 First model for the membrane structure of a rubber particle (Nawamawat et al., 2011)

A previous study (Nawamawat et al., 2011) showed that the mixed layer is composed of 84% proteins and 16% lipids, and the thickness of the mixed layer is approximately 20 nm. Another study reported that the mixed layer is comprised of ω-terminals from 0-3 trans-1,4 isoprene units and 1000-3000 cis-1,4 isoprene units, and α-terminals from two kinds of functional groups namely monophosphate and diphosphate (Wagner., 1976; Cornish et al., 2000; Tanaka et al., 1990; Tanaka et al., 1983; Tangpakdee & Tanaka ., 1997; Tarachiwin et al., 2005). ω-terminals are associated with protein, and α-terminals are associated with phospholipids, and make the network in NR formed by hydrogen bonding or electrostatic forces using some metal ions presented in Figure 2.2 (Wu et al., 2017; Kim et al., 2009; Tangpakdee & Tanaka., 1998; Sakdapipanich et al., 2007).

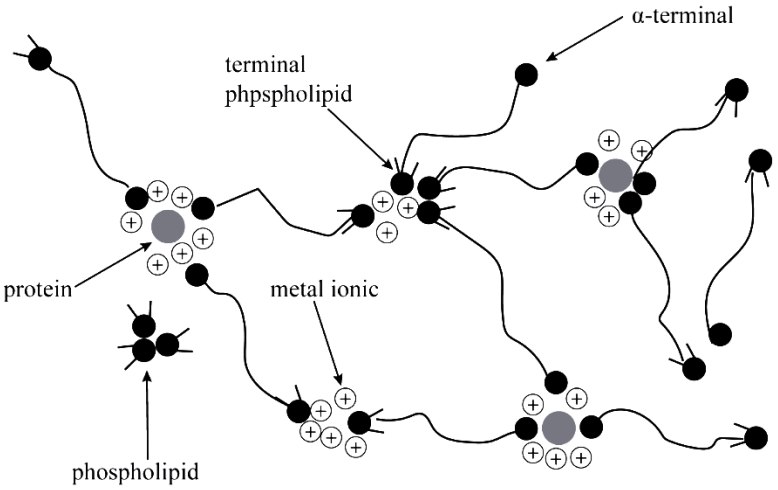

Figure 2. 2 Second model of the membrane structure of a rubber particle (Amnuaypornsri et al., 2008)

Non-rubber substances presence in the rubber product is high when those products are manufactured by raw rubber prepared from field NRL. It is well known that non-rubber substances are responsible for the enhancement of mechanical properties with the development of strain-induced crystallization (amnuaypornsri et al., 2008; Tosaka et al., 2009). The structural changes in the proteins and phospholipids at elevated temperature reduces the mechanical properties (Tuampoemsab et al., 2007) even though rubber product show better mechanical properties at ambient temperature. The microbial degradation of non-rubber substances would be another disadvantage

and cause the lower strength of the product. The proper removal of non-rubber substances and prevention of microbial action using preservatives are essential when field latex is used.

2.1.1.2 Centrifuged natural rubber latex

During concentration, the dry rubber content (DRC) of field NRL is raised to about 60% from about 35%, which is economical for transportation and product manufacture. Additionally, property variation of the product prepared from centrifuged NRL is less as compared to the product prepared by field NRL due to the removal of non-rubber constituents in centrifuged NRL. The centrifuged NRL is considered more uniform in quality than field NRL. NRL concentration by centrifugation, is the most commonly employed method, which involves the separation of preserved field NRL into two fractions; one fraction containing the concentrated latex of about 60% DRC, and the other fraction named 'skim latex' contains 4-5% DRC. Creaming and evaporation are the other two methods of centrifuging latex, less frequently practiced at present. Some of the valuable substances left from the latex during centrifuging may promote mechanical properties of the final rubber vulcanizate; otherwise, those substances might deteriorate mechanical properties while ageing. The lower proportion of water remaining in centrifuged latex causes the minimum problem of thin wall and cellular structure formation compared to field NRL due to the removal of less water during the manufacturing process (Blackley, 1997a).

2.1.2 Raw natural rubber in dry form

NR, as raw rubber in solid form, comes in different types, namely, ribbed smoked sheet (RSS), crepe rubber, technically specified rubber (TSR), and skim rubber. The Purity of raw rubber depends on the production methods and it affects the quality of the products. RSS and crepe rubber are the commonly used raw rubber in the rubber products manufacturing industry in Sri Lanka.

2.1.2.1 Ribbed smoked sheet

The slab of coagulum is prepared using acid as a coagulation agent, mostly formic acid, added to field NRL. It is then sheeted out to a reduced thickness passing

through smooth and diamond roll mill. The ribbed sheets are dried for 5-6 days at around 60 °C in a smoke house where they are suspended on reapers and exposed to smoke from the burning of firewood in a limited supply of air. The moisture content of rubber sheets is reduced to less than 0.8% to develop resistance of the rubber to mold growth (Gu et al., 2009).

2.1.2.2 Crepe rubber

Latex crepe is one of the pure form of NR, which has considerable higher mechanical properties. During processing, the latex is first strained by multiple passes through sieves of different mesh sizes to remove dirt and micro-coagula before subsequent operations. The latex is coagulated, and the coagulum is washed thoroughly by passing it through a series of rollers to produce crinkled laces with several . The laces are dried under controlled conditions over 3-4 days at about 35 °C in drying towers (Nakason et al., 2015). Fractionated bleach (FB), fractionated un-bleached (FUB), and un-fractionated un-bleach (UFUB), yellow fractionated are the main four types of pale crepe. The fractionated pale crepe is produced by removing the yellowish matter of carotenoid particles after the reduction of pH by adding sodium bisulfate before the use of the coagulation step. The little carotenoids left in the fractioned latex are then bleached using thiols to obtain more whitish color in rubber.

2.1.2.3 Technically specified rubber

Technically specified rubber (TSR) is produced to reduce some drawbacks of conventional raw NR. Contamination of foreign matter, storage hardening, and variable in viscosity are some of these drawbacks. The time consumable handling process such as pre-mastication, cutting off large bales, and clearing is required in addition to general manufacturing steps of dry rubber. Otherwise, long mixing time is essential to obtain uniform properties to minimize such drawbacks. The different grades named TSR-L, TSR-5, TSR-10, TSR-20 are produced in various qualities depending on the requirements and demand. The demand for TSR is high compared to its conventional raw rubber forms due to its uniform quality of properties and appearance.

2.1.3 Dry rubber compounding

The compounding ingredients are added into dry rubber based to obtain the rubber vulcanizate with different desired properties is the main function of the dry rubber compounding step. The widely used conventional method for compounding is the mechanical mixing at higher shear rates using internal mixers, two-roll mills, and extruders, etc. Common ingredients such as vulcanizing agents, fillers, antidegradants (antioxidants, antiozonants, age resisters, and protective waxes), and special-purpose ingredients such as coloring pigments, blowing agents, flame retardants, odorants, antistatic agents, and retarders are added to impart different properties in rubber.

The crosslinking agents are necessary to create crosslinks between rubber chains at the molecular level. The cross-linked long-chain rubber molecules form the network structure and transform a viscous liquid to elastic solid. Thus, it improves the strength and elasticity of the final product, which is essential to enhance mechanical properties.

Sulphur is the widely used vulcanizing agent to make crosslinks between rubber chains. The number of sulphur in crosslink strongly influence on physical properties of the final rubber product. The type of vulcanization systems is defined according to the ratio between accelerators to sulphur. The ratio 0.1-0.6, 0.7-2.5, and 2.5-12 are classified as conventional, semi efficient and efficient vulcanizing system respectively. In the conventional vulcanization system, polysulphidic sulphur crosslinks are dominant, which imparts better tensile strength by decreasing modulus at 300% elongation (mod 300%), better tear strength, and good fatigue. The better dynamic properties are also supported by a higher number of sulphur atoms in crosslinks, which prevent the creation of cracks during flexing but gives lower heat resistance and poor aged properties. Short crosslinks of monosulphidic and disulphidic sulphur crosslinks in an efficient vulcanizing system promote better mod 300%, heat resistant, and good aged properties; however, tensile strength and tear strength are decreased. Semi vulcanization systems gives a compromising effect between conventional and efficient vulcanization systems (Datta., 2001).

When sulphur is used alone without accelerators, vulcanization is extremely slow and inefficient even at high temperatures, and usually takes several hours. To

overcome such limitations, accelerators are used, which increases the rate of vulcanization at a lower temperature with high efficiency. Besides, accelerators decrease the quantity of sulphur and improve the 'aged' properties.

Activators are the chemical substances that have strong activation effects on the crosslinking reaction of rubbers. The most common activators used in sulphur vulcanization are zinc oxide and fatty acids. The reaction between zinc oxide and accelerators forms a zinc accelerator complex, which is stabilized by the actions of bases or fatty acids. Fatty acids act as ligands and solubilize the zinc. This complex attacks on the S_8 ring, and as a consequence, it results in chain scission and insertion of sulphur into it. The resulting sulphurating agent is believed to be involved in transferring the molecular sulphur to the hydrocarbon chain to form a crosslink.

The suggested reaction for sulphur vulcanization in Scheme 2.1 begins with the formation of an active accelerator complex formed between activator and accelerators (Heideman et al., 2004).

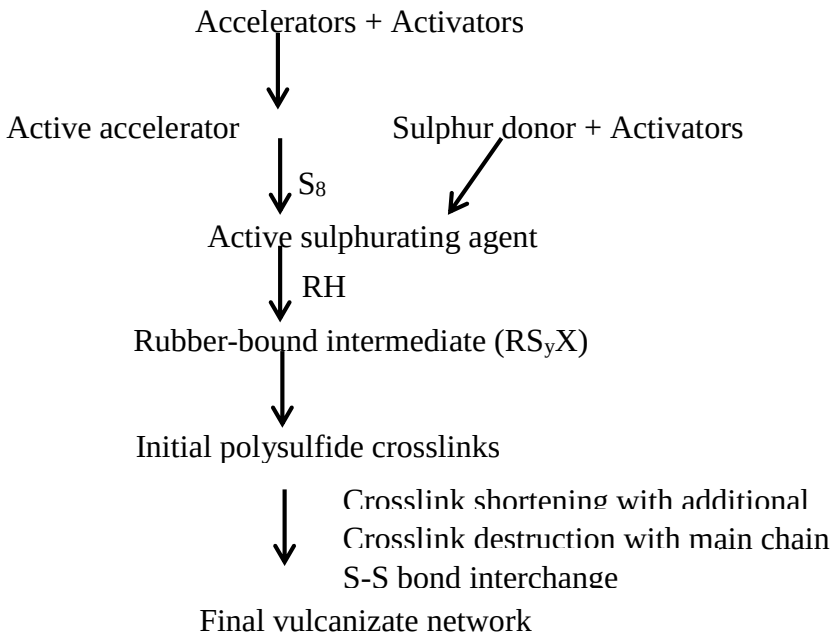

Scheme 2. 1 Outline reaction scheme for sulphur vulcanization of rubber

RH represents the rubber chain, and X-SH is the accelerator.

Sulphur involves vulcanization reaction with the formation of active sulphurating agents after the reaction between sulphur and active accelerator complex

under the influence of vulcanization temperature through ionic and radical pathways (Son et al., 1972). The structures of sulphurating agents are stabilized by the chelation of different ligands such as carboxylates ligands most probably stearic acid and various amines (Ghosh et al., 2003). Once the sulphurating agents are being formed, it reacts with allylic sites of rubber and produces rubber bound intermediates (Parks et al., 1970). The produced pendant group acts as a precursor to form crosslinks. The accelerator-terminated polysulphidic pendent group attached to rubber bound intermediates and crosslink precursor would react with other intermediates or rubber macromolecules to form polysulphidic crosslinks. A large number of sulphur present on crosslink in intermediates convert into shorter crosslinks with the effect of factors such as temperature, amount of zinc oxide, and ratio between sulphur and accelerator, etc. In addition to that precursors are subjected to desulphuration and decomposition reactions (Morrison., 1984).

The presence of zinc in the sulphurating complexes provides a nucleophilic character to the sulphur in the polysulphidic complex and thereby increasing the rate of precursor formation. The presence of natural amines from NR also facilitate the nucleophilicity of the sulphur, and increases the rate of vulcanization, which is the reason why many organoclay based rubber nanocomposite exhibited remarkably reduced cure time with a higher cure rate in many studies because organo clay also contains various types of intercalated amines (Lopez-Manchado et al., 2002; Arroyo et al., 2003; Alex et al., 2006; Teh et al., 2005; Jacob et al., 2006; Sun et al., 2008).

The most common antidegradants is the antioxidant, which protects the rubber from oxidation. Another antidegradant named ‘antiozonant’ prevents the appearance of a surface crack caused by ozone. Antioxidants are mainly divided into two main groups: staining and non-staining. Amine-type antidegradants give the staining effect; however, they act as strong protective agents. Phenolic type antidegradants are less effective but non-staining.

Plasticizers or softeners are added to rubber in the form of low and high viscose liquids or as in solid form making the material softer, flexible, and ease in processability. They also reduce the energy required for processing, assist the incorporation of ingredients, and improve their dispersion. They allow additional fillers to be added by reducing the viscosity of the compound.

2.2 Fillers

2.2.1 Functions of fillers and their importance

The general definition of a filler is a finely divided solid, which is used to fill the surface. One purpose of the addition of filler to rubber is the reduction of cost. However, with the technological advancement and expanded knowledge, treatment of various functional fillers are used to achieve different properties. Other than cheapening the product cost, fillers are incorporated into NR to increase the mod 300%, the hardness, and the abrasion-resistant, which cannot be improved when rubber is used alone. The applied stress concentrated in the rubber matrix is transferred towards the functional fillers, and therefore, the strength and stiffness of the fillers reinforce the rubber. In modern applications, fillers are used to achieve many other important properties such as improved processability, electrical properties, antistatic and magnetic properties, barrier properties, flame retardancy, thermal conductivity, control of density, and thermal expansion, most of which are not shared by rubber itself (Maslowski et al, 2019).

2.2.2 Types of fillers

Fillers are typically classified as particulate fillers and liquid nano-fillers, according to the physical state they are incorporated into rubber. The powdered solid substances with particle size less than 100 μm are generally considered as a particulate filler. Carbon black, silica, clay, and calcium carbonate are the prominent particulate fillers used in the rubber industry. The reinforcement efficiency of particulate fillers depends on particle size, shape, surface area, specific surface activity, and type of the particle structure. Small particle size, less than 1 μm, is a prime requirement to have a better reinforcement effect (Rodriguez & Hamed., 1993; Ames et al., 1996). When the particle size is increased up to the micron level, the reinforcement becomes minimal, especially in the spherical particles. This may be caused by filler particles greatly exceeding the polymer inter-chain distance; hence, developed localized stress by stretching or flexing would rupture the composite from rubber filler interphase. The spherical particle of 1 μm in size covers the specific surface area of 6 m^2/cm^3 and is considered as the lower limit of significant reinforcement. However, the specific

surface area of 300-400 m^2/cm^3 is required to obtain an upper limit of reinforcement (Medalia & Kraus., 1994). Particles with a planar shape have more surface area to contact with rubber matrix than spherical particles with an equivalent size in dimension. However, non-spherical particles such as spheroidal, cubic, tubular, flaky, and elongated, also provide better reinforcement than spherical particles (Blow, 1971; Blow, 1998).

Although a filler offers small particle size, high aspect ratio, and high surface area, it may provide inadequate reinforcement if it has low specific surface activity. Affinity and ability of filler to make a bond or an interaction with the rubber matrix are defined as the surface activity, which is increased by the effect of special functional groups in fillers. Different chemical groups in fillers such as hydroxyl groups in both clay and silica, and quinone and lactone groups in carbon black (Blow, 1971) show specific surface-active for having different types and/or levels of interactions with rubber matrix. Polar rubbers show interactions with polar groups in the fillers. Non-polar interactions are generally improved between NR and filler when the polar nature of filler is reduced by various modifications as to make fillers more compatible with non-polar rubbers. The strong chemical interactions between rubber and conventional fillers provide high mod 300% rather than an increase in tensile properties of a rubber vulcanizate. The structure of the filler such as aggregated structure leads to lower packing density and higher void volume, and thereby to deteriorate the reinforcement.

An increase in surface area by a decrease in particle size would increase viscosity, tensile strength, abrasion resistance, tear strength, and hysteresis; however, this, in turn, gives lower resilience. An increase in surface activity would increase abrasion resistance, modulus at different elongations, and hysteresis, and these behaviors are applicable for modified fillers. An increase in the aspect ratio would increase viscosity, modulus at different elongations, hysteresis, and time for incorporation, but lower the resilience and extrusion shrinkage (Selleh., 2010).

Liquid nano-fillers, prepared by the distribution of particulate fillers in an aqueous medium, show reduced particle size and increased surface area compared to conventional particulate fillers (Thomas & Stephen, 2010). The filled dry rubber compound is then prepared by the incorporation of liquid filler into the latex stage

followed by a step of co-coagulation and drying. This is not the standard method of dry rubber compounding. It was reported that less aggregated filler suspension incorporated into rubber usually gives remarkable properties than direct incorporation of particulate filler by conventional mechanical forces (Tan et al., 2012). Liquid nano-fillers significantly contribute to increased contact between the rubber and filler, and thereby increasing the affinity of rubber matrix to wet the filler surface due to reduction of surface energy.

2.2.2.1 Carbon black

The reinforcement effect of carbon black was discovered in 1904 (Ishikawa., 2011). It is the most widely used filler in NR due to reinforcement ability, relatively low cost, and ease of preparation in fine particle size and shape. Carbon black has an ability to form covalent bonds with NR and creates rather small interphases (Lopez-Manchado et al., 2003). Organic reactive groups on the carbon black surface increase the affinity to make interactions with NR, and therefore, the third ingredient like a coupling agent will not be required to generate strong rubber-filler interactions. Enhanced modulus at different elongations, abrasion resistance, and improved fatigue were the most expected properties achieved by the incorporation of carbon black into NR.

Carbon black is also used to impart electrical conductivity. The morphological form of carbon black is classified into three types, as a particle, aggregate, and agglomerate. The single carbon black particles typically in size range of 15–300 nm are not commonly available in the rubber industry, whereas the particle size of aggregates in the range of 300-500 nm is the popular size. However, further breakdown of aggregates into a smaller size is difficult during rubber compounding. The most commonly used type is agglomerates, which are made up of a group of aggregates and have a particle size in the range of 1-100 μm. However, the breakdown of agglomerates into aggregates during compounding requires high energy (Walter, 2013).

Incorporation of carbon black into high viscous rubber is a challenging process. Higher the carbon black loading, the more will be the average number of particles per aggregate in rubber, which deteriorates the reinforcement of rubber. A higher carbon

black loading should have desirable properties such as higher modulus at a different elongation of the rubber vulcanizate, though it reduces some other vital properties like tensile strength. The appearance of black color, a pollutant in the environment, and dependence on oil feedstock for synthesis were the other drawbacks of carbon black as a useful filler to rubber. However, replacement of carbon black by other fillers has not been yet successful, which may be attributed to poor wetting of naturally hydrophilic surfaces of most non-black fillers with NR.

2.2.2.2 Silica

Silica consists of silicon and oxygen atoms arranged in a tetrahedral structure. It is amorphous and has an average particle size in the range 1-30 nm and a surface area in the range 20-300 m^2/g (Hofman, 1989). Silanol (Si-O-H) groups on the surface of silica particles act as active sites. Even though the mod 300% of silica-reinforced rubber is lower than carbon black reinforced NR, silica provides a unique combination of ageing resistance, tear strength, and adhesion properties (Rattanasom, 2008). Silica is hydrophilic and is not compatible with NR like carbon black. The morphological structures of silica are also of three types: particle, aggregate, and agglomerate. The particle size of physically observable aggregate structures is in the range of 15-20 μm, and therefore, the shear force developed during rubber compounding is not sufficient to disperse aggregate structures efficiently. Chain-like agglomerate structures of silica are generally stable; thus, it needs higher shear forces to make it disperse well (Hofman, 1989).

The water absorbance capacity of silica is high, and it leads to a decrease in cure time, tensile strength, and abrasion resistance (Wagner, 1976). Compatibility difference between hydrophilic silica and hydrophobic NR often causes silica agglomeration in the rubber matrix, which finally results in poor mechanical properties. Silica at higher loading (20 phr) adsorbs zinc complexes in vulcanization reaction causing lower crosslink density (Wolff, 1993) due to inefficient zinc complexes participation in sulphur vulcanization (Rattanasom et al., 2005). The acidic nature of silica also reacts with basic accelerators, which results in a slow cure rate and long cure time (Wolff, 1993). In addition, a higher friction build up between silica particles causes excessive wear and tear of the processing equipment (Dannenberg,

1975). Overcoming such adverse effects of silica is possible by applying a coupling agent, which dramatically reduces the specific surface energy and improves the processing behavior. The addition of glycerol or different amines on silica to interact with such functional groups would soften rubber silica mix by dispersing silica more effectively in the rubber matrix (Kim et al., 2011).

2.2.2.3 Clay or layered silicate

Clay minerals of hydrous aluminum silicates are generally classified as layered silicates. They are formed by a combination of a silicon tetrahedral sheet and an aluminum octahedral sheet.

One tetrahedral layered silicate fused to one octahedral layered silicate (1:1) is known as 'Kaolinite clay' with the general composition of $Al_2Si_2O_5(OH)_5$ and interlayer thickness of 0.7 nm. The crystal lattice consists of one octahedral sheet sandwiched between two tetrahedral sheets (2:1) with a total thickness of 0.94 nm, is well-known as 'phyllosilicates.' The 2:1 phyllosilicate layers can be electrostatically neutral with no interlayer ion present known as 'pyrophyllite.' Due to the absence of interlayer ions, the layers do not expand in water. When silicon in the tetrahedral sheet is substituted by aluminum, the 2:1 structure is called 'mica.' The negative charge induced by this is balanced by the insertion of potassium cations between the layers. Due to the equal size of potassium cation and the hole created by Si/Al tetrahedral sheets, the presence of potassium cation make no interlayer spacing. Consequently, the 2:1 layers are strongly held together.

When in neutral pyrophyllite, the aluminum cations in the octahedral layers are partially substituted by divalent magnesium or iron cations, belonging to smectite clay group. Montmorillonite $(M_x(Al_{4-x}Mg_x)Si_8O_{20}(OH)_4$, Hectorite $M_x(Mg_{6-x}Li_x)Si_8O_{20}(OH)_4$, and Saponite $M_xMg_6(Si_{8-x}Al_x)O_{20}(OH)_4$ are the main types of smectite clay. The negative charge created by the substitution of counter sodium or calcium ions replacing trivalent aluminum cations. The charge created on the layers is not locally constant and varies according to the layer. Due to the unequal size of interlayer cations with the holes of the tetrahedral sheet, the presence of interlayer cations causes an interlayer spacing. Na^+ is the interlayer cation in most pristine clays such as montmorillonite, which is used in many studies to increase the interlayer-

gallery space by cation exchange reaction of long-chain cation; finally, interlayer-gallery space enlarges more than 1.5 nm from its value less than 1.25 nm. The insertion of long-chain cations as a lateral monolayer, lateral bilayer, and paraffin type monolayer and paraffin type bilayer in the interlayer-gallery space cause further increase in its size as shown in Figure 2.3.

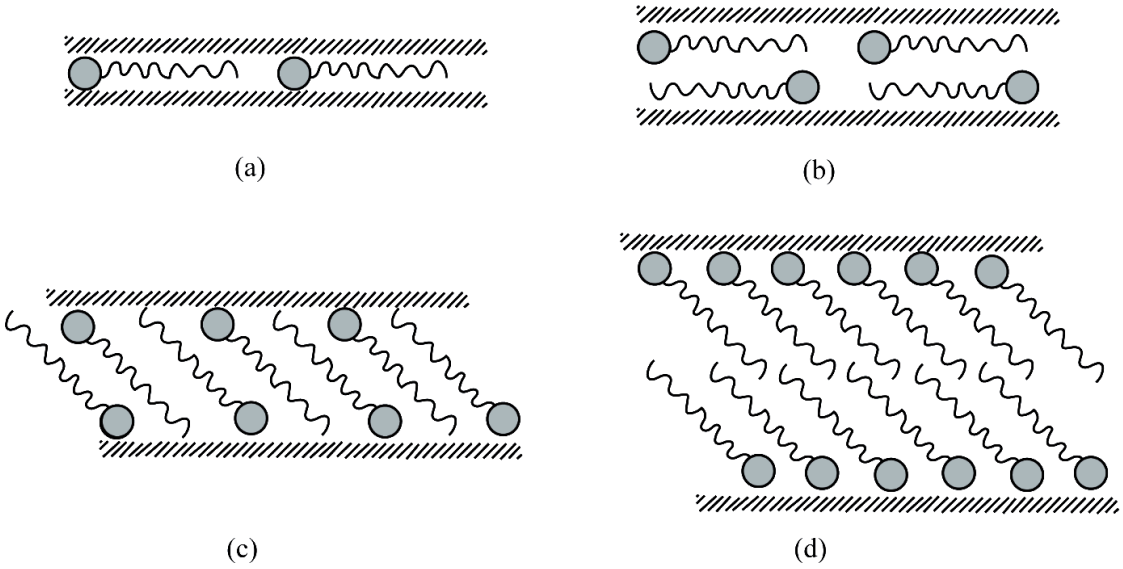

Figure 2. 3 Arrangement of the long-chain cation in layered silicates

(a) Lateral monolayer (b) Lateral bilayer (c) Paraffin-type monolayer (d) Paraffin-type bilayer (Tjong, 2006)

The penetration of polymer molecules into interlayer-gallery space is the most critical process for the preparation of nanocomposite, which directs the formation of different nanostructures in the composite as intercalated, exfoliated, and encapsulated. The presence of water molecules also increases the interlayer-gallery space, a phenomenon called "clay swelling," which is an essential process for further modification of clay by different cation and penetration of polymer molecules into interlayer-gallery space. The increase of interlayer-gallery space of clay by swelling process in an aqueous medium is more effective than direct use of clay as a dry powder (Thomas & Stephan, 2010).

Kaolinite and MMT clay are frequently used to prepare various polymer composites. Kaolinite clay is widely used in the rubber industry to reduce the compound cost but shows inadequate reinforcement. However, MMT clay, compared

to kaolinite clay, imparts better reinforcement in rubber due to its remarkable features as given in Table 2.1 (Miranda-Trevino & Coles., 2003; Uddin., 2018)

Table 2. 1 Features of Kaolinite clay and Montmorillonite clay

Kaolinite clay	**Montmorillonite clay**
The layer consists of 1:1 aluminum octahedral sheet and silica tetrahedral sheet.	The layer consists of 2:1. One aluminum sheet sandwiched between two tetrahedral silicate sheets.
Layers are held together by hydrogen bonds.	Layers are joined by Van-der-Waals forces.
Restrict expansion of layers and limits the reactive area to external surfaces	High expansion of layers and expose of the reactive area to external surfaces
Low swelling capacity	High swelling capacity
Low cation exchange capacity (0-5)	High cation exchange capacity (0-120)
Layers stack up to make large crystals of 70-100 layers thick.	Layers stack up to make small crystals of 20 layers thick.

2.3 Nanocomposites

The Nanocomposite is defined as a composite, in which, at least one dimension of a component is in the nanometer scale (<100 nm). A group of researchers at Toyota-Japan, who developed nylon-6 nanocomposites in 1993 first demonstrated the advantages of nanocomposites containing single silicate layers uniformly dispersed in a polymer matrix (Kajima et al., 1993).

Nanometer range is the dimension which is reflective of bonds and interactions accessible to change in the modification. The different structures of the composite are interacted more efficiently with each other at the highest surface area in the interphase when that dimension found in the nanometer level and imparts superior properties than conventional polymer composite. Further, most of the properties, especially modulus and strength (Vaia et al., 1999; Messersmith & Ginnnelis., 1994), are improved in the nanocomposites conferring to kinetic stability of nanoparticles (Chen et al., 2001). It

shows outstanding reinforcement attributing to the large interfacial area per unit volume or weight of the dispersed phase compared to conventional composites.

Polymer-clay nanocomposite is formed when a polymer penetrated into interlayer-gallery space of clay or penetrated between individual clay layers, which should be made accessible for the polymer chains, otherwise composite is not arranged in nano-scale. The clay-polymer nanocomposite was first reported in 1950 in the patent literature (Carter et al., 1950) but it was not popular at that time until detailed experimentation published by Toyota research. Various engineering plastics such as polypropylene (Kawasumi et al., 1997), polyamide (Fukushima et al., 1988; Reichert et al., 1998), polystyrene (Giannelis., 1996), polyurethane (Wang & Pinnavaia., 1998), epoxy resins (Zilg et al., 1999), poly(ethylene) terepthalate (Yangchuan et al., 1997), poly(ethylene oxide) (Giannelis., 1996), polydimethylsiloxane (Burnside & Giannelis.,2000), polycaprolactane (Messersmith et al., 1995), methyl methacrylate (Dietsche et al., 2000), polyaniline (Biswas & Ray et al., 2000), polyhydroxybutyrate (Gardolinski et al., 2000), and poly(biphenyl ether triphenylphosphate) (Zhou et al., 2001) were synthesized with high stiffness, impact strength, heat distortion temperature, and an improved gas barrier action (Kajima et al., 1993b). However, the polymer-clay nanocomposite is successfully applied to polar polymers, but for nonpolar ones, such as the majority of elastomers, studies started a few years later due to the higher incompatibility between the elastomer and clay (Lopez-Manchado et al., 2003).Polymer-clay nanocomposites have a shown considerable enhancement in thermal properties (Heat resistant and flammability) (Vaia et al., 1999; Messersmith & Giannelis., 1994), barrier properties (Giannelis et al., 1996; Yano et al., 1993; Lan et al., 1994; Strawhecker & Manias., 2000; Matayabas et al., 2001; Yano et al., 1997; Bharadwaj et al., 2002) electrical properties and biodegradability of polymer (Ray et al., 2003(a); Ray et al., 2003(b). The type of nanocomposite can be distinguished depending upon the number of dimensions of the dispersed particles in the nanometer range (Alexandre & Dubois et al., 2000).

The three dimensions of the filler in the range of nanometer-scale (<100 nm) are named as isodimentional nanofillers. The spherical silica nanoparticles obtained by the in situ sol-gel methods (Mark et al., 1996; Wen & Wikes., 1996) or polymerization promoted directly from their surface (Werne et al., 1999) is an example

for this category. The carbon nanotube (Dresselhaus., 2001) or cellulose whiskers (Favier et al., 1997; Chazeau et al., 1999) show two dimensions in the range of nanometer scale. In clay, only one dimension is in the nanometer range, but it shows a remarkable platelet structure with high aspect ratio, and reactive group on the surface to provide different properties not achieved by other fillers.

Lighter weight due to low filler loading, lower cost due to fewer amount of filler used, and improved properties compared with conventional composite at a very low loading of filler are the significant advantages of the nanocomposite. The load transfer from the matrix to the filler is highly efficient due to their increased surface area and good adhesion at the interphase. The crack propagation becomes longer at the interphase because of smaller particle size of nanofiller, which improves both strength and toughness. The disadvantage of the nanocomposite is that nanoparticles tend to aggregate during dry rubber compounding process. Aggregated particles severely affect the thermal and mechanical properties of nanocomposites. It is critical to obtain a homogeneous dispersion of the nanoparticles in the matrix; hence, high-performance nanocomposites are not achieved.

2.3.1 Types of structures in nanocomposites

Three types of nanostructures, namely intercalated structures, exfoliated structures, and encapsulated (un-intercalated) structures, are formed in the rubber-clay nanocomposites, as illustrated in Figure 2.4.

2.3.1.1 Intercalated structures

Intercalated structures are formed when one or more polymer chains are inserted into the interlayer spaces (Aranda & Ruiz-Hitzky., 1992). The presence of polymer chains in the galleries decreases electrostatic forces between the layers. However, the electrostatic forces are not eliminated. This leads to achieving a well-ordered multilayer clay polymer hybrid morphology with different filler-filler, and polymer-filler interactions consisted of polymer chains.

2.3.1.2 Exfoliated structures

Delaminated or exfoliated structures are obtained when individual clay layers are completely and uniformly distributed in a continuous polymer matrix (Ray & Okamato.,2003). Polymer chains lead to an increase in the interlayer-gallery spacing by more than 8-10 nm, which, in turn, gives a high aspect ratio and better dispersion of individual clay layers. Therefore, the most significant improvement in properties is obtained due to large surface interaction between polymer and clay, at lowest clay loading due to its highest phase homogeneity than intercalated structure and greater polymer-filler interactions than filler-filler interaction.

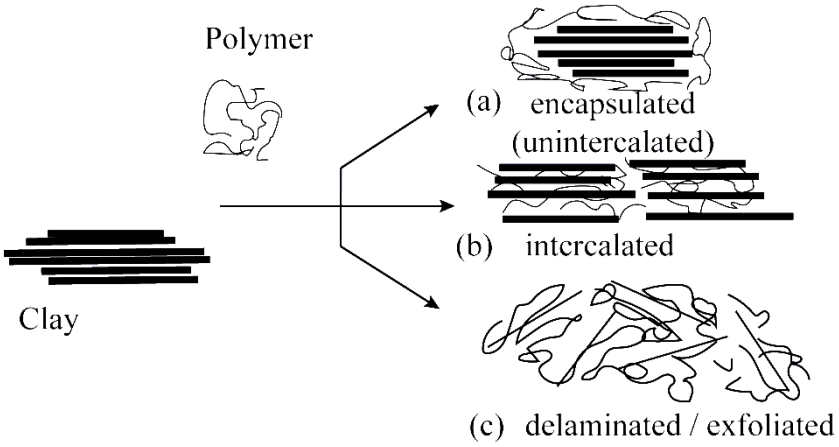

Figure 2. 4 Types of structures in Nanocomposites (Camargo et al., 2009)

2.3.1.3 Encapsulated structures

There is no intercalation of polymer molecules into interlayer-gallery space in clay; hence, the higher number of clay layers are aggregated on each other. Such clay aggregates are encapsulated by polymer macromolecules, therefore, separation into individual clay layers is prevented even at high shear forces. Hence, weak interphase creates between polymer and clay with less interaction. It is not considered as a nanocomposite because even one dimension of the clay layer is not dispersed in the nanometer scale. However, in some studies, clay stack single or very few layers of clay stack is surrounded by polymer without intercalation is called as ‘separated structures.’ which is well-dispersed in the polymer matrix (Wu et al., 2005; Wang et al., 2005).

However, filler-filler interactions are more dominant than polymer-filler interactions due to the highest aggregation behavior of clay structure.

2.3.2 Montmorillonite clay in nanocomposites

Montmorillonite (MMT) is one of the most commonly utilized pristine clay minerals for the preparation of nanocomposites, due to its high cation exchange capacity (Beall & Goss et al., 2009), excellent swelling ability (Adams et al., 1987), high aspect ratio (Wang et al., 2001), and ease of modification (Huskic et al., 2009).

In MMT, at the layer edges, there is a limited number of silanol groups, which increase the polarity. Silanol groups form hydrogen bonds or dipole-dipole interactions with other polar groups and ion-polar interactions with ions. It also can make covalent bonds with various reactive groups (e.g., alkoxy, carboxylic acid, isocyanate groups) in the organic compound. Figure 2.5 presents the structure of MMT.

Frequently, easily exchangeable inorganic cations such as Na^+, K^+, Mg^{2+}, $Ca^{2+,}$ or even organic cations in the interlayer gallery space accounts for its size and cation exchange capacity. Water molecules also can enter into the interlayer gallery space due to the formation of ion-dipole interactions with cations. Some of the oxygen atoms belong to octahedral sheets and tetrahedral sheet; however, hydroxyl ion (silanol group) in the octahedral sheet do not directly link with a tetrahedral sheet and acts as active sites for reaction with other substances (Guggenheim, 2019).

An idealized MMT behaves as a weak acid, and the cation exchange capacity (CEC) of MMT is approximately equal to 0.915 meq/g, and the specific surface area ranges from 750 to 800 m^2/g. MMT is commercially supplied in powder form, in which, the particle size is nearly 8 μm, and it contains about 3000 platelets with a moderate aspect ratio of 10-300 (Khalid et al., 2016). However, the lateral dimension of the individual MMT layer is 200-600 nm, and the thickness of each layer consists of two tetrahedral sheets and one octahedral sheet of a few nanometer thicknesses. MMT is considered as the best option to replace carbon black because of its structural features including the high aspect ratio, exchangeable interlayer cations, hydroxyl groups on the edges of clay platelets, and small dimensions of individual layers.

Another main advantage of an MMT-filled rubber nanocomposite is the enhancement of mechanical properties achieved at lower MMT loading. Therefore,

MMT is considered as a potential substitute for carbon black and silica, which have to be mixed at higher loading to reach the same performance level (Arroyo et al., 2003). The better dispersed MMT layers form thick interphase with large surface area of rubber compared to other fillers due to high aspect ratio of MMT (Ewulunu et al., 2015); it helps reach an optimum dispersion at lower loadings.

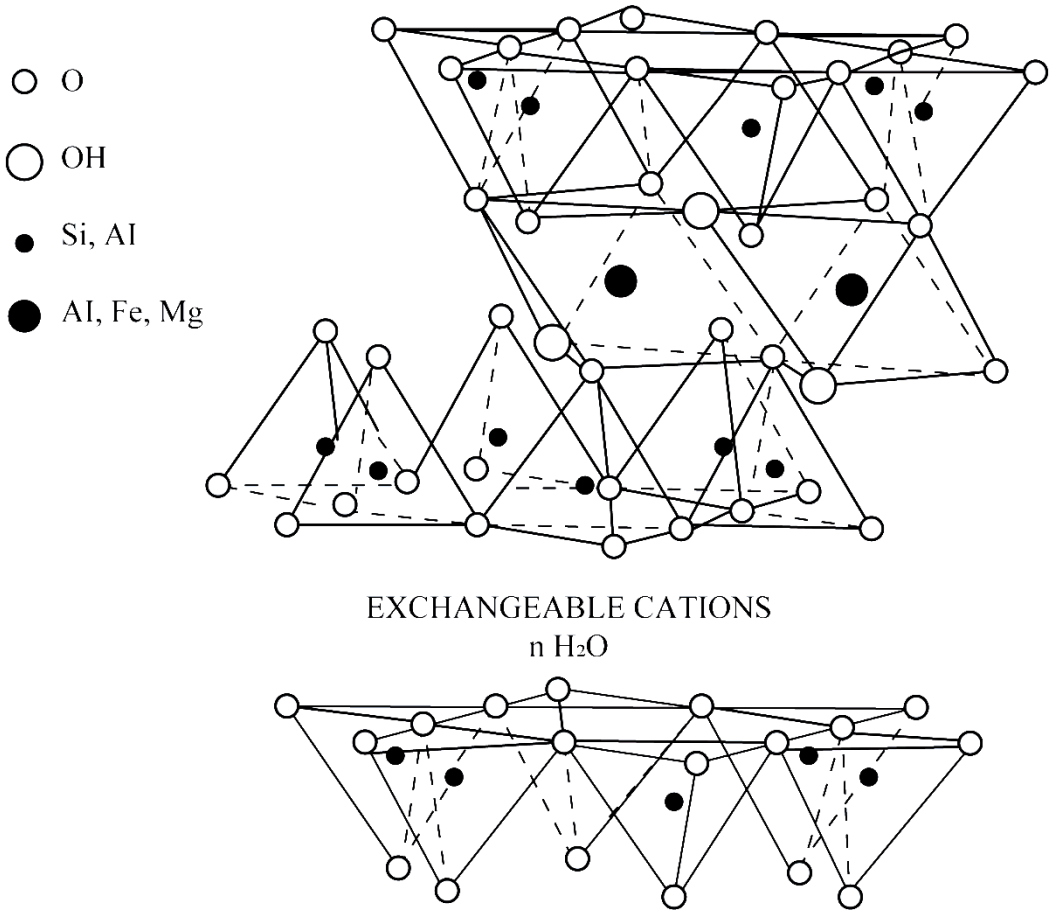

Figure 2. 5 Structure of Montmorillonite clay (Ray & Okamato, 2003)

The incorporation and dispersion of MMT into NRL is easier than NR in the dry stage because MMT is better dispersed in an aqueous medium. In addition to that bound hydrated layers on the surface of the rubber particles interact with hydrophilic MMT at the latex stage (Amarasiri et al., 2013), and provides higher interlayer gallery spaces which are never achieved in solid mixing methods. Therefore, mixing at aqueous medium is proved as a promising method to disperse MMT in NRL. However,

the mixing of MMT would be re-aggregated during drying even though MMT is added to NRL with further dilutions (Amarasiri et al, 2013). Some studies confirmed that the development of strong adhesion between rubber and MMT in nano-scale, especially in the latex stage which accounts for better mechanical properties at final dry vulcanizates (Wu et al., 2005; Valaderes et al., 2006; Amarasiri et al., 2011).

Mixing of MMT in a solid-state with dry rubber is difficult and fails to give a uniform dispersion. The absence or limited hydrophilic layers on the surfaces of rubber particles when rubber is in the solid-state would reduce the compatibility of MMT with rubber due to the removal of hydrophilic non-rubber substances from NRL during raw dry rubber production. MMT also would interact with activators and accelerators in the rubber compound. Further, separation of MMT into individual clay layers in rubber at solid-state is difficult since the shear forces generated during dry rubber compounding are not sufficient to peel-off the layers from MMT stacks. Since the interlayer-gallery spaces of MMT particles are less than 1 nm, polymer chains do not have opportunities to penetrate into smaller spaces and delaminate the clay layers during dry rubber compounding. It is generally accepted that penetration of polymer chain is easier when interlayer-gallery space of clay is high (Galimberti, 2011). However, the optimum size of interlayer-gallery spaces could not be found in NR without MMT modification. MMT is more compatible with polar elastomers than a majority of non-polar rubber elastomers (Lopez-Manchado et al., 2003).

2.3.3 Importance of modification of MMT

Layers of MMT in stacks are held together by weak electrostatic and van-der-Waals forces. The interlayer-gallery space depends on the radius of interlayer cation, charge density on the layers, and the degree of hydration (Ray & Okamato., 2003). According to Galimerti, interlayer-gallery space of the modified MMT highly depends on the length of the alkyl chain, and the ratio of cross-sectional area to the available area per cation (Galimberti, 2011). However, expanding the interlayer gallery space lowers surface energy and decreases cohesive energy, thus facilitating wetting and interaction of rubber macromolecules. Complete dispersion of clay layers in a rubber matrix is achieved by three consecutive steps; first, wetting the surface of

clay tactoids in rubber, then intercalation of rubber into clay galleries, and finally, exfoliation of the clay layers (Ray & Okamato., 2003).

Organoclay, mostly used in previous studies, was prepared by modifying MMT with organophilic ions via cation exchange reaction. As a result, the hydrophilic nature of MMT was converted to hydrophobic nature, and the interlayer-gallery spaces would increase when MMT particles are incorporated into NR (Vaia et al., 1993).

Different intercalation techniques are also used to insert organic molecules into clay layers. Such insertions are done by cation exchange reaction (Fox et al., 2007), anion exchange reaction (Liao et al., 2010), sol-gel reaction (Bottcher et al., 2002), hydrogen bonding (Finocchio et al., 2011), combined ion exchange and hydrogen bonding (Chou et al., 2004), carboxylic acid chelation (Guegan et al., 2010), and carbon dioxide interaction (Lin et al., 2004). Among them, MMT modification by cationic exchange reaction is widely used to prepare organoclay for many applications. Cations in the MMT are usually replaced by alkylammonium, phosphonium, or sulphonium under proper conditions, or by long-chain organic cations such as alkyl primary ammonium ion (Arroyo et al., 2003; Sookyung et al., 2014), alkyl secondary ammonium ion (Hrachova et al., 2013), alkyl tertiary ammonium ion (Hrachova et al., 2013), alkyl quaternary ammonium ion (Paiva et al., 2008; Ghari et al., 2016), alkyl phosphonium ion (Lagaly et al., 2013; Avolos et al., 2008), or by long-chain primary amines (Sun et al., 2008). Alkyl quaternary amines such as dimethyl dehydrogenated tallow ammonium (Tabsan et al., 2010), bis(2-hydroxyethyl), methyl tallow ammonium (Joly et al., 2002), dimethyl benzyl hydrogenated tallow ammonium (Jacob et al., 2007), octadecyl trimethyl ammonium (Keawkumay et al., 2012), distearyl dimethyl ammonium (SI et al., 2011), benzyl trimethyl ammonium, and dihexadecyl dimethyl ammonium (Hrachova et al., 2013) have been frequently used in MMT modification.

Figure 2.6 shows (a) unmodified clay (b) Quaternary amine intercalated organoclay by cation exchange reaction. It is presented that interlayer-gallery space denoted as d(001) of organoclay is greater than that of unmodified MMT due to presence of long chain organic cation.

Intercalation agents create non-covalent bonds and/or covalent bonds with clay surfaces, which cause the separation of clay layers in the clay confinement. Organic

clay intercalation proceeds typically in a stepwise manner that involve ion exchange or polar head chelation towards clay counter ions, followed by further organic incorporation by hydrophobic forces or by hydrogen bonding (Liao et al., 2010). The randomization of layered clay is the final result, which can be controlled. In the past, alkyl quaternary-ammonium salt surfactants were used as intercalating agents, but recently, hydrophobic backboned poly(oxyalkylene) amine derivatives and their corresponding amphiphilic polymers have been structurally tailored to expand the clay interlayer-gallery space (Chou et al., 2004).

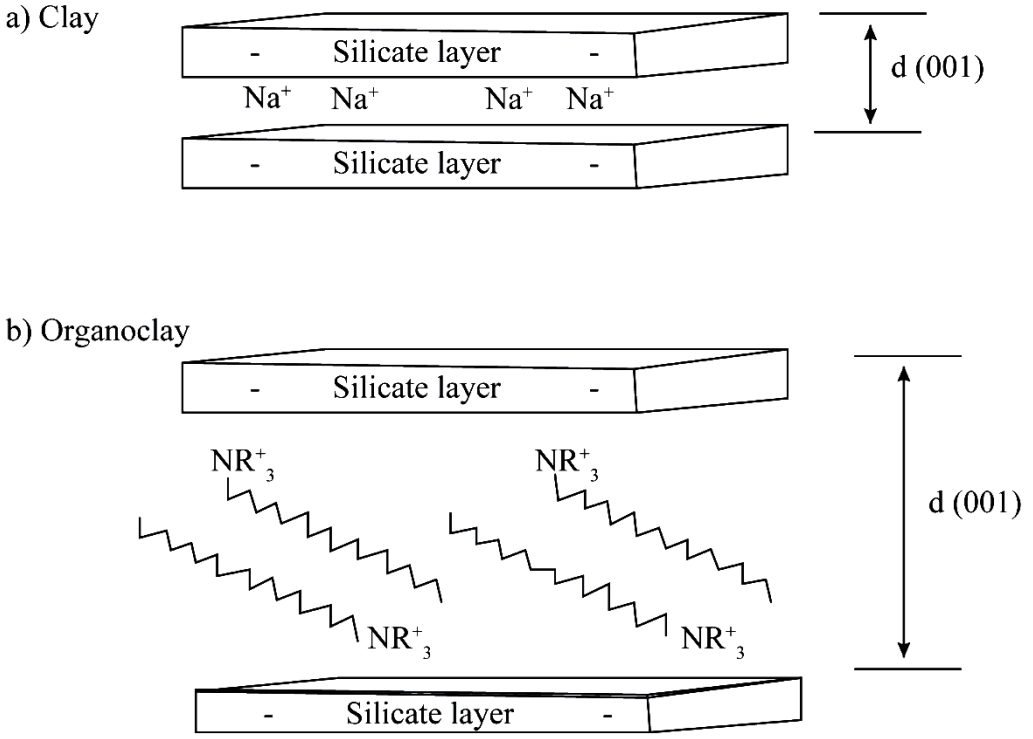

Figure 2. 6 Structure of (a) unmodified Clay (b) Organoclay (Thomas & Stephen., 2010)

Intercalation by sol-gel grafting reaction is one of the leading modification techniques for MMT (Bottcher et al., 2002). The silane coupling agent has both hydrophilic and hydrophobic ends, which enable them to form bonding between clay layers and rubber chains (Thomas & Stephen., 2010). Reactive groups in silane when reacted with silanol surface in the clay allow expansion of the interlayer-gallery spaces with the formation of covalent bonds between clay and silane (Galimberti, 2011).

Figure 2.7 depicts the structure of Bis(triethoxysilylpropyl) tetrasulfide (TESPT) silane agent.

Three reaction mechanisms are involved in systems with sulphidic-alkoxy-based silane. The first silane reacts with clay by silanization (hydrophobation) reaction. Secondly, silane to rubber coupling reaction; and finally, rubber-rubber interaction is promoted by prominent sulphur crosslinks. However, simultaneous reactions are temperature and time-dependent, and show an optimum level at a dump temperature of approximately 140–150 ˚C, as depicted by filler–filler and filler–rubber interactions in Figure 2.8 (Kaewsakul et al., 2015).

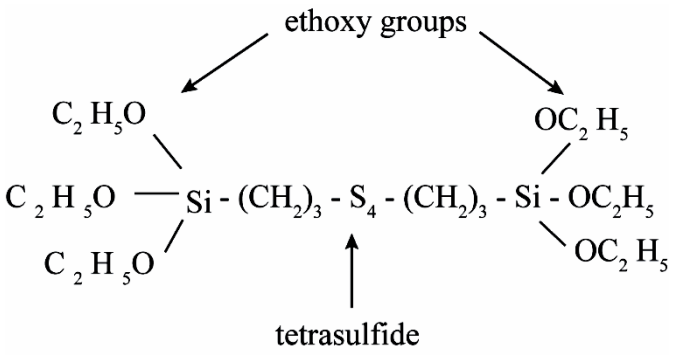

Figure 2. 7 Structure of TESPT coupling agent

The silanization reaction is rather slow at a moderate temperature of 120 ˚C (Goerl et al., 1997). Hence, a higher mixing temperature is necessary to obtain efficient reaction at a short processing time. However, it was noticed that at elevated temperatures, the coupling reaction between rubber and TESPT is triggered and results in premature scorch and undesired high compound viscosity (Reuvekam et al., 2002; Luginsland., 2000). The dump temperature in the range of 145-155 ˚C was reported as the best for both silanization and pre-crosslinking reactions. It is believed that NR can start to react with sulphur from TESPT molecules at the temperature as low as 120 ˚C (Kaewsakul et al., 2015). Sulfidic-alkoxy-based silane coupling agent gives many advantages on silica or clay-filled rubber. Sulfidic-alkoxy silane effectively reduces compound viscosity, filler-filler interactions, and thereby provides relatively high rubber-clay interactions and improvements in mechanical properties. Non-sulphidic-alkoxy silane, due to its bifunctional reactions, provides low rubber-clay interactions. Silane, which has no alkoxy groups but only sulphur

functionality, clearly demonstrates its ineffectiveness in NR, showing poor dispersion and high filler-filler interactions (Kaewsakul et al., 2015).

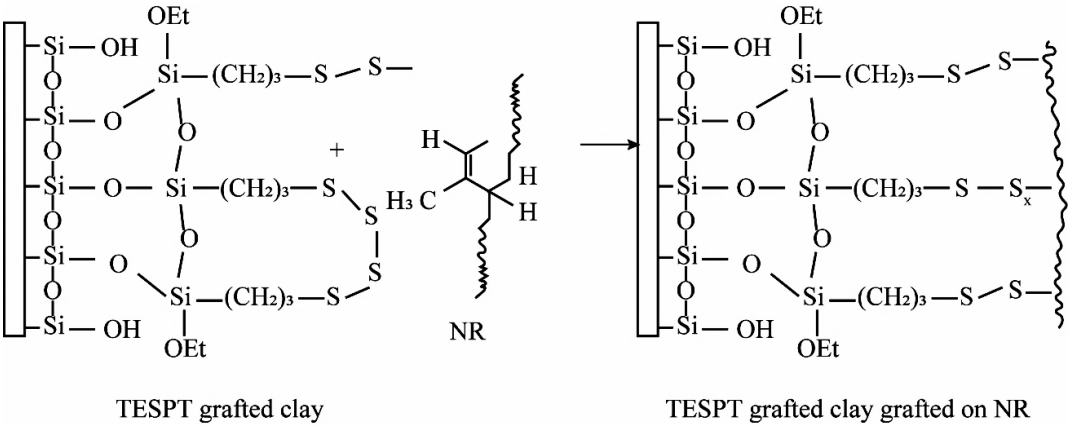

Figure 2. 8 Filler-rubber interaction with TESPT

Silane-grafted MMT (Chow & Neoh., 2009; Xu et al., 2013; Kornmann et al., 1998; Marini & Bretas et al., 2013) or silane-grafted organo modified MMT (Thongpin et al., 2008; Sharif-Pakdaman et al., 2013) was used in previous studies for various polymers (Chow & Neoh., 2009; Xu et al., 2013; Kornmann et al., 1998; Marini et al., 1998; Sharif-Pakdaman et al., 2013), but limited studies were reported for NR (Thongpin et al., 2008). However, the well-known TESPT silane agent used as a coupling agent for NR was not yet studied in using for TESPT grafted MMT or TESPT grafted organo modified MMT for NR compounds.

Direct intercalation of polymers into pristine clay is mostly restricted, but in practice, it was reported that polymers are probably adsorbed onto the external surface of the clay layers. If the layers are exfoliated and well dispersed, then the polymer would intercalate corresponding to one or two linear macromolecule chains between inter- gallery spaces. However, polymer-clay interaction is complex, and it was suggested that loops of polymer chain would penetrate interlayer-gallery space (Sharif-Pakdaman et al., 2013).

2.4 Rubber-clay nanocomposites

Many rubber-clay nanocomposites are implemented after the synthesis of the number of plastic nanocomposites. However, very few studies were done in the early

stages of developing nanocomposite, mainly for synthetic rubber. Okada & Usuki., (1995) prepared nanoclay composite with acrylonitrile-butadiene rubber, by which, they achieved significant improvement of mod 300% by 5 phr of pristine MMT loading but similar mod 300% was obtained by carbon black at 40 phr carbon black. Many synthetic rubbers were used in the preparation of nanocomposite before implementing natural rubber (Wang et al., 2000; Nah et al., 2001; Zhang et al., 2000).

In the development of natural rubber clay nanocomposite, it was reported that nanocomposites achieved superior mechanical properties than conventional composite. However, most significant properties such as tensile strength, tear strength, elongation at break, modulus at different elongations, hardness, and abrasion resistance have not been achieved in a single study. Individual or few combinations of properties were developed with the effect of different processing techniques, types, and loading of clay with different rubber and various types of modification. Arroyo improved the tensile strength without hardly any reduction in the elasticity (Arroyo et al., 2003). However, Verghese et al. (2003) revealed that enhanced strength is given with reduced elongation after the increase at particular loading due to better filler dispersion and strong filler rubber interactions. Mousa et al. (2001) stated that elongation is unaffected with the incorporation of 2 phr organoclay due to higher crosslinking of SBR rubber in the neighborhood of the clay layers by better intercalation and exfoliation behavior. Some studies showed that elongation at break is improved attributing partially to the plasticizing effect of surfactant, located at the rubber clay interphase (Rooj et al., 2012). Wu et al. (2004) stated that tensile strength is affected by two main factors, strain-induced crystallization and the reinforcement of exfoliated clay layers. The same study further explained that tensile strength is improved by the slippage of rubber molecules and the orientation of the intercalated clay layers under tensile stress. This study further showed that exfoliated structures cause good reinforcement, but on the other hand, restrict the deformation of NR molecules; hence, strain-induced crystallization is hindered. Kaewkumay et al. (2010) stated that tensile strength is increased with increasing surfactant content, maybe due to the expansion of interlayer-gallery space in the organoclay. It facilitates the penetration of NR molecules into the gallery space.

Fathurrohman et al. (2015) elaborated that exfoliation of clay in the rubber matrix inhibits the strain-induced crystallization. Some studies showed that a smaller amount of organoclay gives enhanced mechanical properties to rubber compounds due to better dispersion of organoclay in the rubber matrix (Mohan et al., 2011; Bala et al., 2004). Most investigations stated that agglomeration leads to a reduction of tensile characteristics when the content of organoclay reaches higher loading (Bala et al., 2004; Rooj et al., 2012; Amarasiri et al., 2013). Carreto-Gonzalez et al. (2008) introduced a new route to increase the tensile strength without hardly affecting the elongation at the break by using polyethylene glycol, which acts as a swelling agent and improves the dispersion of clay in the rubber matrix. This route tackles the intercalation/exfoliation problems of clays with the organophilization route. Wang et al. (2005) noticed that modulus at different elongations of rubber was low, and slowly intensified with the increase of strain in the lower strain region, and then sharply increased within a smaller strain due to the improvement of tensile crystallization. However, it was mentioned that the modulus at different elongations and tensile strength of nanocomposites were higher than those of pure NR, and stress transition caused by tensile crystallization weakened. It indicated that stress was smoothly developed, possibly caused by the nano effect.

In comparison, some research studies mentioned that high modulus, stiffness, and strength could be achieved by efficient stress transfer from NR macromolecule to filler with a large aspect ratio of nanoclay (Wu et al., 2005). Kim et al. (2006) obtained the highest tensile value using the organoclay without a silane coupling agent, which was due to the significant elongation of the rubber; however, when silane was introduced, the modulus at different elongations was enhanced with lower elongation. Madhusoodanan et al. (2006) reported that tear strength was improved by exfoliation of clay, increased extent of dispersion, and high interfacial action between layers and the rubber. The finely dispersed clay layers divert the tear path and impart higher tear strength in the study.

The highest abrasion resistance could not be obtained by using only organoclay with NR. It was achieved by a hybrid of organoclay and carbon black in some studies (Liu et al., 2010) or nanocomposite with the aid from a silane coupling agent (Tabsan et al., 2010) or epoxidized natural rubber blended with SBR (Rajesekar et al., 2009).

Hardness is also an important parameter which shows similar trend with modulus. It was not increased as carbon black in the filler, but 55-60 IRHD could be obtained by epoxidized natural rubber with 10 phr of organoclay (The et al., 2005) or with the combination of organoclay and carbon black (Galimberti et al., 2009).

Nanocomposites improved barrier properties which are essential for some rubber engineering products containing high-pressure air in the inner tube of the tire, air spring, and cure bladders. The higher barrier to gas permeability is very important for those products. Li et al. (2008) prepared a nanoclay composite to decrease oxygen permeability by more than 40% using 3 phr of organoclay. Molecules, when travel in a longer and more tortuous path takes extra time for diffusion across the membrane. The filler with the same size dispersed uniformly and entirely in the rubber matrix parallel to the surface the composite then matrix properties are not affected for final gas barrier properties. The clay layers with a high aspect ratio would significantly reduce gas permeability (Ray & Okamato., 2003). Wang et al. (2005) also described that gas permeability depends on a function of the aspect ratio of clay and volume fraction in the matrix.

NR-clay nanocomposites show excellent thermal properties compared to pure rubber. The thermal stability was notably improved by the addition of smaller loading of organoclay because well-dispersed clay layers make the path length for the thermally decomposed volatiles to escape and shielding effect imparted by clay layers (Mao et al., 2006; Sharif et al., 2005; Sun et al., 2007).

Five methods have been identified for the preparation of polymer composite nanocomposites (Thyomas, 2010) in the literature: melt blending, solution blending, emulsion blending, in situ polymerization, and in situ template synthesis. Some of these methods are not directly used in the preparation of rubber-clay nanocomposites.

2.4.1 Melt blending

In melt blending, filler is directly mixed with rubber in the molten state and form rubber-clay nanocomposite, which is driven by the enthalpic contribution of the rubber-clay interactions (Qureshi & Qammar., 2010). The steps of melt blending are depicted in Figure 2.9. Initially, a high shear force is applied to break down rubber into small pieces and thereby reducing viscosity. The elevated temperature generated by

the friction of high viscous rubber causes further reduction of viscosity, and fillers and rubber ingredients could be easily incorporated into less viscous rubber. The addition of vulcanizing agents is the last step, during which the temperature is kept minimum to prevent scorch. Hence, vulcanizing ingredients are added at the stage of milling in most of the industrial process to prepare final nanocomposite vulcanizates.

This method is the most direct, environment-friendly, cost-effective, and widely used method in industrial application and academic research to prepare rubber-clay nanocomposite in the literature.

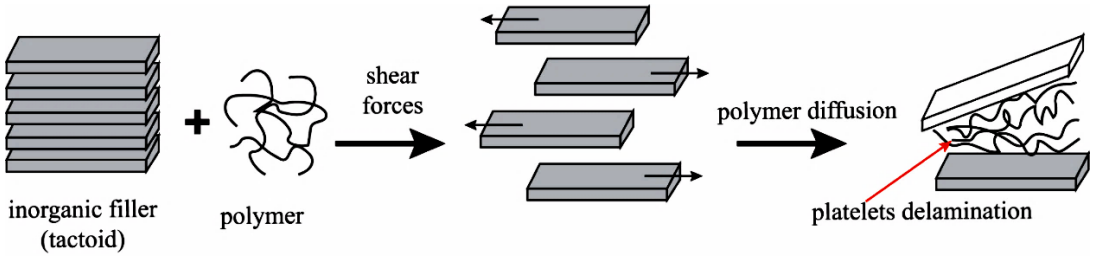

Figure 2. 9 Steps of melt blending (Unalan et al., 2014)

The high viscosity of rubber developed higher friction during mixing, and assist to peel-off the clay layers from the clay stacks, and encourage towards the formation of the exfoliated structures. Melt blending is performed using the standard processing machineries of the rubber industry, including internal mixers such as brabender plasticoder and Banbury, open mills, and twin screw extruders. The final product depends on the processing parameters such as mixer type, mixing time, and temperature, and chemical ingredients in the rubber formulation such as compatibilizer/s and accelerator/s. Compatibilizers such as silanes (Jang et al., 2012) and titanates (Alkadsi, 2008) were required in many melt blending processes to increase interfacial interactions between rubber and clay. Otherwise, re-aggregation and/or de-intercalation of clay layers in rubber would occur (Guo et al., 2018).

In comparison to rubber, exfoliation of clay is difficult in plastic phase due to its lower viscosity (Wong et al., 2013). Commercially available organoclay in a solid-state is incorporated directly into rubber, and therefore, the preparation of an aqueous suspension of organoclay, which is considered as a most challenging process in the latex industry, is not required. However, the use of aqueous suspension of

organoclay in the dry rubber industry is difficult as the processing equipment is not designed to handle liquids in large volumes.

Grafting of functional groups to NR to make NR more compatible with clay is also a common technique used in the preparation of rubber-clay nanocomposites. Grafting of functional groups onto NR is also possible simultaneously with melt blending (Juntuek et al., 2012). This route is the easiest way to modify clay while mixing it with rubber because of its simplicity (Varghese et al., 2003; Vijayalekshmi et al., 2010). When clay layer surfaces are sufficiently compatible with the chosen rubber, it is believed that loops of rubber macromolecules will crawl into interlayer-gallery space and form intercalated and/or exfoliated structures in the nanocomposites. Epoxidized NR was successfully mixed with an organoclay (The et al., 2005) and showed improved mechanical properties due to the high compatibility of epoxidized NR with polar clay in the composite than unmodified NR. Further, some studies exhibited better mechanical properties by incorporating clay with polyethylene glycol, which forms intermolecular forces with polar clay and non-polar NR (Carreto-Gonzalez et al., 2008). The property improvements were not as much as expected, because none of the studies confirmed the formation of fully exfoliated structure, and thereby achieved better results.

The effort of direct use of powdered organoclay into rubber matrix was successful and improved the properties even though the exfoliate structure did not remain in the final stage of vulcanization (Varghese et al., 2003; Bala et al., 2004; The et al., 2005; Carreto-Gonzalez et al., 2008). However, the use of a solvent in the process is not required, and mixing of the large extent of filler is done at higher shear forces; those are the few advantages of the melt blending method.

2.4.2 Solution blending

Solution blending includes several steps, as illustrated in Figure 2.10 (Premanik et al., 2003). A clay suspension is made as to the first step, in which, clay layers are exfoliated into single platelets using a polymer-soluble solvent. The polymer is then mixed with the clay suspension to adsorb clay platelets onto the polymer. The solvent is finally eliminated from the polymer-clay complex through evaporation.

The driving force of solution blending is the entropy, gained by desorption of the solvent. Polar polymers are most preferred for solution blending rather than non-polar polymers; hence, for rubber-clay nanocomposite, NR grafted by epoxy, polyimide, and polymethylmethacrylate are widely applied. A few studies were reported on NR, but this blending method was mostly used for synthetic rubbers (Ganter et al., 2001; Sadhu & Blowmick., 2008).

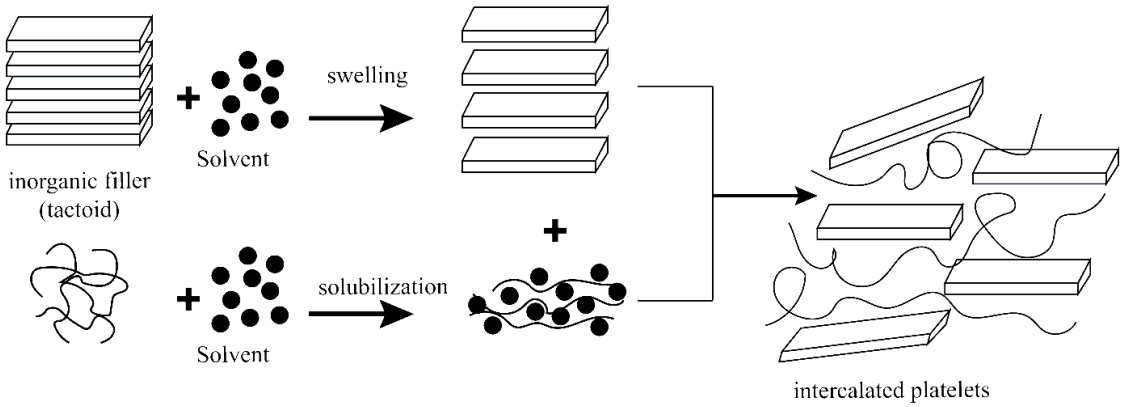

Figure 2. 10 Steps of solution blending (Unalan et al., 2014)

Toluene, methylethylketone, N,N-dimethylacetamide (Karger-Kocsis and Wu., 2004), and chloroform and carbon tetrachloride (Sadhu et al., 2004) are the most common organophilic solvents used in solution blending, which are compatible with an organoclay (Sadhu & Blowmick., 2004). Hence, unmodified MMT was not commonly used with solvent blending as it is easily agglomerated and separate clay from the polymer. Organoclay-filled NR composites prepared by solution blending showed higher bound rubber content than those prepared by mechanical blending (Lopez-Manchado et al., 2004). It was reported that intense intercalation appears with the increased effect of interlayer-gallery space and intercalation of soluble rubber into the gallery space (Lopez-Manchado et al., 2004), and resulted in the formation of exfoliation structures more easily (Joly et al., 2008).

The nature of the solvent influences the mechanical properties of nanocomposites. In a study based on styrene butadiene rubber (SBR) latex, the higher tensile strength and modulus at different elongations of nanocomposites were observed when toluene acted as the solvent in solvent blending, compared to the use of

chloroform and carbon tetrachloride as solvents. It revealed the importance of having similar polarity and solubility of rubber to the solvent as vital for de-coiling the rubber chains and obtain complete exfoliation of organoclay (Sadhu & Blowmick., 2004).

The effect of the final processing temperature is also significant since a few solvent molecules remain even after the vaporization stage. The presence of exfoliated structures is dominant as residual solvent molecules within silicate interlayers facilitate exfoliation during thermal treatment at higher temperatures, beyond 140 $^{\circ}$C, at atmospheric conditions. Also, complete de-intercalation of rubber molecules may occur with the effect of motion of residual solvent molecules within clay layers under extra pressure, exerting conditions at relatively lower temperatures (Thomas & Stephen., 2010).

The disadvantage of solution blending is that it needs a compatible polymer-solution system, as well as organoclay for better dispersion. Moreover, eradicating the solvent from the composite is also tricky due to desorption of the solvent (Wang et al., 2000). The solvent vaporization process is not environment-friendly and also causes health hazards to human beings. Since this method requires a high amount of solvent for large-scale production, hence solution blending is limited for use in the industry.

2.4.3 Emulsion blending

Emulsion blending is the popular method, in which nanoclay and other compounding ingredients are added into the latex stage and stirred well to obtain a uniform mix. At this stage, a higher degree of exfoliation would occur at minimum energy consumption. After that, clay-filled latex is destabilized using a co-coagulation agent and dried. Figure 2.11 presents the steps of emulsion blending. When acid is used as a destabilization of clay-filled latex, most commonly, it is called co-coagulation method.

The prepared rubber-clay nanocomposite is then mixed with rubber compounding ingredients at the latter stages, which in turn gives additional intercalated structures and exfoliated structures by the effect of melt blending. In emulsion blending, clay layers are separated from the rubber phase when co-coagulation time is too long. The other adverse effect is the development of

viscosity with higher loss of mechanical energy as heat. However, less energy consumption is required for incorporation of clay into rubber matrix, which is an added advantage in emulsion blending. This blending gives better clay dispersion in the nanometer level with effective moderate viscosity. The size of the latex particle, rubber to clay ratio, and the co-coagulation rate are the primary factors to be considered for effective dispersion of clay in NR (Thomas & Stephen., 2010).

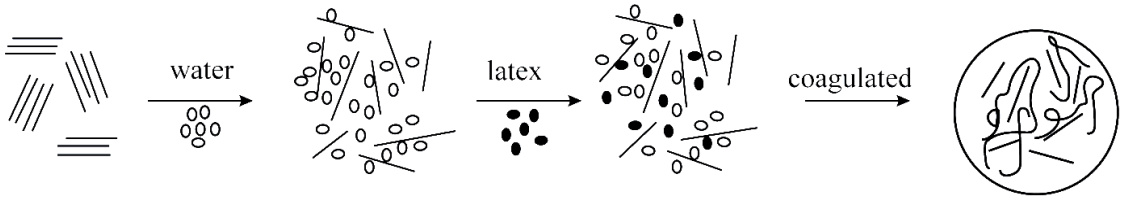

Figure 2. 11 Steps of emulsion blending (Wang et al., 2005)

This blending method is frequently studied in the preparation of rubber-clay nanocomposites during the last two decades in research after Zhang et al. (2000) introduced the method with SBR latex. A similar process was first developed in 1957 to destabilize NR latex with a clay mineral (Giger & Liponski., 1957). In latex, the clay is swollen by hydration and makes it good for dispersion at the molecular level in the rubber matrix. However, the application of this process was limited due to the lack of identified knowledge on nanoclay and clay modifications at that time. Until 2005, this blending method was not a research interest for academics, however, Wu prepared NR-clay nanocomposite in 2005 with improved mechanical properties using this method (Wu et al., 2005). After various modifications were done for both rubber and clay to enhance different properties of the nanocomposites by many research-based on emulsion blending (Alex et al., 2006; Abdhollahi et al., 2008; Rattanasom et al., 2009; Bhowmick et al., 2010; Lee et al, 2011; Tan et al., 2012; Tan et al., 2016). Even though this is a promising method in most of the academic research, its expansion for industrial applications is limited, this could be the reason why dry rubber industry is not equipped to handle both dry rubber and rubber latex in industrial premises. Generally, it is considered that the incorporation of clay directly into NRL is easier than the incorporation of clay into dry NR using melt blending and solution blending. Among the fillers, clay is the one which is easily dispersed in water, as clay acts as a

swelling agent owing to its hydration ability of cations such as Na^+ or K^+ (Theng, 1979).

Reinforcement in a composite is outstanding due to the uniform mixing of clay in rubber if the emulsion blending is used. Hence, properties of the composites, such as hardness, tear strength, and tensile strength, show its highest value, and sometimes exceeding the properties resulting from carbon black (Arroyo et al., 2003). Further, it was confirmed that the mechanical properties of NR-clay nanocomposites prepared by emulsion blending are considerably higher than those prepared by solution blending (Wang et al., 2000). However, interlayer-gallery spaces in clay particles were not increased even by 1 nm in many studies carried out on the preparation of NR–clay nanocomposites by emulsion blending (Wu et al., 2005; Valadares et al., 2006), which shows that it separates the clay into either individual layers or aggregates of nanometer thickness without the intercalation of rubber molecules into clay galleries. The specific structure named as "separated" has a unique behavior on improving the properties by homogeneous dispersion of less aggregated clay structure. This structure is also a type of encapsulated structure; the only difference is that single or very few layer-thick clay stack dispersed well in the rubber matrix. Few studies specifically suggested that separated structures are easily produced by the emulsion blending method (Wu et al., 2005; Wang et al., 2005).

Except for the step of addition of clay into latex, the other steps of emulsion blending are closely related to the production of dry rubber sheets. It is an advantage that the production of nanocomposites starting from NRL with modifications is more effective than starting from dry rubber. However, a few drawbacks in the emulsion blending limit its usage in large-scale production. The main problem is caused by a co-coagulation agent such as hydrogen ion (H^+) from acid, which would replace the Na^+ ions in the interlayer-gallery space and thereby decrease space (Abdollahi et al., 2008). This effect mainly contributes to the re-aggregation of clay layers, so that rubber latex particles between the clay layers may be expelled (Wu et al., 2005). MMT suspension may increase the viscosity in NRL, which causes resistive to coagulation of NR and delaying the process (Choi & Chung., 2008). The sudden co-coagulation of NR without proper dispersion of clay may cause phase separation if the most potent coagulating agent is used (Jurkowska et al., 2007). However, clay and rubber may

coagulate at different times if the co-coagulation rate is slow and result in phase separation in the nanocomposite. Maintaining a balanced rate of co-coagulation is another challenge associated with the emulsion blending method. On the other hand, the low denser NR after coagulation would float on water, while high denser MMT coagulates would settle in the bottom of the mixing vessel, leading to a phase separation. The addition of filler in the latex stage is also possible in the co-coagulation method, but retaining the fillers is difficult due to excessive use of water to wash the rubber during the processing stage (Jurkowska et al., 2007).

2.4.4 In-situ polymerization

Under this method, various monomers are intercalated into interlayer-gallery space in clay and those are polymerized within gallery space using a catalyst, pre-intercalated initiators and heat radiation. The driving force of the process depends on the intercalation strength between the monomer, and the clay surface, and enthalpy evolvement during the interlayer polymerization (Theng et al., 1982). The rubber monomers are not generally available. Hence, this method is not suited for the application of rubber but is widely used in Nylon 6, epoxy, polyurethane, polystyrene, polyurethane oxide, unsaturated polyesters, and polyethylene terephthalate nanocomposites (Rezende et al., 2010).

2.4.5 In situ template synthesis

In the current method, an aqueous solution is used to dissolve primary clay building block material and polymer. Clay layers are produced in the polymer dissolved medium by its primary building block material under favorable processing conditions. Lithium fluoride, silica, and magnesium hydroxide are the major building block materials used with the polymer in a solvent. The resultant slurry or gel is refluxed at a higher temperature. Washing and drying are also necessary for the process. Polymers are then trapped into clay layers which are grown by nucleation. The advantage of this process is that modification of clay by increasing interlayer-gallery space is not required because clay layers may well disperse within polymer chains. For rubber, this method has no demand due to processing problems. It may be a reason that high temperatures applied for the synthesis of clay layers may

cause decomposition of rubber. This method is only limited to few nanocomposites prepared by hectorite clay with heat resistant polymers such as polyacrylonitrile and polyvinyl alcohol (Pinnavaia & Beall., 2001).

2.5 Properties of NR-clay nanocomposites prepared by different methods

Various rubber-clay nanocomposites have been developed in laboratory-scale by academics and researchers in the industry. However, the application of such inventions into industrial-scale production is still a challenge. None of the findings in previous studies showed that the optimum levels of properties were obtained as expected from nano behavior in the single study. Property fluctuation in nanocomposites was high in large-scale production due to the formation of combination clay structures of aggregated, intercalated, and exfoliated during processing; hence, it limits the applications of nanocomposites in the rubber industry. Most interestingly, producing the lightest weight rubber vulcanizates with remarkable mechanical properties with the use of small amounts of nanoclay loading is the main aim of the dry rubber industry.

The current knowledge and technology would be helpful to develop the co-coagulation concept while preparing NR-clay nanocomposites, which is still being developed to fulfill such objectives. The main advantage of this method is that it provides pathways to modify both clay and NR during the stage of nanocomposite preparation. Besides, the emulsion blending process with an acid-free environment opens a new path to obtain undisturbed exfoliated structures and thereby achieving superior properties. However, suitable modifications are necessary to increase the compatibility between rubber and clay under a less disturbed environment to obtain exfoliated clay structures.

Most of the properties in NR-clay nanocomposite are different, and those are impossible to compare due to different methods and techniques with various modifications. Properties of NR-clay nanocomposites varied in the highest range, the properties of clay-filled NR nanocomposite prepared from melt blending (Table 2.2), solution blending (Table 2.3), and emulsion blending (Table 2.4) can be tabulated as below.

Table 2. 2 Properties of nanocomposites prepared by melt blending

Property	Values	Reference	
		MMT	Organo MMT
Tensile strength	Less than 20 MPa	(Arroyo et al., 2003; Sharif et al., 2005; Wu et al., 2005; Tabsan et al., 2010)	(Arroyo et al., 2003; Lopez-Manchado., 2003; Sharif et al., 2005; Sukumar & Menaon., 2008; Chattopadhray et al., 2010)
	20-30 MPa	-	(The et al., 2004; Liu et al., 2006; The et al., 2006; Jacob et al., 2007; Sun et al., 2008; Avalos et al., 2008; Bhattacharya et al., 2008, Li et al., 2008; Viet et al., 2008; Hakeem et al., 2009; Qu et al., 2009; Tabsan et al., 2010; Yahaya et al., 2010; Ismail et al., 2011; Kaewkumay et al., 2012; Rooj et al., 2012; Alwis et al., 2014; Nematollahi et al., 2014; Fathurrhman et al., 2015; Ratnayaka et al., 2015; Zhang et al., 2018)
	30 – 35 MPa	-	(Madhusoodanan et al., 2006; Harahap et al., 2013; Ghari et al., 2016)
Elongation at break	Less than 500%	-	(Arroyo et al., 2003; Lopez-Manchado et al., 2004; Li et al., 2008)
	500 - 700%	(Arroyo et al., 2003; Sharif et al., 2005; Wu et al., 2005; Tabsan et al., 2010)	(Madhusoodanan et al., 2006; Sun et al., 2007; Sukumar & Menon., 2008; Hakeem et al., 2009; Tabsan et al., 2010; Chattopadhray et al., 2010; Ismail et al., 2011; Harahap et al., 2013; Nematollahi et al., 2014; Fathurrhman et al., 2014; Ratnayaka et al., 2015; Ghari et al., 2016; Zhang et al., 2018)
	Above 700%	-	(The et al., 2004;Sharif et al., 2005; Liu et al., 2006; The et al., 2006; Jacob et al., 2007; Avalos et al., 2008; Bhattacharya et al., 2008; Kaewkumay et al., 2012; Rooj et al., 2012; Alwis et al., 2014)

Modulus at 300% elongation	Less than 3 MPa	(Arroyo et al., 2003; Sharif et al., 2005; Wu et al., 2005; Tabsan et al., 2010)	(Sharif et al., 2005; The et al., 2005; The et al., 2006; Bhattacharya et al., 2008; Viet et al., 2008; Hakeem et al 2009; Kaewkumay et al., 2012; Rooj et al., 2012; Harahap et al., 2013)
	3 -5 MPa	-	(Arroyo et al., 2003;Varghese et al., 2003; Liu et al., 2006; Madhusoodanan et al., 2006; Jacob et al., 2007; Sun et al., 2007; Sukumar & Menon., 2008; Tabsan et al., 2010; Yahaya et al., 2010; Ismail et al., 2011; Alwis et al., 2014; Fathurrhman et al., 2014; Ratnayaka et al., 2015;)
	Greater than 5 MPa	-	(Li et al., 2008; Chattopadhray et al., 2010; Nematollahi et al., 2014)
Hardness	Less than 50 IRHD	(Arroyo et al., 2003; Wu et al., 2005; Tabsan et al., 201)	(Arroyo et al., 2003; Liu et al., 2006; Sun et al., 2007; Avalos et al., 2008; Viet et al., 2008; Tabsan et al., 2010; Alwis et al., 2014, Zhang et al., 2018)
	50 – 60 IRHD	-	(Lopez-Manchado et al., 2004; Madhusoodanan et al., 2006; Yahaya et al., 2010; Nematollahi et al; 2014; Fathurrhman et al., 2014; Ghari et al., 2016)
	Greater than 60 IRHD	-	(The et al., 2006; Ismail et at., 2011)
Abrasion loss	Less than 200 mm^2	-	(Madhusoodanan et al., 2006)
	Greater than 200 mm^2	-	(Arroyo et al., 2003)
Tear strength	Less than 30 N/mm	-	(Liu et al., 2006; Sun et al., 2007; Li et al., 2008)
	30-50 N/mm	-	(Madhusoodanan et al., 2006; Jacob et al., 2007; Bhattacharya et al., 2008; Yahaya et al., 2010; Alwis et al., 2014; Fathurrhman et al., 2014; Ratnayaka et al., 2015; Ismail & Veerasamy., 2011)

	Greater than 50 N/mm	(Tabsan et al., 2010)	(The et al., 2006; Tabsan et al., 2010)

Table 2. 3 Properties of nanocomposite prepared by solution blending

Property	**Values**	**Reference**	
		MMT	**Organo MMT**
Tensile strength	Less than 20 MPa	-	(Jeon et al., 2003; Vu et al., 2000)
	20-30 MPa	-	
	30 – 35 MPa	-	(Magaraphan et al., 2003)
Elongation at break	Less than 500 %	-	(Vu et al., 2000)
	500 -700 %	-	(Jeon et al., 2007),
	Above 700%	-	(Magaraphan et al., 2003)
Modulus at 300% elongation	Less than 3 MPa	-	
	3 -5 MPa	-	(Magaraphan et al., 2003; Jeon et al., 2007)
	Greater than 5 MPa	-	(Vu et al., 2000)
Hardness	Less than 50 IRHD	-	
	50 – 60 IRHD	-	
	Greater than 60 IRHD	-	(Magaraphan et al., 2003)

Table 2. 4 Properties of nanocomposite prepared by emulsion blending

Properties	**Values**	**Reference**	
		MMT	**Organo MMT**
	Less than 20 MPa	(Lee et al., 2011)	(Bhowmick et al., 2010)
	20-30 MPa	(Wu et al., 2005; Varghese et al., 2003; Abdhollahi et al., 2008;	(Alex et al., 2006)

Tensile strength		Rattanasom et al., 2009; Tan et al., 2012; Tan et al, 2016)	
	30 – 35 MPa	(Amarasiri et al., 2013)	-
Elongation at break	Less than 500 %	-	-
	500 -700 %	(Wu et al., 2005; Abdhollahi et al., 2008; Tan et al., 2012; Tan et al, 2016)	(Alex et al., 2006)
	Above 700%	(Varghese et al., 2003; Abdhollahi et al., 2008; Amarasiri et al., 2013)	(Bhowmick et al., 2010)
Modulus at 300% elongation	Less than 3 MPa	(Lee et al., 2011)	-
	3 -5 MPa	(Amarasiri et al., 2013; Tan et al, 2016)	(Alex et al., 2006; Bhowmick et al., 2010)
	Greater than 5 MPa	(Wu et al., 2005; Rattanasom et al., 2009; Tan et al., 2012)	-
Hardness	Less than 50 IRHD	(Varghese et al., 2003; Lee et al., 2011)	-
	50 – 60 IRHD/Shore A	(Wu et al., 2005; Rattanasom et al., 2009; Tan et al, 2016)	-
	Greater than 60 IRHD	(Tan et al., 2012)	-
Tear strength	30-50 N/mm	(Wu et al., 2005; Varghese et al., 2003; Tan et al., 2012)	-
	Greater than 50 N/mm	(Rattanasom et al., 2009; Amarasiri et al., 2013)	-

Most studies in the literature showed that tensile strength less than 30 MPa with 500-700% elongation at break. mod 300% and tear strength were less than 5 MPa 50 N/mm tear strength respectively and the hardness was also developed in the range of 40-50 IRHD/Shore. None of the studies do not reported the overall improvement the above mentioned properties in a single study. Many investigations described that tensile strength is improved due to the effect of better dispersion of clay with minimum aggregation. The improved elongation at break is obtained by a higher degree of exfoliation of clay with minimum nanoclay loading. Very few studies obtained the mod

300% greater than 5 MPa and a hardness greater than 55 shoreA/IRHD (Nematollahi et al., 2014)), and abrasion loss close to 200 mm^2 (Arroyo et al., 2003; Madhusoodanan et al., 2006). Those properties were improved by an increase of interaction between clay and rubber; hence, other properties like tensile strength and elongation at break were reduced. It is a challenge to increase those properties by a well-balance the degree of exfoliation, strain-induced crystallization, and rubber-clay interaction. Literature reports a few attempts made to reduce the abrasion loss using the NR-clay nanocomposite as well. Those studies were also based on the combination of clay and carbon black, and limited studies achieved an abrasion loss of less than 200 mm^2 using only clay (Madhusoodanan et al., 2006).

For unmodified MMT, the higher tensile strength, mod 300%, and elongation at break are obtained by the incorporation of MMT into latex by the emulsion blending method (Abdhollahi et al., 2008). Incorporation of MMT into dry rubber by melt blending method does not provide better mechanical properties in most studies (Arroyo et al., 2003; Sharif et al., 2005; Wu et al., 2005). This phenomenon behaves differently in organoclay with two methods, as organoclay gives better mechanical properties in melt blending (Harahap et al., 2013; Madhusoodanan et al., 2006), but the application of organoclay in emulsion blending was rare in research, maybe due to the difficulty in the preparation of organoclay suspension and its less compatibility with the aqueous medium. However, polar MMT clay is dispersed well in aqueous latex medium (Amarasiri et al., 2013). This could be the reason that many research carried out organoclay with dry rubber and MMT in latex medium.

Further, the tensile strength of NR-organoclay nanocomposite is below 20 MPa in emulsion blending but achieved 20-30 MPa in the method of melt blending. Elongation at break also shows a similar trend with tensile strength, and very few studies obtained elongation at break less than 500% due to the improvement of interaction between clay and rubber or higher aggregated behavior. The improved mod 300% and hardness, and reduced abrasion loss are obtained by the synergistic effects of combining clay with other fillers such as carbon black (Li et al., 2008; Chattopadhray et al., 2010), grafting the NR with various functional groups (Tabsan et al., 2010; Nematollahi et al., 2014), and the use of various compatibilizers to increase the interaction between clay and rubber (Tan et al., 2012). Obtaining improved mechanical properties using only

MMT or organoclay without further modification is rare in past studies. However, Madhusoodanan et al. (2006) obtained the most remarkable balance mechanical properties by only using organoclay by melt blending without any other modification (Tensile strength 32.5 MPa, modulus 300%, 4.5 MPa, elongation at break 690%, hardness 51 shore A, tear strength 40 kNm, and abrasion loss 90 mm^3).

Tasban et al. (2010) obtained the tensile strength 30.1 MPA, elongation at break 636%, mod 300%, 4.57 MPa, Tear strength 61 kN/m, and hardness 50.3 shore A using compatibilizing agent (TESPT) with 10 phr of organoclay by melt blending method. In another study, with the use of epoxidized NR and a combination of organoclay and carbon black dual filler system, Chattopadhyray (2010) obtained the higher mod 300% (6.18 MPa), elongation at break (706.5%) with reduction of the tensile strength (17.4 MPa) by melt blending method. Li et al. (2008) achieved the higher mod 300% (13.0 MPa) with moderate tensile strength (22.2 MPa) by melt blending method with the addition of 3 phr of organoclay and 47 phr of carbon black. The tear strength was also improved (46.7 N/mm), with the reduction of elongation at break (436%). Vu et al, (2000) also obtained higher mod 300% (9.82 MPa), with the reduction of tensile strength (9.89 MPa) and elongation at break (392 %) when organoclay (30 phr loading) was incorporated into epoxidized NR by melt blending. Grafted maleic anhydride into NR with organoclay by melt blending method permitted better mechanical properties with mod 300%, 5.09 MPa, tensile strength 27.9 MPa, elongation at break 593%, and hardness 52 shore A (Nematollahi et al., 2014). The other promising method in acid-free co-coagulation (AFCC method) for the preparation of NR-MMT nanocomposite was probably discussed for the first time in recent literature by Rattanasom et al., (2009) obtaining 30MPa tensile strength, 5MPa modulus at 300% elongation, 90 N/mm tear strength, and 52 shore A hardness. The AFCC method is similar to emulsion blending, but the only difference was that latex was not destabilized using the coagulation agent; hence, the oven drying method was used. However, neither of the results improved tensile strength (greater than 35 MPa) mod 300% (higher than 6 MPa) with satisfactory properties of elongation at break (not less than 600%), tear strength (greater than 40 N/mm), hardness (greater than 50 IRHD), and reduction of abrasion loss (less than 200 mm^3); hence, further investigations are necessary to obtain such properties by suitable modifications.

CHAPTER 3

MATERIALS & METHODS

3.1 Materials

The materials used in this study are mainly classified as NR, nanoclay, and chemical ingredients, and their technical details are given in the following sections.

3.1.1 Natural rubber

Two types of NRL, namely field NRL, and high ammonia preserved centrifuged NRL, were purchased from Hanwalla Rubber (Pvt) Ltd, Sri Lanka, and were used in the preparation of NR-clay nanocomposite nanocomposites by different manufacturing methods. Characteristics of the field NRL (Appendix A), centrifuged NRL (Appendix B) and pale crepe (Appendix C) were within the standard specifications. The centrifuged NRL was already preserved with zinc oxide and tetramethyl thiurium disulfide (TMTD) at 0.0125 % (w/w) loading of each. Pale crepe, a type of dry rubber supplied by Samson Compounds PLC, Sri Lanka, was used in the preparation of NR-clay nanocomposites by mechanical mixing method.

3.1.2 Nanoclay

MMT was used as a reinforcing filler (Arroyo et al., 2003) and which was supplied by Southern Clay Products, USA, under the trade name of Cloisite-116. MMT has a cation exchange capacity (CEC) of 80 meq/100 g and an interlayer distance of 1.25 nm (in non- hydrous form).

3.1.3 Chemical ingredients

Various chemicals were used in the preparation of nanocomposites in the study. The function/category and the supplier details of each ingredient are given in Table 3.1. All the ingredients were of industrial grade and were used without further purification.

Table 3. 1 Chemical ingredients

Ingredient	**Function/Category**	**Supplier**
Acetone	Solvent	Glorchem Enterprise, Sri Lanka
25 % (w/w) Ammonia	Stabilizer, Modifier	
Benzyl alcohol	Solvent	Sigma-Aldrich USA
Bis(triethoxysilylpropyl) tetrasulfide (TESPT)	Compatibilizer	Evonic catalyst (Pvt.) Ltd., India
Cetyl trimethyl ammonium bromide (CTAB)	Cataionic surfactant, Modifier	Glorchem Enterprise, Sri Lanka
Chloroform	Solvent	
Cumene Hydroperoxide	Polymer initiator	Merck, German
Diammonium hydrogen phosphate (DAHP)	Removal of excess Mg^{2+} in NRL	BDH Chemicals, UK
Diethyl ether	Solvent	Glorchem Enterprise, Sri Lanka
99.8 % (w/w) Ethanol	Solvent	Sigma-Aldrich USA
85 % (w/w) Formic acid	Coagulant	Glorchem Enterprise, Sri Lanka
Hydrochloric acid (HCl)	Reagent for titration	
Isopropanol	Solvent	Sigma-Aldrich USA
Lowinox CPL	Antioxidant	Addivant, USA
Mercaptobenzothiazole sulphanamide, MBTS	Accelerator	Merchem Ltd., India
Maleic Anhydride (MAH)	Modifier	Organic trading (Pvt.) Ltd., Sri Lanka
Methanol	Solvent	Glorchem Enterprise, Sri Lanka
Phenolphthalein	Acid base indicator	
Potassium hydroxide (KOH)	Reagent for titration	
Silver Nitrate ($AgNO_3$)	Test for Bromide ions	
Sodium dodecyl sulfate (SDS)	Anionic Surfactant, Emulsifier	
Sodium salt of condensed arylsulfonic acid (Dispersol LR)	Dispersing agent	
Sodium silicofluoride (SSF)	Gelling agent	
Stearic acid (Lubstric)	Organic Activator	Golrej industries, India
Sulphur (Rub-O-Sulf)	Vulcanizing agent	Industrial and fine chemicals, India
Tetraethylenepentamine, (TEPA)	Redox initiator	Merck, German
Toluene	Solvent	

Urea	Deproteinization agent	Glorchem Enterprise, Sri Lanka
Xylene	Solvent	
Zinc Oxide, ZnO (White seal; ACPL-P999)	Inorganic Activator	Associated Rubber Chemicals (Pvt.) Ltd, India

3.2 Methodology – preparation of nanocomposites

Series of NR-clay nanocomposites (hereafter will be referred as nanocomposite) were prepared by incorporating unmodified and modified MMT into either field NRL or centrifuged NRL, by three different processing methods, namely acid co-coagulation (ACC), acid-free co-coagulation (AFCC) and acid-free co-coagulation with gelling agents (AFCC-G1, AFCC-G2, and AFCC-G3). Three different gelling agents, SSF (G1), CTAB (G2), and CTAB, and SDS (G3) were used. Nanocomposites from the pale crepe were also prepared by the mechanical mixing method. MMT modified with CTAB hereafter will be referred as OMMT and OMMT modified by TESPT as the grafting agent hereafter will be referred as OMMT-S, respectively. NRL was modified with Succinimide (SI) called as SI grafted NRL. The methods of preparation of solutions, suspensions, preparation of latex for modification, and modification of both latex and clay are described in detail in Sections 3.2.1 to 3.2.6.

3.2.1 Preparation of suspensions, dispersions and solutions

Several suspensions, dispersions, and solutions were prepared to the required concentrations using the materials listed in Table 3.1. The concentration of the suspensions, dispersions and solutions, solutes and solvents, and the special instruments used are given in Table 3.2.

In addition, aqueous Maleamic acid (MA) was prepared using Maleic Anhydride (MAH) and ammonia. MAH was heated to its melting temperature. 25 % (w/w) ammonia and molten MAH were mixed together according to 1:1 molar ratio. Then 12.5 % (w/w) MA solution is prepared by adding distilled water.

Table 3. 2 Concentrations of the suspensions, dispersions and solutions

Ingredient	**Solvent**	**Concentration of solution/dispersion/ suspension**	**Special equipment and conditions**
85 % (w/w) formic acid	Distilled water	1 % (w/w) solution	Magnetic stirrer
DAHP	Distilled water	15 % (w/w) solution	Magnetic stirrer
ZnO	Distilled water with 1 % (w/w) dispersol LR	50 % (w/w) dispersion	48 h, in ball mill
SSF	Distilled water	20 % (w/w) dispersion	Emulsifier
CTAB	Distilled water	10 wt % dispersion	Emulsifier
SDS	Distilled water	10 wt % dispersion	Emulsifier
Cumyl Hydroperoxide	Distilled water	25 % (w/w) dispersion	Emulsifier
TEPA	Distilled water	25 % (w/w) solution	Magnetic stirrer

3.2.2 Removal of ammonia and magnesium ions from field latex

The magnesium content of field NRL was reduced from 200 to 50 ppm using DAHP solution. The required amount of DAHP in grams (W_p) was calculated according to Equation 1 (Seneviratne et al., 2003).

$$W_p = \frac{(m-50)\times W_l \times 132}{10C \times 24} \quad (1)$$

m = Magnesium content of latex in ppm

W_l = Weight of latex in kg

C = Concentration of DAHP solution as a percentage

The sludge formed as magnesium ammonium phosphate was removed. Field NRL was then de-ammoniated by continuous stirring at 50 rpm for 3 hours, while blowing air prior to use in the preparation of the product. Alkalinity was maintained less than less than 0.1 % (w/w).

3.2.3 Preparation of de-proteinized centrifuged latex

Dry rubber content (DRC) of centrifuged NRL was adjusted to 30% (w/w) with deionized water. Urea 0.1% (w/w), SDS 1% (w/w) and 0.025% (w/w) each of the solvents (acetone, ethanol and isopropanol) were mixed in centrifuged NRL. It was then centrifuged to obtain de-proteinized centrifuged NRL having a DRC of 60% (w/w) (Wongthong et al., 2013).

3.2.4 Preparation of 3 % (w/w) MMT suspension

Aqueous suspension of MMT 3% (w/w) was prepared at 40-50 $^{\circ}$C under vigorous stirring using a magnetic stirrer. Further stirring was carried out by means of an attrition mill of the model 01HD made in Union Process, USA, operated at 600 rpm for 30 minutes. It was then mixed at a frequency of 20 kHz for 15 minutes using model Qsonica ultrasonic stirrer made in the U.S.A.

3.2.5 Modification of MMT

MMT was modified by CTAB as the intercalating agent to prepare OMMT, which is further modified by TESPT as the grafting agent. The modified OMMT hereafter will be referred as OMMT-S. Both OMMT and OMMT-S were prepared in two different forms, as suspensions, and powders. The resultant products are given in Table 3.3. The methods of modifications are given in detail in Section 3.2.5.1 and Section 3.2.5.2.

Table 3. 3 Modifying agents for MMT and resultant products

Type of MMT	**Modifying Agent**	**Resultant product**
MMT	CTAB	Powder
		Suspension
OMMT	TESPT	Powder
		Suspension

3.2.5.1 Preparation of OMMT powder

MMT suspension of 3% (w/w) was prepared according to the procedure described in Section 3.2.4. Eighteen millimoles of CTAB were added into 500 ml of 3% (w/w) MMT suspension and mixed for 30 minutes in the attrition mill operated at 600 rpm at room temperature. The suspension was further sonicated at a frequency of 20 kHz for 15 minutes using the ultrasonic stirrer. The suspension was left aside overnight and the product was filtered. The de-watered suspension was washed several times with distilled water using vacuum filtration until no white precipitate was observed in the filtrate with 0.1 M $AgNO_3$. Finally, bromide free CTAB modified MMT was prepared as a de-watered suspension, which was then mixed with 500 ml of distilled water and further mixed in the attrition mill and the ultrasonic stirrer under the process conditions given in Section 3.2.4. The suspension was dried in a vacuum oven at 60 $^{\circ}$C for 2 days. The resultant OMMT crystals were then ground using a mortar and pestle into a fine powder (Singla et al., 2012).

3.2.5.2 Preparation of 3% (w/w) OMMT suspension

A paste was prepared by mixing of OMMT powder (Section 3.2.5.1) with 15% (w/w) Dispersol LR together with a small quantity of distilled water. After that 500 ml of 3% (w/w) OMMT suspension was prepared by mixing the paste with distilled water using a mechanical stirrer at a speed of 200 rpm followed by further mixing in the attrition mill and the ultrasonic stirrer under the process conditions given in Section 3.2.4.

3.2.5.3 Preparation of OMMT-S powder

The amount of TESPT required for modification of MMT was determined according to Equation 2 (Subramani et al., 2007).

$$\text{Amount of TESPT (g)} = \frac{\text{CEC} \times 1.2 \times \text{M.wt. of TESPT} \times \text{Amount of MMT}}{1000} \quad (2)$$

Molecular weight, (M.wt.) of TESPT, CEC of MMT and amount of MMT used in modification were taken as 538.95 g, 80 meq per 100 g of MMT and 20 g, respectively. 1.035 g of TESPT was dissolved in 200 ml of absolute ethanol, and then

0.1 M hydrochloric acid was added to the suspension until the pH was 4. After that, 20 g of OMMT was added into the solution and was mixed at 70 ˚C for 2 hours under reflux. Distilled water was then added to the solution to make the concentration of ethanol to 90% (w/w). Mixing was continued for 14 hours under the same conditions. The product was filtered and washed with distilled water three times at room temperature to remove the un-reacted TESPT, and then dried in an oven at 60 ˚C for 48 hours. The prepared OMMT-S crystals were ground into powder form.

3.2.5.4 Preparation of 3% (w/w) OMMT-S suspension

OMMT-S (Section 3.2.5.3) suspension was prepared using powdered OMMT-S as per the method described in Section 3.2.5.2.

3.2.6 Modification of NRL

The de-proteinized centrifuged NRL (Section 3.2.3) was stabilized by the addition of SDS dispersion, and transferred into a 500 ml reactor equipped with a reflux condenser, a mechanical stirrer, and a thermometer. Isopropanol and MA solution were then added according to the formulation given in Table 3.4.

Table 3. 4 Formulation of SI grafted NRL

Ingredient	**Loading, in dry weight, phr**
60% (w/w) de-proteinized centrifuged NRL	85 phr
12.5% (w/w) MA solution	15 phr
10% (w/w) SDS dispersion	1.3 phr
Isopropanol	7.6 pph
25% (w/w) TEPA dispersion	0.5 pph
25% (w/w) Cumene hydroperoxide	0.1 pph

pph = parts per hundred parts of the organic component, which includes both rubber content of the centrifuged latex and MA solution.

The mixture was stirred for 30 minutes under a nitrogen atmosphere to remove dissolved oxygen. Afterward the mixture was heated up to a 50 ˚C and homogenized dispersion of TEPA and Cumene hydroperoxide were added. The

mixture was then kept at the same temperature for another 2 hours to complete the grafting reaction of SI into NRL and is called SI grafted NRL. The grafting efficiency of SI grafted NRL is determined in Section 3.3.1.5.

3.2.7 Preparation of NR-clay nanocomposite

Twelve series of NR-clay nanocomposites, were prepared with MMT and modified MMT in aqueous suspensions or in powder form by three different processing methods, namely acid co-coagulation (ACC), acid-free co-coagulation (AFCC), acid-free co-coagulation supported by gelling agent (AFCC-Gx; x=1, 2,3 for three types of gelling agents) and mechanical mixing. A summary of the preparation method of each nanocomposite from different materials and processes is described in Table 3.5. These nanocomposites were prepared by varying the modified (OMMT and OMMT-S) or unmodified MMT in different loading. The processing methods are described in Section 3.2.7.1 to Section 3.2.7.7. Either field NRL or centrifuged NRL or SI grafted NRL was used as the base material in the preparation of nanocomposite. The pale crepe was used to prepare nanocomposite by mechanical mixing method. The general code system is denoted as P/QQ/RR/SS-X. P represents the processing method, in which code is given for each main method; A for ACC, B for AFCC, and C for mechanical mixing. QQ is for the type of latex or rubber, FL for field latex, CL for centrifuged latex, gL for grafted latex, and PC for pale crepe rubber. RR represents the gelling agents, G1 for SSF, G2 for CTAB, and G3 for a combination of CTAB, and SDS. RR code is not used in the coding system when the gelling agent is not used. SS is used for clay type, M for MMT, O for OMMT and OS for OMMT-S. The loading of clay in the nanocomposite is represented by x. CT is used at the beginning of the coding system with the hyphen separating from the name of the nanocomposite to represent the control. The loading of the clay is not mentioned in the coding system of control.

3.2.7.1 Preparation of A/FL/M series nanocomposites

NR-clay nanocomposite having MMT loadings of 2, 5, 8, 12, and 20 phr were prepared by incorporating 3% (w/w) aqueous suspension of MMT into de-ammoniated field NRL using ACC method. The MMT suspension was mixed with field NRL using

mechanical stirrer at a speed of 50 rpm for 3 hours until a homogeneous latex-MMT mix was obtained. The latex-MMT mix was co-coagulated with 10 ml of 1 % (w/w) formic acid for 1 kg of DRC in latex. The coagulum was washed thoroughly with water to remove acid and was then pressed firstly in a smooth roll mill and secondly in a diamond roll mill. The milled sheets were dried for 3 days at 50 $^{\circ}$C in a smoke house. This preparation method was called acid co-coagulation (ACC) method and the dried sheets are called A/FL/M series nanocomposites. The nanocomposite without MMT was taken as the CT-A/FL.

Table 3. 5 Raw materials and methods used in preparation of nanocomposites

Nanocomposite Series	**Type of NRL**	**Type of nanoclay**	**Gelling agent/s**	**Method of preparation**
A/FL/M	Field NRL	MMT	-	ACC
B/FL/M	Field NRL	MMT	-	AFCC
B/FL/G1/M	Field NRL	MMT	SSF	AFCC-G1
B/FL/G2/M	Field NRL	MMT	CTAB	AFCC-G2
B/CL/G2/M	Centrifuged NRL	MMT	CTAB	AFCC-G2
B/CL/G3/M	Centrifuged NRL	MMT	CTAB and SDS	AFCC-G3
B/CL/O	Centrifuged NRL	OMMT	-	AFCC
B/CL/G3/O	Centrifuged NRL	OMMT	CTAB and SDS	AFCC
B/CL/G3/OS	Centrifuged NRL	OMMT-S	CTAB and SDS	AFCC-G3
B/gL/G3/OS	SI grafted NRL	OMMT-S	CTAB and SDS	AFCC-G3
C/PC/O	Pale crepe	OMMT	-	Mechanical mixing
C/PC/OS	Pale crepe	OMMT OMMT-S	-	Mechanical mixing

3.2.7.2 Preparation of B/FL/M series nanocomposites

NR-clay nanocomposite having MMT loadings of 2, 5, 8, 12, and 20 phr were prepared using acid-free co-coagulation (AFCC) method using field NRL and MMT. The latex-MMT mixes were poured into aluminum pans of 2-3 mm height, and were dried in an air circulated oven for 2 days at 50 $^{\circ}$C. Dried rubber was milled to obtain sheets having even thickness and the milled sheets were dried again for another day in the oven under the same drying conditions. The dried sheets are called B/FL/M series nanocomposites. The nanocomposite without MMT was taken as the CT-B/FL.

3.2.7.3 Preparation of B/FL/G1/M series nanocomposites

NR-clay nanocomposites having MMT loadings of 2, 4, 6, and 8 phr were prepared to mix of field NRL with MMT suspension for 3 hours using a mechanical stirrer to get a homogeneous mix. 5 phr loading of 50 % (w/w) ZnO dispersion and 1.2 phr loading of 20% (w/w) SSF dispersion was added to the latex-MMT mix to destabilize the latex by gelation. The destabilized mix was then dried according to the method described in section 3.2.7.2. The preparation method is called AFCC-G1. The nanocomposite without MMT was taken as the CT-B/FL/G1 and nanocomposite with MMT is named as B/FL/G1/M.

3.2.7.4 Preparation of B/FL/G2/M series nanocomposites

In preparation of B/FL/G2/M series nanocomposites, 2 phr of MMT in the form of MMT suspension was added into field NRL and MMT suspension was mixed with field NRL using mechanical stirrer at a speed of 50 rpm for 3 hours until a homogeneous latex-MMT mix was obtained. Then 2 phr loading of CTAB suspension was added and stirred well for another 15 minutes. The destabilized mix was then dried according to the method described 3.2.7.2. The preparation method is called as AFCC-G2.

3.2.7.5 Preparation of B/CL/G2/M series nanocomposites

B/CL/G2/M series nanocomposite was prepared using the same procedure for preparing B/FL/G2/M series nanocomposite used in the preparation of B/FL/G2/M,

however, centrifuged NRL instead of field NRL was used. The destabilized mix was then dried according to the method described 3.2.7.2.

3.2.7.6 Preparation of B/CL/G3/M series nanocomposites

In preparation of B/CL/G3/M series nanocomposite, 2 phr loadings of MMT suspension was added into de-ammoniated centrifuged NRL in the presence of 1 phr loading of SDS and mixed using the mechanical stirrer at a speed of 60 rpm for 24 hours. The loading (2 phr) of CTAB was mixed with, NRL-MMT in the aluminum pan for gelling. The destabilized mix was then dried according to the method described in section 3.2.7.2.The preparation method is called AFCC-G3 method.

3.2.7.7 Preparation of B/CL/O series nanocomposites

NR-clay nanocomposites having OMMT were prepared using centrifuged NRL and OMMT suspension. The nanocomposite without OMMT was taken as CT-B/CL. The nanocomposites were prepared by the AFCC method, which was discussed under Section 3.2.7.2.

3.2.7.8 Preparation of B/CL/G3 series nanocomposites

The loading of 2 and 5 phr of OMMT and OMMT-S in the form of suspensions were added into de-ammoniated centrifuged NRL in presence of 1 phr loading of SDS in the form of dispersion and mixed using the mechanical stirrer at a speed of 60 rpm for 24 hours. 2 phr loading of CTAB was mixed with, NRL-OMMT and NRL-OMMT-S mix in the aluminum pans for gelling and nanocomposites were prepared using AFCC-G3 method. The formulation of the B/CL/G3 series nanocomposites is given in Table 3.6. The nanocomposites without either OMMT or OMMT-S is called CT-B/CL/G3.

3.2.7.9 Preparation of B/gL/G3 series nanocomposites

The loading 15 phr of OMMT-S filled NRL nanocomposite was prepared with SI grafted NRL (Section 3.2.6) and OMMT-S suspension (Section. 3.2.5.4). 500 ml of OMMT-S suspension was added to SI grafted NRL and stirred using a mechanical

stirrer at a speed of 50 rpm for 24 hours. The dry weight ratios of OMMT-S:MA was kept as 1:1.

Two nanocomposites having OMMT-S loadings of 2 and 5 phr were prepared by adding small portions of NRL OMMT-S mix into the selected quantity of de-ammoniated centrifuged NRL while stirring in the aluminum pans for gelling and nanocomposites were prepared using AFCC-G3 method. The nanocomposites prepared without OMMT-S, and 2 phr and 5 phr of OMMT-S were called CT-B/gL/G3, B/gL/G3/OS2, and B/gL/G3/OS5. The formulation of the B/gL/G3/OS series nanocomposites is given in Table 3.7.

Table 3. 6 Formulation of B/CL/G3 series nanocomposites

	CT-B/CL/G3	**B/CL/G3/O2**	**B/CL/G3/O5**	**B/CL/G3/OS2**	**B/CL/G3/OS5**
Ingredient	Loading, phr				
Centrifuged latex	100 (dry weight)				
OMMT	-	2	-	2	-
OMMT-S	-	-	5	-	5

Table 3. 7 Formulation of B/gL/G3 series nanocomposites

	Loading, phr		
Ingredient	CT-B/gL/G3	B/gL/G3/OS2	B/gL/G3/OS5
SI grafted NRL	100 (dry weight)		
OMMT-S	-	2	5

3.2.7.10 Preparation of C/PC series nanocomposites

2 and 5 phr loadings of OMMT, OMMT-S in powder form were mixed with a pale crepe in a Brabender plasticorder of model ME made in Toyo Seiki Seisaku-Sho, Japan operated at a speed of 60 rpm for 5 minutes. TESPT was used as the coupling agent. The formulation of C/PC nanocomposites series is given in Table 3.8. The nanocomposite without OMMT or OMMT-S was called as CT-C/PC.

Table 3. 8 Formulation of C/PC series nanocomposites

	Loading, phr				
Ingredient	**CT-C/PC**	**C/PC/O2**	**C/PC/O5**	**C/PC/OS2**	**C/PC/OS5**
Pale crepe	100				
OMMT	-	2	5	-	-
OMMT-S	-	-		2	5

3.2.8 Preparation of NR-clay nanocomposite compounds

Zinc oxide, stearic acid, and antioxidants were incorporated into NR-clay nanocomposites as per the formulation given in Table 3.9, using the Brabender plasticorder operated at a speed of 60 rpm for 5 minutes. Zinc oxide was not added to B/FL/G1/M Series nanocomposites and CT-B/FL/G1 at the compounding stage, since it was already added to the NR-clay mix while preparation of nanocomposites. Sulphur and MBTS were then added to the compounds using a two-roll mill for another 2 minutes.

Table 3. 9 Formulation of nanocomposite compound

Ingredient	**Loading, phr**
NR-clay nanocomposite	100
Sulphur	2
ZnO	5
Stearic acid	2
MBTS	2
Antioxidant	1

3.2.9 Preparation of NR-clay nanocomposite vulcanizates

The prepared NR-clay nanocomposite compounds were vulcanized to obtain nanocomposite vulcanizates using a hydraulic press of model Moore made in England at 140 $^{\circ}$C under 15 MPa pressure for the respective cure times, $t_{90,}$ determined from the cure curves given in chapter 4. (Refer Tables 4.1, 4.6, 4.8, 4.10 and Figures 4.35, 4.53, 4.67, 4.77).

3.3 Characterization of materials, nanocomposites and nanocomposite vulcanizates

Characterizations of NRL, CTAB, and modified and MMT were described in Section 3.3.1. The Characterizations of nanocomposites were described in Section 3.3.2. Characterizations of nanocomposite compounds and nanocomposite vulcanizates were described in Section 3.3.3 and Section 3.3.4 respectively.

3.3.1 Characterization of NRL, CTAB and modified and unmodified MMT

Methods of determination of nitrogen content of NRL (Section 3.3.1.1), FTIR spectroscopic analysis of CTAB, MMT, OMMT, and OMMT-S (Section 3.3.1.2), FTIR spectroscopic analysis of NRL and SI grafted NRL (Section 3.3.1.3) were discussed. The Spectroscopic analysis of NRL and SI grafted NRL was mentioned in Section 3.3.1.4. Grafting Efficiency of SI grafted NRL was also determined and the method was given in Section 3.3.1.5.

3.3.1.1 Determination of nitrogen content of NRL

Nitrogen content of the centrifuged NRL and the de-proteinized centrifuged NRL, CT-A/FL, and CT-B/FL were determined by the semi-micro method using Kjeldahl apparatus according to ISO 1656: 2014.

The weight of 5 g of rubber sample was placed into a digestion flask, followed by 5g of potassium sulphate and 20 ml of sulfuric acid 98% were added. The sample was suspended by gently swirling the tube. The digestion flask was heated to 350 $^{\circ}$C until white fumes can be seen. Heating was continued for about 180 minutes. The vapour of water and sulphuric acid were bubbled through a solution of sodium hydroxide to neutralize them. The sample was allowed to cool to room temperature and 100 ml of water was added. It was titrated by 0.25 moldm^{-3} NaOH.

$$\text{Nitrogen content} = \frac{[(\text{ml. acid x N of acid}) - (ml\ blank\ x\ N\ of\ base)] - (ml.standard\ base\ x\ N\ of\ base] x\ 1.4}{\text{Weight of sample in grams}} \quad (3)$$

3.3.1.2 Spectroscopic analysis of CTAB and modified and unmodified MMT

Fourier transform infrared (FTIR) spectra of CTAB, MMT, OMMT, and OMMT-S were obtained using a Bruker Alpha model FTIR spectrometer under ATR

mode. The spectra were taken using KRS-5 prism placed at an angle of incident of 45° at a resolution of 4 cm^{-1}. One hundred scans were signal averaged for each material over the spectral range of 400-4000 cm^{-1}. The area under the peak is calculated by using origin 2017 software.

3.3.1.3 X-ray diffraction analysis of modified and unmodified MMT

X-ray diffraction (XRD) technique was used to evaluate structural behavior of powder form of MMT, OMMT and OMMT-S at a wavelength of 1.54 Å of Cu Kα radiation using a model D8 advance diffractometer made in Bruker, Germany. Scanning was carried out over a Bragg angle (2θ) ranging from 3 – 10° at a rate of 0.01° of step size. Interlayer-gallery space, d, of MMT was calculated using the conventional Bragg equation, given by equation (4).

$$N\lambda = 2d \sin \theta \quad (4)$$

where, λ – Wave length of X-rays

θ- Angle between incident radiation and scattering plan

n – Order of diffraction

3.3.1.4 Spectroscopic analysis of NRL and SI grafted NRL

NRL (CT-B/CL/G3 in Section 3.2.7.8) and SI grafted NRL (CT-B/gL/G3 in Section 3.2.7.9) were prepared using combined gelling agent-G3 by AFCC-G3 method. Unreacted MA in the SI grafted NR was extracted with diethyl ether for 24 hours using a Soxhlet extraction apparatus (Saelao & Phinyocheep et al., 2005). The grafted NR after extraction was dissolved in chloroform and cast as a thin film. The spectrum of the thin film was analyzed using the FTIR spectrometer over the spectral range of 400-4000 cm^{-1} under the conditions described in Section 3.3.1.2.

3.3.1.5 Determination of grafting efficiency of SI grafted NRL

The intensity of the succinimide absorption peak area of function at 1713 cm^{-1} of SI grafted NR and peak area for the absorption of methyl group of NR at 1373 cm^{-1} were determined from the FTIR spectroscopic analysis. The grafting efficiency was calculated by equation (5).

$$\text{Grafting efficiency} = \frac{A\,1713}{A\,1373} \times 100 \quad (5)$$

where,

A 1713 - Peak area at 1713 cm^{-1} for SI in SI grafted NR

A 1373 - Peak area at 1373 cm^{-1} for methyl group in NR

3.3.1.6 Thermogravimetric Analysis

Thermogravimetric analysis (TGA) was carried out for OMMT-S clay from model SDT-Q600 made in TA instruments USA over the temperature range from room temperature to 800 ˚C at a heating rate of 20 ˚C /min for rubber vulcanizates. Nitrogen flow (80 ml min^{-1}) was utilized to remove all corrosive gases involve in the degradation and avoid thermos oxidative degradation.

3.3.2 Characterization of nanocomposites

Metal ion contents of the A/FL/M series (Section 3.2.7.1) and B/FL/M series (Section 3.2.7.2) of nanocomposites were determined using the absorption spectrometric method as described in Section 3.3.2.1. The bound rubber content of B/CL/G3 series (Sections 3.2.7.8) and B/gL/G3 series (Section 3.2.7.9) nanocomposites were determined as per the method described in Section 3.3.2.2. The viscosities of B/CL/G3 series and B/gL/G3 series nanocomposites was determined using moving a die rheometer (Section 3.3.2.3). Scanning electron microscopy (SEM) images of A/FL/M series and B/FL/M series nanocomposites were analyzed (Section 3.3.3.4). XRD technique was used to evaluate the structural behavior of A/FL/M series, B/FL/M series and, B/CL/O series nanocomposites by the method described in Section 3.3.1.3. Dynamic mechanical thermal analysis (DMTA) of B/CL/O series nanocomposites was carried out as described in Section 3.3.2.5. Ash content of A/FL/M and B/FL/M nanocomposites was determined in Section 3.3.2.6. TGA of B/gL/G3/OS5 for nanocomposites and its control prepared in the sections 3.2.7.9 and was determined in Section 3.3.1.6.

3.3.2.1 Determination of metal ion content

Content of copper (Cu), manganese (Mg), iron (Fe), and manganese (Mn) in nanocomposites were analyzed using an absorption spectrometric method. About 5 g

of nanocomposite was accurately weighed and burnt in a muffle furnace at 550 °C. The ash was digested with concentrated hydrochloric acid and was filtered before analyzing using an atomic absorption spectrophotometer of model GBC Avanta M made in the USA.

3.3.2.2 Determination of bound rubber content

Each nanocomposite, 0.2 g was cut into small pieces of approximately 1 mm^3 in size and was placed into a stainless steel cage of a known weight. The cage was then immersed in 50 ml of toluene at room temperature for 72 hours. Nanocomposite specimens were taken out and vacuum dried at 60 °C to a constant weight. Bound rubber content was measured, according to equation (6) (Lopez-manchado et al., 2004)

$$\text{Bound rubber content} = \frac{W_{fg} - W\,[\,m_f/(m_f+m_p)\,]}{W\,[m_p/(m_f+m_p)\,]}/ \times 100 \qquad (6)$$

where w_{fg} is the weight of MMT added, m_f is the weight of the filler in the nanocomposite, m_p is the weight of the polymer in the nanocomposite, and W is the weight of the specimen.

3.3.2.3 Viscosity

The viscosities of nanocomposites were determined using rubber process analyzer model RPA Flex, MDR made in TA Instruments USA operated at 100 °C for 10 minutes.

3.3.2.4 Morphology

Nanocomposites were fractured under liquid nitrogen and their SEM images were taken using a scanning electron microscope of the model Evo 18 made in Carl-Zeiss, Germany. Fracture surfaces were gold sputter coated to prevent charging under the electron beam.

3.3.2.5 Dynamic mechanical thermal analysis

Dynamic mechanical thermal analysis (DMTA) of nanocomposite was carried out using a Dynamic mechanical analyzer of model Q 800 of TA instrument, USA. The dual cantilever mode of deformation was selected. Rectangular test specimens

having dimensions of 40 mm x 12 mm x 2 mm were examined over temperature a range of -80 °C to 80 °C, at a heating rate of 2 °C/min. Liquid nitrogen was used as the cooling medium. Storage modulus, loss modulus and tan δ of each nanocomposite were recorded in temperature sweep mode at 1.0 Hz.

3.3.2.6 Ash content

The weight 6g of sample was placed into a dried pre-weighted porcelain crucible. Then the crucible was heated at 800 °C for 60 minutes. After the ash of the sample was obtained, it was left to cool down to room temperature. Crucible with ash was reweighed and the real weight of the ash was calculated. The percentage of the weight of the ash to the weight of the original sample is considered as ash content.

3.3.3 Characterization of nanocomposite compound

Cure characteristics of A/FL/M series (Section 3.2.7.1), B/FL/M series (Section 3.2.7.2), and B/CL/O series (Section 3.2.7.7) nanocomposite compounds were obtained using oscillating disc rheometer of model Rheo-line made in Prescott Instruments Ltd, UK and B/CL/G3 Series (Section 3.2.7.8), B/gL/G3 series (Section 3.2.7.9) and C/PC series (Section 3.2.7.10) nanocomposite compounds using rubber process analyzer model of RPA flex made in TA Instrument U.S.A as described in Section 3.3.3.1. The activation energy of B/CL/G3 series, B/gL/G3 series, and C/PC series nanocomposite compounds were determined using a moving die rheometer according to the method and condition described in Section 3.3.3.2. The viscosity B/CL/G3 series and B/gL/G3 series nanocomposite compounds were determined using a moving die rheometer according to the method and condition described in Section 3.3.2.3.

3.3.3.1 Cure characteristics

Cure characteristics of nanocomposite compounds were obtained from oscillating disc rheometer and rubber process analyzer operated at a temperature of 140 °C as per ASTM standard D 2048-95. Maximum torque (M_H) and minimum torque (M_L), scorch time that represents the time for a rise by two units from minimum

torque (t_{s2}) and cure time that corresponds to 90% of cure (t_{90}) were determined. The cure rate index (CRI) is expressed as Equation (7).

$$CRI = \frac{100}{t_{90} - t_{s_2}} \quad (7)$$

3.3.3.2 Determination of activation energy

The cure characteristics of nanocomposite compounds were determined using a moving die rheometer at temperatures of 140 °C, 150 °C, and 160 °C. The energy of activation of curing (E_a) was determined using the Arrhenius equation given by equations (8) and (9). (Alex et al., 2006).

$$k = A \exp(-\frac{E_a}{RT}) \quad (8)$$

$$\log k = \log A - \frac{E_a}{2.303\ RT} \quad (9)$$

Where, A is the Arrhenius constant, R is the universal gas constant, T is the absolute temperature, and k is the cure rate constant. The cure rate constant was determined from the rheograph as per equation (10).

$$\ln(M_H - M_t) = -kt + \ln(M_H - M_L) \quad (10)$$

where, M_H is the maximum rheometric torque, M_L id the minimum rheometric torque and M_t is the rheometric torque at time t.

The slope of the plot of $\ln(M_H - M_t)$ versus time t from the rheograph directly gives the cure rate constant.

3.3.4 Characterization of nanocomposite vulcanizates

B/CL/O series, B/CL/G3 series, B/GL/G3 series, and C/PC series nanocomposite vulcanizates were characterized using XRD analysis as described in Section 3.3.1.3. Morphology of tensile fracture surfaces of B/CL/O series nanocomposite vulcanizates and that of surfaces fractured under liquid nitrogen of B/CL/G3 series, B/gL/G3 series, and C/PC series nanocomposite vulcanizates were analyzed as described in Section 3.3.2.4. DMTA of B/CL/O series, B/CL/G3 series, and B/gL/G3 series nanocomposite vulcanizates were done as described in Section 3.3.2.5.

Crosslink densities of A/FL/M series, B/FL/M series, B/CL/O series, B/CL/G3 series, B/gL/G3 series, and C/PC series nanocomposite vulcanizates and respective control of vulcanizates were determined according to the method described in Section 3.3.4.1. Rubber-clay interactions of A/FL/M series and B/FL/M series nanocomposite vulcanizates, CT-A/FL, and CT-B/FL were determined as described in Section 3.3.4.2. Glass transition temperatures of nanocomposite vulcanizates of A/FL/M and B/FL/M series were determined using differential scanning calorimetry (DSC) as per the procedure described in Section 3.3.4.3.

Mechanical properties such as tensile properties, tear strength, and hardness of all nanocomposite vulcanizates and the control of vulcanizates prepared were determined. Abrasion loss was determined only for B/CL/G3 series, B/gL/G3 series, and C/PC series nanocomposite vulcanizates and their control of vulcanizates. Methods of determination of mechanical properties are described in Section 3.3.4.4. Abrasion loss of B/CL/G3, B/gL/G3, and C/PC nanocomposite vulcanizates were determined as described in Section 3.3.4.5. Ageing properties of A/FL/M series, B/FL/M series, B/CL/G3 series, B/gL/G3 series, and C/PC series nanocomposite vulcanizates and their control of vulcanizates were determined as described in Section 3.3.4.6. All tests were carried out at 28±2 $^{\circ}$C. DMTA properties of B/CL/O series, B/CL/G3 series, and B/gL/G3 series nanocomposite vulcanizates were determined as per the methods described in Section 3.3.2.5.

3.3.4.1 Determination of crosslink density

Specimens from nanocomposite vulcanizates having dimensions of 20 mm×20 mm×2 mm were immersed in toluene for 48 hours in a dark environment until absorption equilibrium and were dried in a vacuum oven at 60 $^{\circ}$C until a constant weight was achieved. Weights of a specimen before swelling, swollen gel, and after drying, were recorded and were used to determine crosslink density. Volume fraction, v, is defined as the crosslink density by mol per gram and is given by equation (11).

$$v = {}^{1}/_{2\,M_c} \tag{11}$$

where, M_c is the molar mass between the crosslink of rubber vulcanizate and it was calculated by Flory-Rehner equation (Flory & Rehner., 1943) which is given by equation (12).

$$M_c = \frac{-\rho_r \times V_s \times V_r^{1/3}}{\ln(1-V_r) + (V_r + \varkappa V_r^2)} \quad (12)$$

where, ρ_r - density of NR (0.92 gcm^{-3})

V_s - Molar volume of toluene (106.35 cm^3mol^{-1})

$\varkappa$ - Flory-Hugging polymer-solvent interaction, (0.39) for NR-toluene

V_r - volume of fraction of rubber in swollen gel

V_r was calculated using Ellis and Welding equation (Ellis & Welding., 1964) as given in Equation (13).

$$V_r = \frac{(D-FW)/\rho_r}{\frac{(D-FW)}{\rho_r} + \frac{A_o}{\rho_s}} \quad (13)$$

where, A_o - weight of absorbed solvent

ρ_s - Density of solvent (0.87)

D - De-swollen weight

F - Weight fraction of the filler

W - Initial weight of the sample

3.3.4.2 Determination of rubber-clay interaction

The rubber-clay interaction, Q_f/Q_g which is defined by Lorenz and Parks (Lorenz & Parks.,1961) and given in equation (14), was determined from the swelling parameters, which were obtained by the method described in Section 3.3.4.1.

$$Q_f/Q_g = ae^{-z} + b \quad (14)$$

where, f, g – Subscripts refer to filled and gum nanocomposite vulcanizate

z – Ratio by weight of filler to rubber in the nanocomposite vulcanizate

a and b – Constants

Q was determined by measuring the weight of toluene absorbed per gram of nanocomposite vulcanizate as per equation (15).

$$Q = \frac{W_s - FW}{D - FW} \quad (15)$$

W_s – Weight of the swollen rubber nanocomposite vulcanizate, after equilibrium attained.

The lower Qf/Qg values give a higher the extent of the interaction between the filler and the rubber matrix.

3.3.4.3 Different scanning calorimetry analysis

Glass transition temperatures of nanocomposite vulcanizates were determined using a differential scanning calorimeter (DSC) of model Q20 made in TA instruments, USA according to ISO 22768:2006. Approximately 7 mg of each nanocomposite vulcanizate was placed in a tzero pan and the test was run at a heating rate of 3 °C/min over a temperature range of -75 to -55 °C, in nitrogen environment maintained at a flow rate of 35 ml/min.

3.3.4.4 Determination of mechanical properties

Tensile properties such as tensile strength, elongation at break and modulus at 300% elongation (mod 300%), and tear strength were measured using Hounsfield H10KT tensile tester as per ISO 37:2011 and ISO 34-1:2010, respectively. Dumbbell specimens (type1) and angle specimens were punched from 2 mm thick vulcanized sheets and strained at a rate of 500 mm/min. Crosshead movement was taken as the extension.

The Hardness of nanocomposite vulcanizates was determined using a deadload hardness tester of model H14/PC made in Wallace Instruments, UK according to ISO 48:2010. Specimens having a thickness of 12.5 ± 0.5 mm and a diameter of 29.0 ± 0.5 mm were used.

3.3.4.5 Abrasion loss

Abrasion loss of nanocomposite vulcanizates was measured according to ASTM D5963-04(2015) using electromechanical abrasion tester of model Zwick 6102 made in the USA. The cylindrical shape specimens having a diameter of 16 ± 0.3 mm

and height 6 mm, were kept on a rotating sample holder and 5 N load was applied. The abrasion loss was calculated according to equation (16)

$$\Delta V = \frac{\Delta m}{\rho} \quad (16)$$

where, Δm is the mass loss of the sample during the abrasion test, ρ is the density of the specimen and ΔV is the abrasion loss in cm^3.

3.3.4.6 Determination of ageing properties

Ageing properties of nanocomposite vulcanizates were determined based on tensile strength, elongation at break, and mod 300%. The dumbbell specimens (Type1) were aged at 70 $^{\circ}$C for 120 hours an air circulating oven according to ASTM D 573-04. The aged specimens were kept for a period of 40 hours at room temperature to obtain thermal equilibrium before measuring their physical properties. The property retention values (PRV) of tensile strength, elongation at break, and mod 300% were calculated using respective properties of the un-aged specimens, and presented as a percentage in the following equation (17).

$$PRV = \frac{A}{O} \times 100 \quad (17)$$

P = percentage of property retention

O = Original value before ageing

A = value after ageing

CHAPTER 4

RESULTS AND DISCUSSION

4.1 NR-Clay nanocomposites with MMT

MMT filled NR-clay nanocomposite vulcanizates from two series of nanocomposites A/FL/M and B/FL/M were prepared by the ACC method (Section 3.2.7.1) and AFCC method (Section 3.2.7.2), respectively using field NRL. The effect of the processing method and the effect of MMT loading on properties of MMT filled NR-clay nanocomposite vulcanizates are discussed in Section 4.1.1. The gelling agents, G1 (SSF), G2 (CTAB), and G3 (a combination of CTAB and SDS) were used to reduce surface drying in nanocomposites prepared by the AFCC method in Section 4.1.2 and discusses the effect of gelling agents on properties.

4.1.1 Effect of processing method and MMT loading on properties

The two processing methods, AFCC, and ACC methods are evaluated based on the properties. The ash content (Section 4.1.1.1), XRD analysis (Section 4.1.1.2), morphology (Section 4.1.1.3), cure characteristics (Section 4.1.1.4), crosslink density (Section 4.1.1.5), mechanical properties (Section 4.1.1.6), and metal ion content and ageing properties (Section 4.1.1.7) are discussed.

4.1.1.1 Ash content

The percentage of ash content in A/FL/M8 and B/FL/M8 nanocomposites are 92% (w/w) and 81% (w/w) respectively. The lower value of A/FL/M8 nanocomposites indicates that removal of MMT with washing process is high. However, this value is significantly low in B/FL/M8 nanocomposites due to less chance of MMT loss along with water vapour.

4.1.1.2 XRD analysis

Figure 4.1 (a) shows the XRD diffractogram of B/FL/M nanocomposites at different MMT loadings, and Figure 4.1 (b) illustrates the XRD diffractogram of MMT. A peak can be seen in MMT diagram at a diffraction angle of 6°. With the

incorporation of MMT into NRL, the diffraction angle moves to the lower side, approximately 4°. Further, XRD diffractograms disclosed that the intensity of peak and the interlayer-gallery space vary with the MMT loading. The higher interlayer-gallery spaces (2.21 nm) is shown by B/FL/M8 nanocomposites among B/FL/M nanocomposites. However, B/FL/M nanocomposites with other MMT loadings show lower interlayer-gallery space compared to B/FL/M8 nanocomposite, corresponding to the existence of a large interlayer-gallery spaces. It might be due to better dispersion of the higher number of clay stack with a lower number of clay layers at 8 phr clay loading.

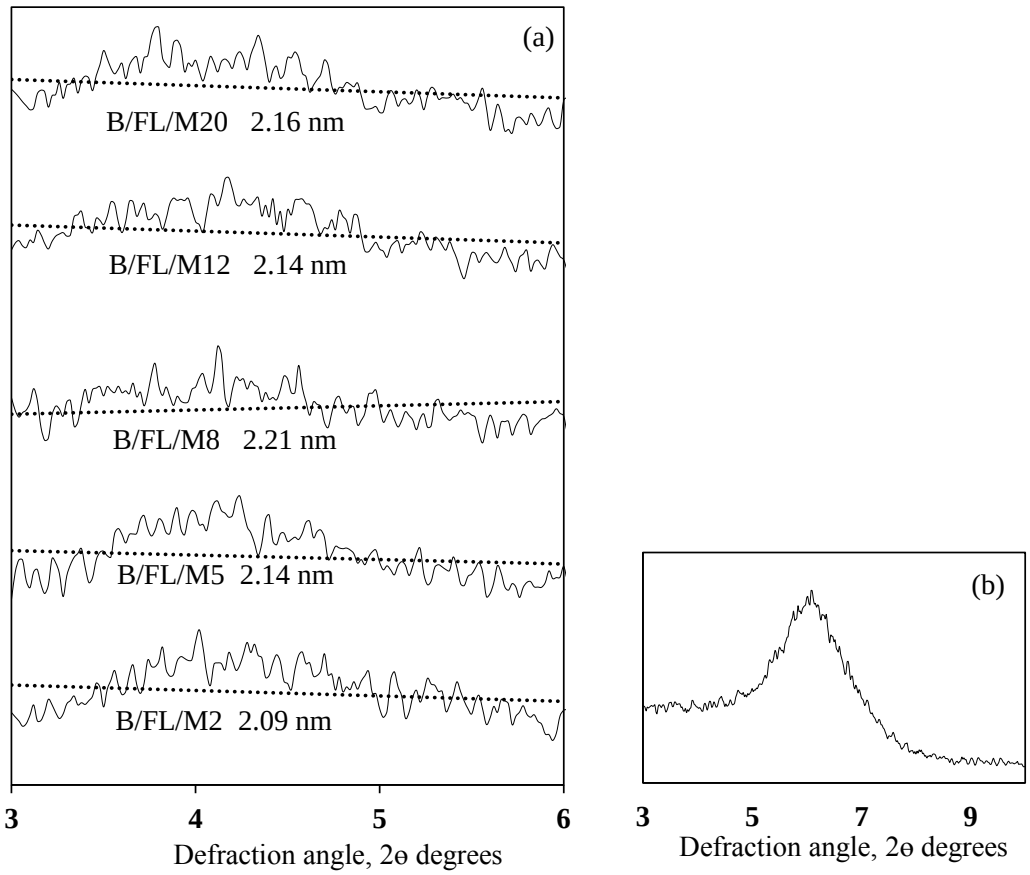

Figure 4. 1 XRD diffractogram of (a). B/FL/M nanocomposite (b). MMT

MMT was noted to prevent the coagulation of rubber particles and made them stabilized due to the formation of exfoliated and/or intercalated clay structures homogeneously dispersed in NRL. During mechanical mixing, rubber particles penetrate through clay layers to form the said structures. It was reported (Wu et al.,

1997) that 2θ was shifted to the lower side with an increase of interlayer-gallery space when partially exfoliated clay structures were formed in nanocomposites and it may be due to the function of MMT as a steric stabilizer. In the non-acidic medium MMT and clay particles are negatively charge, hence there is a repulsion between them. However, MMT is dispersed well in rubber latex because of its hydrophilic nature. Therefore clay layers are neither highly aggregated nor better dispersed. It is assumed that clay stacks with few clay layers are better dispersed. When MMT loading is increased up to 8 phr, there is a chance to increase the higher number of such clay stacks formation. This structures are believed to be in between nano and micro. This means that most of those clay stacks dispersed in the micron range due to the effect of MMT function as a steric stabilizer with the balance of total interactions and repulsions.

Figure 4.2 presents the XRD diffractogram of A/FL/M8 and B/FL/M8 nanocomposites where A/FL/M8 shows 2θ value 4.24 corresponding to interlayer-gallery space 2.08 nm while B/FL/M8 shows 2θ value 3.99 corresponding to interlayer-gallery space 2.21 nm. This implies that B/FL/M8 nanocomposite contains smaller clay stacks with a better dispersion as compared to A/FL/M8 nanocomposite. When clay layers are dispersed as smaller clay stack in NR under acid-free environment, it needs significant amount of clay loading for better distribution in the entire rubber matrix to have optimum properties due to formation of less aggregated clay structures.

It was identified during the study that the recommended acid level (Ratnayake et al., 2003a) in the RSS rubber manufacturing process was not satisfactory because the NRL was stabilized due to the addition of MMT. The stabilized NRL prevents co-coagulation unless the high quantity of acid is used. Therefore, adding more acid was necessary to co-coagulate the NRL in the preparation stage of A/FL/M nanocomposites. Highly variable interlayer-gallery spaces at different intensities were observed in A/FL/M nanocomposites at 8phr MMT loading in Figure 4.2, which may be due to the poor degree of dispersion of MMT in NR matrix associated with highly aggregated MMT stacks formed in the presence of acid.

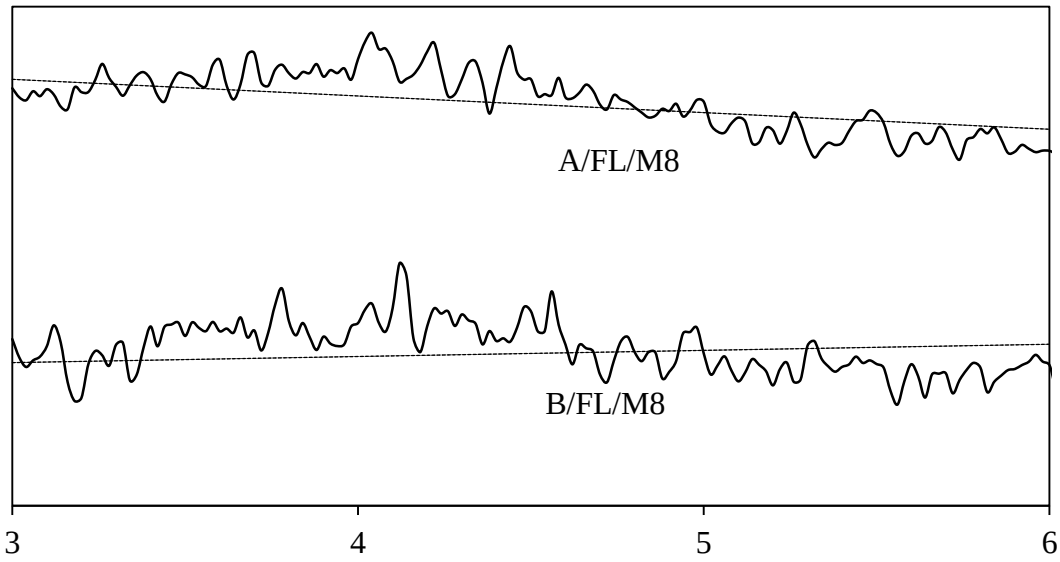

Figure 4. 2 XRD diffractogram of A/FL/M8 and B/FL/M8 nanocomposites

4.1.1.3 SEM analysis

Figure 4.3 and Figure 4.4 illustrate the SEM images of the nanocomposites prepared by the two processing methods.

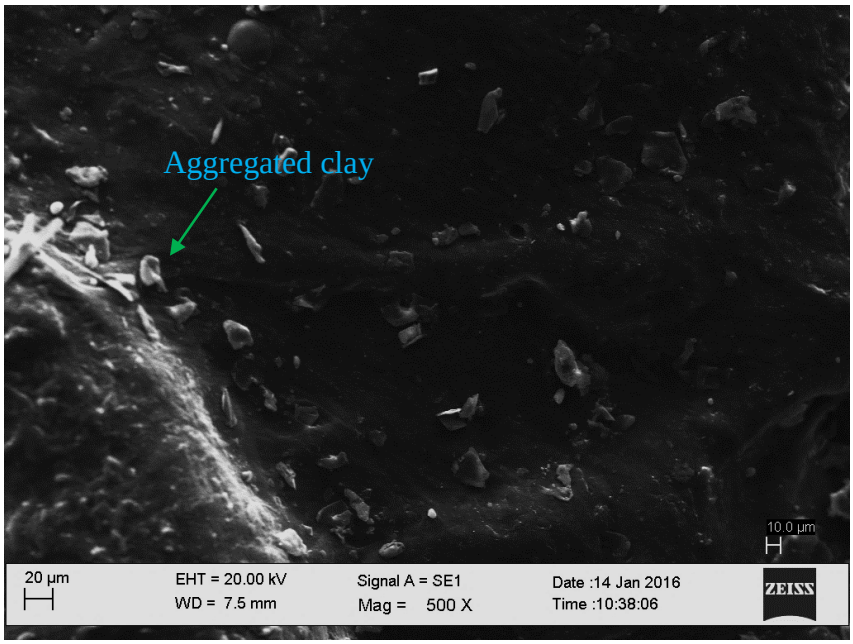

Figure 4. 3 SEM image of A/FL/M8 nanocomposite

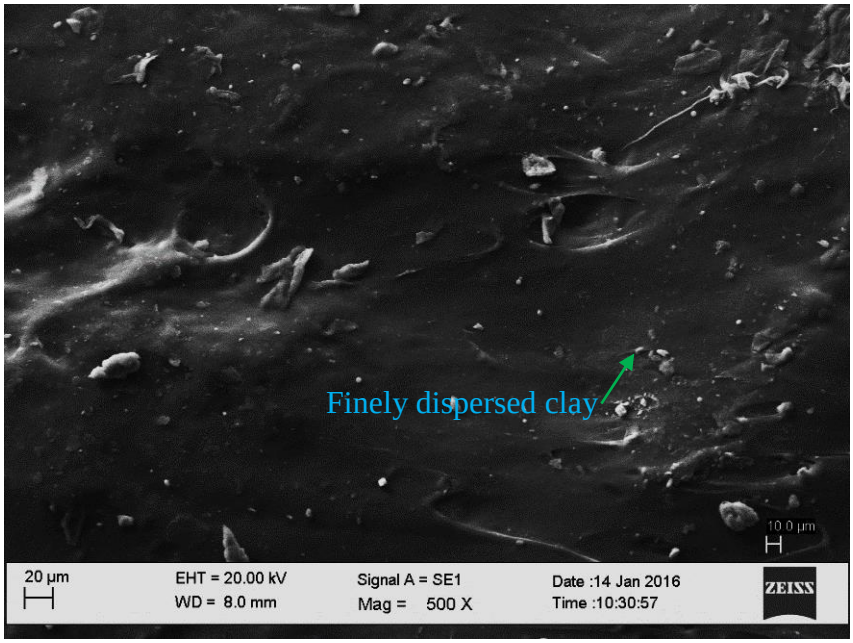

Figure 4. 4 SEM image of B/FL/M8 nanocomposite

The SEM image of A/FL/M8 nanocomposite (Figure 4.3) shows aggregated clay stacks than fine morphology, while that of B/FL/M8 nanocomposite (Figure 4.4) indicates homogeneously distributed and finely dispersed clay stacks. This is expected since clay aggregates could be formed due to the presence of acid in the ACC method.

4.1.1.4 Cure characteristics

Table 4.1 presents the cure properties of NR-clay nanocomposite compounds prepared with A/FL/M and B/FL/M nanocomposites at different MMT loadings. Table 4.1 shows that t_{90} of B/FL/M nanocomposite compounds are approximately four times lower than those of A/FL/M nanocomposite compounds at the same MMT loading. Further, cure rates of B/FL/M nanocomposite compounds are higher than those of A/FL/M nanocomposite compounds while t_{s2} of B/FL/M nanocomposite compounds are lower than those of A/FL/M nanocomposite compounds at every MMT loading. In preparation for B/FL/M nanocomposites, water is only removed by evaporation, and hence, natural substances like proteins and phospholipids remain in the nanocomposites. In preparation of A/FL/M nanocomposites, many natural substances are extracted with water at the stage of sheeting and milling. Natural substances in the rubber would act as an accelerator, and thus, reduce the cure time significantly (Zhong

et al.,2009). As a consequence, the presence of natural subtances in B/FL/M nanocomposite compounds accelerates the vulcanization process. The natural substances removed in CT-A/FL is higher those of CT-B/FL. The nitrogen content of CT-A/FL and CT-B/FL was 1.56% and 3.43% respectively. A lower level of zinc-ammine complexes produced with a lower level of nitrogen containing substances in A/FL/M series compounds delay the initiation of the vulcanization process, and thereby increase the t_{s2}. The formic acid which was used to destabilize NRL may react with basic curatives and would increase the cure time in A/FL/M nanocomposite compounds. Martin & Davey et al., (1934) also described the effect of acid on increasing the cure time by reacting with rubber curatives.The increase of t_{s2} and the decrease of cure rates for A/FL/M nanocomposite compounds lengthen the resultant t_{90} cure times compared to those of B/FL/M nanocomposite compounds.

The cure time of A/FL/M nanocomposite compounds decreases with an increase in MMT loading. Hydrogen ions in the acid can exchange with the cations in the interlayer-gallery spaces of MMT. The remaining hydrogen ions in small quantities will react with basic curatives, delaying the first step of the vulcanization process. An excess amount of acid used for co-coagulation of A/FL/M nanocomposites would replace zinc ions in the interlayer-gallery spaces of MMT. Hence, zinc ion concentration available for the curing process is high, and the cure time decreases with MMT loading in A/FL/M nanocomposite compounds. Such variation of cure time was not observed in B/FL/M nanocomposite compounds due to the acid-free environment. Some studies (Lopez-Manchado et al., 2003; Rooj et al., 2012) described that exfoliation of clay would reduce the activation energy of the curing reaction, and thereby reduce t_{90}. This phenomenon is evident frequently in nanocomposites prepared with organically modified MMT. However, the M_H-M_L value, which provides direct relationship to the crosslink density, increases with MMT loading and decreases thereafter, passing through an optimum at 8 phr. The lowes t_{s2}, the highest cure rate, and thereby the lowest t_{90} were obtained for B/FL/M nanocomposite compounds at 8 phr. This may be due to better distribution of a higher number of smaller clay stacks in B/FL/M8 nanocomposite compound. It was reported (Sun et al.,2007; Rooj et al., 2012) that various accelerators, especially the ammine group and

organo cations dispersed well in exfoliated structures, would increase the cure rate. Similarly, higher levels of natural proteins and phospholipids in B/FL/M nanocomposite compounds would disperse well in between well-distributed smaller clay stacks at MMT loading of 8 phr and increases the cure rate.

Table 4. 1 Cure characteristics of A/FL/M and B/FL/M nanocomposite compounds

	t_{s2}, min	t_{90}, min	$M_H - M_L$, dN	CRI, min^{-1}
CT-A/FL	12.7	41.6	163.6	3.5
A/FL/M2	10.3	49.7	154.5	2.5
A/FL/M5	8.8	44.8	151.3	2.8
A/FL/M8	7.8	41.2	181.8	3.0
A/FL/M12	8.0	36.1	180.5	3.6
A/FL/M20	7.6	36.3	169.4	3.5
CT-B/FL	2.0	11.2	167.5	10.0
B/FL/M2	2.9	12.5	144.9	10.4
B/FL/M5	3.2	12.3	187.5	11.0
B/FL/M8	2.2	11.0	197.7	11.4
B/FL/M12	2.5	12.1	183.1	10.4
B/FL/M20	3.2	13.8	170.6	9.4

4.1.1.5 Crosslink density

Figure 4.5 presents the crosslink densities of A/FL/M and B/FL/M nanocomposite vulcanizates at different MMT loadings. The crosslink densities of B/FL/M nanocomposite vulcanizates show higher values than those for A/FL/M nanocomposites at every MMT loading. Controls of their nanocomposites also show the same trend. In A/FL/M nanocomposite vulcanizates and its control retard the

formation of crosslinks between rubber macromolecules, and thereby exhibiting a lower crosslink density due to the presence of a minimum of natural substances. MMT aggregation in A/FL/M series prepared under acidic environment may adversely influence on the decline of the crosslink density. The long-chain natural fatty acids formed by hydrolysis of proteins in B/FL/M nanocomposite vulcanizates increase the solubility of ZnO and produce more zinc ammine complexes. The higher soluble zinc complexes combine with accelerators to form active accelerator complexes and thereby reacting with sulphur more easily. The higher accelerator sulphur ratio produces an increased number of active sulphureting agents, resulting in a higher number of short length mono and di sulphidic crosslink rather than the formation of polysulpidic crosslinks (Heideman et al., 2004). Higher the number of short-chain sulphur crosslinks has an influence on increasing the crosslink density. This is another reason for increasing the crosslink density in B/FL/M nanocomposite vulcanizates rather than A/FL/M nanocomposite vulcanizates. The improved barrier properties developed due to better dispersion of clay layers in B/FL/M also has an effect on increasing the crosslink density than A/FL/M nanocomposite vulcanizates (Amarasiri et al., 2013; Ismail & Veerasamy., 2011).

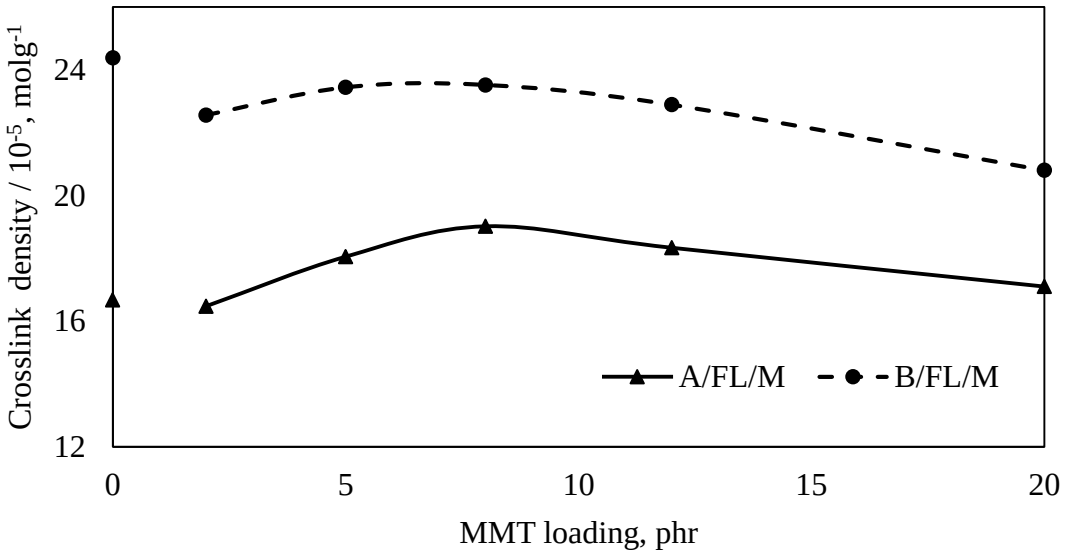

Figure 4. 5 Crosslink densities of B/FL/M and A/FL/M nanocomposite vulcanizates

The addition of MMT to nanocomposites decreases the crosslink density due to the filler effect. Further, the addition of MMT either to A/FL/M nanocomposite vulcanizates or to B/FL/M nanocomposite vulcanizates at lower loadings causes nano-dispersed reinforcement due to the high surface area of MMT, and the formation of physical crosslinks between rubber and clay. However, with the increase of MMT loading, it is well known that the aggregated clay stacks are formed, and thereby the size of the dispersed phase is increased while reducing the surface area. Both nanocomposite vulcanizates show an increase of crosslink density with MMT loading at lower loadings and a decrease at higher loadings, passing through an optimum. The crosslink density of B/FL/M nanocomposite vulcanizates shows the highest at 8 phr loading, after that it decreases with a higher amount of clay aggregation.

4.1.1.6 Mechanical properties

Figure 4.6 provides the stress-strain curves of A/FL/M and B/FL/M nanocomposite vulcanizates at selected MMT loadings. As per Figure 4.6, a more significant strain-induced crystallization was observed for B/FL/M nanocomposite vulcanizates compared to A/FL/M nanocomposite vulcanizates. This may be due to the effect of micro gel with the effect of higher non-rubber substances presence in B/FL/M. The micro gel structures are eliminated by acidic effect due to reduction of interactions between proteins (Ehabe et al., 2014), and thereby decreasing strain-induced crystallization (Manzur et al., 1997). Further, the nano-scale dispersion of MMT layers in rubber provides an efficient reinforcement without aggregation and improves stiffness due to the formation of immobilized or partially immobilized rubber (Kajima et al., 1993b). The nano-structures distribute stress evenly throughout rubber phase resulting in a minimum crack growth even at a higher elongation at break, leading to higher tensile stress before fracture (Rattanasom et al., 2009) However, the tensile properties of nanocomposite vulcanizates prepared by the co-coagulation method are better than those developed by mechanical mixing (Wu et al., 2005; Gu et al., 2009). Strain-induced crystallization is promoted by clay loading up to a certain optimum level, but more clay layers with aggregated structures result in early rupture when stress is applied.

The tensile strength of CT-B/FL is 62% greater than CT-A/FL due to improved strain-induced crystallization with the presence of higher non-rubber substances in CT-B/FL. Strain-induced crystallization was increased with the increase in MMT loading, and thereby the elongation at break decreased. This behavior is evident in the stress-strain curves of nanocomposite vulcanizates. The fracture initiation point occurred at lower elongations for higher MMT loadings due to a higher degree of clay aggregation. The lower level of aggregated clay structures dispersed properly in the rubber matrix, and the improved interactions between polar MMT and non-polar rubber in B/FL/M nanocomposite vulcanizates at MMT loading of 8 phr gives better tensile properties.

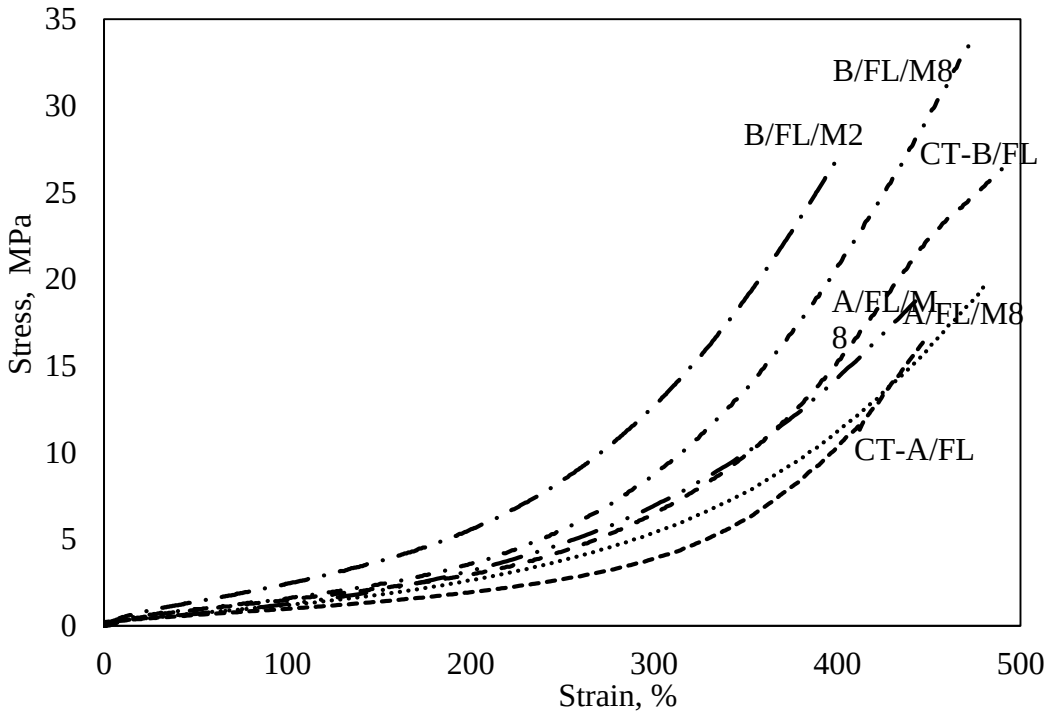

Figure 4. 6 Stress-strain curves of A/FL/M and B/FL/M nanocomposite vulcanizates

The formation of a crosslinked network in NR is reduced by aggregated polar MMT structures in the non-polar NR matrix. Hence, an incompatible particle of MMT may scavenge the rubber radicals and hinder the radical–radical interactions (Sharif et al., 2005). Further, under the effect of external load, the aggregated sites may act as fracture initiation points and fail at lower elongation (Moczo & Punanszky ., 2008),

whereas the propagation of crack is limited in nanocomposite vulcanizates under significant high stress due to the formation of a high number of exfoliated and less aggregated structures. As a result, tensile strength increases with MMT loadings and approaches 35 MPa at MMT loading of 8 phr in B/FL/M nanocomposite vulcanizate, and decreases thereafter.

A/FL/M12 nanocomposite vulcanizate with an optimum tensile strength at 12 phr loading of MMT produced a similar variation (Figure 4.7). However, the drop of tensile properties is high in A/FL/M nanocomposite vulcanizate because nanostructures are not evenly distributed in the acidic environment. On the other hand, due to the increase of the presence of aggregated clay structures in A/FL/M nanocomposite vulcanizates deteriorate tensile properties with MMT loading. Exfoliation will be difficult when clay stacks are encapsulated by rubber at a coagulated state. Accordingly, due to the poor distribution of stresses under highly aggregated MMT structures in an acid environment, the A/FL/M nanocomposite vulcanizates fail at the low stresses, resulting in relatively low tensile properties.

The maximum tensile strength of B/FL/M nanocomposite vulcanizates was observed at MMT loading of 8 phr, while that of A/FL/M nanocomposite vulcanizates was at MMT loading of 12 phr. Mechanical properties were improved promoting the strain-induced crystallization by natural proteins and phospholipids in natural rubber which form natural network structure (Amnuaypornsri et al., 2008).

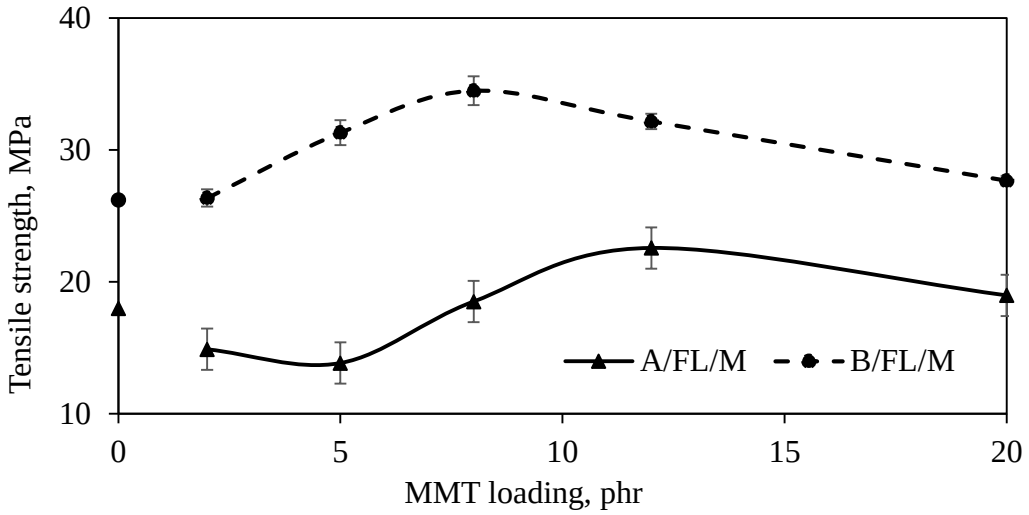

Figure 4. 7 Tensile strength of A/FL/M and B/FL/M nanocomposite vulcanizates

The elongation at break of both nanocomposite vulcanizates decreases after MMT loading of 8 phr, however, those values show a significant reduction (Figure 4.8) compared to that of gum rubber vulcanizates in common literature (greater than 600%) (Verghese et al., 2003a; Abdollahi et al., 2008). Some researchers revealed (Wang et al., 2005; Wu et al., 2005) that the addition of MMT would add stiffness to NR, thus, resulting in the reduction of elongation at break after a particular loading of MMT.

mod 300% increases with the increase of MMT loading (Figure 4.9) since the aggregated MMT particles behave like a conventional filler and cause an early rupture with lower tensile strength and elongation at breaks. However, if the clay layers are dispersed at nano-scale with a higher degree of exfoliation, the increase of mod 300% is limited by lowering the stress as associated with its remarkable structures. mod 300% reduction at a lower value is a significant advantage to the latex industry, but in the dry rubber industry, it is aimed to increase both mod 300% and tensile strength with a minimum change of elongation at break using minimum clay loading.

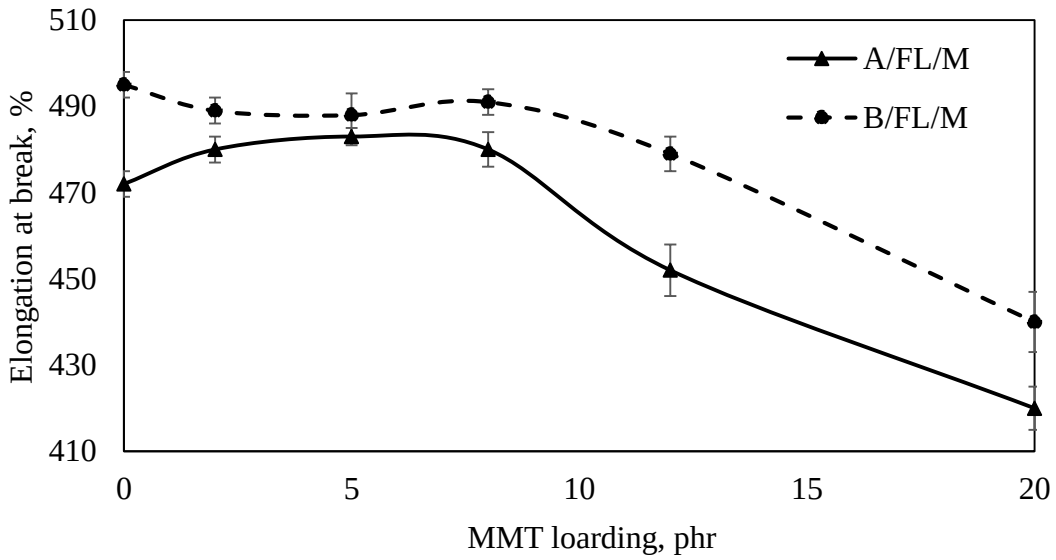

Figure 4. 8 Elongation at break of A/FL/M and B/FL/M nanocomposite vulcanizates

Figure 4.10 illustrates the tear strengths of A/FL/M and B/FL/M nanocomposite vulcanizates at different MMT loadings. The tear strength of MMT-filled rubber nanocomposite vulcanizates was not highly improved because

applied stresses might be concentrated at the sharp edges of layers and promote early breakdown compared to spherical fillers (Rattanasom et al., 2015). However, the lack of higher exfoliated clay structures in both nanocomposite vulcanizates imparts significantly lower tear strength. Strain-induced crystallization has no great effect on improving the tear strength. However, tear strength of A/FL/M and B/FL/M nanocomposite vulcanizates are not developed as expected and are not greater than 25 N/mm.

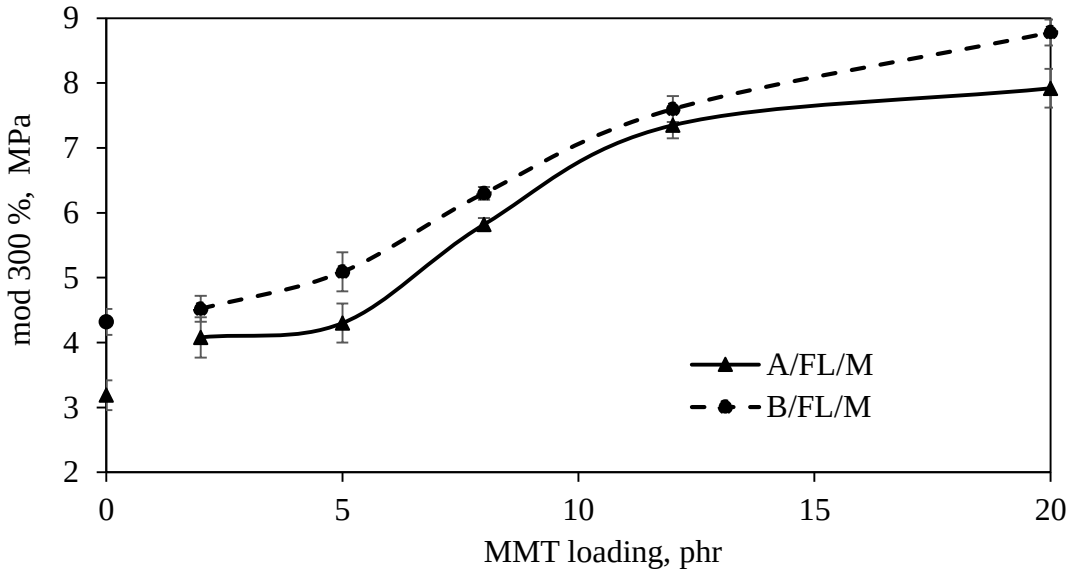

Figure 4. 9 mod 300% of A/FL/M and B/FL/M nanocomposite vulcanizates

The hardness of B/FL/M nanocomposite vulcanizates shows increasing trend with the maximum value given at 8 phr MMT loading (Figure 4.11), even though mod 300% exhibits a gradual increase with MMT loadings. Conventional fillers, in general, provide an increase in hardness and mod 300% together with the increase in filler loading (Blackley, 1997(a)). Such improvement of hardness at MMT loading of 8 phr is due to fine dispersion of clay stacks in rubber matrix. The hardness of nanocomposite vulcanizates may vary with crosslink density and morphology. The hardness of B/FL/M series nanocomposite vulcanizates shows higher than A/FL/M nanocomposite vulcanizates at higher MMT loading due to the better dispersion of less aggregated clay structures and improved crosslink density in A/FL/M nanocomposite vulcanizates. It is interesting to note that A/FL/M nanocomposite vulcanizates show greater hardness than B/FL/M nanocomposite vulcanizates at lower MMT loadings

since acid coagulation causes rigid coagulum in A/FL/M nanocomposite vulcanizates with the effect of rubber particles held together closely by acid coagulation.

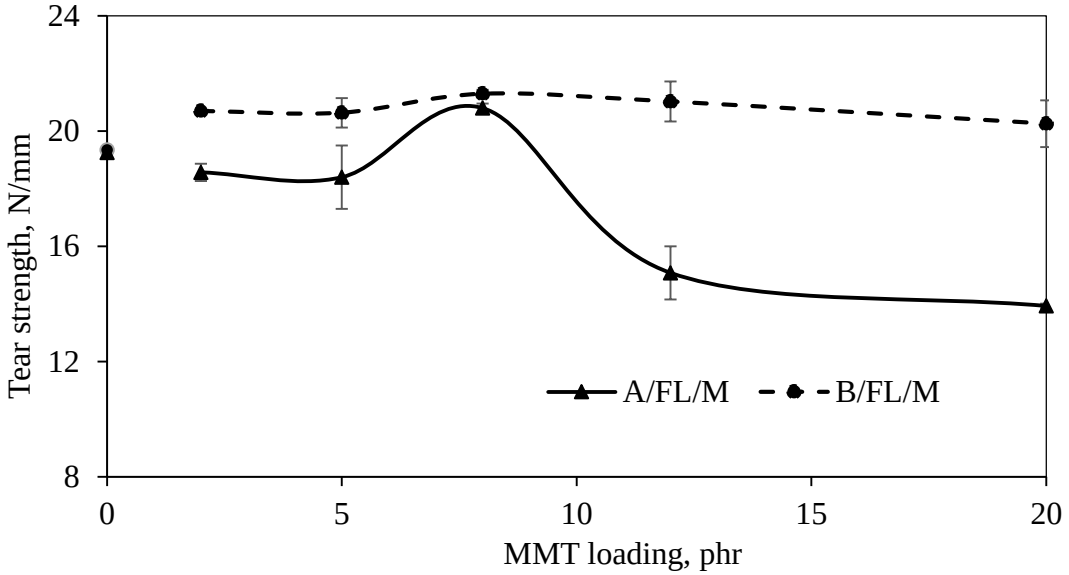

Figure 4. 10 Tear strength of A/FL/M and B/FL/M nanocomposite vulcanizates

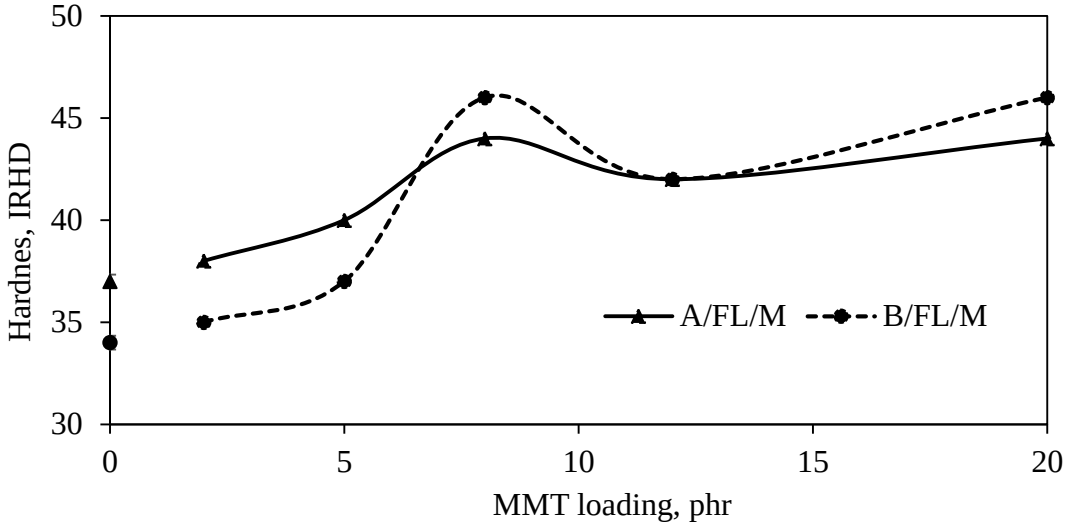

Figure 4. 11 Hardness of A/FL/M and B/FL/M nanocomposite vulcanizates

4.1.1.7 Metal ion content and ageing properties

Na, K, Mg, Ca, Rb Al, Si, Fe, Mn, and Cu are the main metallic ions found in lutoid phase in the field NRL (Rippel et al., 2002). Na, K, and Ca are the major metallic ions in the serum (Rippel, et al., 2003). Transition metallic ions especially Fe, Mn, and Cu may cause thermal ageing on the degradation of solid rubber by induced fragmentation of polyisoprene chain (Rippel, et al.,2002). When nanocomposites were

prepared by the AFCC method (B/FL/M), metal ions and other non-rubber substances were remained with rubber because only water was removed by evaporation. The metal ion content of CT-A/FL, CT-B/FL, and B/FL/M12 is described in Table 4.2.

Table 4. 2 Content of metal ion

	CT-A/FL	CT-B/FL	B/FL/M12
Mn, ppm	1	1	2.7
Fe, ppm	1320	20	960
Mg, ppm	240	480	4260
Cu, ppm	8	3	4

However, the nanocomposites prepared by the ACC method (A/FL/M) consist of a lower amount of metal ions, as part of them were removed with washed water used for the removal of acids.

Mg ion content in CT-A/FL and CT-B/FL is in the range similar to the Mg ion content in centrifuged NRL (Santipanuscopon & Riyajan, 2009) and for of B/FL/M, the value is quite high due to the remaining of all cations in field latex without removing. The effect of Mg ions on the ageing of rubber is less significant than the effect of Cu, Mn, and Fe ions, which can decrease the activation energy of thermal oxidation of NR, and thereby accelerate the thermo-oxidative degradation (Goh & Phang., 1978). Concentrations of Cu and Mn ions below 8 ppm are not significant for thermal ageing as per ISO 6101-3:2014 and ISO 6101-4:2014 (2014a; b). High Fe ion content in CT-A/FL may result due to the contamination during manufacturing especially from processing water (Ratnayaka et al., 2011) or an increase of free Fe with the effect of acid which would affect the ageing properties of NR.

It was reported (Uddin, 2008) that MMT contains substantial amounts of Mg and Fe ions, and those ions may also be responsible for increasing the ion content in the nanocomposites. However, the remarkable ageing resistance of MMT may reduce such adverse effects (Park et al., 2012; Jurkowska, 2007). It is found that property retention value (PRV) of tensile strength, elongation at break, and mod 300% in CT-A/FL vulcanizate is lower than that of CT-B/FL vulcanizate after ageing corresponding to ageing properties in Table 4.3. The higher percentage of property

reduction occurred in CT-A/FL vulcanizate produced by the ACC method than in CT-B/FL vulcanizate produced by the AFCC method. The higher content of Fe ions in CT-A/FL vulcanizate would cause thermal ageing with the oxidation of poly isoprene chain.

Table 4. 3 Ageing properties of CT-A/FL and CT-B/FL nanocomposite vulcanizates

Mechanical properties	**CT-A/FL**			**CT-B/FL**		
	Before ageing	**After ageing**	**PRV, %**	**Before ageing**	**After ageing**	**PRV, %**
Tensile strength, MPa	18.0	11.7	65	26.2	19.9	76
Elongation at break, %	486	394	81	495	416	84
Mod 300%, MPa	3.2	3.0	94	4.3	4.0	93

Degradation of a large number of proteins and phospholipids remained in CT-B/FL vulcanizate may cause a reduction of mechanical properties (Tuampoemsab & Skadapipanich., 2007) which is not the effect of oxidative thermal ageing. However both effects reduce the mechanical properties, therefore, it is difficult to analyze which effect is highly contributing to the reduction of mechanical properties. The results of both control samples show that the effect of metal ion on thermal ageing is greater than the effect of degradation of protein and phospholipids when MMT is not used as a filler. The prominent natural antioxidant tocotrienols together with other antioxidants protein and amino acid are believed to be lower in CT-A/FL vulcanizate due to removable with water and effect of the acid (Hasma & Othman, 1990) but in CT-B/FL vulcanizate, natural oxidant substances are high and may reduce the thermal ageing.
Ageing properties of A/FL/M8 and B/FL/M8 nanocomposite vulcanizates are given in Table 4.4. In A/FL/M8 nanocomposite vulcanizate, the PRV of tensile strength, elongation at break, and mod 300% are higher than that of B/FL/M8 nanocomposite vulcanizate. With the addition of MMT, the ageing resistance was improved compared to control, but, B/FL/M nanocomposite vulcanizates show the highest reduction of properties than A/FL/M nanocomposite vulcanizates. This shows that degradation of non-rubber content is a bigger contributor to the reduction of mechanical properties

rather than thermal ageing rendered by metallic ions found in the study. It is also interesting to note that ageing of A/FL/M nanocomposite vulcanizates is reduced significantly with the addition of MMT. It indicates that thermal ageing corresponding to oxidation of isoprene chain due to metallic ions could be prevented by the effect of MMT but the degradation of protein and phospholipid could not be prevented by a similar way. It is believed that ageing resistance of MMT is more prominent than the effect of natural antioxidant effect in nanocomposite vulcanizates. Ageing results propose the necessity to have a proper investigation of this behavior in another study and it is necessary to introduce a method to prevent the reduction of mechanical properties by the degradation of proteins at elevated temperature.

Table 4. 4 Ageing properties of A/FL/M8 and B/FL/M8 nanocomposite vulcanizates

Mechanical properties	**A/FL/M8 nanocomposite**			**B/FL/M8 nanocomposite**		
	Before ageing	**After ageing**	**PRV, %**	**Before ageing**	**After ageing**	**PRV, %**
Tensile strength, MPa	18.5	16.8	91	34.5	27.2	79
Elongation at break, %	481	452	94	488	424	87
Mod 300%, MPa	5.8	5.6	97	6.3	5.7	90

4.1.1.8 DSC analysis

Figure 4.12 illustrates the DSC thermograms of CT-A/FL, CT-B/FL, A/FL/M nanocomposite vulcanizates and B/FL/M nanocomposite vulcanizates at two different MMT loadings. T_g of the controls and the nanocomposite vulcanizates exhibited the same value and is approximately -63°C. This implies that strong rubber-clay interactions are not developed in the nanocomposite vulcanizates for the enhancement of mechanical properties. Hence, the greater property enhancement in B/FL/M nanocomposite vulcanizates at MMT loading of 8 phr might be mainly due to the effective dispersion of small clay stacks and the increased crosslink density. It can be argued that T_g of both nanocomposite vulcanizates should be different due to change

of crosslink density but an increase of crosslink density in B/FL/M nanocomposite vulcanizates is not strong enough to change T_g. It shows that mechanical properties of B/FL/M is greatly influenced by strain induced crystallization rather than effect from crosslink density.

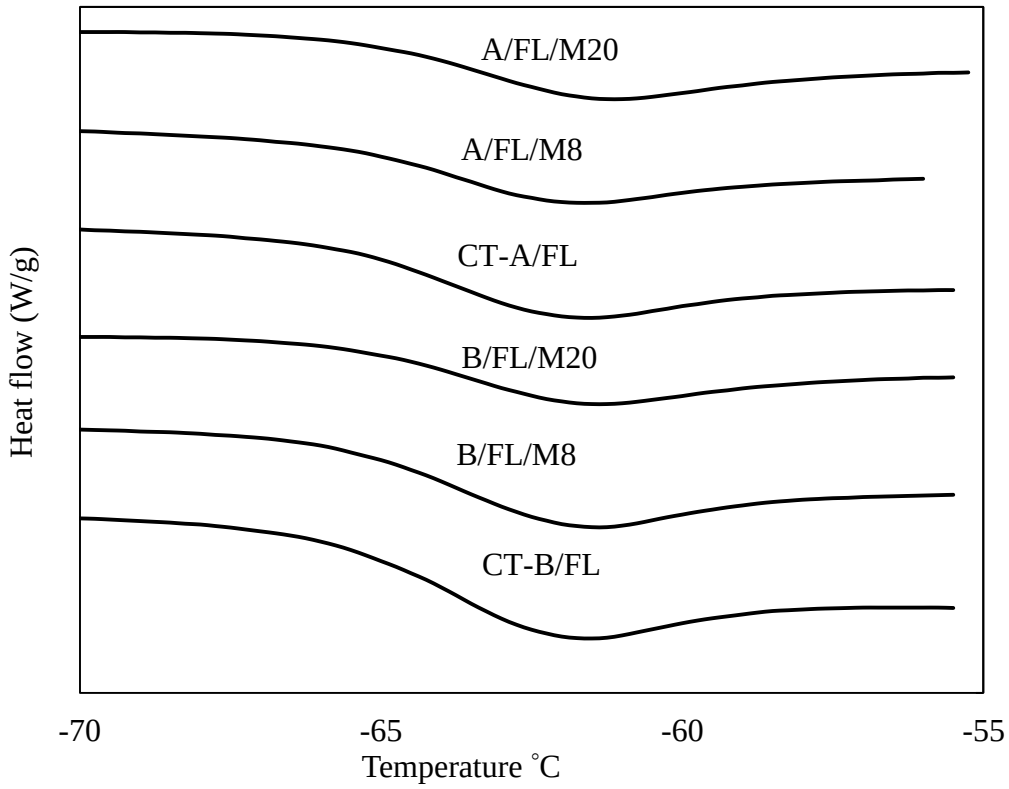

Figure 4. 12 DSC thermograms of A/FL/M and B/FL/M nanocomposite vulcanizates

Low tear strength (less than 25 N/mm)(Figure 4.10 in Section 4.1.1.7) and poor thermal ageing (Table 4.2 and Table 4.3 in Section 4.1.1.8) are the major drawbacks of B/FL/M nanocomposite vulcanizates, even though it shows better tensile strength and mod 300% in un-aged conditions. Besides, large-scale production of B/FL/M nanocomposites could not be implemented due to slow drying. Hence, surface layers of the NRL-MMT mix are only dried as a thin layer and prevent destabilization of the bottom layers in the mix due to the hindrance of water evaporation. This phenomenon is named as surface drying. The addition of an effective gelling agent to prevent surface

drying is an essential requirement of the study; otherwise, the separation of MMT from NRL is high and would cause a higher fluctuation of properties.

4.1.2 Effect of gelling agent

The large-scale production of B/FL/M nanocomposites is limited due to the thin layer surface drying of nanocomposites even though the AFCC method gives better properties. Use of a gelling agent such as SSF to speed-up the coagulation and increase the mass production of coagulum with the aid of oven-drying was successful. SSF is normally used in the latex foam rubber industry as a gelling agent (Blacklley, 1997b). Two types of nanocomposites, B/FL/G1/M nanocomposites at MMT loadings from 2 to 8 phr (Section 3.2.7.3), and B/FL/G2/M nanocomposite at MMT loadings from 2 phr (Section 3.2.7.4) prepared using SSF (G1), and CTAB (G2) respectively were considered for the study. Properties of B/FL/G1/M and B/FL/G2/M nanocomposite vulcanizates are compared with those of B/FL/M nanocomposite vulcanizates, as discussed in Section 4.1.2.1 and Section 4.1.2.2 respectively. Section 4.1.2.3 presents the effect of type of latex, field NRL and centrifuged NRL, on the properties of the nanocomposite vulcanizates prepared with G2. The properties of the nanocomposite vulcanizates prepared with G3 using centrifuged NRL is discussed in Section 4.1.2.4.

4.1.2.1 SSF gelling agent

The pH of the NR-MMT mix was reduced to a range of 8.0 to 8.5 when G1 is added to obtain the gelling effect. The reduction of pH is mainly due to the formation of hydrofluoric acid after SSF hydrolysis. The acidic effect of silicic acid produced by hydrolysis of SSF as in below reaction plays a vital role in the gelation and destabilization of the latex (Blacklley, 1997c).

$$Na_2SiF_6 \longrightarrow 2\,Na^+ + SiF_6^{2-}$$

$$SiF_6^{2-} + H_2O \longrightarrow Si(OH)_4 + 4\,H^+ + 6\,F^-$$

Besides, the produced ammine complexes with the reaction from zinc oxide and added soaps induce further destabilization of NRL by forming insoluble zinc soaps.

The Siloxane network is created by a polymerization reaction of silicic acid given by hydrolysis of SSF. Figure 4.13 shows the suggested structure of the siloxane

network around MMT layers. Similar phenomenon of formation of siloxane network from silicic acid is discussed in another study in the literature (Belton et al., 2012). It is the network consisted of Si-O-Si bonds which further reacts with silanol bonds (Si-O-H) in MMT and expands its structure. Those areas are considered as most polar sites in the NR matrix and compatibility with NR is significantly reduced due to different solubility parameters between NR and siloxane network.

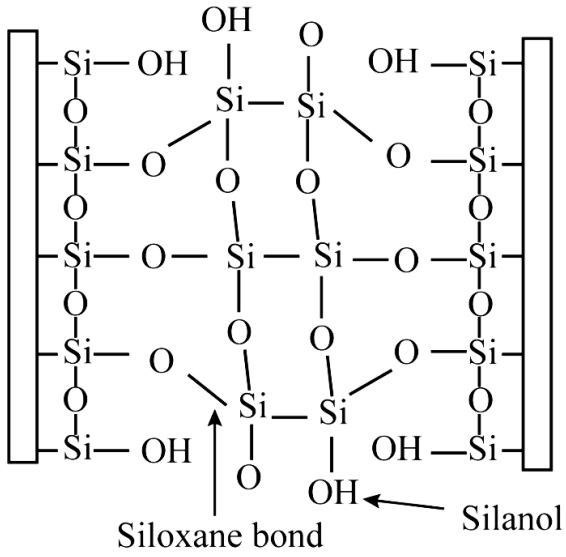

Figure 4. 13 Structure of the siloxane network between MMT layers

The crosslink density of B/FL/M nanocomposite vulcanizates is higher than that of B/FL/G1/M nanocomposite vulcanizates at all MMT loadings (Figure 4.14). The crosslink density of B/FL/G1/M nanocomposite vulcanizate is reduced by poor distribution of polar curatives in the rubber phase, and interact with the siloxane network. This is happened due to the difference of solubility parameter between NR and siloxane network around clay layers. This effect is more pronounced with an increase of MMT loading. A similar effect was reported in the NR-EPDM blend in another study due to the migration of curatives from the EPDM phase to NR phase (Brown & Tinker., 1990).

Figure 4.15 shows the variation of tensile strength and elongation at break against MMT loadings of B/FL/G1/M nanocomposite vulcanizates. The tensile strength of B/FL/G1/M nanocomposite vulcanizates shows a gradual decrease with an increase of MMT loading up to 8 phr, while B/FL/M nanocomposite vulcanizates show

a gradual increase up to 8 phr. The reduction of the tensile strength of B/FL/G1/M8 nanocomposite vulcanizate is 57% compared to B/FL/M8 nanocomposite vulcanizate due to the reduction of crosslink density. The siloxane network around MMT is increased with the effect of gelling agent, however, that polar network is less compatible with non-polar NR, and may be due to lack of strong interaction between NR and siloxane network at higher MMT loading, is another reason for reduction of tensile strength. Each sample used the same quantity of SSF; however, the tensile strengths of CT-B/FL/G1 and B/FL/G1/M2 nanocomposite vulcanizates show significant improvements than that of CT-B/FL and B/FL/M2 nanocomposite vulcanizates. This may be due to the interaction of the siloxane network and polar non-rubber substances in rubber particles. Such interactions are weakened by an increase in MMT loading due to a lack of compatibility.

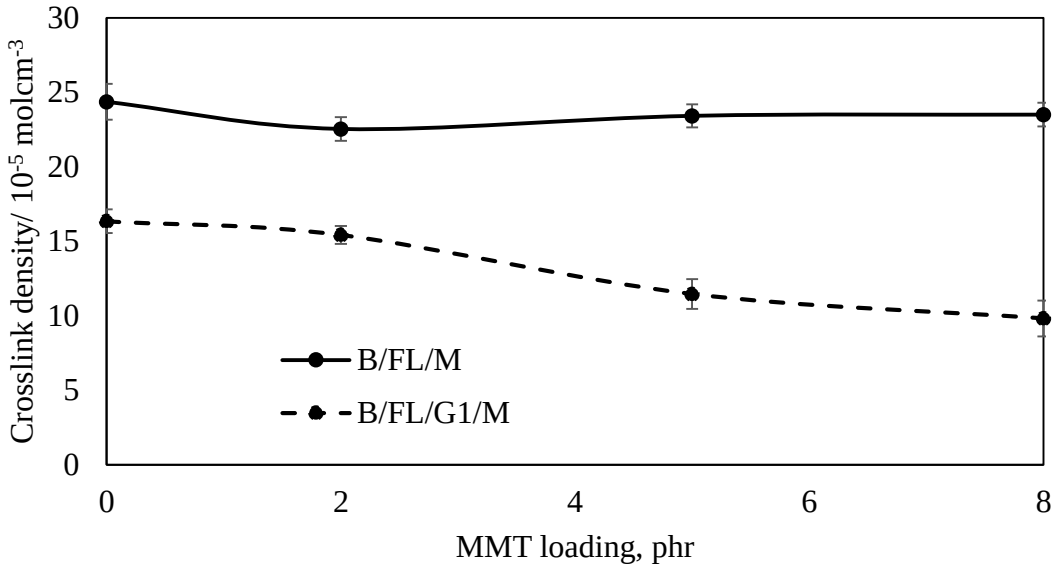

Figure 4. 14 Crosslink density of B/FL/M and B/FL/G1/M nanocomposite vulcanizates

The elongation at the break of B/FL/G1/M nanocomposite vulcanizates at every MMT loadings is higher than those of B/FL/M nanocomposite vulcanizates (Figure 4.16). This may be due to lower crosslink densities in B/FL/G1/M nanocomposite vulcanizates than those of B/FL/M nanocomposite vulcanizates. The increased polar content of the siloxane network in B/FL/G1/M nanocomposite vulcanizates may cause a plasticizing effect and thereby reduce the crosslink density.

The plasticizing effect would increase the elongation at break in B/FL/G1/M nanocomposite vulcanizates compared to that of B/FL/M nanocomposite vulcanizates.

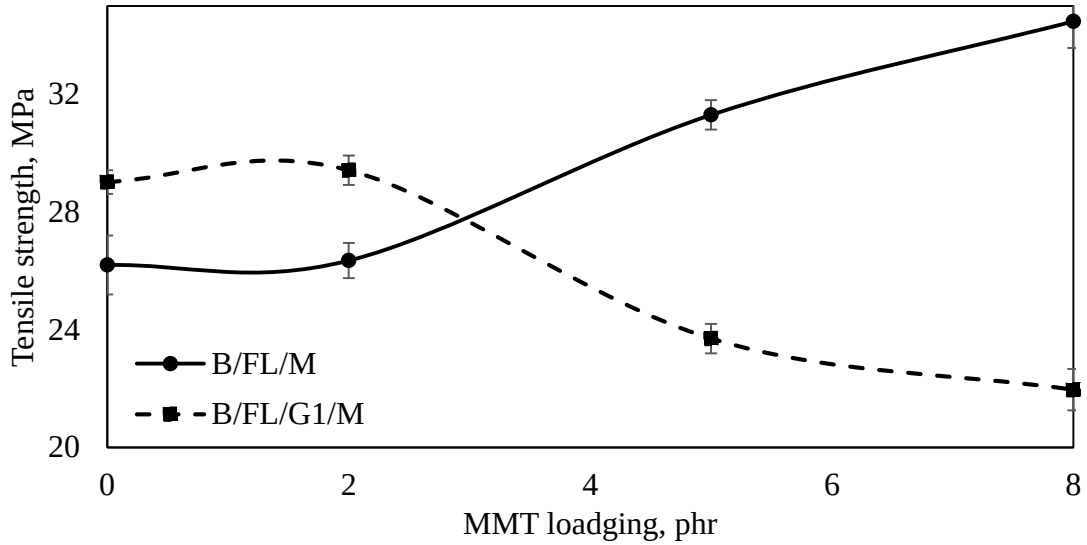

Figure 4. 15 Tensile Strength of B/FL/M and B/FL/G1/M nanocomposite vulcanizates

mod 300% at all loadings of B/FL/G1/M nanocomposite vulcanizates are lower than that of B/FL/M nanocomposite vulcanizates (Figure 4.17) due to lower crosslink density of B/FL/G1/M nanocomposite vulcanizates. mod 300% of B/FL/M nanocomposite vulcanizates show a gradual increase with an increase in MMT loading, but it decreases through the maximum for B/FL/G1/M nanocomposite vulcanizates. An increase of density of siloxane network would improve the mod 300% at lower MMT loadings due to interaction between siloxane network and polar non-rubber substances of rubber particle, but it decreases at higher MMT loadings with lack of rubber clay interactions improved with MMT loading. It shows that rubber clay compatibility was reduced with the higher MMT loadings. Bond strength of siloxane is considerably low and more flexible than sulphur crosslinks, hence the increased density of siloxane network found between MMT layers at higher MMT loadings suppresses the rise of stress or acts as a point vulnerable to rupture.

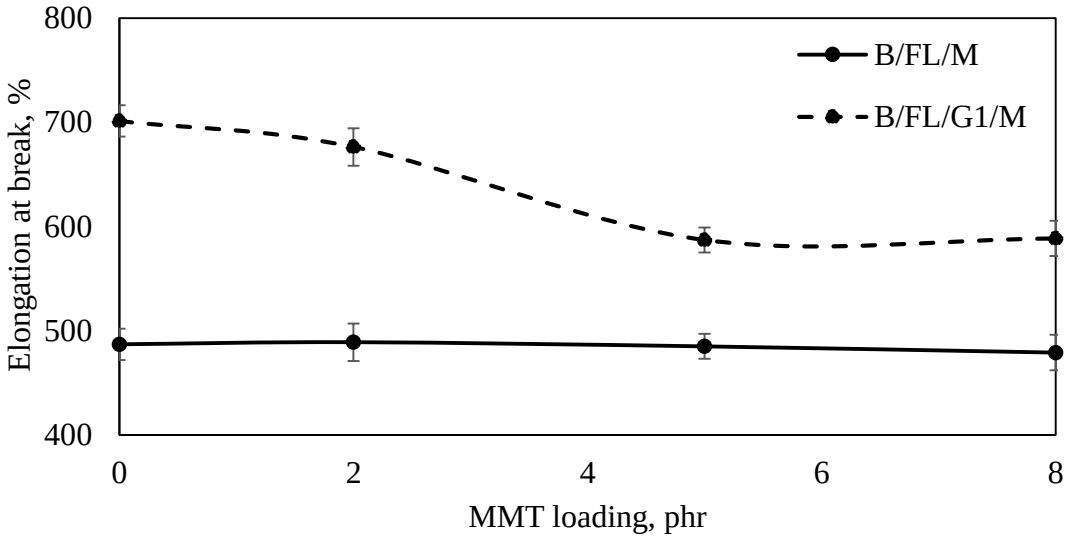

Figure 4. 16 Elongation at break of B/FL/M and B/FL/G1/M nanocomposite vulcanizates

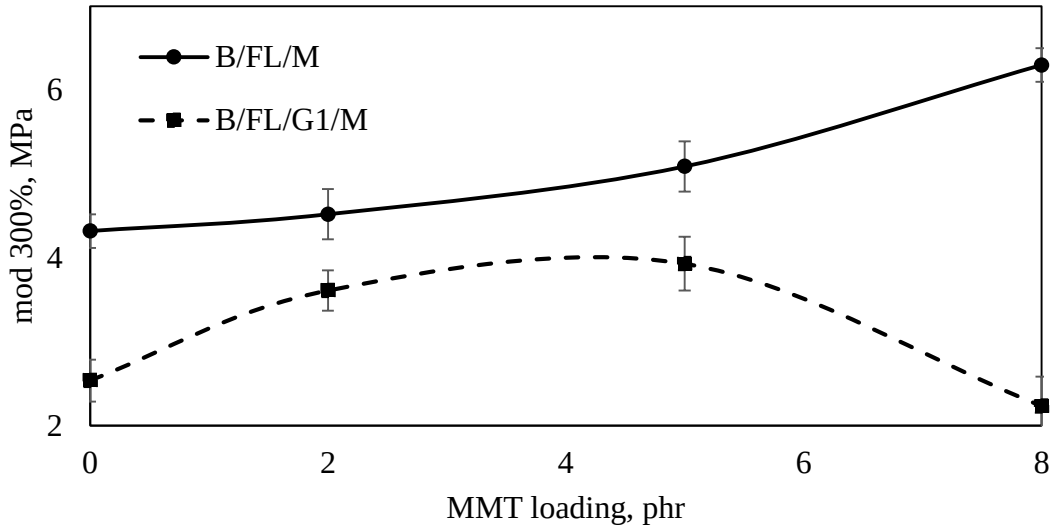

Figure 4. 17 mod 300% of B/FL/M and B/FL/G1/M nanocomposite vulcanizates

Interestingly, the tear strengths of B/FL/G1/M nanocomposite vulcanizates show higher values than those of B/FL/M nanocomposite vulcanizates at every MMT loading, even though the tensile strengths of B/FL/G1/M nanocomposite vulcanizates were inferior to those of B/FL/M nanocomposite vulcanizates (Figure 4.18).

The smaller size of clay aggregates dispersed in medium with a plasticizing agent would increase the tear strength. However, aggregated clay structures act as a point of crack initiation and rupture easily when tensile stress is applied. The initiation and propagation of cracks are different during tearing compared to tensioning. The initiation point of the crack in tear specimens occurs at an angular point and propagates through the weakest interphase between rubber and filler. An increase of flexibility bonds in siloxane network and propagation of strain in longer tear path in zigzag direction by the effect of MMT would improve the tear strength, especially at lower loadings of B/FL/G1/M nanocomposite vulcanizates. However, the tear strength decreases at higher MMT loadings due to the formation of larger aggregated clay structures and the effect of lower crosslink density.

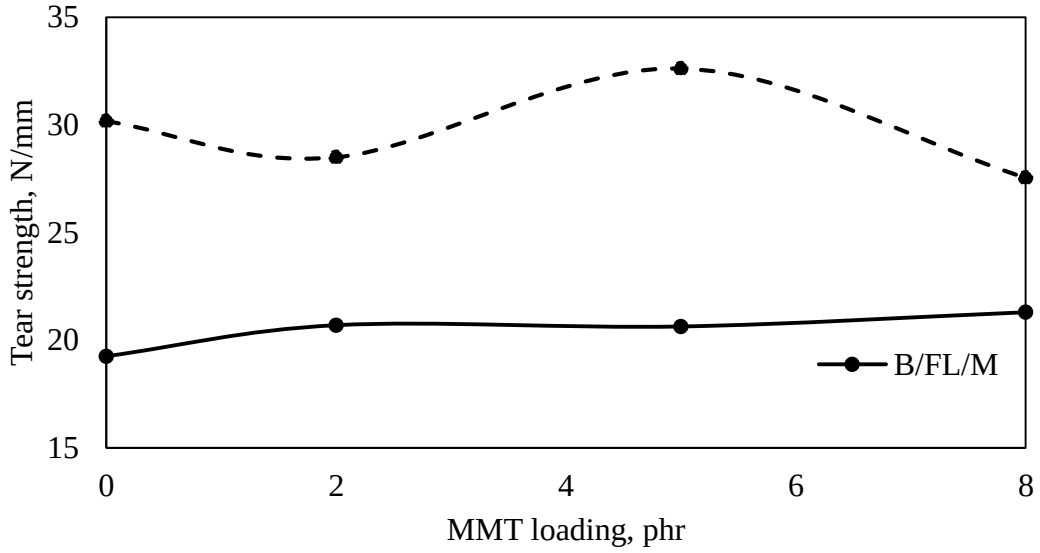

Figure 4. 18 Tear strength of B/FL/M and B/FL/G1/M nanocomposite vulcanizates

The tensile and tear properties of nanocomposite vulcanizates are improved due to the creation of siloxane networks surrounded by the smaller clay aggregates (at lower MMT loadings of MMT especially at 2 phr). Further enhancement of these properties could be obtained by the development of rubber-clay interactions through suitable modifications. However, the results confirmed that SSF is not a suitable gelling agent to use with MMT, even though the problem associated with surface drying of AFCC is solved.

4.1.2.2 CTAB gelling agent

Table 4.5 presents the mechanical properties of the two nanocomposite vulcanizates, prepared with and without CTAB gelling agent at the MMT loading of 2 phr and named as B/FL/M2 and B/FL/G2/M2 respectively.

Table 4.5 Mechanical properties of B/FL/M2, B/FL/G2/M nanocomposite vulcanizate

Mechanical properties	**Type of nanocomposite vulcanizates**	
	B/FL/M2	**B/FL/G2/M2**
Tensile strength, (MPa)	26.4	15.8
Elongation at break, (%)	489	492
mod 300% (MPa)	4.5	3.9
Tear strength (N/mm)	20.7	29.2

CTAB (G2) was used as a gelling agent in the study because the positively charged CTAB ions destabilize the negatively charged NRL by creating electrostatic interactions. An increase of the non-polar nature of MMT by intercalation of CTAB was also considered as an added advantage. However, the tensile strength and mod 300% of the B/FL/G2/M nanocomposite vulcanizate are reduced by 26% and 13% respectively, as compared to the B/FL/M2 nanocomposite vulcanizate. Non-rubber content including proteins remained in field NRL was considerably high, and those proteins may form protein-CTAB clusters. CTAB is responsible to cause denaturation of proteins and thereby converting folded proteins into unfolded (Wang et al., 2005; Chakraborty & Basak., 2008; Saha et al., 2018). The positively charge head group of CTAB interacts with proteins by via electrostatic interactions and hydrophobic tail of CTAB interacts with protein by hydrophobic interaction (Chakraborty & Basak., 2008; Pongnara et al., 2008). One of the studies also proposed that such structure with CTAB is like beads on a string chain like complex. It further revealed that the unfolded protein can bind with CTAB surfactant micelles in the protein-CTAB complexes when concentration of CTAB is increased. As a result of that micelles get elongated and the number of micelles per cluster is decreased. Finally, Protein-CTAB cluster merges to

form large micelle with unfolded proteins wrapping the micelle surface (Saha et al., 2018). This phenomenon is common in field NRL is used with CTAB due to presence of higher protein content. Those aggregated clusters would act as fracture initiation points and thereby reducing tensile strength. The effect of strain-induced crystallization with the change of protein structure may also decrease the tensile strength. In addition to that higher number of fracture initiation points may decrease the tensile strength and presence of CTAB as a plasticizing agent decreases the mod 300%. The elongation at break was the same, and the tear strength of B/FL/G2/M nanocomposite vulcanizate was increased by 41%, compared to B/FL/M2 nanocomposite vulcanizate, due to the plasticizing effect of CTAB used in the B/FL/G2/M nanocomposite vulcanizate. Replacing the field NRL by centrifuged NRL is suggested in the study to obtain better mechanical properties if G2 is used in future studies as protein content in the centrifuged latex was considerably low.

4.1.2.3 Effect of type of latex

The loading of 2 phr CTAB was used as a gelling agent to prepare both B/FL/G2/M and B/CL/G2/M nanocomposite (Section 3.2.7.3) from field NRL and centrifuged NRL respectively with MMT loading of 2 phr.

Table 4. 6 Mechanical properties of B/FL/G2/M and B/CL/G2/M nanocomposite vulcanizates

Mechanical properties	**Nanocomposite vulcanizate**	
	B/FL/G2/M	**B/CL/G2/M**
Tensile strength (MPa)	15.8	28.5
Elongation at break (%)	492	579
mod 300% (MPa)	3.9	4.2
Tear strength (N/mm)	29.2	33.8

Tensile strength, elongation at break, mod 300%, and tear strength of the B/CL/G2/M nanocomposite vulcanizate are increased by 80%, 18%, 8%, and 1.5% than those of the B/FL/G2/M nanocomposite vulcanizate (Table 4.6). The presence of less protein content in the centrifuged NRL may form a lesser number of protein-CTAB complexes. As a result, the fracture initiation points are reduced, and

the mechanical properties were increased in the B/CL/G2/M nanocomposite vulcanizate compared to those of the B/FL/G2/M nanocomposite vulcanizate.

However, it was noted that the gelation time for the destabilization of the B/CL/G2/M nanocomposite was considerably longer (about 20-25 min) than that of the B/FL/G2/M nanocomposite (about 12 min) during the latex stage. The evidence, thus, suggests that it is worthy of adding another gelling agent together with CTAB to speed-up the gelling process; otherwise, the clay aggregates would be separated from the latex phase during the period of longer gelation time and deplete mechanical properties.

4.1.2.4 Effect of the combination of CTAB gelling agent with SDS

The gelling agent CTAB was combined with SDS (G3) to speed-up the gelling process and the nanocomposites prepared with G3 were named as B/CL/G3/M2 nanocomposite (Section 3.2.7.6). It is expected that negative charge SDS would combine with positively charge CTAB and form a gelling structure quickly. The cure properties of B/CL/G3/M2 nanocomposite compound and the mechanical properties of the B/CL/G3/M2 nanocomposite vulcanizate are evaluated with respective nanocomposite compound and nanocomposite vulcanizates of B/CL/G2/M (Section 3.2.7.3).

Gelation time for the destabilization of the latex-clay mix was considerably low (1 minute) with the addition of SDS. The negatively charged SDS denatures the latex particle-bound folded protein into unfolded and increases the negative sites on the protein (Jelinska et al., 2017). The positively charged head group of CTAB adsorbed on both NRL particles and SDS by electrostatic attractions and increases gelling efficiency. The higher the adsorption capacity of CTAB cause de-stabilization of NRL more quickly than NRL with the absence of SDS (Pongnara et al., 2008).

t_{s2}, t_{90}, and CRI of the B/CL/G3/M2 nanocomposite compound show similar values compared to those of the B/CL/G2/M2 nanocomposite compound, indicating that the effect of SDS on cure characteristics and CRI is negligible (Table 4.7). Tensile strength, elongation at break, and tear strength of the B/CL/G3/M2 nanocomposite vulcanizates show 15%, 3%, and 7.5% increase compared to those of the B/CL/G2/M2 nanocomposite vulcanizates respectively due to better dispersion of clay in

B/CL/G3/M2 nanocomposite vulcanizates. Quick Gelation limits the time for the separation of clay stacks from NRL and prevents the formation of aggregated clay structures and thereby improves mechanical properties. The better dispersed clay retained in latex may increase the mechanical properties. It is also well known that clay layers are fully separated with the addition of an anionic surfactant (Gunister et al., 2004). However, mod 300% of the B/CL/G3/M2 nanocomposite vulcanizate shows a slight reduction than that of B/CL/G2/M2 nanocomposite vulcanizate, owing to the use of CTAB and SDS which act as a plasticizer.

Table 4. 7 The cure and mechanical properties of B/CL/G2/M2 and B/CL/G3/M2 nanocomposites

Properties	**Type of nanocomposite**	
	B/CL/G2/M2	**B/CL/G3/M2**
t_{s2}, min	2.2	2.3
$t_{90,}$ min	8.2	8.3
M_H-M_L, dN	8.2	8.9
CRI, min^{-}	16.7	16.8
Tensile strength, MPa	28.5	32.7
Elongation at break, %	579	597
mod 300%, Mpa	4.2	4.0
Tear strength, N/mm	33.8	36.3

In the current Section, CTAB was not used to increase the interlayer- gallery space of MMT. Quaternary amines such as CTAB is generally used to make organoclay as well, which is also important study to improve the mechanical properties. It was done under gelling agent free environment to understand effect of CTAB as intercalation agent on mechanical properties of nanocomposite in the next Section of 4.2.

4.2 NR- clay nanocomposites with OMMT

Section of 4.2.1 discusses the characterization of modified MMT clay with CTAB, and Section 4.2.2 explains the effect OMMT loading on properties of the B/CL/O nanocomposites prepared by the AFCC method (Section 3.2.7.7).

4.2.1 Characterization of OMMT

FTIR spectroscopy and XRD analysis used to characterize the MMT modified by CTAB, are discussed in Section 4.2.1.1 and Section in 4.2.1.2 respectively.

4.2.1.1 FTIR analysis

Figure 4.19 shows the FTIR spectra of CTAB, MMT, and OMMT. OMMT was used after washing with water to remove bromide ions.

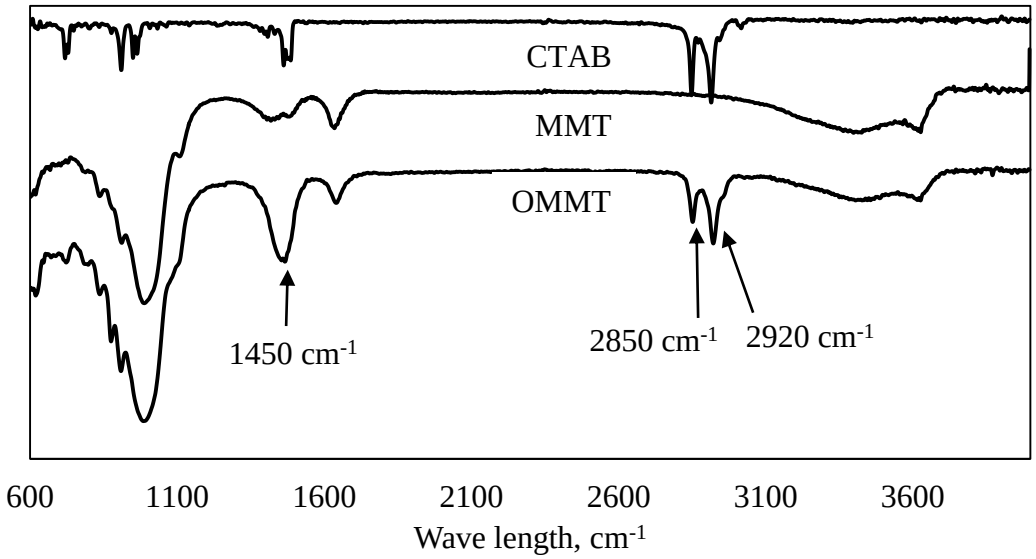

Figure 4. 19 FTIR spectra of CTAB, MMT, and OMMT

Three additional peaks are found at 2919, 2851, and 1450 cm^{-1} spectrum of the OMMT, when compared to the spectrum of MMT. The appearance of these additional peaks (Table 4.8) confirms that the retention of CTAB without washing away during bromide ion removal.

Table 4. 8 Peak assignment of the FTIR spectrum for CTAB

Wave number (cm^{-1})	Structure	Reference
2919	C-H asymmetric stretching	Ling et al., 2016
2851	C-H symmetric stretching	Ling et al., 2016
1450	CH_3 bending vibration	Ashraf et al., 2009

4.2.1.2 XRD analysis

Figure 4.20 illustrates the XRD diffractograms of MMT and OMMT. The peak at 2θ of 4.02 shows the successful intercalation of CTAB into the interlayer-gallery space of MMT in organoclay (OMMT). The inter gallery spaces of OMMT was 2.20 nm, while that of MMT was 1.41nm. It is confirmed that the interlayer-gallery space of the OMMT increased by 56% after modifying MMT with CTAB.

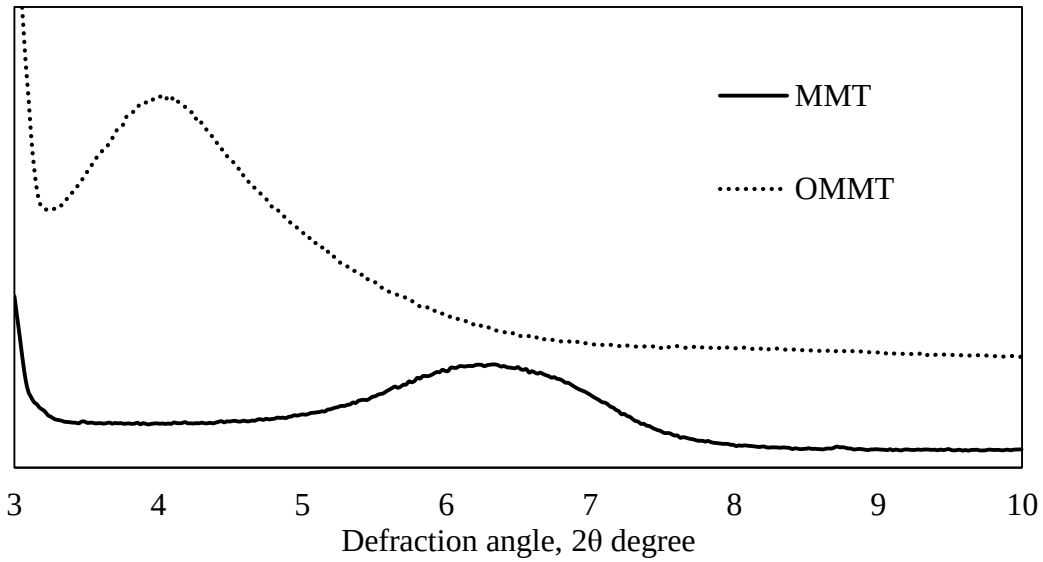

Figure 4. 20 XRD diffractograms of MMT, and OMMT

4.2.2 Effect of OMMT loading

B/CL/O nanocomposites at OMMT loading from 2-8 phr were taken. Cure characteristics (Section 4.2.2.1), XRD analysis (4.2.2.2), morphology (Section 4.2.2.3), crosslink density, and rubber-clay interaction (Section 4.2.2.4), DMTA

(4.2.2.5), and mechanical properties (Section 4.2.2.6) of the B/CL/O nanocomposite are discussed in this section.

4.2.2.1 Cure characteristics

Table 4.9 presents the cure characteristics such as t_{s2}, t_{90}, M_H, and M_L of B/CL/O nanocomposite compounds, while Figure 4.21 presents M_H-M_L and CRI. B/CL/O nanocomposite compounds at every OMMT loading exhibit drastic drops of t_{s2} and t_{90} than those of CT-B/CL. In literature, many researchers have described that organoclay would accelerate the curing process, mainly by a primary amine in the organoclay, which forms the zinc-amine complexes (Alex et al., 2006; Kim et al., 2006). It was also reported that quaternary amine accelerates the first stage of the curing process, although the proper mechanism of quaternary amine for curing was not yet suggested in the literature (Teh et al., 2004; Lopez-Manchado., 2004). It may be due to the fact that quaternary amine does not have a lone-pair electron for the formation of zinc-ammine complexes. It is confirmed that the tertiary amines are produced from the quaternary amines after the nucleophilic substitution of oxygen anion connected with Si in the clay layers (Galimberti., 2011) as in Figure 4.21.

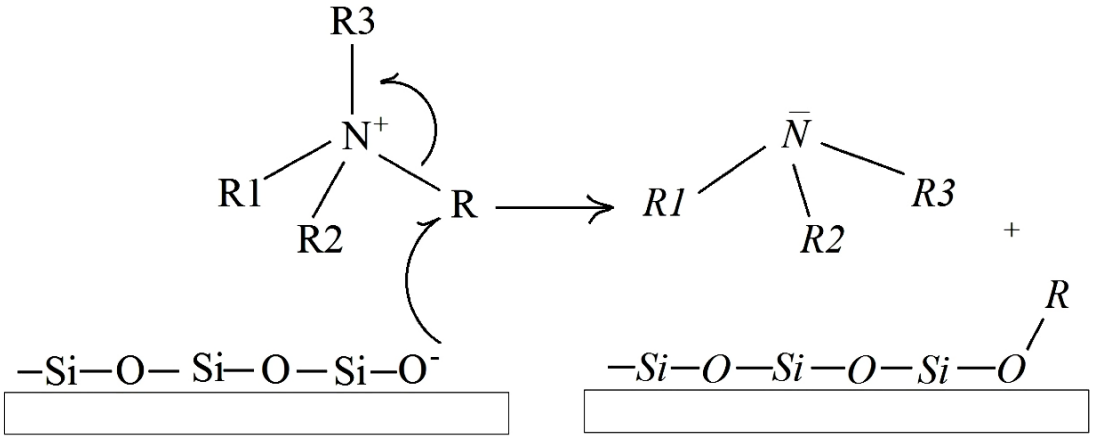

Figure 4. 21 Nucleophilic substitution of quaternary ammonium cation by oxygen anion of clay (Galimberti., 2011)

The amines produced by the degradation of CTAB have a higher influence on the formation of zinc-ammine complexes with soluble zinc ions and increases the rate of crosslinking and the degree of crosslink density while reducing t_{90}. (Lopez-Manchado et al., 2003).

t_{s2} and t_{90} of nanocomposite compounds are significantly lower than those values of the control compound. The amines degraded by CTAB would form zinc ammine complexes and thereby reduce t_{s2} and t_{90}.

Table 4. 9 Cure characteristics of B/CL/O nanocomposite compounds

Nanocomposite compound	t_{s2}**, min**	t_{90}**, min**	M_H**, dN**	M_L**, dN**
CT-B/CL	10.8	28.6	12.23	3.98
B/CL/O2	4.4	14.8	14.57	3.25
B/CL/O4	4.7	14.2	14.59	3.64
B/CL/O6	4.9	14.1	14.53	2.44
B/CL/O8	5.0	13.5	14.80	2.32

However, a few studies described the ability of CTAB on denaturing the structure of a protein (Chakraborty & Basak., 2008; Wang et al., 2005). Denaturation helps change the native quaternary structure of the folding of peptide backbones of protein into an unfolded, insoluble, and crystallized structure (Deller et al., 2016). Generally, it is accepted that hydrophobic side chains of the proteins are hidden inside, while the polar side chains are protruded out in the globular protein, primarily in the aqueous phase. When CTAB damages this native structure, protein is more soluble in NR, especially in the absence of an acidic environment. In an acidic medium, denaturation is also possible with acid, but acid would interact and react with basic curatives to delay the cure time. It is also observed that mechanical properties of B/CL/O nanocomposites are greater than that of A/FL/M nanocomposite discussed in Section 4.1.1. The denaturation effect of CTAB in B/CL/O nanocomposite is totally different from that of acid in A/FL/M nanocomposite. CTAB would enhance cure characteristics and contribute to improving mechanical properties whereas acid could not behave similarly.

With the addition of 2 phr of OMMT loading, M_H shows an increment and remains almost constant thereafter at every OMMT loading in nanocomposite compound (Table 4.9). On the contrary, M_L was reduced by an increased amount of

CTAB with an increase in OMMT loading due to the plasticizing effect. The almost constant of M_H and decrease of M_L occurred with the addition of OMMT into NRL resulting in an increase in M_H-M_L. It is interesting to note that the values of crosslink density were not directly proportional to M_H-M_L (Figure 4.22). It shows an increase of M_H-M_L may depend on the loading of OMMT and the effect of the plasticizing agent rather than crosslinking density.

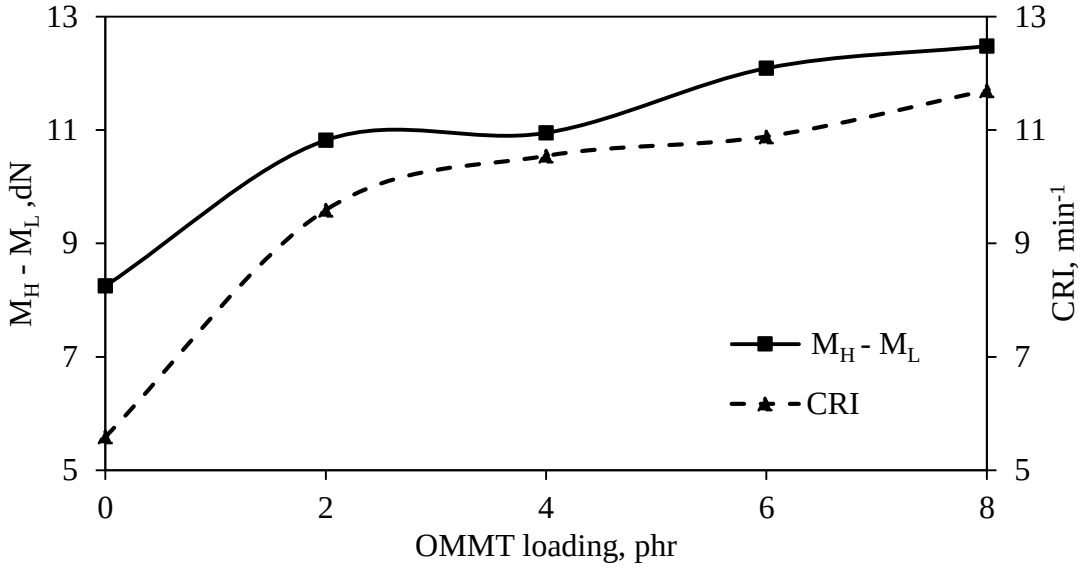

Figure 4. 22 M_H-M_L and CRI of B/CL/O nanocomposite Compounds

4.2.2.2 XRD Analysis

Figure 4.23 illustrates the X-ray diffractograms of OMMT and B/CL/O nanocomposite vulcanizates at different OMMT loadings. CT-B/CL vulcanizate does not show any peak because of the absence of OMMT clay layers. It is also evident that B/CL/O2 nanocomposite does not show any significant peak, suggesting that exfoliated clay structures present in the nanocomposite in unvulcanized state. It shows that rubber macromolecules penetrate to inter layer-gallery spaces between OMMT clay layers in the stacks or around the OMMT clay stacks generating both exfoliated structures and encapsulated structures (separated structures) having few clay layers in the stack in the nanocomposite stages. In encapsulated structures, clay layers are not intercalated by rubber macromolecules, instead of that clay stacks with few clay layers are encapsulated by rubber macromolecules (Wu et al., 2005). In contrast, two separate

peaks appear at 2θ of 4 and 6.2 in the B/CL/O nanocomposite vulcanizates after vulcanization at every OMMT loading, and are due to the presence of aggregated clay structures having two different interlayer-gallery spaces. The appearance of the two peaks at different intensities seems to suggest that the curing is not favorable for exfoliation.

Verghese & Karger-Kocsis (2003b) also noticed similar behavior in a study and called this phenomenon "confinement." Authors further explained that intercalated amine would remove from interlayer-gallery space of clay and involve in the formation of zinc-ammine complexes. Hence, peaks in XRD appear in different intensities as confirmed to unmodified MMT. Those aggregated clay structures were named as confinement structures. It was also found in the study that an increase of 55% peak area of confined structures in the B/CL/O8 nanocomposite vulcanizate greater than peak area in the B/CL/O2 nanocomposite vulcanizate. The presence of high amount of CTAB in B/CL/O8 nanocomposite vulcanizate was responsible for a higher degree of de-intercalation and greater intensity of the peak. However, this clay confinement does not occur before vulcanization due to the absence of ZnO in the B/CL/O2 nanocomposite. In contrast to this, few studies elaborated that curing reaction could facilitate the intercalation of rubber macromolecules in interlayer-gallery space of clay favoring exfoliated structures (Labaron et al., 2001; Wu et al., 2001; Usuki et al., 2002; Ma et al., 2007). It may be due to this reason that well-dispersed rubber macromolecules penetrate into interlayer-gallery space and form zinc-ammine complexes within the interlayer-gallery spaces hence confinement is not necessary.

However B/CL/O nanocomposite vulcanizates may consist of three possible clay structures, namely, confined MMT, intercalated OMMT, and encapsulated OMMT, but it does not mean that exfoliated OMMT layers are completely absent. The distribution pattern of clay could be further verified later in the study by the SEM images. The higher amount of confined structures found at higher OMMT loadings would be the main cause of the inferior mechanical properties. Further, the limited rubber-clay interactions between rubber and clay lead to an aggregation of clay structures. Further, the confinement of clay could be prevented by the addition of a greater amount of CTAB beyond its requirement for intercalation. This was achieved

by the addition of a higher quantity of CTAB into rubber clay nanocomposite before vulcanization (refer Section 4.2.3).

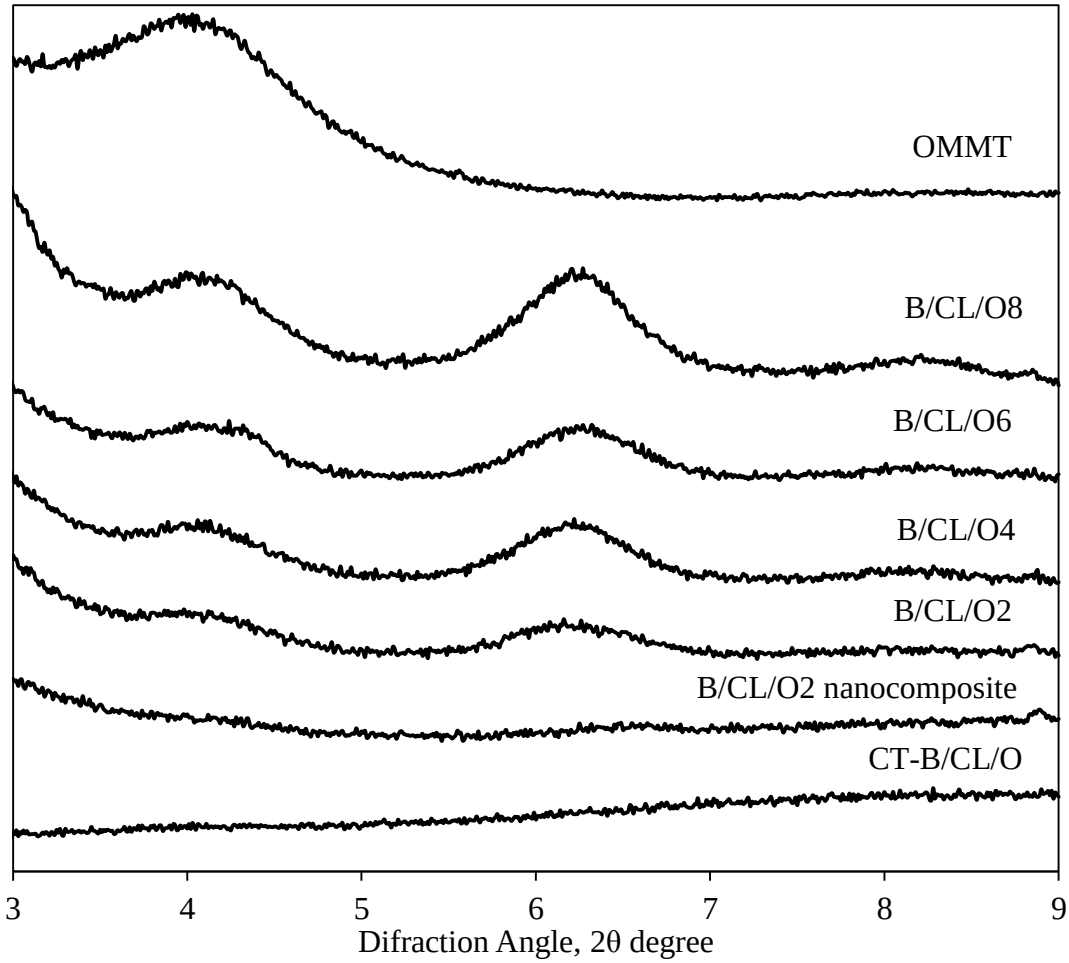

Figure 4. 23 The X-ray diffractogram of OMMT and B/CL/O nanocomposite vulcanizates

4.2.2.3 Morphology

Figure 4.24 and 4.25 show SEM images of tensile fracture surfaces of B/CL/O2 and B/CL/O8 nanocomposite vulcanizates respectively. A rough fracture surface with curved tears and fewer voids in B/CL/O2 nanocomposite vulcanizate, suggests better compatibility and/or adhesion between phases (Hakim & Ismail., 2009). In comparison to that, a smooth fracture surface in B/CL/O8 nanocomposite vulcanizate indicates poor compatibility. Further, B/CL/O8 nanocomposite

vulcanizate shows OMMT aggregates, and more voids as shown in Figure 4.24 indicate the fracture occurred due to poor adhesion between phases.

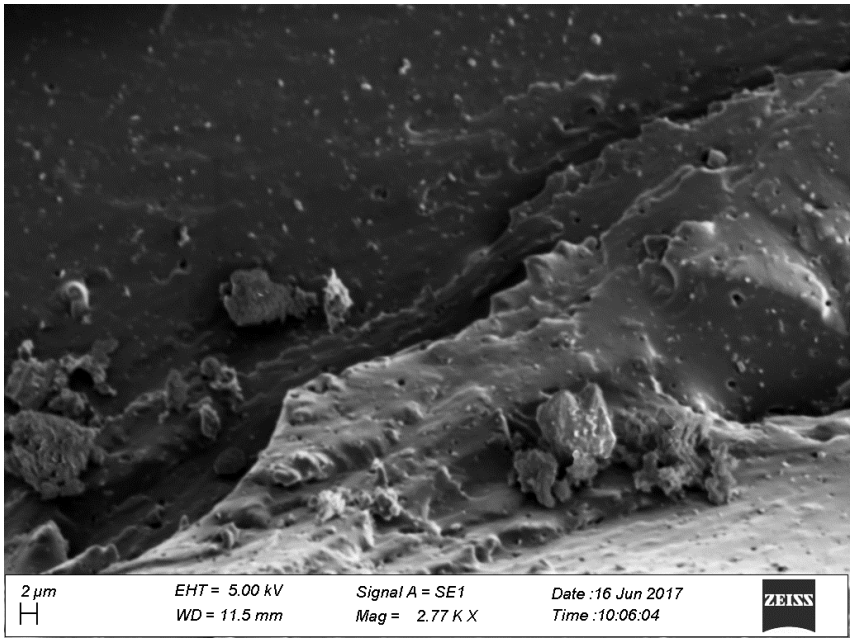

Figure 4. 24 SEM image of a tensile fracture surface of B/CL/O2 nanocomposite vulcanizate

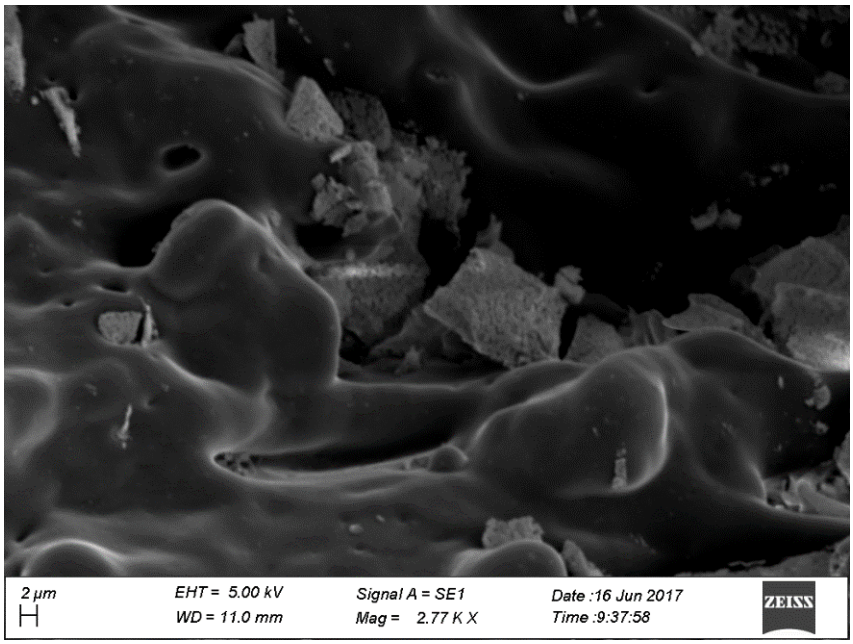

Figure 4. 25 SEM image of a tensile fracture surface of B/CL/O8 nanocomposite vulcanizate

4.2.2.4 Crosslink density and rubber-clay interaction

The crosslink density and the rubber-clay interaction through Q_f/Q_g of the B/CL/O nanocomposite vulcanizates at different OMMT loadings are given in Figure 4.26. Low Q_f/Q_g corresponds to more rubber-clay interaction. B/CL/O2 nanocomposite vulcanizate shows a 20% increase of crosslink density compared to CT-B/CL vulcanizate and is due to the formation of more crosslinks in the presence of additional zinc-ammine complexes. Also, at lower OMMT loading of 2phr, B/CL/O2 nanocomposite vulcanizate may improve the barrier properties and reduces the degree of swelling, which increases the crosslink density due to better distribution of smaller clay stacks. It imparts synergistic contribution to the barrier properties and may improve the crosslink density by a blend of exfoliated clay structures and smaller clay stacks with few clay layers in the rubber matrix formed at lower OMMT loading (Valadares et al., 2006).

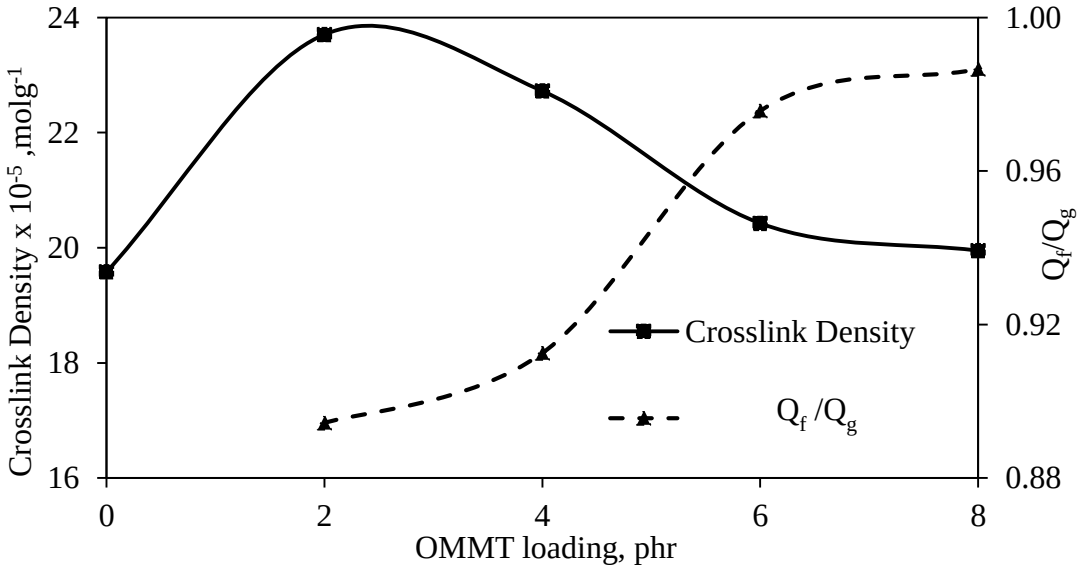

Figure 4. 26 Crosslink density and Q_f/Q_g of B/CL/O nanocomposite vulcanizates

Crosslink density is shown as decreased at higher OMMT loadings, attributed to the increase in the degree of swelling caused by dominant aggregated clay structures which result in reduced surface area of the clay (Amarasiri et al., 2013). Moreover, greater interactions of negatively charged both OMMT and rubber particles in NRL

with positively charged CTAB ions decreases Q_f/Q_g in B/CL/O2 nanocomposite vulcanizate. Otherwise, at higher OMMT loadings, it shows greater Q_f/Q_g, due to the formation of aggregates, thereby decreasing the level of rubber-clay interactions. It is worthy to note that the formation of interactions between rubber and OMMT through CTAB ions could be prevented by the presence of small positive ions in the acid found in the conventional ACC method. This negative effect was prevented by using the AFCC method to prepare B/CL/O nanocomposites. It is also interesting to note that M_H-M_L is lower at 2 phr OMMT loading at which crosslink density shows higher value. It may be due to the reason that M_H-M_L depends on the stiffness of clay and plasticizing effect of CTAB whereas crosslink density may depend due to improved barrier properties by a better distribution of smaller clay stacks.

4.2.2.5 Dynamic mechanical thermal analysis

Figure 4.27 depicts storage modulus of B/CL/O nanocomposite vulcanizates at different OMMT loadings.

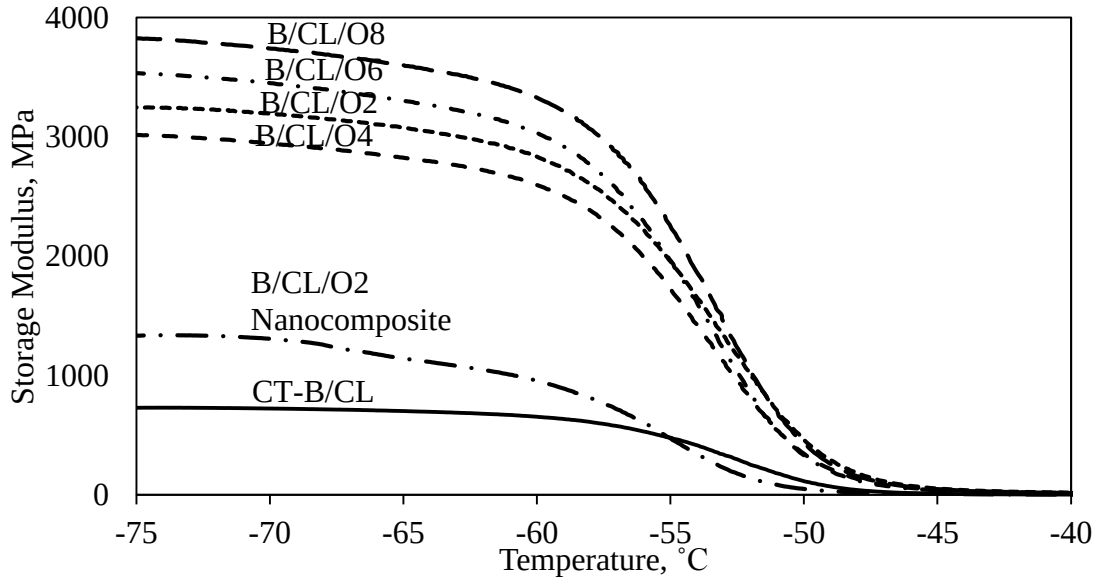

Figure 4. 27 Storage moduli versus temperature curves of B/CL/O nanocomposite vulcanizates

In the glassy state, the B/CL/O2 nanocomposite shows a greater storage modulus than CT-B/CL vulcanizate, confirming the formation of rubber-clay interactions. Further, higher storage moduli exhibited at higher OMMT loadings in

nanocomposite vulcanizates was due to the enhancement of the degree of crystallinity in B/CL/O nanocomposites. Introduction of crystalline clay structures to amorphous rubber and their fine dispersion by smaller clay stacks and crystallization of protein by denaturation with the addition of CTAB increases the degree of crystallinity of the nanocomposites. Research in different fields revealed that native crystalline structures in proteins are changed by the denaturation in the excess use of plasticizers and forming new crystalline structures (Lent et al., 1998). Additionally, some crystallinity at the surface is generated by electrostatic interactions between positively charged CTAB and negatively charged rubber. The B/CL/O2 nanocomposite vulcanizate shows higher storage moduli over the B/CL/O2 nanocomposite, which may also be due to the effect of sulphur crosslinks presence in B/CL/O2 nanocomposites. Further, it can be confirmed that the effect of sulphur crosslinks on storage moduli is dominant than the effect of OMMT loadings.

Figure 4.28 shows the loss factor ($\tan\delta$) versus temperature curves of B/CL/O nanocomposite vulcanizates at different OMMT loadings. T_g is also analyzed from the data of $tan\ \delta$. T_g of B/CL/O2 nanocomposite and CT-B/CL vulcanizate are -47.7 $^{\circ}$C and -44.5 $^{\circ}$C respectively. B/CL/O2, B/CL/O4, B/CL/O6, and B/CL/O8 nanocomposite vulcanizates show T_g in between -45.5 $^{\circ}$C and 46.0 $^{\circ}$C. The change of T_g the B/CL/O series of nanocomposite vulcanizates mainly depends on the plasticizing effect of CTAB, which decreases T_g compared to CT-B/CL vulcanizate. T_g does not vary with OMMT loading, due to an increase of loss moduli with the plasticizing effect which overrides the increase of storage moduli with increment in OMMT loading.

$\tan\delta$ of the nanocomposite and the nanocomposite vulcanizates of B/CL/O are lower than that of CT-B/CL vulcanizate. It indicates a significant reduction of dissipation energy with a lesser variation of storage moduli due to enhanced reinforcement in B/CL/O nanocomposite vulcanizates than CT-B/CL vulcanizate. This also may be due to the enhancement of attractions between negatively charged rubber particles and positively charged OMMT in the acid-free environment. The reinforcement of rubber nanocomposite vulcanizates improved by shifting the T_g to the higher temperature side was reported in the literature (Varghese et al., 2003; Karger-Kocsis and Wu., 2004). However, this behavior is different in B/CL/O

nanocomposite vulcanizates which may be due to the presence of a higher amount of CTAB in rubber phase de-intercalated from interlayer-gallery spaces of OMMT by confinement process discussed at Section in 4.2.2.2.

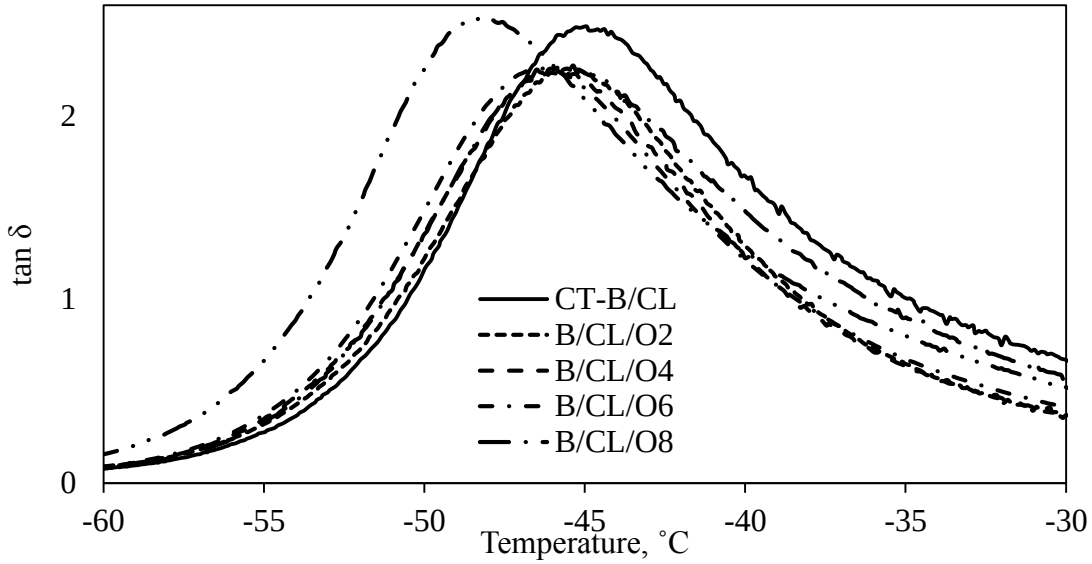

Figure 4. 28 tan δ vs temperature curves of B/CL/O nanocomposite vulcanizates

4.2.2.6 Mechanical properties

Figure 4.29 presents the stress-strain curves of B/CL/O nanocomposite vulcanizates at OMMT loadings of 2 phr and 8 phr. B/CL/O nanocomposite vulcanizates exhibited improved strain-induced crystallization behavior than that of CT-B/CL vulcanizate due to crystallinity developed with storage moduli as confirmed by DMTA study. Rubber macromolecules aligned with a high amount of OMMT clay layers would cause a higher strain-induced crystallization in B/CL/O8 nanocomposite vulcanizate. However, before attaining the maximum strain induced crystallization, nanocomposite specimen broke at a lower elongation possibly due to the presence of aggregated clay structures formed at higher OMMT loadings.

Figure 4.30 presents tensile strength and elongation at break of B/CL/O nanocomposite vulcanizates at different OMMT loadings, while Figure 4.31 illustrates mod 300% and tear strength. It is evident that tensile strength, elongation at break, and mod 300% of B/CL/O nanocomposite vulcanizate at 2 phr OMMT loading show 7% MPa increment, 10% reduction and 1.4% MPa increment respectively, compared

to the CT-B/CL vulcanizate. This confirms that the reinforcing effect of OMMT in NR is caused by a higher degree of strain-induced crystallization. The increase of the tensile strength with a minimum reduction of elongation at break is the effect due to the improvement of strain-induced crystallization by the orientation of fine clay layers along with the direction of stress (Madhusoodanan et al., 2006). High aspect ratio and large surface area of OMMT increase interfacial interactions between OMMT and NR effectively and transfer the stress between NR and OMMT. The improved interactions between rubber and OMMT also increase the crystallinity and improve the reinforcing effect (Usuki et al., 1995).

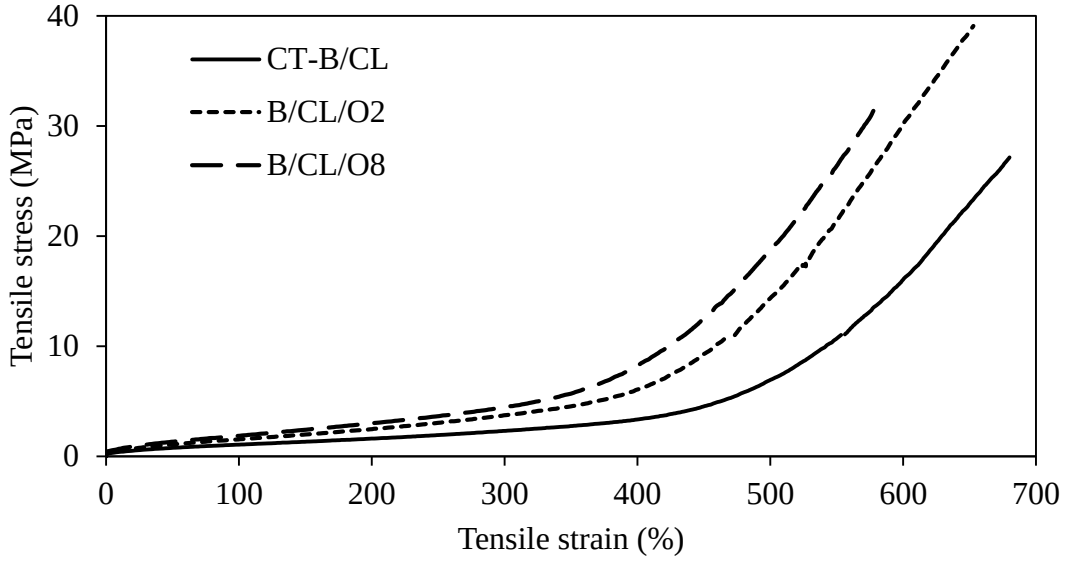

Figure 4. 29 Stress versus strain curves of B/CL/O nanocomposite vulcanizates

The crosslink density could be improved by the formation of zinc amine complexes with the effect of quaternary amine (Mousa & Karger-kocsis., 2001) and the effect of better dispersion of organoclay (Varghese et al., 2003; Madhusoodanan et al., 2006; Zhang et al., 2008). However, the excess use of quaternary amine would cause a plasticizing effect (SI et al., 2011; Kim et al., 2006) and weaken mod 300%. Hence, a proper balance of CTAB and OMMT should be maintained to achieve a higher tensile strength in the nanocomposite vulcanizate. It was achieved by OMMT loading of 2 phr at B/CL/O2 nanocomposite vulcanizate. It was reported that an enhancement in the tensile strength is improved by exfoliation (Hakim et al., 2009; Varghese et al., 2003; Madhusoodanan et al., 2006). The contradictory statement was

also discussed in the literature as the strain-induced crystallization is inhibited by exfoliated clay structures and thereby reducing the tensile strength (Fathurrohman et al., 2015). The tensile strength and elongation at break of such nanocomposite vulcanizates are improved with the reduction of mod 300%. However, B/CL/O nanocomposite vulcanizates at low OMMT loadings show high tensile strength with an increase of mod 300% and a decrease of elongation at break. The improvement of mod 300% is not as satisfactory as expected possibly due to a lack of improved rubber clay interactions.

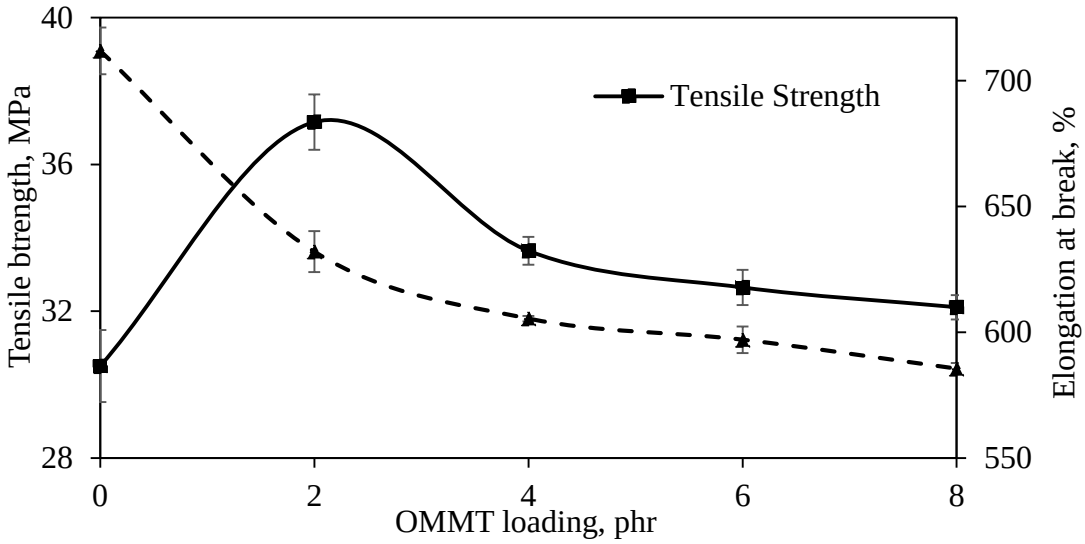

Figure 4. 30 Tensile strength and elongation at break of B/CL/O nanocomposite vulcanizates

The study further discloses that a decrease of both tensile strength and elongation at break resulted together with an increase of mod 300% when OMMT at higher loadings are incorporated. This property variation is mainly due to aggregated clay structures present in such nanocomposites. Higher clay aggregation increases the formation of rupture initiation points (Mousa & Karger-Kocsis., 2001; Zhang et al., 2008; Fathurrohman et al., 2015; Sharif et al., 2005). Thus, the nanocomposite vulcanizates are broken easily at weak points, resulting in a low elongation at break before the maximum tensile strength achieved (Sharif et al., 2005).

The literature described the same phenomenon in different ways. The limited rubber phase to disperse of clay also creates the aggregated clay structures (Teh et al., 2006) and reduces the exfoliated clay structures. However, the formation of aggregated clay structures is prevented by diluting the NRL by water in many industrial applications. The limited rubber phase in the composite may cause clay aggregation again at drying stages. This could be minimized by the use of lower loading of nanoclay better dispersed at the rubber phase (Amarasiri et al., 2013; Mousa & Karger-Kocsis., 2001; Teh et al., 2006). Most of such nanocomposite vulcanizates exhibited enhanced mechanical properties with the improvement of crosslink density together with an increment of T_g. The most promising finding of B/CL/O nanocomposite vulcanizate is that it obtained higher tensile strength at 2 phr of OMMT in B/CL/O2 nanocomposite vulcanizate by decreasing of T_g compared to that of CT-B/CL vulcanizate.

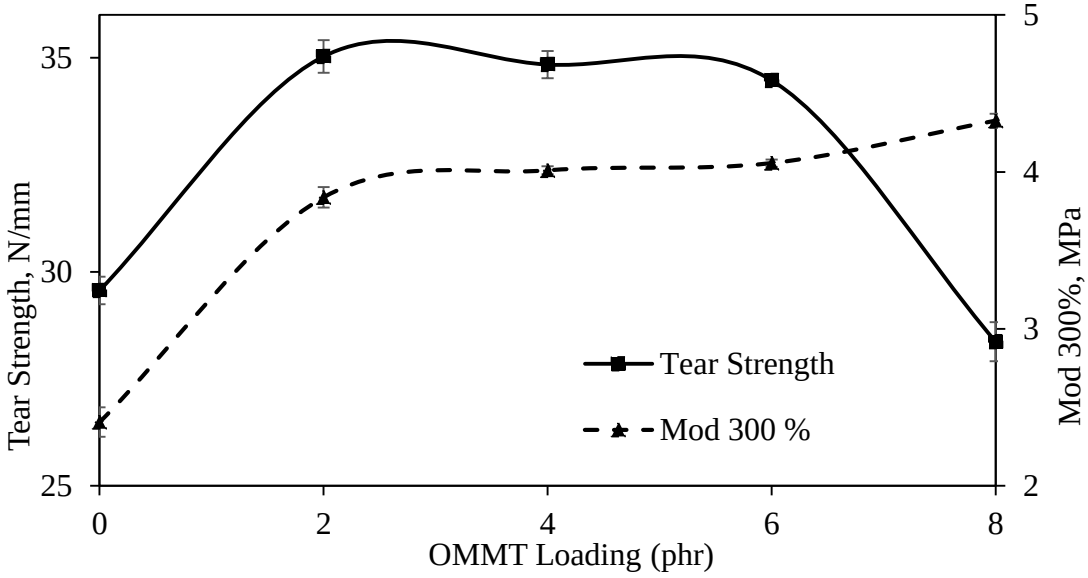

Figure 4. 31 mod 300% and tear Strength of B/CL/O nanocomposite vulcanizates

The tear strength of nanocomposite vulcanizates is slightly improved when 2 phr loading of OMMT is incorporated into NR in B/CL/O2 nanocomposite vulcanizates. It is mainly due to the creation of voids in their vicinity by a fine dispersion of clay layers. It supports the dissipation of high energy and thereby, withstands greater strains. Clay layers divert the zigzag tear path to provide a higher tear strength (Madhusoodanan et al., 2006). However, at higher OMMT loadings,

especially in B/CL/O8 nanocomposite vulcanizates, tear strength reduces with the effect of a high degree of clay aggregation. Such aggregates, may act as stress concentrators (Ishiaku et al., 2000).

The tear strength is not enhanced as expected due to lower rubber-filler interactions in the B/CL/O nanocomposite vulcanizates. It is necessary to develop such interactions between NR and exfoliated clay structures by suitable modifications if tear strength is to improve further.

Figure 4.32 provides the hardness of B/CL/O nanocomposite vulcanizates at different OMMT loadings.

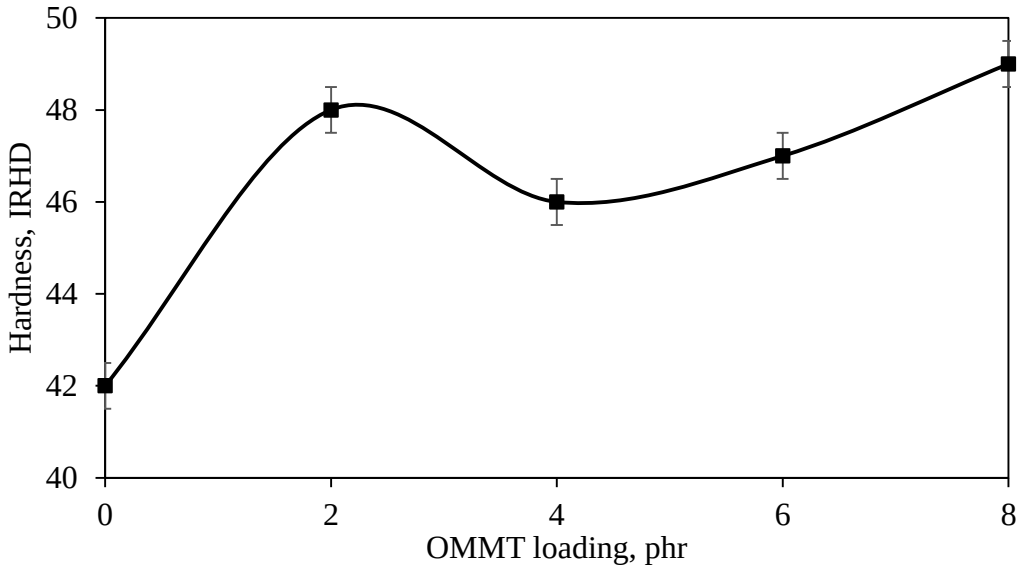

Figure 4. 32 Hardness of B/CL/O nanocomposite vulcanizates

Hardness generally shows a substantial increase with filler loading. It is generally accepted that when more filler is incorporated into the rubber matrix, hardness is improved due to a decrease of plasticity and an increase of rigidity (Ewulonu et al., 2015). In addition, hardness is improved by increasing crosslink density (Alwis et al., 2013). The hardness of B/CL/O nanocomposite vulcanizates shows an increasing trend with OMMT loading with the minimum at 4 phr loading. At this loading, better distribution of the smaller number of clay stack is less and the filler effect is not high enough to increase the hardness. However, the improved rubber-clay interactions due to better distribution of smaller clay stacks may increase the hardness at lower OMMT loadings below 2 phr. The filler effect under the studied range of the

OMMT loadings overrides an increase of plasticizing effect; hence, hardness is improved with the OMMT loading. However, hardness could be further increased if crosslink density is increased by improving rubber-clay interaction. It was not achieved in B/CL/O nanocomposite vulcanizates due to the presence of aggregate clay structures prepared at higher loadings.

The ageing resistance of B/CL/O nanocomposite vulcanizates is improved significantly than A/FL/M and B/FL/M nanocomposite vulcanizates, which may be due to consequence of replacing the field NRL by centrifuged NRL and or effect of organically modified clay used in B/CL/O nanocomposite vulcanizates (Table 4.10). PRV of tensile strength and elongation at break of CT-B/CL and B/CL/O2 nanocomposite vulcanizates show a decreasing trend after ageing while CT-B/CL and B/CL/O2 vulcanizates show increasing trend after ageing.

Table 4. 10 Ageing properties of B/CL/O nanocomposite vulcanizates

Tensile properties	**CT-B/CL**			**B/CL/O2**		
	Un-aged	**Aged**	**PRV, %**	**Un-aged**	**Aged**	**PRV, %**
Tensile strength, MPa	30.5	26.8	88	37.2	34.2	92
Elongation at break, %	712	655	92	632	594	94
mod 300%, MPa	2.4	2.9	120	3.8	4.4	116

The major drawback of the preparation B/CL/O nanocomposite vulcanizates was the surface drying. NRL clay mix was not co-coagulated at below the dried surface of the coagulum. The evaporation of water prevented by the dried top surface of the coagulum causes this surface drying. It is suggested that the use of gelling agents to prevent this undesirable effect is vital in the study.

The study of B/CL/O nanocomposite vulcanizates shows that increment of non-polar content of clay by modification of CTAB under acid-free environment is not necessary to increase all mechanical properties as expected. Even though the tensile strength is improved with the incorporation of lower loadings of OMMT in B/CL/O nanocomposite vulcanizates, the tear strength, mod 300%, and hardness of B/CL/O

nanocomposite vulcanizates were not increased. This could be overcome by increasing the compatibility between rubber and clay by suitable modifications.

4.2.3 The effect of gelling agent

The effect of gelling agent G3 comprising of CTAB and SDS on the properties of B/CL/G3/O2 nanocomposite (Section 3.2.7.8) and gelling agent free B/CL/O2 nanocomposite (Section 3.2.7.7) at 2 phr OMMT loading together with their Controls are evaluated and discussed under this Section.

These properties including cure characteristics (Section 4.2.3.1), crosslink density (Section 4.2.3.2), mechanical properties (Section 4.2.3.3), and glass transition temperature (Section 4.2.3.4) are given in Table 4.8.

Table 4. 11 Properties of B/CL/O2 and B/CL/G3/O2 nanocomposite compound and vulcanizate of controls

	CT-B/CL	**CT-B/CL/G3**	**B/CL/O2**	**B/CL/G3/O2**
t_{s2} (min)	10.8	1.9	4.4	2.1
t_{90} (min)	28.6	3.9	14.8	8.8
CRI (min^{-1})	5.9	12.0	9.6	14.8
Crosslink density ($x\ 10^{-5}$ $molg^{-1}$)	19.6	19.8	23.7	20.6
Tensile strength (MPa)	30.5	15.2	37.2	35.8
Elongation at break (%)	711	462	632	650
mod 300% (MPa)	2.4	3.9	3.8	3.2
Tear Strength (N/mm)	29.6	33.0	35.0	39.6
Hardness (IRHD)	42	44	42	44
T_g ($^{\circ}C$)	-44.5	-45.7	-45.5	-48.8

4.2.3.1 Cure characteristics

t_{s2} and t_{90} of CT-B/CL/G3 compound is drastically lowered compared to those of CT-B/CL compound (Table 4.11). Although OMMT (MMT modified with CTAB) was not present in CT-B/CL/G3 compound, CTAB used as a gelling agent in

it, decreases t_{s2} and t_{90} . Similar trend of cure properties are seen in B/CL/G3/O2 nanocomposite compound compared to B/CL/O2 nanocomposite compound, due to presence of the higher amount of CTAB in B/CL/G3/O2 nanocomposite compound added as intercalation agent and gelling agent. The effect of a quaternary amine such as CTAB contribution on the formation of zinc ammine complexes was evaluated by much research in the literature (Teh et al., 2004; Lopez-Manchado., 2004). The higher number of zinc ammine complexes created in CT-B/CL/G3 and B/CL/G3/O2 nanocomposite compound give lower t_{s2} and t_{90} with the increment of CRI compared to CT-B/CL compound and B/CL/O2 nanocomposite compound. t_{s2} and t_{90} of CT-B/CL/G3 compound are less than those of B/CL/G3/O2 nanocomposite compound due to the effect of clay when CTAB is excess in both vulcanizates. This shows the addition of clay may intercalate zinc ammine complexes into interlayer-gallery space and its use for vulcanization is limited compared to its control.

4.2.3.2 Crosslink density

A higher crosslink density in B/CL/G3/O2 nanocomposite vulcanizate was expected due to the formation of a higher amount of zinc-ammine complexes. However, due to the dissolution of a higher amount of gelling agent, the crosslink density of B/CL/G3/O2 nanocomposite vulcanizate shows a lower value than B/CL/O2 nanocomposite vulcanizate (Table 4.11). In comparison, the crosslink density of CT-B/CL vulcanizate and CT-B/CL/G3 vulcanizate shows similar values, indicating that the gelling agent does not have a greater influence on the crosslink density in the absence of clay. This shows that leaching of clay with the dissolution of the gelling agent may have a greater influence on reducing the crosslink density.

4.2.3.3 Mechanical properties

The tensile strength and the elongation at break of CT-B/CL/G3 vulcanizate are significantly lower than those of CT-B/CL vulcanizate (Table 4.11). The presence of both cationic and anionic surfactants in CT-B/CL/G3 vulcanizate causes the formation of gelling clusters by a combination of both CTAB and SDS surfactants. The structure of the gelling cluster is proposed and given in Figure 4.43 in Section 4.2.5. The interface between two surfactants in a cluster has the lowest strength; hence,

it may act as a fracture initiation point when tensile stress is applied. mod 300%, hardness, and tear strength of CT-B/CL/G3 vulcanizate are higher than those of CT-B/CL vulcanizate because of the increase of the total number of interactions between gelling agents. Interestingly, the gelling clusters may not reduce tear strength as a consequence of initiation and propagation of cracks are different during tearing compared to tensioning. The initiation point of the crack in tear specimens may occur at an angular point and propagates through the weakest interphase between rubber and clay. The increase of the slippery action by plasticizing agents and propagation of strain in longer tear path in zigzag direction by the effect of OMMT would improve the tear strength, especially at lower loading of B/CL/G3/O2 nanocomposite vulcanizate. The hardness of B/CL/G3/O2 nanocomposite vulcanizate is similar to that of CT-B/CL/G3 vulcanizate, and it shows that the addition of OMMT at 2 phr loading does not affect on the increase of hardness. However, an increased amount of CTAB in B/CL/G3/O2 nanocomposite vulcanizate improves hardness slightly compared to B/CL/O2 nanocomposite vulcanizate.

Keawkumay mentioned that tensile strength depends on both organoclay and the content of primary and quaternary amine surfactant, and mod 300% depends mostly on content of organoclay clay (Keawkumay et al., 2012). This study of B/CL/O2 nanocomposite revealed that both organoclay and surfactant affect the tensile strength, mod 300%, elongation at break, tear strength and hardness due to excess use of surfactant together with 2 phr loading of OMMT.

4.2.3.4 Glass transition temperature

T_g of CT-B/CL/G3 vulcanizate is lower than that of CT-B/CL vulcanizate and T_g of B/CL/G3/O2 nanocomposite vulcanizate is also lower than that of B/CL/O2 nanocomposite vulcanizate (Table 4.11). This shows that the higher amount of surfactants used as gelling agents in CT-B/CL/G3 vulcanizate and B/CL/G3/O2 nanocomposite vulcanizate decrease T_g due to higher plasticizing effect. This also shows that T_g of B/CL/O2 and B/CL/G3/O2 nanocomposite vulcanizates were decreased after the incorporation 2 phr of OMMT from their T_g of controls due to the same effect. The Presence of CTAB either as an intercalation agent or gelling agent in the nanocomposite may act as a plasticizing agent and may decrease the T_g, which is

more prominent when a higher amount of CTAB is introduced to nanocomposite as a gelling agent.

Large-scale production is successful without the problem of surface drying after the addition of gelling agent G3, although G3 causes a smaller reduction of tensile strength and mod 300%. Despite such smaller differences in properties, this study confirmed that the use of gelling agent G3 is effective to overcome the problem of surface drying and could be used in future studies.

4.2.4 Type of clay

The effect of type of clay was studied using B/CL/G3/O2 nanocomposite vulcanizate prepared with OMMT (Section 3.2.7.8) and B/CL/G3/M2 nanocomposite vulcanizate prepared with MMT with G3 gelling agent (Section 3.1.7.6) under the acid- free environment and tensile properties are given in Table 4.12.

Table 4. 12 Mechanical properties of B/CL/G3/M2 and B/CL/G3/O2 nanocomposite vulcanizates

Mechanical Properties	**Nanocomposite vulcanizate**	
	B/CL/G3/M2	**B/CL/G3/O2**
Tensile strength, MPa	32.9	35.8
Elongation at break, %	597	650
mod 300 %, MPa	4.0	3.2
Tear strength, N/mm	36.3	39.6

The loading of 2 phr clay was used in the preparation of both nanocomposite vulcanizates with the intension to compare mechanical properties and thereby understanding the effect gelling agent on MMT and OMMT. Tensile strength, elongation at break, and tear strength of B/CL/G3/O2 nanocomposite vulcanizate were enhanced by 9.5%, 8.7%, and 9.0% respectively compared to B/CL/G3/M2 nanocomposite vulcanizate. Good dispersion of OMMT in the B/CL/G3/O2 nanocomposite vulcanizate results in better mechanical properties compared to the B/CL/G3/M2 nanocomposite vulcanizate, which consists of higher aggregated MMT layers and is further confirmed by the SEM image in Figure 4.33 in comparison to the

image of B/CL/G3/O2 nanocomposite vulcanizate shown in Figure 4.34. However, mod 300% of B/CL/G3/O2 nanocomposite vulcanizate was lowered by 26% compared to that of B/CL/G3/M2 nanocomposite vulcanizate. The large amount of CTAB used as a gelling agent and intercalation agent in B/CL/G3/O2 nanocomposite vulcanizate shows lower mod 300% due to greater plasticizing effect. Generally, plasticizing agent increases elongation at break while reducing tensile strength and mod 300%. The trend is quite different in the application of nanoclay, because the better dispersed nanoclay with the use of surfactant increases tensile strength as well. Higher the interfacial surface area with minimum aggregated clay influences on increasing tensile strength (Keawkumay et al., 2012).

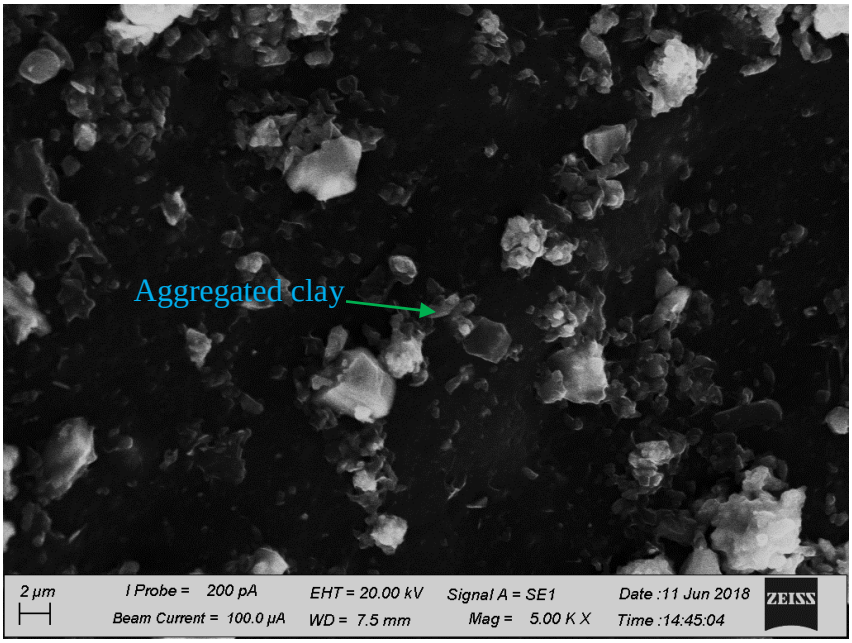

Figure 4. 33 SEM image of B/CL/G3/M2 nanocomposite vulcanizate

Properties of nanocomposite vulcanizates show that the nanocomposite vulcanizates prepared with OMMT give better mechanical properties compared to that with MMT under the gelling condition. However, it is necessary to introduce a suitable modification to increase mod 300% in further studies without reducing other mechanical properties, if OMMT is selected as the clay for further studies. As per literature, the use of OMMT was a success in many nanocomposite vulcanizates using

as a filler incorporated into NR by mechanical blending (Jacob et al., 2007; Viet et al., 2008; Yahaya et al., 2010), and none of studies have used the emulsion blending especially under acid-free environment with a gelling condition. Therefore, it is necessary to compare nanocomposite vulcanizates prepared from both methods of mechanical blending and emulsion blending using OMMT.

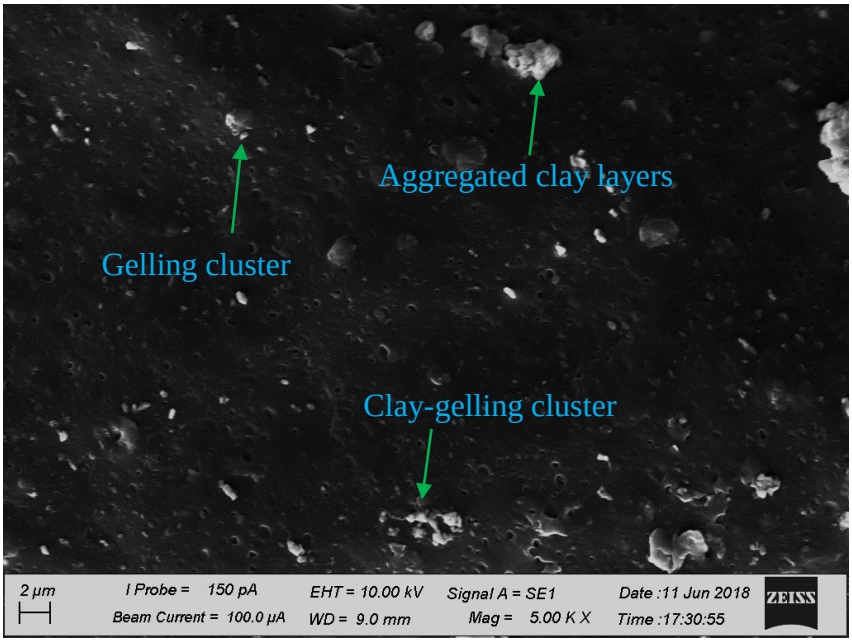

Figure 4. 34 SEM image of B/CL/G3/O2 nanocomposite vulcanizate

4.2.5 Effect of processing method

The effect of processing method (mechanical blending and emulsion blending under the acid-free environment with the gelling condition) used to prepare nanocomposites are discussed as a comparative study between CT-B/CL/G3, B/CL/G3/O2, B/CL/G3/O5 nanocomposites (Section 3.2.7.8), and CT-C/PC, C/PC/O2, and C/PC/O5 in C/PC nanocomposites (Section 3.2.7.9), respectively. Properties such as cure characteristics (Section 4.2.5.1), morphology (Section 4.2.5.2), XRD analysis (Section 4.2.5.3), crosslink density (Section 4.2.5.4), bound rubber content (Section 4.2.5.5), DMTA (Section 4.2.5.6), mechanical properties (Section 4.2.5.7), abrasion loss (Section 4.2.5.8), and ageing properties (Section 4.2.5.9) are discussed.

4.2.5.1 Cure characteristics

Figure 4.35 shows t_{s2}, t_{90} and CRI of B/CL/G3 and C/PC nanocomposite compounds. CT-B/CL/G3, B/CL/G3/O2, and B/CL/G3/O5 nanocomposite compounds show lower t_{s2} values compared to those of C/PC nanocomposite compounds. This is attributed to the higher number of CTAB and thereby increasing the amount of zinc-ammine complexes in B/CL/G3 nanocomposite compounds compared to C/PC nanocomposite compounds.

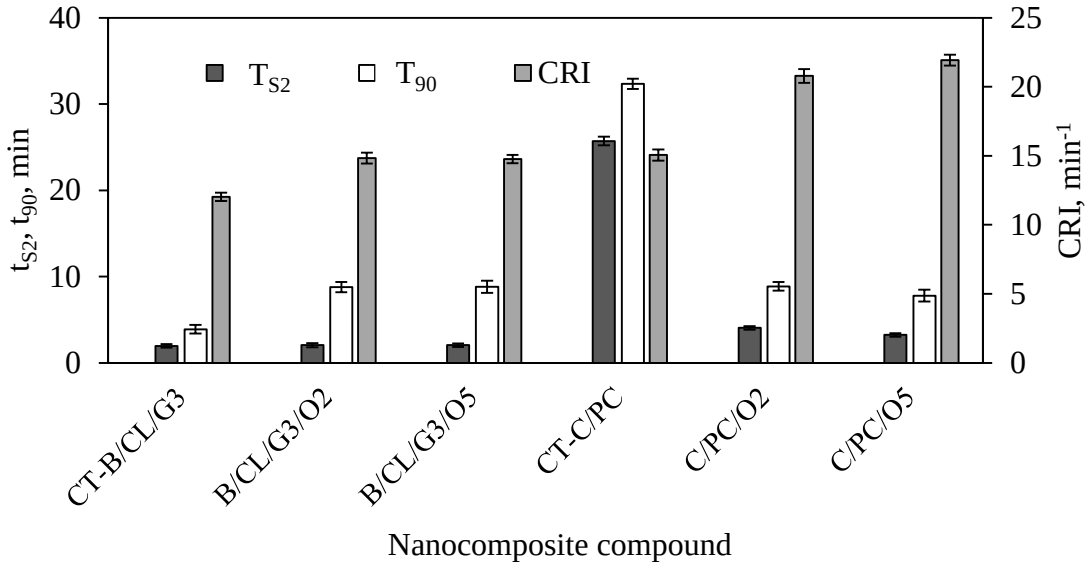

Figure 4. 35 t_{s2},t_{90} and CRI of B/CL/G3 & C/PC nanocomposite compounds

t_{90} of B/CL/G3/O2 and B/CL/G3/O5 nanocomposite compounds show higher values compared to those of C/PC/O2 and C/PC/O5 nanocomposite compounds. This may due to different crosslink densities shown by B/CL/G3 and C/PC nanocomposite (Refer Section 4.2.5.4). CT-C/PC shows higher t_{s2} and t_{90} corresponding to their C/PC/O2 and C/PC/O5 nanocomposite compounds due to the absence of CTAB via a gelling agent or intercalation agent. t_{s2} and t_{90} values are lowered in C/PC/O5 nanocomposite compound compared to that of C/PC/O2 nanocomposite compound with the presence of more OMMT in C/PC/O5 nanocomposite compound. However, it is interesting to note that CRI of C/PC nanocomposite compounds is greater than those of B/CL/G3 nanocomposite compounds. The reason may be due to the smaller values of t_{90}- t_{s2} found in C/PC nanocomposite compounds to form a smaller number

of crosslinks compared to those of B/CL/G3 nanocomposite compounds and that value is inversely proportional to CRI.

Figure 4.36 presents the activation energy of the vulcanization process in B/CL/G3 & C/PC nanocomposite compounds. The activation energy of vulcanization reaction of B/CL/G3/O2, B/CL/G3/O5 nanocomposite compounds and CT-B/CL/G3 is lower than that of C/PC/O2, C/PC/O5 and CT-C/PC. It may be confirmed that the presence of a higher number of zinc-ammine complexes in B/CL/G3 nanocomposite compounds and its control decreases the activation energy showing similar trend with t_{s2} values.

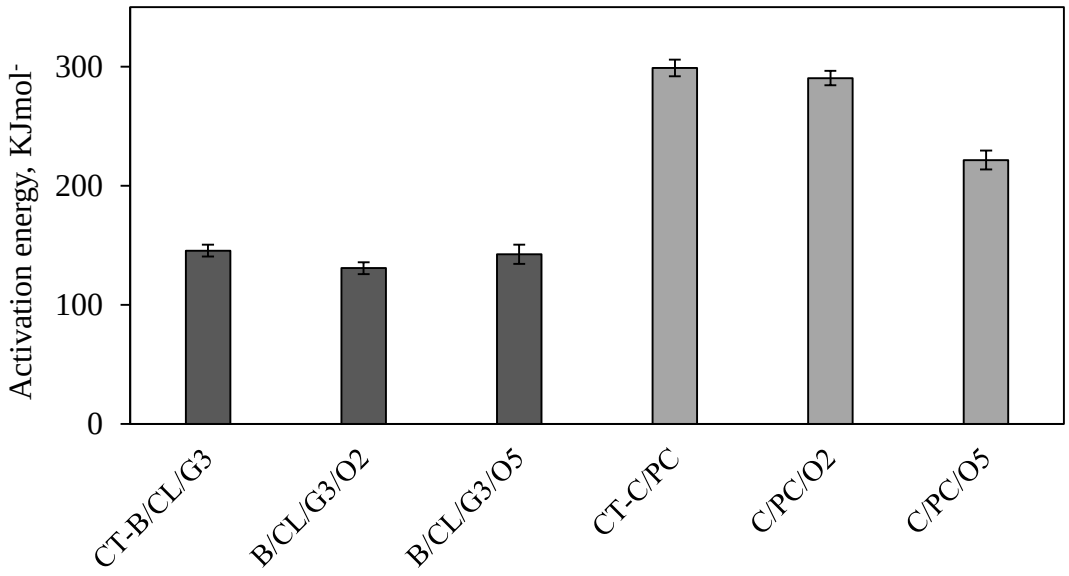

Figure 4. 36 Activation energy of B/CL/G3 & C/PC nanocomposite compounds

M_H - M_L of CT-B/CL/G3 is greater than that of CT-C/PC, and may be due to the formation of a higher number of Sulphur crosslinks in CT-B/CL/G3 (Figure 4.37).

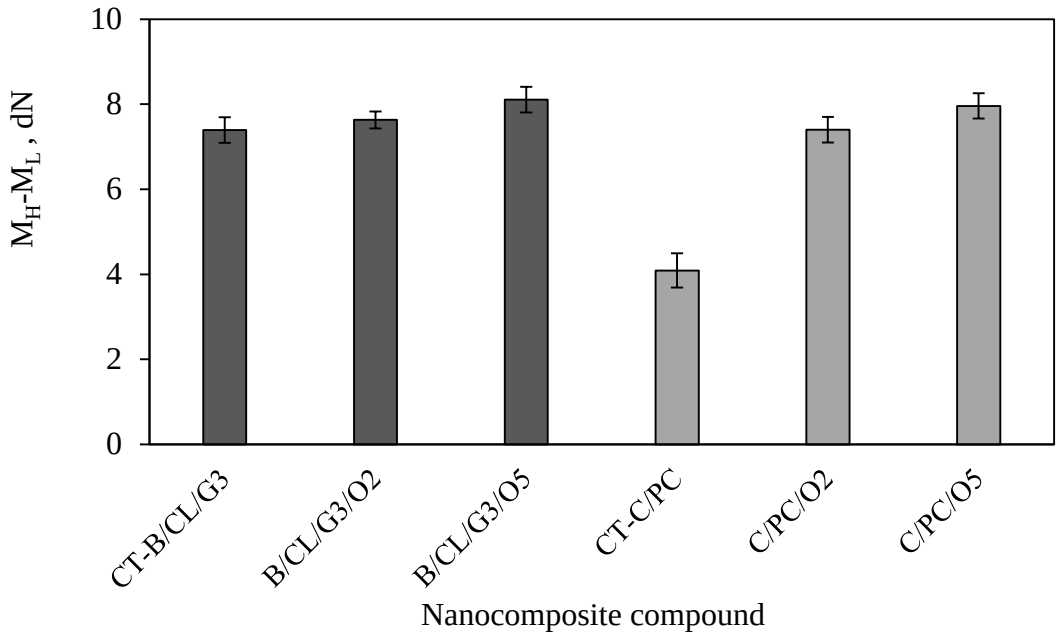

Figure 4. 37 M_H-M_L of B/CL/G3 and C/PC nanocomposite compounds

M_H - M_L of such nanocomposite compounds does not vary significantly with the addition of gelling agents.

4.2.5.2 Morphology

Figure 4.38 Figure 4.34 Figure 4.39, Figure 4.40, and Figure 4.41 illustrate SEM image of CT-B/CL/G3, B/CL/G3/O2, C/PC/O2, B/CL/G3/O5, and C/PC/O5 nanocomposite vulcanizates. Observation on SEM image of such nanocomposite vulcanizates and controls is described in Table 4.13.

In CT-B/CL/G3, the white color particles, believed to be gelling clusters produced by the combination of CTAB and SDS, are distributed throughout the rubber matrix. SEM images showed that OMMT dispersed by emulsion blending in B/CL/G3/O2 and B/CL/G3/O5 nanocomposite vulcanizates are better than compared to mechanical blending in C/PC/O2 and C/PC/O5 nanocomposite vulcanizates.

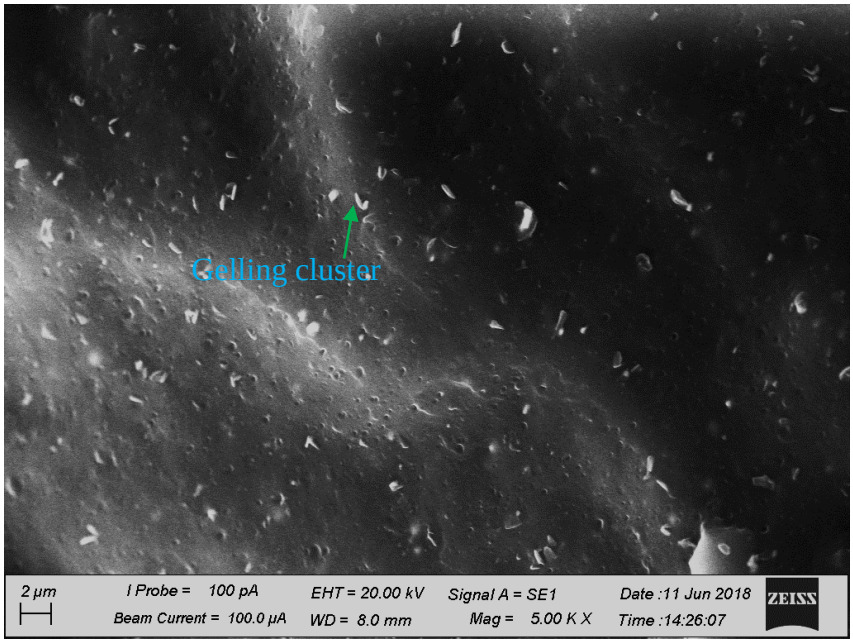

Figure 4. 38 SEM image of CT-B/CL/G3

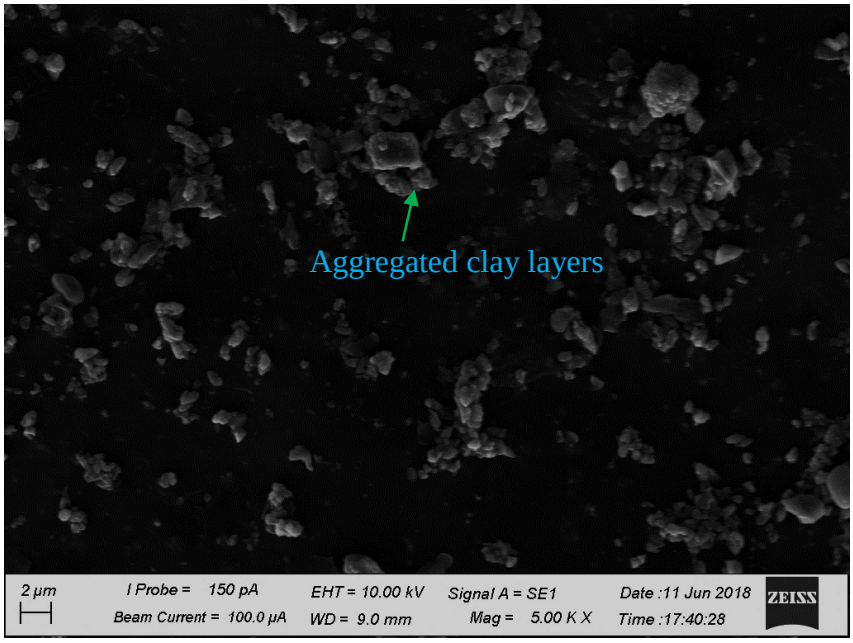

Figure 4. 39 SEM image of C/PC/O2 nanocomposite vulcanizate

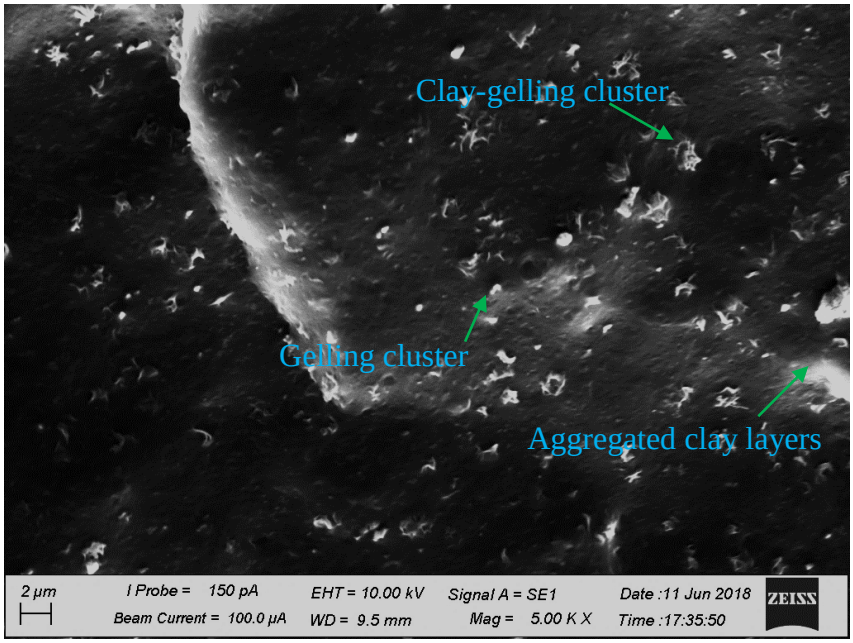

Figure 4. 40 SEM image of B/CL/G3/O5 nanocomposite vulcanizate

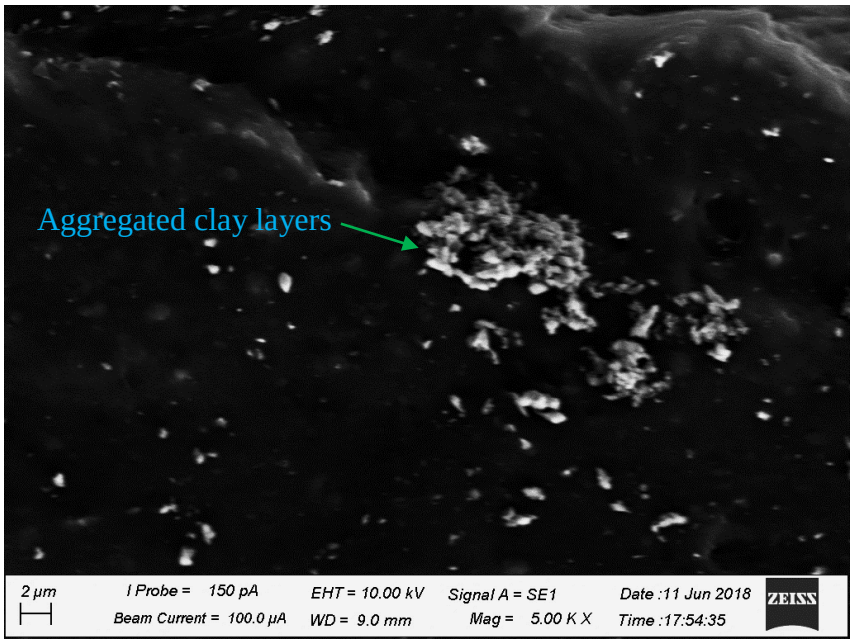

Figure 4. 41 SEM image of C/PC/O5 nanocomposite vulcanizate

Table 4. 13 Observations on SEM images of B/CL/G3 and MB- G nanocomposite vulcanizates

Nanocomposite	**Appearance**
CT-B/CL/G3	• No aggregated clay structures. • Presence of a large number of small gelling clusters. • Proper distribution of gelling clusters
B/CL/G3/O2	• Lower number of aggregated structures • Presence of very few number of clay-gelling clusters • Proper distribution of gelling clusters • Uneven distribution of clay structures
B/CL/G3/O5	• Higher number of aggregated structures • Presence of few clay-gelling clusters • Proper distribution of gelling clusters • Uneven distribution of clay structures
C/PC/O2 & C/PC/O5	• Higher number of aggregated structures • Higher number of layers in the aggregate • Uneven distribution of clay structures with separation from rubber phase

4.2.5.3 XRD analysis

Figure 4.42 presents the XRD diffractograms of SDS, CTAB, B/CL/G3/O2, B/CL/G3/O5, C/PC/O2, and C/PC/O5 nanocomposite vulcanizates and respective controls. SDS gives peaks at 2θ of 7.08, 4.80, and 9.32 while CTAB gives a peak at 2θ of 7.5. Three prominent peaks were appeared in the diffractograms of the CT-B/CL/G3, B/CL/G3/O2 nanocomposite vulcanizates at 2θ of 4.4, 6.6, and 8.2 and are due to the presence of excess CTAB and SDS which consist of different crystalline arrangements in NR. Some research also show that similar crystalline peaks with other chemicals found in vulcanized rubber (Fathurrohman et al., 2019; Kim et al., 2019).

The 2θ value slightly decreased from their original value with the effect of interaction between CTAB and SDS in the gelling cluster as proposed by figure 4.43. It shows those two surfactants are packed in a crystalline structure. The XRD observations are in agreement with the morphology of the nanocomposite vulcanizates characteristic peak corresponds to MMT at 2θ of 6.2 (Bao & LiGong., 2010) is not visible in the B/CL/G3/O2 nanocomposite vulcanizate, and it may be due to exfoliation of clay layers at low clay loading with excess surfactants. The diffractogram of the B/CL/G3/O5 nanocomposite vulcanizate shows the overlapping of a few peaks corresponding to aggregated clay structures and gelling clusters. The evidence, thus suggests the peaks corresponding to aggregate clay structure occurred in the nanocomposite at OMMT loading at 5 phr. XRD further confirms that confinement of OMMT structures is absent in B/CL/G3/O2 and B/CL/G3/O5 nanocomposite vulcanizates as discussed in B/CL/O nanocomposite vulcanizates (Section 4.2.2.2). Excess CTAB in rubber matrix in B/CL/G3 nanocomposite vulcanizate form zinc-ammine complexes hence CTAB in interlayer-gallery space is not necessary to use and confinement is restricted. C/PC/O2 and C/PC/O2 nanocomposite vulcanizates also produce a higher intensity peak corresponding to the intercalated OMMT layers.

Both CTAB and SDS can denature the protein in the latex. Charged polar segment of protein prefers to contact with the polar head group of CTAB while SDS directly contact with the protein by nonpolar hydrophobic tail (Chakraborty et al., 2008). When SDS is incorporated before addition of CTAB, SDS are adsorbed into denatured protein in latex and negative charge of rubber particles is increased. When CTAB is added later, those are adsorbed on the surface of protein by electrostatic interactions of polar head group and the hydrophobic interactions by hydrophobic tail. The ability of CTAB absorption on protein is further increased by pre-adsorbed SDS on surface of CTAB because CTAB and SDS form head to head electrostatic interactions. When excess CTAB is added, it forms a bilayer structure via tail to tail hydrophobic interactions with CTAB and SDS around first layer (Pongnara et al.,2008). All surfactants arrange in micelle structure to reduce surface tension on the surface of denatured proteins according to the proposed structure given by Figure 4.43. However the polar head group of CTAB and SDS could interact polar OMMT, but

aggregated clay stacks prevent proper interaction between clay layers and gelling agent, hence formation of clay-gelling clusters is minimum in B/CL/G3/O2 and B/CL/G3/O5 nanocomposite vulcanizates. The structure of the clay-gelling structure is suggested in figure 4.93 under Section 4.3.6.

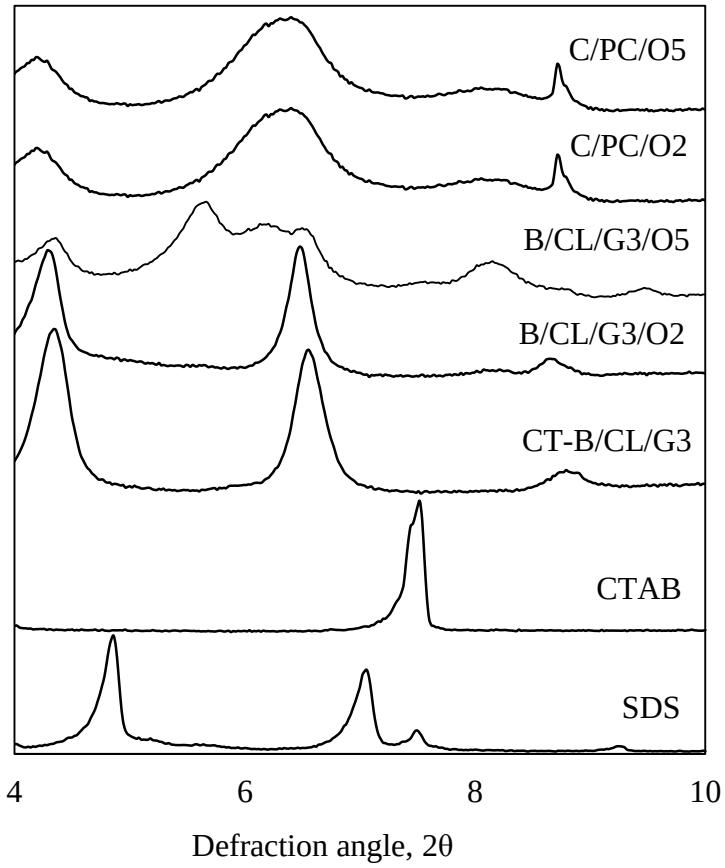

Figure 4. 42 XRD diffractogram of B/CL/G3 and C/PC nanocomposites vulcanizates

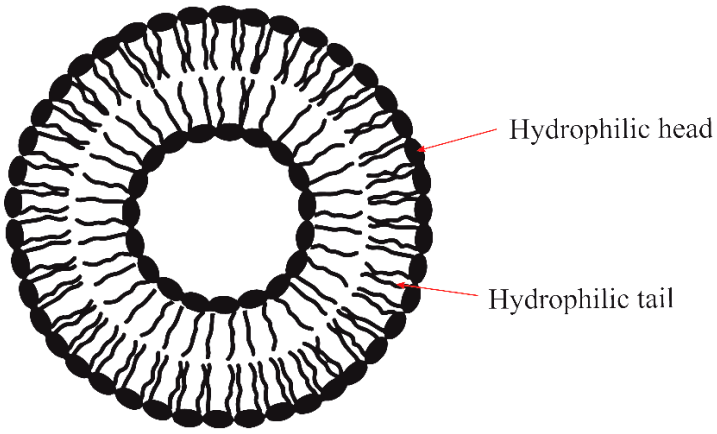

Figure 4. 43 Suggested structure for the gelling cluster

4.2.5.4 Crosslink density

Figure 4.44 presents the crosslink density of nanocomposite vulcanizates and bound rubber content of B/CL/G3 and C/PC nanocomposite vulcanizates. The crosslink density of B/CL/G3/O2, B/CL/G3/O5, and CT-B/CL/G3 nanocomposite vulcanizates are greater than that of C/PC/O2, C/PC/O5 nanocomposite vulcanizates and CT-C/PC vulcanizates due to presence of CTAB as a gelling agent in B/CL/G3 nanocomposite vulcanizates and thereby producing higher amount of zinc-ammine complexes.

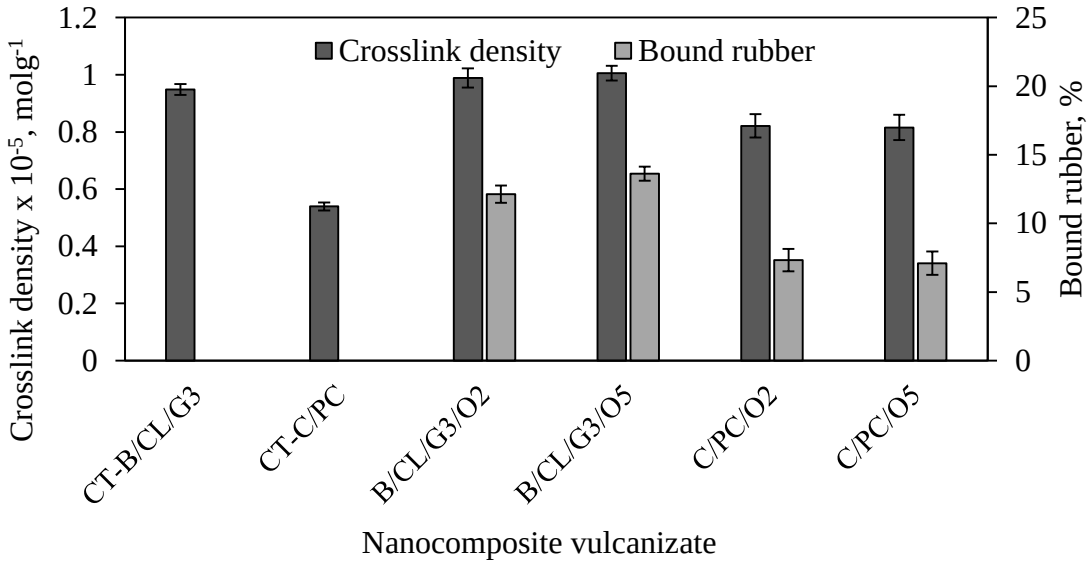

Figure 4. 44 Crosslink density and bound rubber content of B/CL/G3 and C/PC nanocomposite vulcanizates

However, prepared with OMMT, the crosslink densities of B/CL/G3/O2 and B/CL/G3/O5 nanocomposite vulcanizates do not show a significant increase compared to CT-B/CL/G3. It may be the reason that the dissolution amount of sol in B/CL/G3/O2 and B/CL/G3/O5 nanocomposite vulcanizates are similar with CT-B/CL/G3 due to the presence of gelling agent. The crosslink density of C/PC/O5 nanocomposite vulcanizate should be improved than that of C/PC/O2 nanocomposite vulcanizate due to increase of zinc ammine complexes, but an aggregation of OMMT at the higher loading may decrease the crosslink density as suggested by many research (Arroyo et

al., 2003; Vijaylekshmi et al., 2010). This shows that direct use of mechanical mixing is not a suitable method to incorporate OMMT into rubber even though it is widely used in many industrial-based applications.

4.2.5.5 Bound rubber content

Bound rubber content of B/CL/G3/O2 and B/CL/G3/O5 nanocomposite vulcanizates are greater than that of C/PC/O2 and C/PC/O5 nanocomposite vulcanizates (Figure 4.44). The improved compatibility between rubber and OMMT is increased in B/CL/G3/O2 and B/CL/G3/O5 nanocomposite vulcanizates by the use of a higher amount of CTAB under acid-free environment. CTAB forms electrostatic interactions with negatively charged rubber and MMT. Further, the long-chain hydrocarbon tail of CTAB increases the organophilicity of hydrophilic clay, thereby it increases rubber-clay interactions. The SDS also would balance those electrostatic interactions and increase the dispersion of OMMT. However, by neglecting the presence of higher content of CTAB and SDS as plasticizers, B/CL/G3/O5 nanocomposite vulcanizates show higher bound rubber content due to the presence of improved rubber-clay interactions than plasticizing effect. Instead, a significant reduction of bound rubber content is found in C/PC nanocomposite vulcanizates due to poor interaction between rubber and aggregated OMMT structures under limited CTAB content.

4.2.5.6 DMTA study

Figure 4.45 shows tan δ of B/CL/G3 and C/PC nanocomposite vulcanizates. T_g of CT-B/CL/G3 vulcanizate (-45.7 $^{\circ}$C) is greater than that of CT-C/PC vulcanizate (-47.9°C) by 1.2 $^{\circ}$C, which is due to high crosslink density given by the presence of a higher number of zinc-ammine complexes in CT-B/CL/G3 vulcanizate with the effect of CTAB. However, T_g of B/CL/G3/O2 nanocomposite vulcanizate (-48.8 $^{\circ}$C) is reduced compared to that of CT-B/CL/G3 vulcanizate. This evidence suggests that the presence of OMMT with the gelling agent lowers the T_g due to the plasticizing effect. However, further increase of OMMT loading in B/CL/G3/O5 nanocomposite vulcanizate, T_g (-46.1 $^{\circ}$C) is increased by 2.7 $^{\circ}$C compared to that of B/CL/G3/O2

nanocomposite vulcanizate with the effect of improved bound rubber content due to rubber-clay interactions.

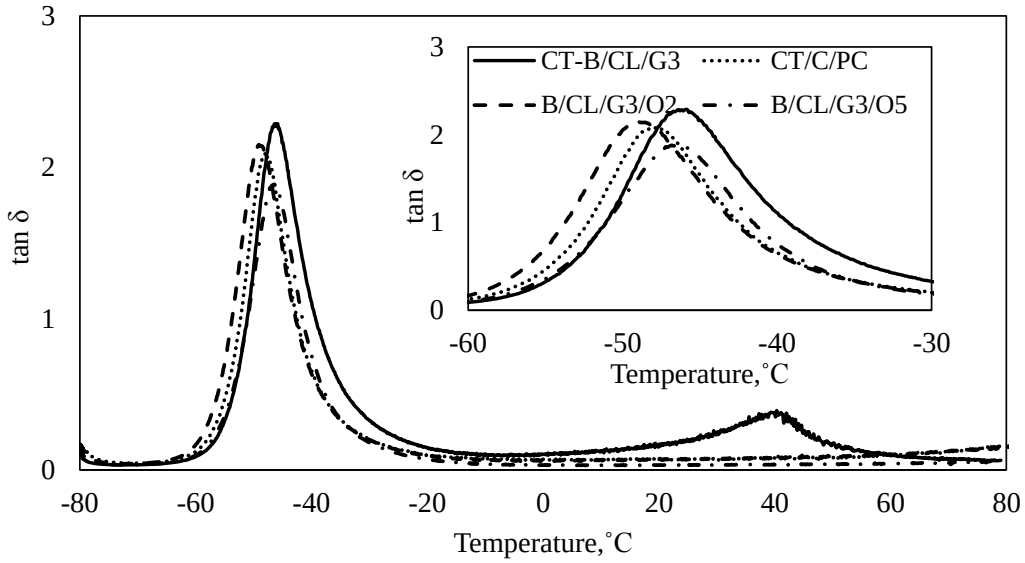

Figure 4. 45 tan δ of B/CL/G3 and C/PC nanocomposite vulcanizates

tan δ of B/CL/G3/O2 and B/CL/G3/O5 nanocomposite vulcanizates are reduced by the addition of OMMT due to the reinforcement effect, and the higher reduction is shown in B/CL/G3/O5 nanocomposite vulcanizates. It is also interesting to note that CT-B/CL/G3 vulcanizate gives secondary relaxation peak due to undisturbed ionic crosslink between CTAB and SDS in the gelling clusters. However, such interaction would be weakened by the effect of clay-gelling clusters when OMMT is incorporated

4.2.5.7 Mechanical properties

Stress-strain curves of B/CL/G3/O2, C/PC/O2 nanocomposite vulcanizates, and their controls are shown in Figure 4.46. CT-B/CL/G3 vulcanizate shows an initial increment of strain-induced crystallization than CT-C/PC, however, CT-B/CL/G3 vulcanizate breaks early at lower elongation before the maximum strain-induced crystallization was achieved. The greater strain-induced crystallization shown by CT-B/CL/G3 vulcanizate is due to the presence of higher non-rubber substances than CT-C/PC vulcanizate. Many works in the literature described that strain-induced crystallization is increased at higher non-rubber substances. The terminal isoprene

units in NR forms bonding network structure with proteins and phospholipids in the rubber particle membrane. This naturally occurring network plays a significant role in the orientation of isoprene molecule during deformation, hence strain-induced crystallization is improved. (Amnuaypornsri et al., 2008; Tosaka et al., 2009). It is believed that non-rubber substances were removed during the preparation of pale crepe while in the raw rubber processing stage. However, non-rubber content in NRL remains in CT-B/CL/G3 vulcanizate because the water was only removed by evaporation at the drying stage by the AFCC method. The tensile strength was not increased as expected from the result of strain-induced crystallization, which may be due to weak interphase build up between CTAB and SDS in gelling agent clusters (Figure 4.43) while stretching. Therefore, tensile strength and elongation at break of CT-B/CL/G3 vulcanizate are reduced by 35% and 55% respectively compared to those of CT-C/PC vulcanizate. Strain-induced crystallization of both B/CL/G3/O2 and C/PC/O2 nanocomposite vulcanizates show a similar trend but C/PC/O2 nanocomposite vulcanizate breaks early at comparative lower elongation to B/CL/G3/O2 nanocomposite vulcanizate due to presence of higher clay aggregation.

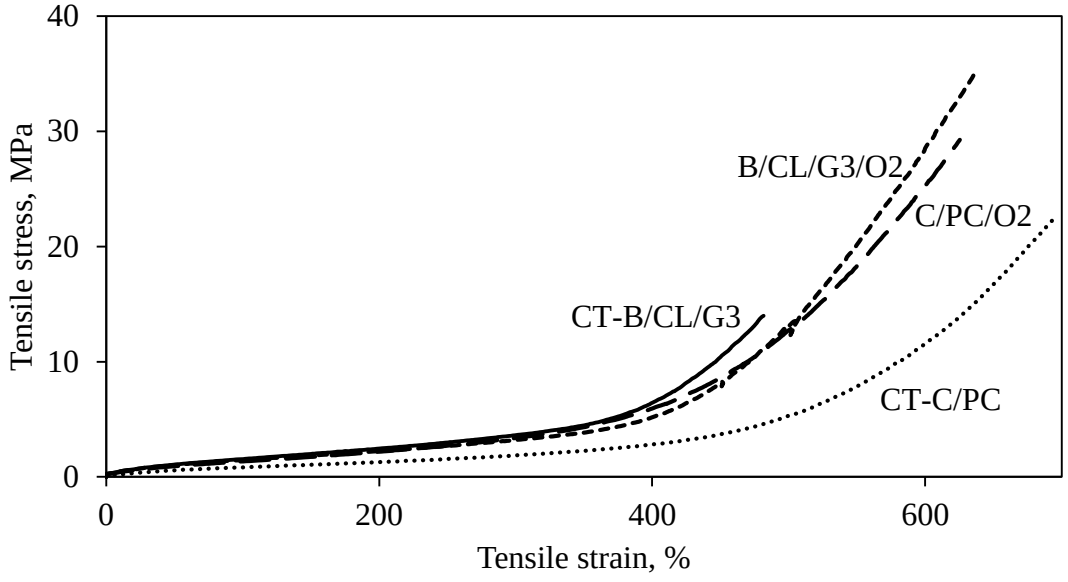

Figure 4. 46 Stress strain curves of B/CL/G3 and C/PC nanocomposite vulcanizates

Figure 4.47 presents the tensile strength, elongation at break, and mod 300% of C/PC nanocomposite vulcanizates and B/CL/G3 nanocomposite vulcanizates.

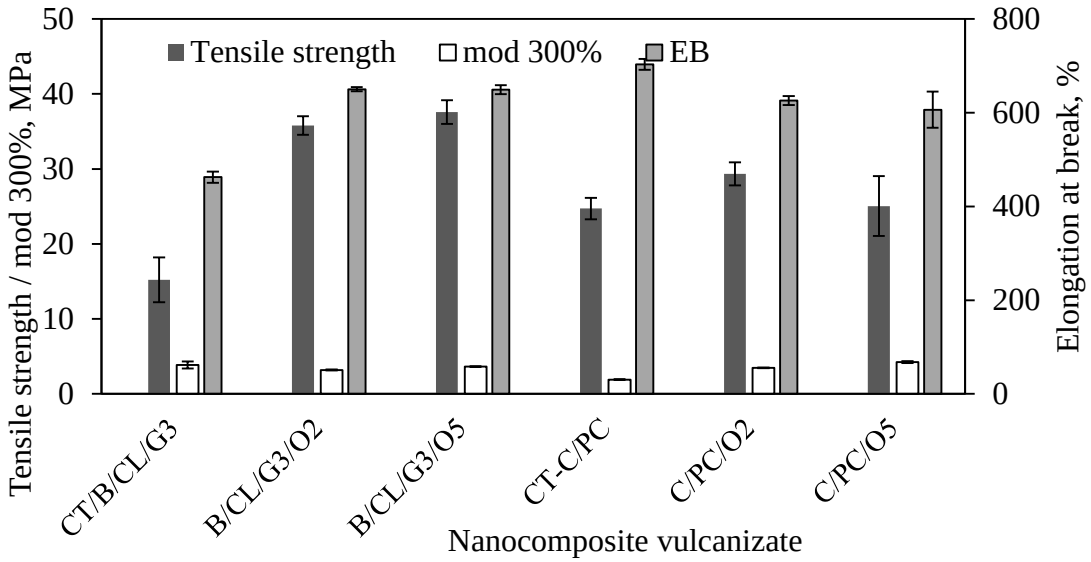

Figure 4. 47 Tensile properties of B/CL/G3 and C/PC nanocomposite vulcanizates

The tensile strength and elongation at break of CT-C/PC vulcanizate are 38.5% and 52% higher respectively, compared to those of CT-B/CL/G3 vulcanizate. The lower tensile strength and elongation at break are caused by fracture initiation at weak interphase between CTAB and SDS in gelling clusters. However, with the addition of OMMT, both B/CL/G3 and C/PC nanocomposite vulcanizates showed increased their tensile strength and elongation at break due to the reinforcement effect. It is interesting to point out that fracture initiation points in gelling clusters reduced by reinforcement of OMMT, would give a greater improvement of such properties in B/CL/G3 nanocomposite vulcanizate compared to that of CT-B/CL/G3. Further, the tensile strength of B/CL/G3/O2 and B/CL/G3/O5 nanocomposite vulcanizates are increased by 22% and 26% compared to that of C/PC/O2 and C/PC/O5 nanocomposite vulcanizates respectively. With the further addition of OMMT, at 5 phr, the tensile strength of B/CL/G3/O5 nanocomposite vulcanizate is further increased but the tensile strength of C/PC/O5 nanocomposite vulcanizate is reduced. It shows that the presence of a higher amount of aggregated structures decreases the tensile strength and elongation at break in C/PC/O5 nanocomposite vulcanizate than that of C/PC/O2 nanocomposite vulcanizate. However, The tensile strength of B/CL/G3/O5 nanocomposite vulcanizate is comparatively high due to better dispersion of OMMT with minimum aggregation thereby reinforcement is further increased. This evidence

shows that the preparation of nanocomposites by AFCC method in B/CL/G3 nanocomposite vulcanizates is more effective than for nanocomposite vulcanizates prepared by mechanical mixing. This effect also decreases elongation at break in C/PC/O5 nanocomposite vulcanizate than C/PC/O2 nanocomposite vulcanizate with the addition of OMMT but gives similar elongation at break values in both B/CL/G3/O2 and B/CL/G3/O5 nanocomposite vulcanizates which are slightly greater than C/PC/O2 and C/PC/O5 nanocomposite vulcanizates. The improved slippery action of OMMT with the effect of gelling agent in B/CL/G3/O2 and B/CL/G3/O5 nanocomposite vulcanizates may also increase the elongation at break. However, B/CL/G3/O5 nanocomposite vulcanizate shows the highest tensile strength (37.6 MPa), and CT-C/PC vulcanizate shows the highest elongation at break (703%) among in B/CL/G3 and C/PC nanocomposite vulcanizates. It is well known that gum rubber gives better elongation at break without incorporation of filler, hence CT-C/PC vulcanizate exhibits higher elongation at break.

The mod 300% of CT-B/CL/G3 vulcanizate is 103% greater than that of CT-C/PC vulcanizate due to higher crosslink density in CT-B/CL/G3 vulcanizate. Interestingly, with the addition of OMMT, the mod 300% of B/CL/G3/O2 and B/CL/G3/O5 nanocomposite vulcanizates decrease than that of C/PC/O2 and C/PC/O5 nanocomposite vulcanizates, which may be due to an increased plasticization effect by the gelling agent in B/CL/G3 nanocomposite vulcanizates. However that increment of mod 300% for B/CL/G3/O5 nanocomposite vulcanizate is 14% greater than that of B/CL/G3/O2 nanocomposite vulcanizate. For C/PC/O5 nanocomposite vulcanizate, mod 300% is 22% greater than that of C/PC/O2 nanocomposite vulcanizate. It shows that a higher amount of aggregated structures and the absence of gelling agents in C/PC nanocomposite vulcanizates may increase the mod 300%, even though controls of those behave differently.

Figure 4.48 illustrates the tear strength and hardness of B/CL/G3, and C/PC nanocomposite vulcanizates and its controls. The tear strength of CT-B/CL/G3 vulcanizate is 37% greater than that of CT-C/PC vulcanizate due to higher crosslink density in CT-B/CL/G3 vulcanizate. Propagation of tear path does not break at weaker interphases in gelling clusters, whereby it travels between such interphases for longer distances to obtain moderately higher tear strength. Both nanocomposites show higher

tear strength than respective controls by means of better dispersion of clay. It is further confirmed that tear strength of B/CL/G3/O5 nanocomposite vulcanizate shows higher tear strength (42.7 N/mm), which is 20% greater than that of C/PC/O5 nanocomposite vulcanizate, and the B/CL/G3/O2 nanocomposite vulcanizate is 26% greater than that of C/PC/O2 nanocomposite vulcanizate. Higher values of crosslink density, bound rubber content, and plasticizing effect of B/CL/G3 nanocomposite vulcanizates impart higher tear strength than C/PC nanocomposite vulcanizates.

The hardness of CT-B/CL/G3 vulcanizate is 12.8% greater than that of CT-C/PC vulcanizate (Figure 4.48) and is mainly due to the increase of crosslink density. Hardness is further increased by the addition of OMMT in both nanocomposite vulcanizates than their corresponding controls by filler effect. B/CL/G3/O5 nanocomposite vulcanizate shows the highest hardness (49 IRHD), which is 11.3% higher than that of C/PC/O5 nanocomposite vulcanizate. The hardness of B/CL/G3/O2 nanocomposite vulcanizate is 9.3% higher than that of C/PC/O2 nanocomposite vulcanizate. These results imply that hardness is not reduced by the plasticizing effect with the addition of gelling agents, but is due to an increase of crosslink density and bound rubber content.

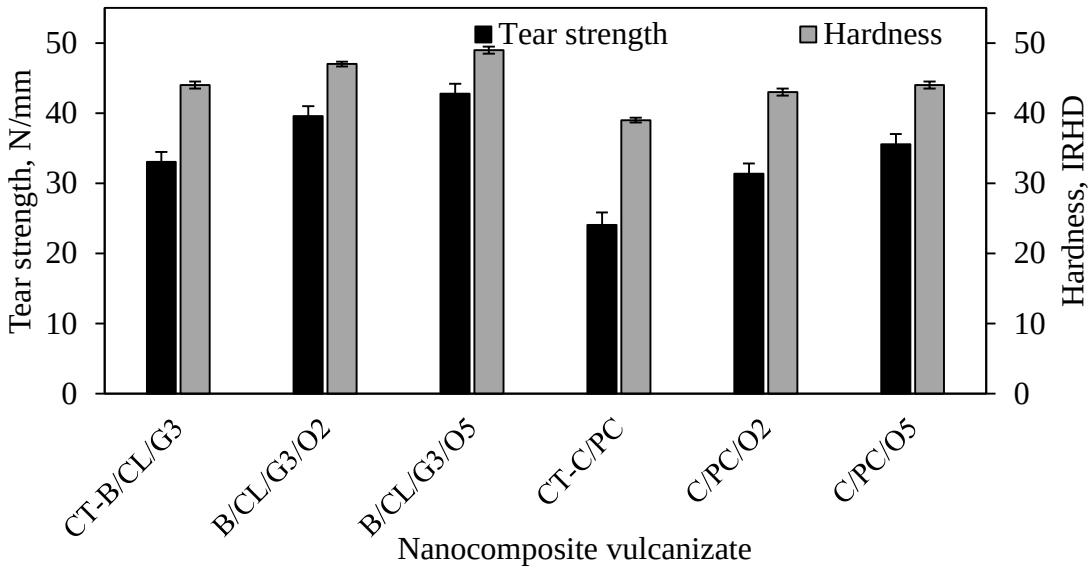

Figure 4. 48 Tear strength and hardness of B/CL/G3, and C/PC nanocomposite vulcanizates

4.2.5.8 Abrasion loss

Figure 4.49 shows the abrasion loss of B/CL/G3 and C/PC nanocomposite vulcanizates and their controls. B/CL/G3/O2, B/CL/G3/O5, C/PC/O2, and C/PC/O5 nanocomposite vulcanizates and controls do not show a general pattern of abrasion loss. This implies the improved rubber-clay interactions in both nanocomposite vulcanizates are not sufficiently strong to reduce abrasion loss in the study of B/CL/G3 and C/PC nanocomposite vulcanizates.

4.2.5.9 Ageing properties

Figure 4.50 provides the PRV of tensile strength, mod 300%, and elongation at break in B/CL/G3 and C/PC nanocomposite vulcanizates after thermal ageing. The mechanical properties of aged CT-B/CL/G3 nanocomposite vulcanizate and CT-C/PC vulcanizate are greater than that of un-aged samples.

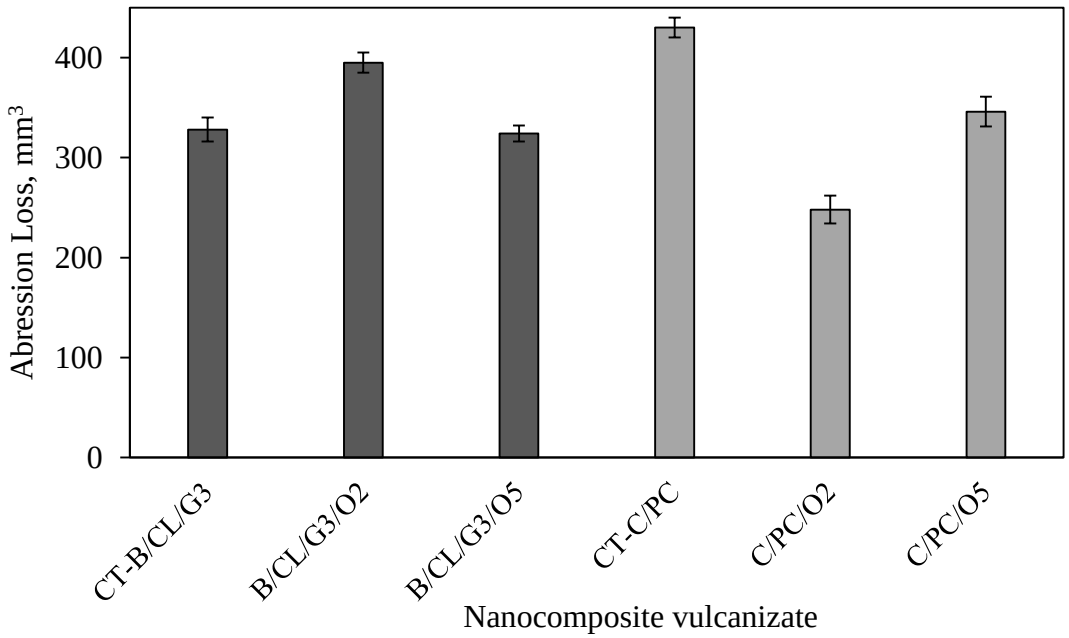

Figure 4. 49 Abrasion loss of B/CL/G3 and C/PC nanocomposite vulcanizates

The mechanical properties mainly depend on the thermal stability of the rubber during ageing. The thermal stability is reduced due to a decrease in material rigidity and an increase in chain mobility described in the literature (Sharma et al., 2015). The increasing amount of plasticizers decreases the material rigidity (Marcin et al., 2019)

and increase flexibility and chain mobility (Vieira et al., 2011). In the presence of higher OMMT loading and absence of surfactants, C/PC/O5 nanocomposite vulcanizate shows better aging resistance compared to B/CL/G3/O2, and B/CL/G3/O5 nanocomposite vulcanizates. However, PRV of all samples show greater than 90% due to better aging resistant compared to other studies in the literature (Caril et al., 2011)

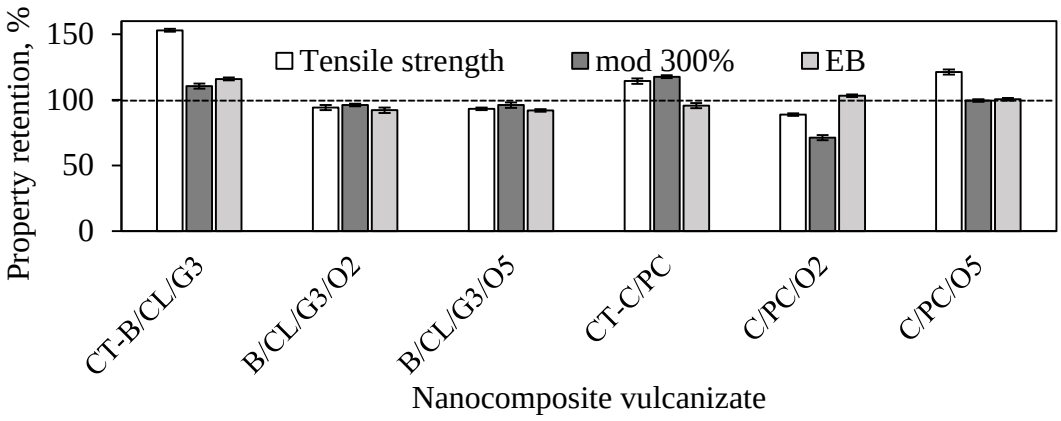

Figure 4. 50 Ageing properties of CT-B/CL/G3 and CT-C/PC vulcanizates

The mechanical properties of B/CL/G3 nanocomposite vulcanizates were improved after solving the problem of surface drying with the use of gelling agent G3. It is confirmed that the gelling agent has no significant adverse effect on decreasing the mechanical properties.

4.3 NR-Clay nanocomposites with modified OMMT and NRL

The OMMT modified with the TESPT silane coupling agent (OMMT-S) is characterized and discussed in Section 4.3.1. The effect of OMMT-S on properties B/CL/G3 nanocomposite vulcanizates (B/CL/G3/OS2 and B/CL/G3/OS5) is discussed in Section 4.3.2 and is compared with B/CL/G3 nanocomposite vulcanizates (B/CL/G3/O2 and B/CL/G3/O5) prepared with OMMT. Properties of nanocomposite vulcanizates prepared with OMMT-S using different processing methods, by mechanical mixing (C/PC/OS2 and C/PC/OS5) and emulsion blending (B/CL/G3/OS2 and B/CL/G3/OS5), are discussed in Section 4.3.3. Effect on SI grafted NR on properties of nanocomposite vulcanizates is discussed in Section 4.4.4 as a comparative study between B/gL/G3 nanocomposite vulcanizates (B/gL/G3/OS2 and

B/gL/G3/OS5) and B/CL/G3 nanocomposite vulcanizates (B/CL/G3/OS2 and B/CL/G3/OS5). A structure for nanocomposite vulcanizates is proposed in Section 4.3.5 which mechanism is proposed in Section 4.3.6.

4.3.1 Characterization of OMMT-S

Figure 4.51 shows the FTIR spectra of OMMT and Table 4.14 describes its peak assignment.

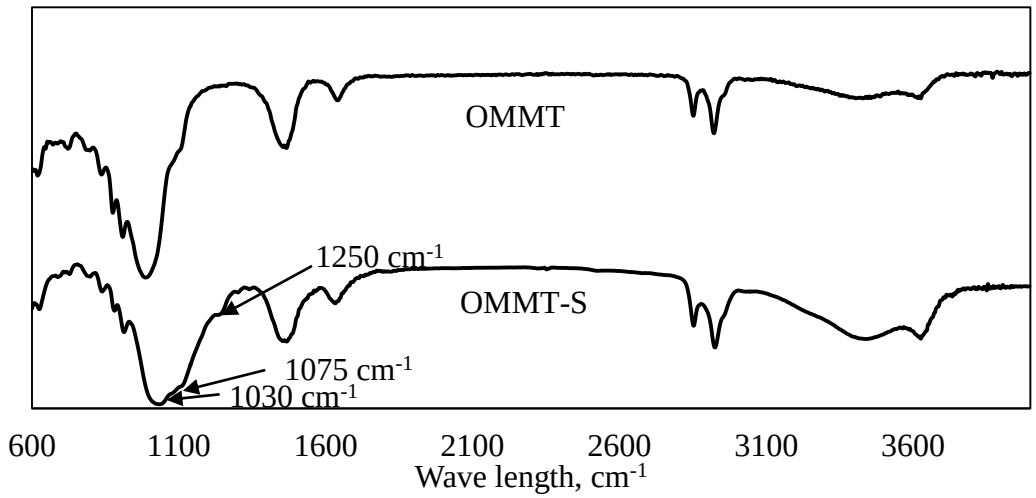

Figure 4. 51 FTIR spectrum of CTAB, MMT, OMMT and OMMT-S

Table 4. 14 Peak assignment of the FTIR spectrum for OMMT-S

Wave number (cm^{-1})	Structure	Reference
1250	Si-CH_2 deformation	Bellamy., 1975
1075	Si-O-C stretching vibration	Tan et al., 2012
1030	Si-O-Si streching vibration	Sengloyluank etal., 2017

Some studies stated that the grafting of TESPT on the surface of MMT could be identified in absorption peaks at 2925 and 2852 cm^{-1} corresponding to C-H stretching vibrations (Kim et al, 2011). Such a method may not valid for OMMT due to appearance of same peak for CTAB (Viana et al., 2012). A strong absorption peak at 1030 cm^{-1} is observed, corresponding to the Si-O-Si stretching vibration of the silicate. (Tan et al., 2012), which also could not be used to confirmation of grafting due to the appearance of the same peak in OMMT. The appearance of the absorption

peak of Si-O-C stretching (Sengloyluan et al., 2017) and Si-CH_2 deformation in TESPT (Bellamy., 1975) confirm the grafting of TESPT on OMMT in OMMT-S.

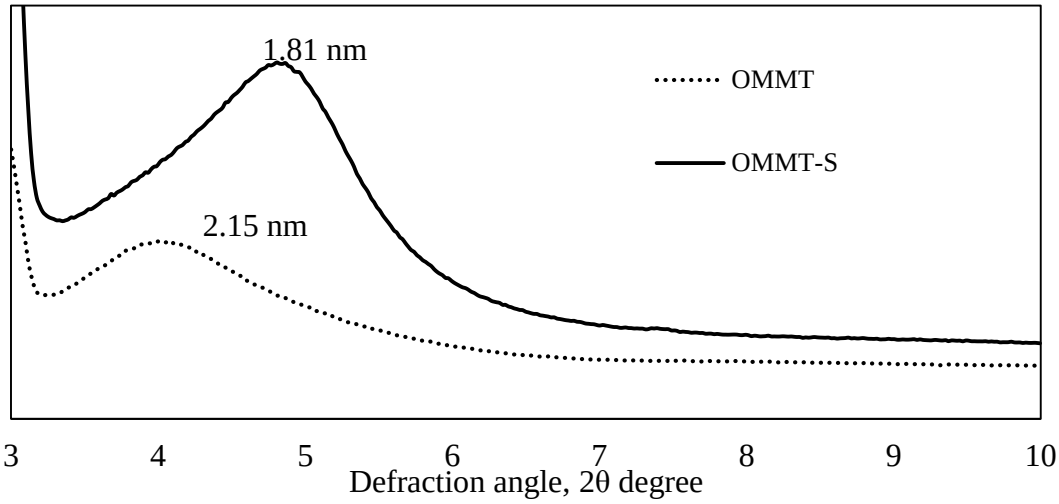

Figure 4. 52 XRD diffractogram of OMMT and OMMT-S

Modification of OMMT to OMMT-S is successful and is confirmed by the shift of diffraction angle to high value. After modification, the interlayer distance of OMMT is reduced from 2.15 nm into 1.81 nm corresponding to their intrinsic peaks at diffraction angles of 4.11 and 4.88 degrees respectively. However, the broad and higher intense peak of OMMT-S represents peaks for interlayer-gallery spaces of OMMT as well. The other study also described a similar effect and the reason for the lower interlayer-gallery space of silane grafted organoclay compared to that of organoclay due to formation of chemical bonding in silane grafted organoclay (Bharadwaj, et al, 2013).

4.3.2 The effect of OMMT-S on properties of nanocomposite vulcanizates

The impact of OMMT-S on properties of B/CL/G3/OS2 (2 phr) and B/CL/G3/OS5 (5 phr) nanocomposite vulcanizates is compared with that of OMMT in B/CL/G3/O2 (2 phr) and B/CL/G3/O5 (5 phr) nanocomposite vulcanizates (Section 3.2.7.8). The properties include cure characteristics (Section 4.3.2.1), morphology (Section 4.3.2.2), XRD analysis (Section 4.3.2.3), viscosity (Section 4.3.2.4), bound rubber content (Section 4.3.2.5), crosslink density (Section 4.3.2.6), DMTA (Section 4.3.2.7), mechanical properties (4.3.2.8), abrasion loss (Section 4.3.2.9), and ageing

properties (Section 4.3.2.10). OMMT-S is produced by grafting the TESPT on to OMMT (Section 3.2.5.3) to reduce the surface energy of clay and to increase rubber-clay interactions.

4.3.2.1 Cure characteristics

Figure 4.53 shows $t_{s2}, t_{90,}$ and CRI of B/CL/G3 nanocomposite compounds. Figure 4.54 and 4.55 illustrate activation energy and M_H-M_L of B/CL/G3 nanocomposite compounds. t_{s2} and t_{90} of B/CL/G3/OS2 and B/CL/G3/OS5 nanocomposite compounds show similar values with that of B/CL/G3/O2 and B/CL/G3/O5 nanocomposite compounds. It shows that grafting TESPT on OMMT does not affect cure characteristics. As a result of that CRI of those nanocomposite compounds show similar values. However, it was evident in other research that silica treated by TESPT interacts with polar curatives and delays t_{s2} (Lapattananon et al., 2011). Another research described those cure properties depend on TESPT according to the type of vulcanizing system. In the presence of TESPT, the efficient vulcanizing system increases cure time but conventional vulcanizing system has no significant effect on cure time (Sae-oui et al, 2005). The result of cure properties of the current section shows that the used semi efficient vulcanization system has also no effect on cure properties.

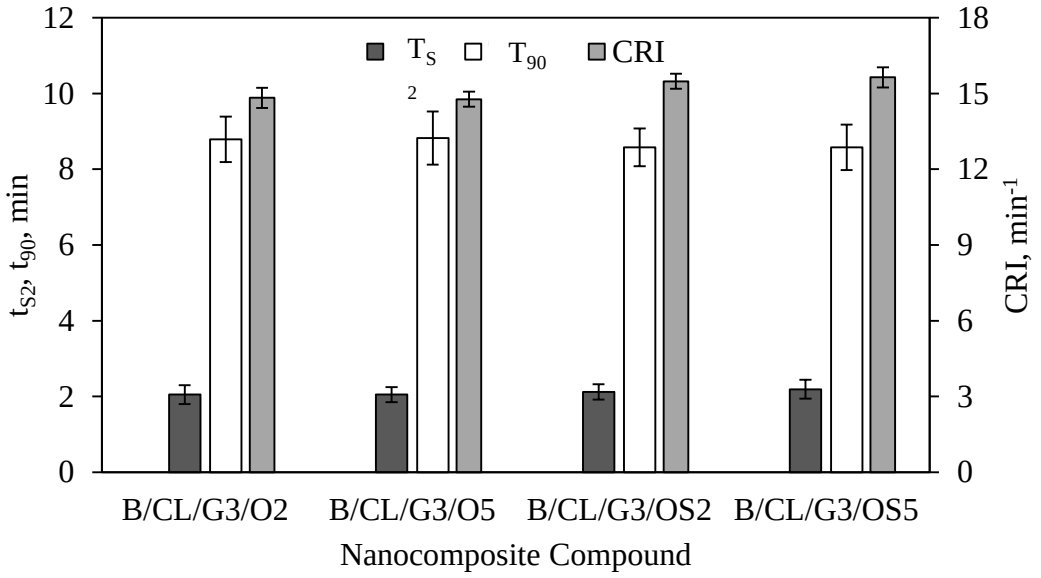

Figure 4. 53 t_{s2}, t_{90}, and CRI of B/CL/G3 nanocomposite compounds

The activation energy of vulcanization reaction in B/CL/G3/OS2 and B/CL/G3/OS5 nanocomposite compounds is slightly greater than the respective B/CL/G3/O2 and B/CL/G3/O5 nanocomposite compounds (Figure 4.53). The siloxane network created by OMMT-S would interact with polar curative, thereby increasing the activation energy. However, the small difference of such activation energies shown by B/CL/G3 nanocomposite compounds has no significant effect on change of cure characteristics.

The higher amount of clay layers having lower surface energies and better dispersion of clay in rubber matrix in B/CL/G3/OS5 nanocomposite compound may show slightly higher M_H-M_L (Figure 4.55) than the other three nanocomposite compounds. Surface energy is believed to be reduced by the siloxane network in OMMT-S, whereas the presence of a higher amount of silanol groups in OMMT increases the surface energy. Silanols (Si-O-H) group has relatively high acidic hydrogen because Si-O bond increases the polarity of O-H bond. The bond between the silicon and oxygen is σ and pπ-dπ in nature which would increase the polarity of O-H in silanol and increases the acidity and surface energy (Lebrun et al., 1989). However acidity and surface energy of silanol are decreased when silicon substituents such as siloxane network is grafted to OMMT. The grafted siloxane network increases the inductive effect +I on silicon atom in terminal silanol group (Matwiyoff et al., 1965). As a result of that OMMT-S separates individual clay layers from clay stacks efficiently than OMMT due to the reduction of surface energy.

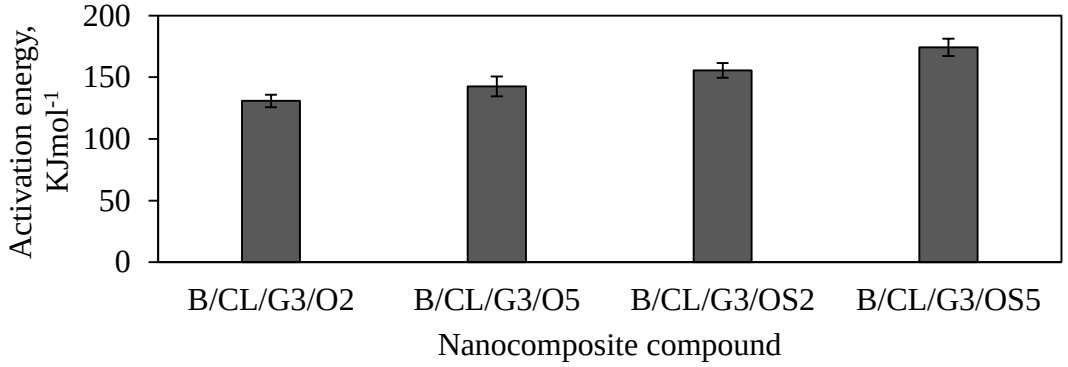

Figure 4. 54 Activation energy of vulcanization in B/CL/G3 nanocomposite compounds

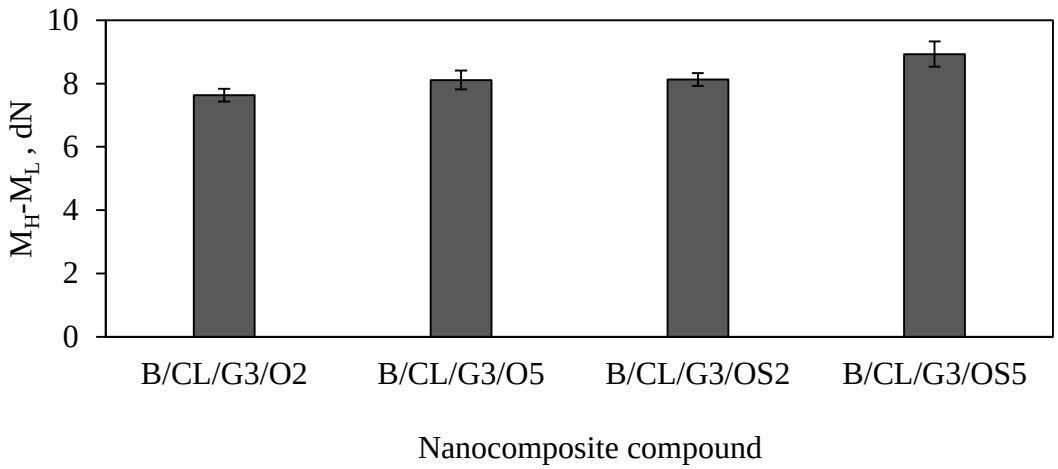

Figure 4. 55 M_H-M_L of B/CL/G3 nanocomposite compounds

4.3.2.2 Morphology

Figure 4.56 shows the SEM image of B/CL/G3/OS2 nanocomposite vulcanizate, while Figure 4.57 shows that of B/CL/G3/OS5 nanocomposite vulcanizate. B/CL/G3/O2 (Figure 4.34) and B/CL/G3/O5 (Figure 4.40) nanocomposite vulcanizates have randomly distributed large clay stacks.

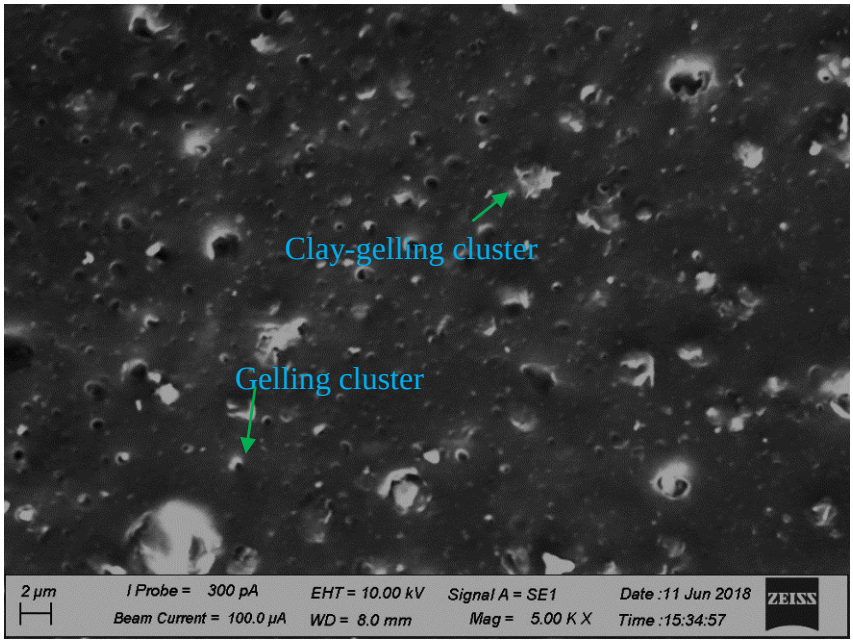

Figure 4. 56 SEM graph of B/CL/G3/OS2 nanocomposite vulcanizate

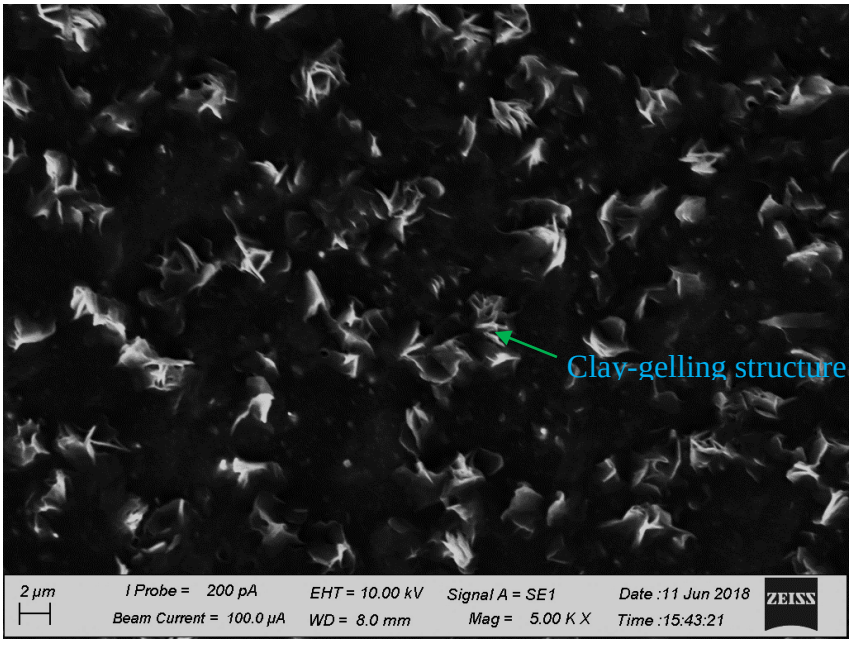

Figure 4. 57 SEM graph of B/CL/G3/OS5 nanocomposite vulcanizate

Observation of SEM image of B/CL/G3/O2 and B/CL/G3/O5 nanocomposite vulcanizates is described in Table 4.12 and observation of B/CL/G3/OS2 and B/CL/G3/OS5 nanocomposite vulcanizates are described in Table 4.15. The formation of large clay stacks in B/CL/G3/OS2 and B/CL/G3/OS5 nanocomposite vulcanizates are limited due to low surface energies and higher separation of clay layers, attributing to the effect of grafted TESPT. The separated smaller clay structures are more finely distributed in the entire rubber matrix, and apparently shown in B/CL/G3/OS5 nanocomposite vulcanizate, having OMMT-S loading at 5 phr. Gelling clusters are visible in B/CL/G3/O2 and B/CL/G3/O5 nanocomposite vulcanizates but less in B/CL/G3/OS2 and B/CL/G3/OS5 nanocomposite vulcanizates because they combine with clay and form clay gelling structures.

This observation confirmed that the presence of a higher number of better dispersed OMMT-S layers (confirmed by XRD in Section 4.3.2.3) finely distributed in the rubber matrix and disturb the arrangement of gelling clusters with the formation of the higher number of clay-gelling structures in B/CL/G3/OS5 nanocomposite. The polar positive charged head of CTAB may interact with polar negatively charged clay layers and form clay-gelling structures. The structure of a randomly distributed clay-gelling structure is suggested in Figure 4.95 in section 4.4.

Table 4. 15 Evaluation of SEM images of B/CL/G3 nanocomposite vulcanizates

Nanocomposite	Appearance
B/CL/G3/OS2	• Presence significant amount of clay-gelling clusters • Proper distribution of gelling clusters • Uneven distribution of clay structures
B/CL/G3/OS5	• Presence higher number of clay-gelling structures • limited distribution of gelling clusters • Even distribution of clay-gelling structures

4.3.2.3 XRD analysis

Figure 4.58 presents the XRD diffractograms of B/CL/G3 nanocomposite vulcanizates. Both nanocomposite vulcanizates prepared with 2 phr of OMMT (B/CL/G3/O2) and 2 phr of OMMT-S (B/CL/G3/OS2) show same peaks due to presence of crystalline structures of gelling agent. It shows that peaks for clay structures are absent because clay layers are aligned in crystalline structures or exfoliated at lowest loading. However, both peaks related to crystalline and aggregated clay structures appear in B/CL/G3/O5 nanocomposite vulcanizate, the crystalline peak and aggregated clay structures are minimized in B/CL/G3/OS5, may be due to presence of higher amount of well dispersed OMMT-S clay layers as clay-gelling structures, evenly distributed in the entire rubber matrix, disturb the crystalline structures. This effect is visible in the SEM image in Figure 4.57 as well.

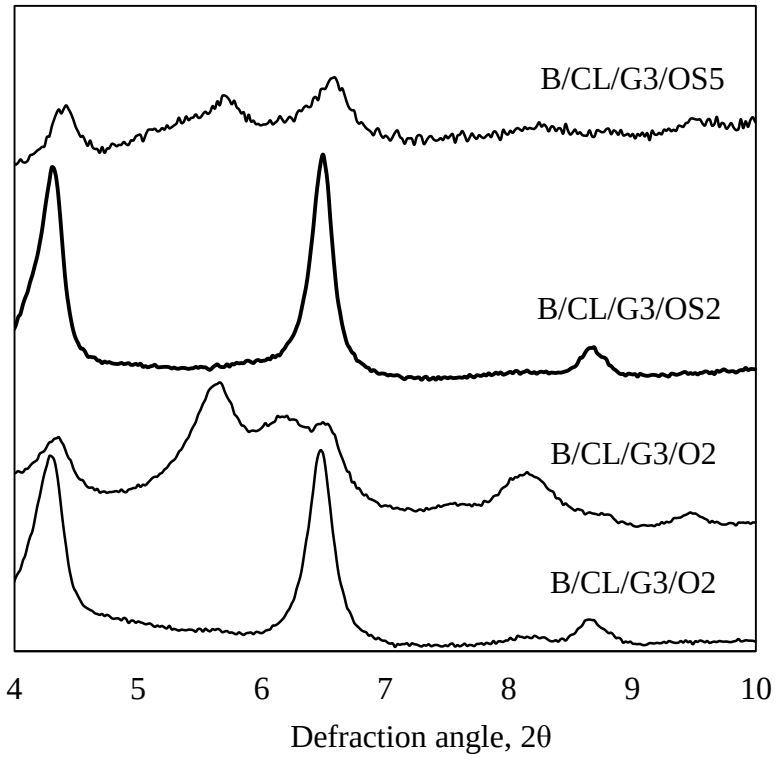

Figure 4. 58 XRD diffractograms of B/CL/G3 nanocomposite vulcanizates

4.3.2.4 Viscosity

Figure 4.59 presents the viscosity of B/CL/G3 nanocomposite prepared at 5 phr of OMMT and OMMT-S loading. The viscosity of B/CL/G3/OS5 nanocomposite is lower than that of B/CL/G3/O5 nanocomposite due to a better dispersion of higher amounts of smaller OMMT-S as stacks in the rubber matrix. A similar effect in TESPT modified silica is found in other studies (Goerl et al., 1997; Reuvekamp et al., 2002).

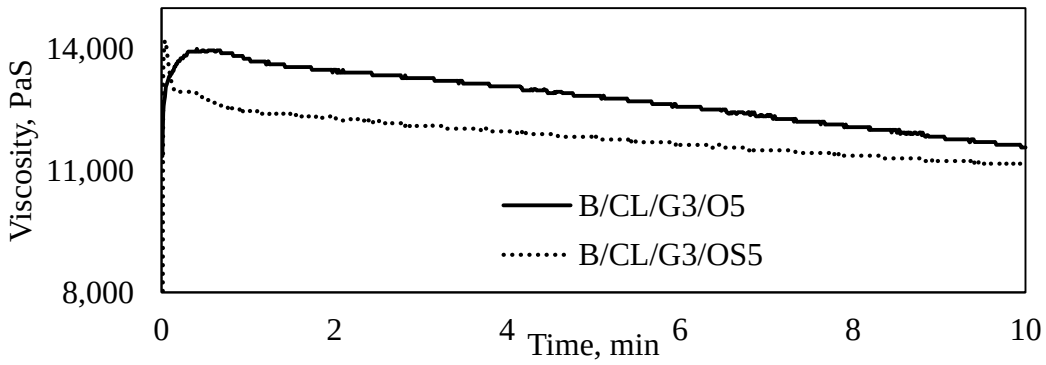

Figure 4. 59 Viscosity of B/CL/G3 nanocomposites

4.3.2.5 Bound rubber content

Figure 4.60 illustrates the bound rubber content of B/CL/G3 nanocomposites. The bound rubber contents of B/CL/G3/OS2 and B/CL/G3/OS5 nanocomposites are greater than that of B/CL/G3/O2 and B/CL/G3/O5 nanocomposites.

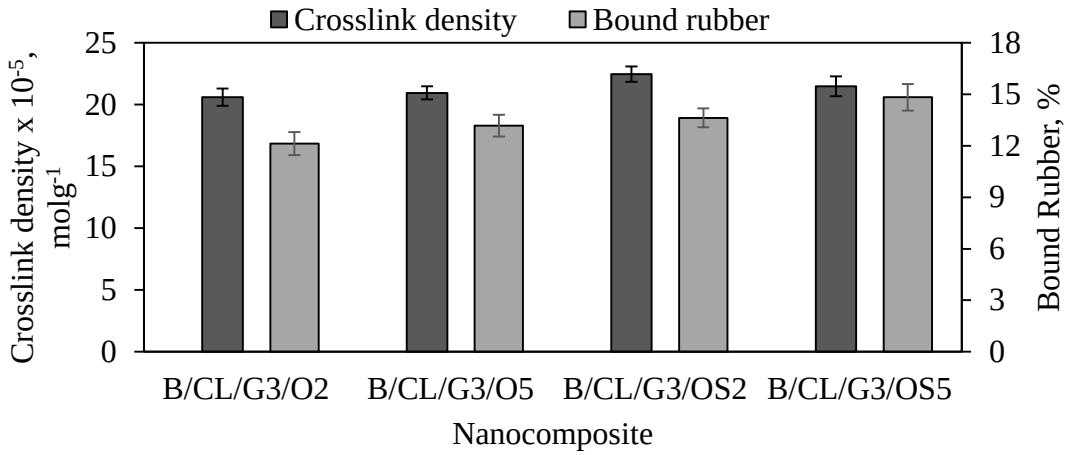

Figure 4. 60 Bound rubber content of B/CL/G3 nanocomposites and crosslink density of B/CL/G3 nanocomposite vulcanizates

It indicates that the grafted TESPT in B/CL/G3/OS2 and B/CL/G3/OS5 nanocomposites cause extra rubber-clay interactions. The interactions created between siloxane bonds in hydrolyzed TESPT and the silanol group in clay layers improve the rubber-clay compatibility. Besides, sulphur crosslinks occurred between rubber macromolecules and grafted TESPT, further increases the rubber-clay interactions (Sae-oui et al., 2005). The principal advantage of the use of TESPT grafted OMMT-S in the current study is that, it reduces the surface energy of OMMT, and it disperses OMMT-S evenly in the rubber matrix. The finely distributed higher number of clay-gelling structures in the rubber phase increases bound rubber content in B/CL/G3/OS5 nanocomposite compared to the other three nanocomposites.

4.3.2.6 Crosslink density

The crosslink densities of B/CL/G3/OS2 and B/CL/G3/OS5 nanocomposite vulcanizates are higher than those of B/CL/G3/O2 and B/CL/G3/O5 nanocomposite vulcanizates (Figure 4.60).

It demonstrates that TESPT influences the increase of rubber-clay interactions by formation of sulphur crosslinks between clay and NR during the vulcanization stage of B/CL/G3/OS2 and B/CL/G3/OS5 nanocomposite vulcanizates because TESPT donates active sulphur radicals to form sulphidic bonds between rubber and OMMT-S. The crosslink density of B/CL/G3/OS5 nanocomposite vulcanizate is slightly reduced compared to B/CL/G3/OS2 nanocomposite vulcanizate, which may be due to an effect of better dispersion of higher number of clay-gelling structures, and hence it may reduce the formation of sulphur crosslinks between rubber macromolecules. However, a study reported that a silane coupling agent could react with the vulcanization curatives (Arrighi et al., 2003), and decrease the crosslink density. Moreover, some literature discusses both self-condensation of TESPT and steric hindrance for vulcanization in the excess use of silane (Sae-Oui et al., 2006). Therefore, silane agents are mixed into clay filled rubber at the compounding stage before the addition of curatives. Another study described that silane agents would react with non-rubber content in rubber (Sarkawi et al., 2013) hence direct addition of silane agents is not effective. In the current investigation, these undesirable effects are prevented by grafting the TESPT on OMMT before incorporation into rubber and hence clay layers are dispersed in rubber more effectively.

4.3.2.7 DMTA study

Figure 4.61 shows the tan δ versus temperature curve of B/CL/G3 nanocomposite vulcanizates. The study in Section 4.2.5 shows that T_g increases in B/CL/G3/O5 nanocomposite vulcanizate (-46.1 $^{\circ}$C) than B/CL/G3/O2 nanocomposite vulcanizate (-48.8 $^{\circ}$C) with the addition of OMMT. When OMMT is replaced by OMMT-S at 2 phr clay loading, T_g of B/CL/G3/OS2 nanocomposite vulcanizate (-46.1 $^{\circ}$C) is increased by 2.7 $^{\circ}$C than that of B/CL/G3/O2 nanocomposite vulcanizate due to the effect of improved rubber-clay interactions. This shows that the change of T_g by modification of TESPT is effective in lower clay loading. B/CL/G3/O5, and B/CL/G3/OS5 nanocomposite vulcanizates show similar T_g values around -46.1 $^{\circ}$C, revealing that modification of TESPT has no effect on T_g at higher loading (5 phr). The tan δ of B/CL/G3/O2 nanocomposite vulcanizate is similar to B/CL/G3/OS2 nanocomposite vulcanizate and B/CL/G3/O5 nanocomposite vulcanizate is similar

with B/CL/G3/OS5 nanocomposite vulcanizate due to similar reinforcement given by similar clay loading.

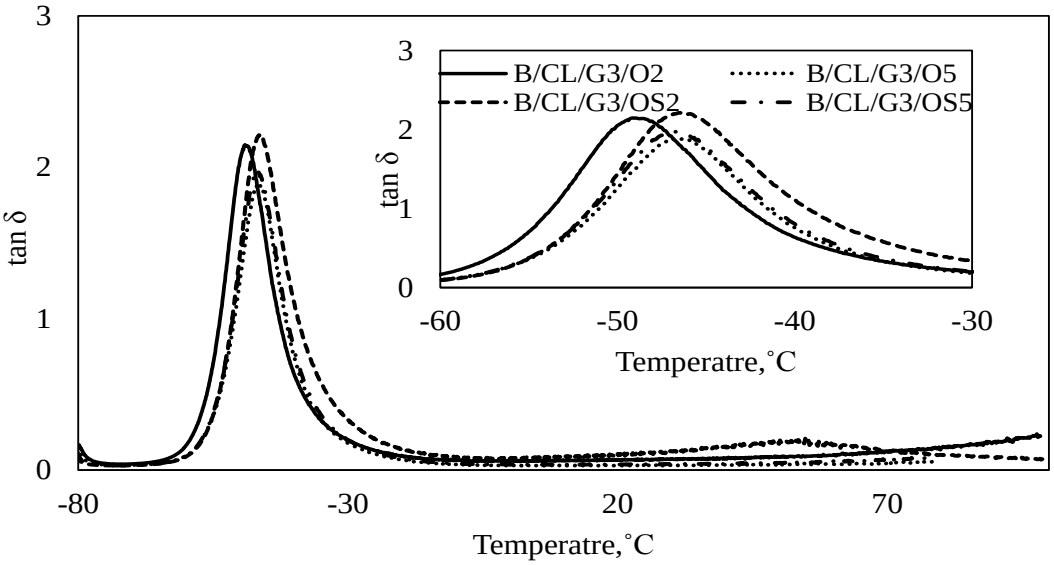

Figure 4. 61 tan δ of B/CL/G3 nanocomposite vulcanizates

T_g of B/CL/G3/OS2 and B/CL/G3/OS5 nanocomposite vulcanizates are almost similar but tan δ of B/CL/G3/OS5 nanocomposite vulcanizate is lower than that of B/CL/G3/OS2 nanocomposite vulcanizate due to reinforcement of higher filler loading.

4.3.2.8 Mechanical properties

Figure 4.62 shows the stress-strain curves of B/CL/G3 nanocomposite vulcanizates. The B/CL/G3/OS5 nanocomposite vulcanizate exhibits the higher strain- induced crystallization, but it breaks early before it attained a higher elongation compared to the other three nanocomposite vulcanizates. The siloxane network at lower OMMT-S loading (2 phr) shows more flexible and tougher without the loss of high tensile strength. On the other hand, the siloxane network at higher OMMT-S loading (5 phr) became harder and stronger with the reduction of flexibility and toughness. A similar phenomenon was described in silica filled NR in another study. (Premachandra et al., 1996).

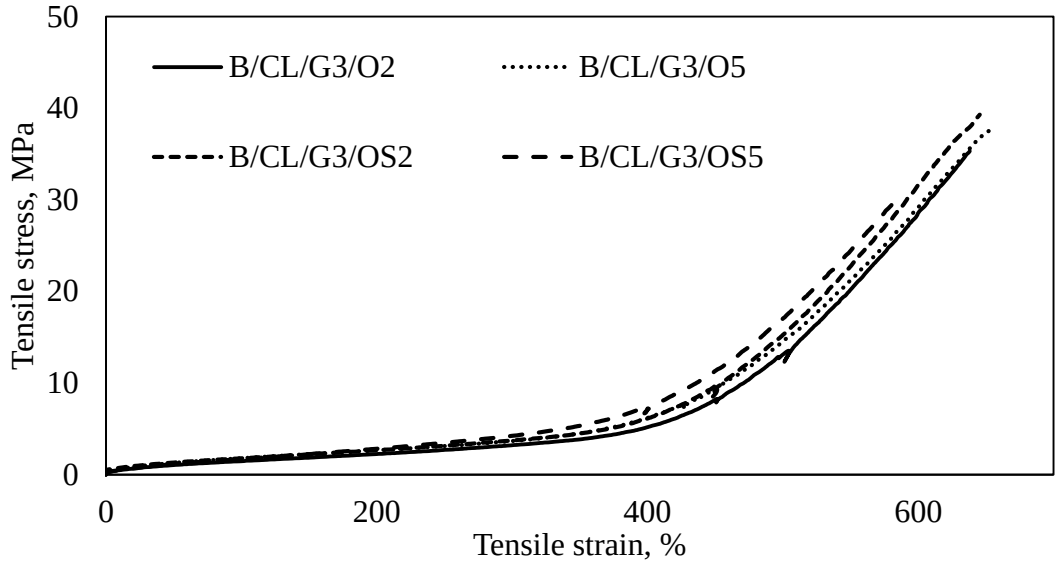

Figure 4. 62 Stress strain curve of B/CL/G3 nanocomposite vulcanizates

Figure 4.63 shows tensile strength, elongation at break, and mod 300% of B/CL/G3 nanocomposite vulcanizates. The B/CL/G3/OS2 nanocomposite vulcanizate shows higher tensile strength (39.4 MPa) than that of B/CL/G3/O2, B/CL/G3/O5, and B/CL/G3/OS5 nanocomposite vulcanizates. The better dispersion of clay layers with higher flexibility and toughness at lower OMMT-S loading increases the tensile strength. The increase of bound rubber content and crosslink density in B/CL/G3/OS2 nanocomposite vulcanizate further increase its tensile strength to achieve higher value. Instead, the elongation at break of B/CL/G3/O2, B/CL/G3/O5, and B/CL/G3/OS2 nanocomposite vulcanizates show similar values around 650%. The minimum reduction of elongation at break occurs with the effect of improved slippery action due to the addition of a higher amount of plasticizers at lower clay loading (Wu et al., 2004; Kim et al., 2006). Siloxane network around clay layers at higher OMMT-S loading (5phr) causes lower elongation at break (575%) and tensile strength (31.3 MPa) in B/CL/G3/OS5 nanocomposite vulcanizate. This may be due to the formation of harder and stronger but inevitably less flexible siloxane network around clay layers with higher OMMT loading.

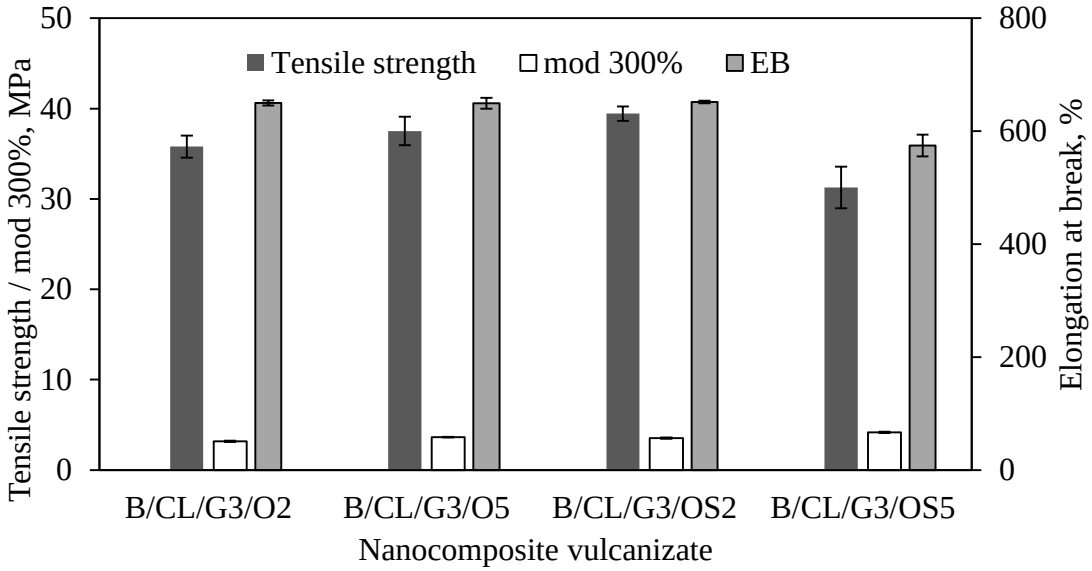

Figure 4. 63 Tensile properties of B/CL/G3 nanocomposite vulcanizates

When OMMT-S loading is increased (5 phr), the improved mod 300% and lack of strength of siloxane network around OMMT-S causes catastrophic failure. One of the study described that the network structure of siloxane would reduce the tensile strength of the silica reinforced rubber composite due to plasticization effect of siloxane network (Sae-oui et al., 2005). An increase of OMMT-S loading together with grafted siloxane network may act as rubber incompatible structure and causes possible rupture. The tensile strength and elongation of B/CL/G3/O5 nanocomposite vulcanizate show higher values due to better dispersion of higher amount of OMMT but those values could not override those properties of B/CL/G3/OS2 nanocomposite vulcanizate due to lack of flexibility similar to B/CL/G3/OS2 nanocomposite vulcanizate.

B/CL/G3/OS5 nanocomposite vulcanizate shows higher mod 300% than the other three nanocomposite vulcanizates due to higher rubber-clay interactions as suggested by increased bound rubber content and/or filler effect. The mod 300% of other B/CL/G3 nanocomposite vulcanizates do not improve significantly, however tensile strength is improved to a higher extent with a minimum reduction of elongation at break especially at lower OMMT-S loading (2phr).

Tear strength and hardness of B/CL/G3/O5 and B/CL/G3/OS5 nanocomposite vulcanizates are similar and slightly greater than that of B/CL/G3/O2 and

B/CL/G3/OS2 nanocomposite vulcanizates, which also show similar tear strength and hardness (Figure 4.64).

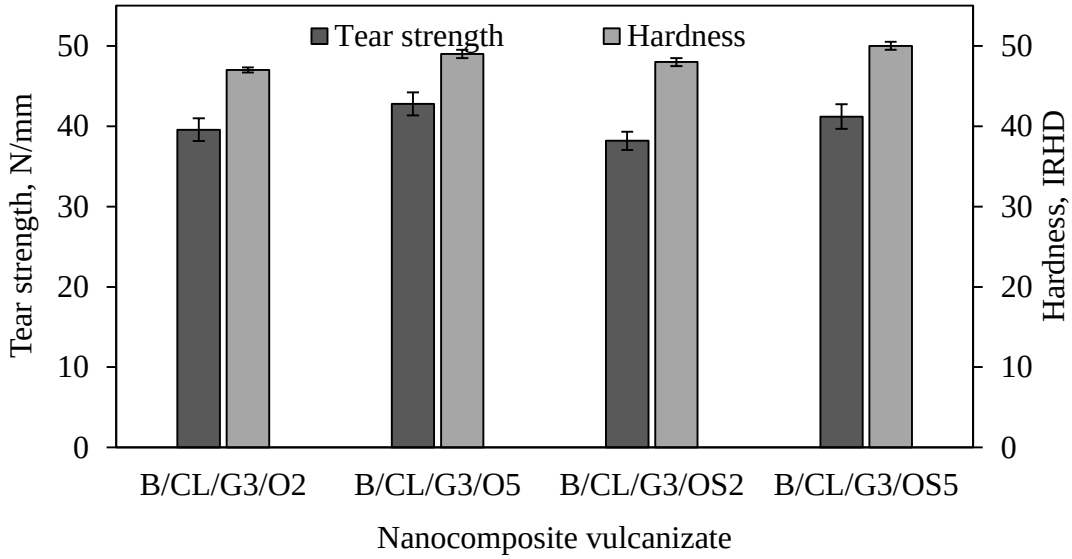

Figure 4. 64 Tear strength and hardness of B/CL/G3 nanocomposite vulcanizate

It denotes that tear strength mainly depends on the amount of finely dispersed clay layers than the effect of silane modification. The siloxane network has no interactions with rubber phase similar with sulphur crosslinks. The better dispersed OMMT-S clay layers with lower surface energy would enhance the tear strength and hardness. It suggests that suitable modification of rubber to interact with the siloxane network on OMMT-S is necessary for further enhancement of these properties.

4.3.2.9 Abrasion loss

Figure 4.65 presents the abrasion loss of B/CL/G3 nanocomposite vulcanizates. The abrasion loss of B/CL/G3/OS2 and B/CL/G3/OS5 nanocomposite vulcanizates are similar and lower than that of B/CL/G3/O2 and B/CL/G3/O5 nanocomposite vulcanizates. The properly dispersed higher number of OMMT-S clay layers together with improved rubber-clay interactions in B/CL/G3/OS2 and B/CL/G3/OS5 nanocomposite vulcanizates show lower abrasion loss.

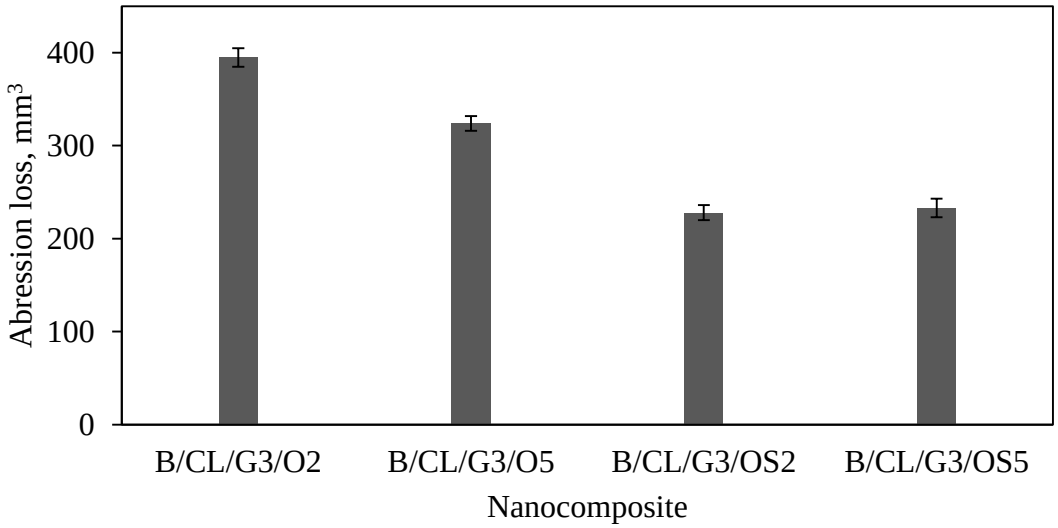

Figure 4. 65 Abrasion loss of B/CL/G3 nanocomposite vulcanizates

4.3.2.10 Ageing properties

Figure 4.66 illustrates the values of PRV of tensile strength, mod 300%, and elongation at break of B/CL/G3 nanocomposite vulcanizates after thermal ageing.

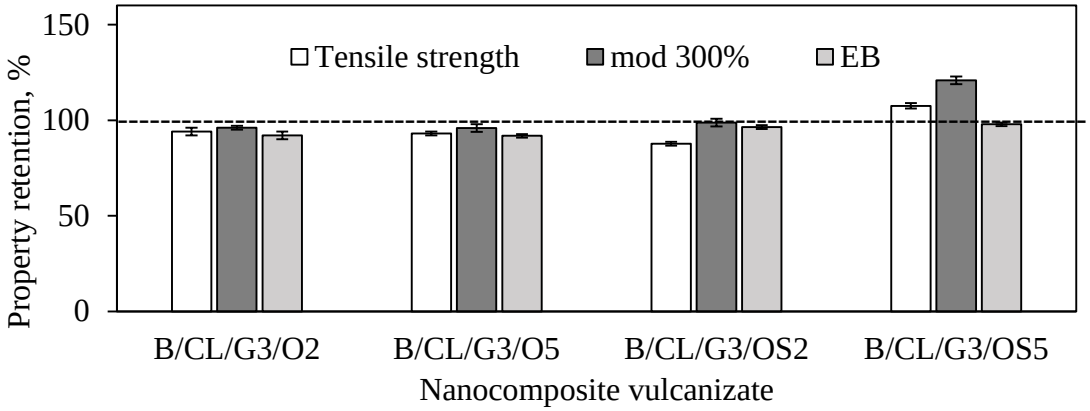

Figure 4. 66 Ageing properties of B/CL/G3 nanocomposite vulcanizates

The PRV of tensile strength, elongation at break, and mod 300% of B/CL/G3/O2, B/CL/G3/O5, and B/CL/G3/OS2 nanocomposite vulcanizates show a similar trend. The tensile strength and mod 300% of B/CL/G3/OS5 nanocomposite vulcanizate show improved properties having higher PRV greater than 100%. The higher the OMMT-S loading and an increase of bound rubber due to better rubber-clay

interactions could be the reason for higher PRV in B/CL/G3/OS5 nanocomposite vulcanizate. An increase of rigidity and a decrease of chain mobility in rubber also improve the ageing resistance overriding the surfactant effect in B/CL/G3/OS5 nanocomposite vulcanizate. Nevertheless, all B/CL/G3 nanocomposite vulcanizates show excellent ageing resistance.

The modification of organoclay by grafting of the silane group is successful. It decreases polar properties on the surface and reduced polar energy. As a result of that clay layers are well separated from clay stacks and disperse properly in the rubber phase. The bound rubber content, crosslink density, and mechanical properties are also increased. However, those properties are obtained with the proper balance between polar clay and non-polar rubber especially at lower loading. When loading of OMMT-S is increased, such polar-non polar balance is disturbed. Hence all mechanical properties are not increased properly as expected. This effect could be minimized if NR is modified by polar groups and maintain the proper balance of polar and non-polar even at effective higher OMMT-S loading. In addition to that it is appropriate to compare properties of OMMT-S based nanocomposite vulcanizates (B/CL/G3/OS2 and B/CL/G3/OS5) with nanocomposite vulcanizates prepared by mechanical blending using OMMT-S and commonly used raw rubber. Further modification of NRL by AFCC method using gelling agent G3 is necessary to be checked with industrial mechanical mixing with the use of OMMT-S.

4.3.3 The effect of OMMT-S on properties of nanocomposites prepared using different processing methods

The effect of OMMT-S on the properties of the nanocomposite vulcanizates prepared using AFCC method (B/CL/G3/OS2 and B/CL/G3/OS5) and mechanical mixing (C/PC/OS2 and C/PC/OS5) are discussed. These properties include cure characteristics (4.3.3.1), crosslink density (4.3.3.2), morphology (4.3.3.3), mechanical properties (4.3.3.4), abrasion loss (4.3.3.5), and Ageing properties (4.3.3.6).

4.3.3.1 Cure characteristics

Figure 4.67 shows t_{s2}, t_{90} and CRI of B/CL/G3/OS2, B/CL/G3/OS5, C/PC/OS2, and C/PC/OS5 nanocomposite compounds. Higher quantities of

non-rubber substances remained in the nanocomposites when they were prepared using the AFCC method.

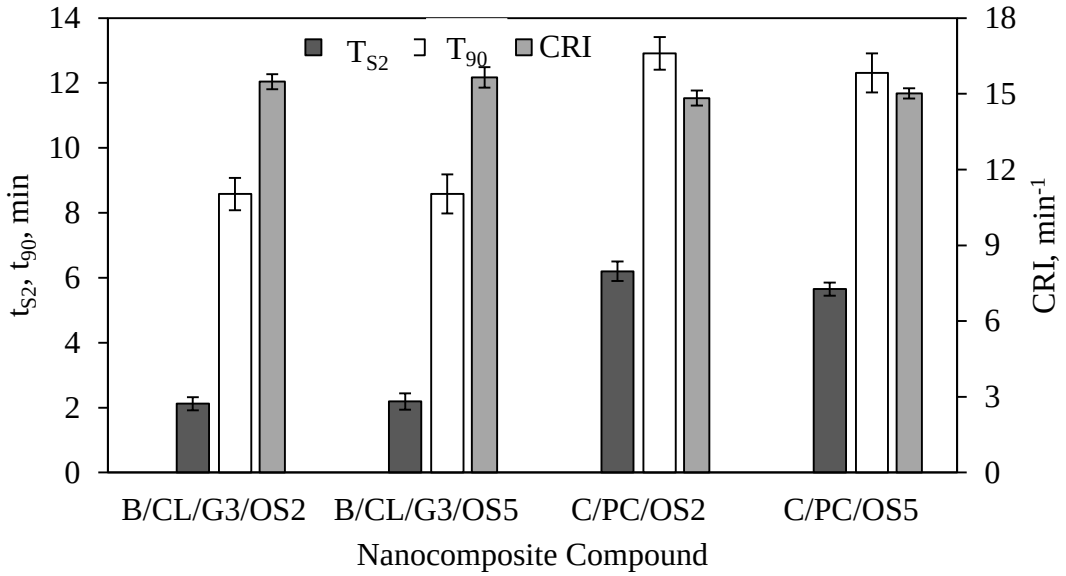

Figure 4. 67 $t_{s_2}, t_{90,}$ and CRI of B/CL/G3 and C/PC nanocomposite compounds

B/CL/G3/OS2 and B/CL/G3/OS5 nanocomposite compounds show lower t_{s2} and t_{90} and higher CRI compared to that of C/PC/OS2 and C/PC/OS5 nanocomposite compounds due to presence of higher amount of non-rubber substances in B/CL/G3/OS2 and B/CL/G3/OS5 nanocomposite compounds than those in C/PC/OS2 and C/PC/OS5 nanocomposite compounds. It is well known that non-rubber substances accelerate vulcanization reaction.

M_H-M_L of B/CL/G3/OS2 and B/CL/G3/OS5 nanocomposite compounds is greater than that of C/PC/OS2 and C/PC/OS5 nanocomposite compounds (Figure 4.68), and it may be due to higher crosslink density of B/CL/G3 nanocomposite compounds.

4.3.3.2 Morphology

SEM images of C/PC/OS2 (Figure 4.69) and C/PC/OS5 (Figure 4.70) nanocomposite vulcanizates show that there are a higher aggregation of OMMT-S compared to B/CL/G3/OS2 (Figure 4.56) and B/CL/G3/OS5 (Figure 4.57) nanocompositevulcanizates.

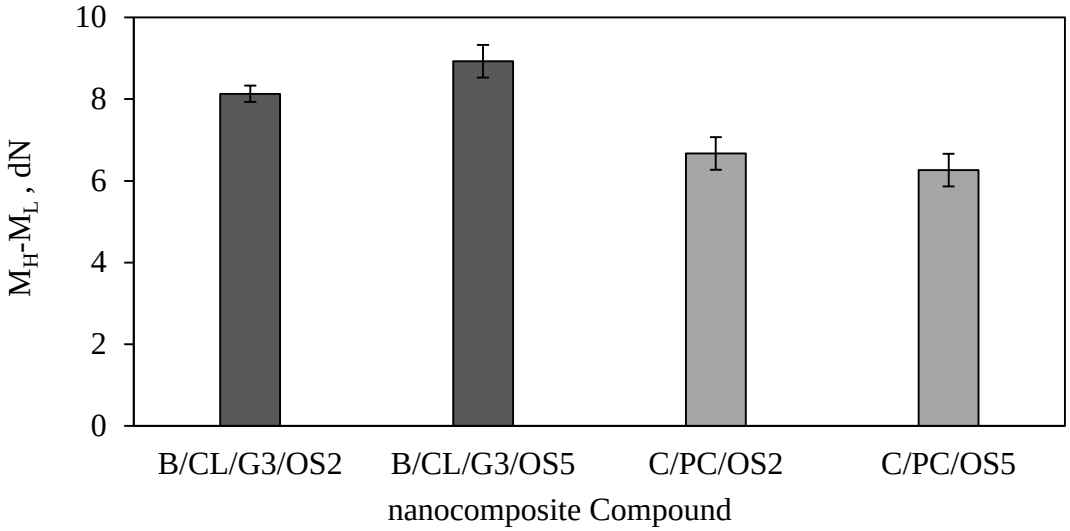

Figure 4. 68 M_H-M_L of B/CL/G3 and B/CL/O nanocomposites

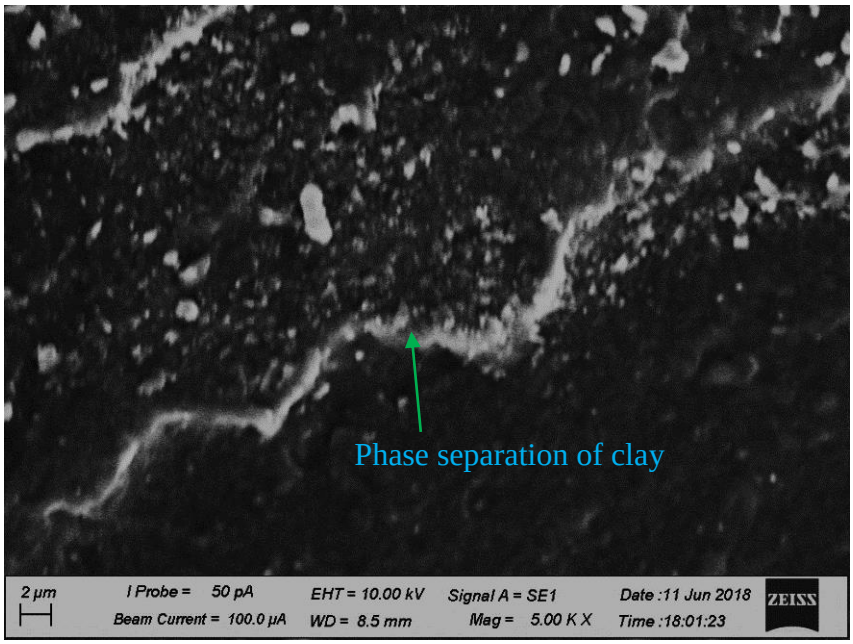

Figure 4. 69 SEM image C/PC/OS2 nanocomposite vulcanizate

The incorporation of OMMT-S only by mechanical mixing in the dry rubber route causes higher aggregation and even creates the separation of clay from the rubber phase. It reveals that the effect of emulsion blending and the presence of higher surfactant content as a gelling agent in B/CL/G3/OS2 and B/CL/G3/OS5 nanocomposite vulcanizates cause better dispersion of OMMT-S in B/CL/G3 nanocomposite vulcanizates compared to C/PC nanocomposite vulcanizates.

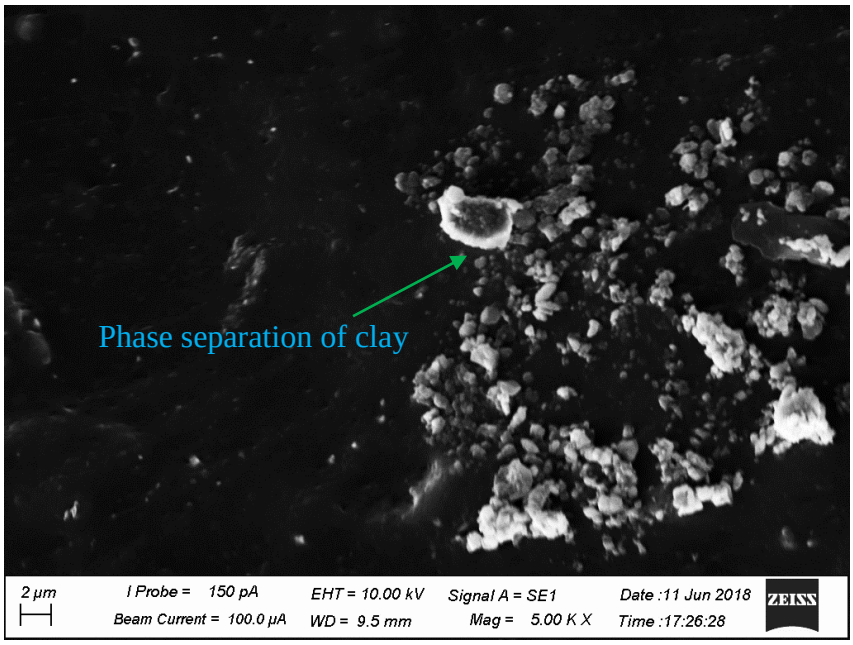

Figure 4. 70 SEM image of C/PC/OS5 nanocomposite vulcanizate

4.3.3.3 Crosslink density

Figure 4.71 displays the crosslink densities of B/CL/G3/OS2, B/CL/G3/OS5, C/PC/OS2, and C/PC/OS5 nanocomposite vulcanizates.

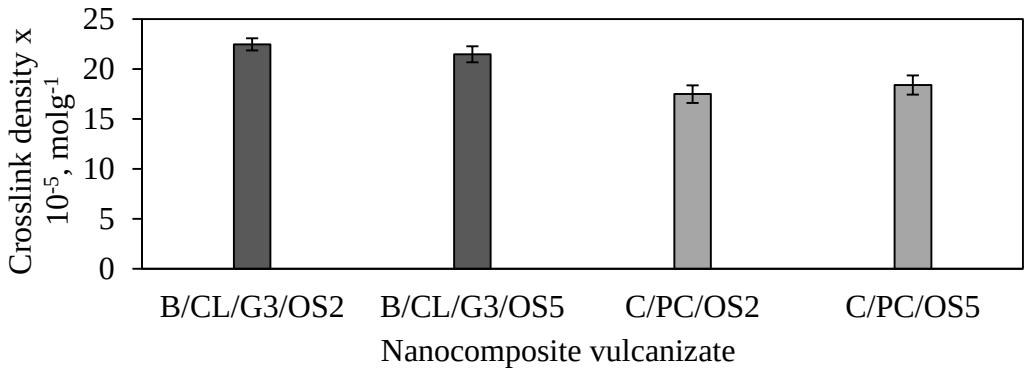

Figure 4. 71 Crosslink Density of B/CL/G3 and C/PC nanocomposite vulcanizates

4.3.3.4 Mechanical properties

Figure 4.72 presents tensile strength, elongation at break, and mod 300% of B/CL/G3/OS2, B/CL/G3/OS5, C/PC/OS2, and C/PC/OS5 nanocomposite vulcanizates. The tensile strength of B/CL/G3/OS2 and B/CL/G3/OS5 nanocomposite

vulcanizates are greater than that of C/PC/OS2 and C/PC/OS5 nanocomposite vulcanizates respectively.

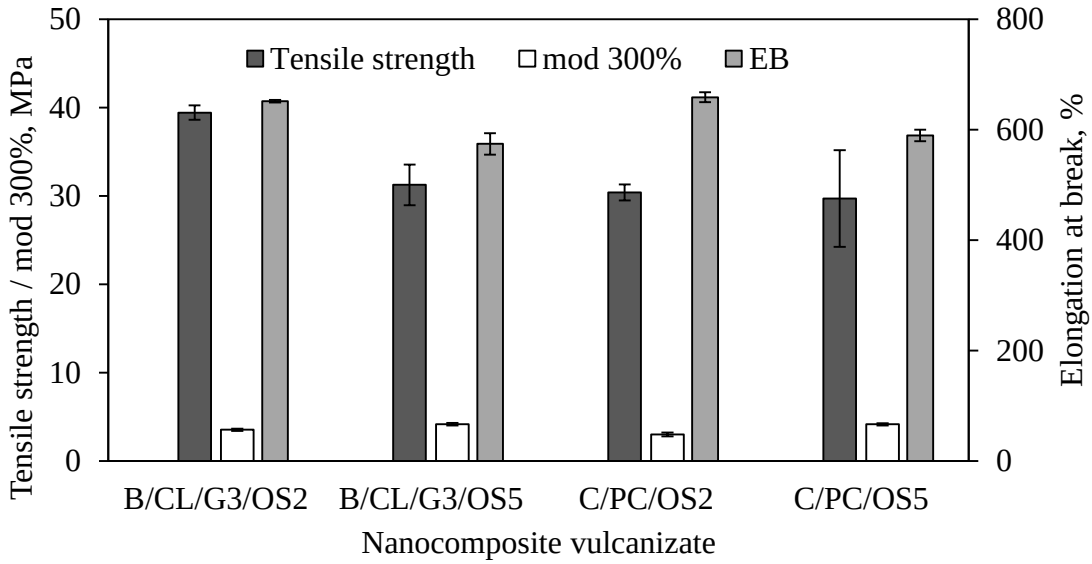

Figure 4. 72 Tensile properties of B/CL/G3 and C/PC nanocomposite vulcanizates

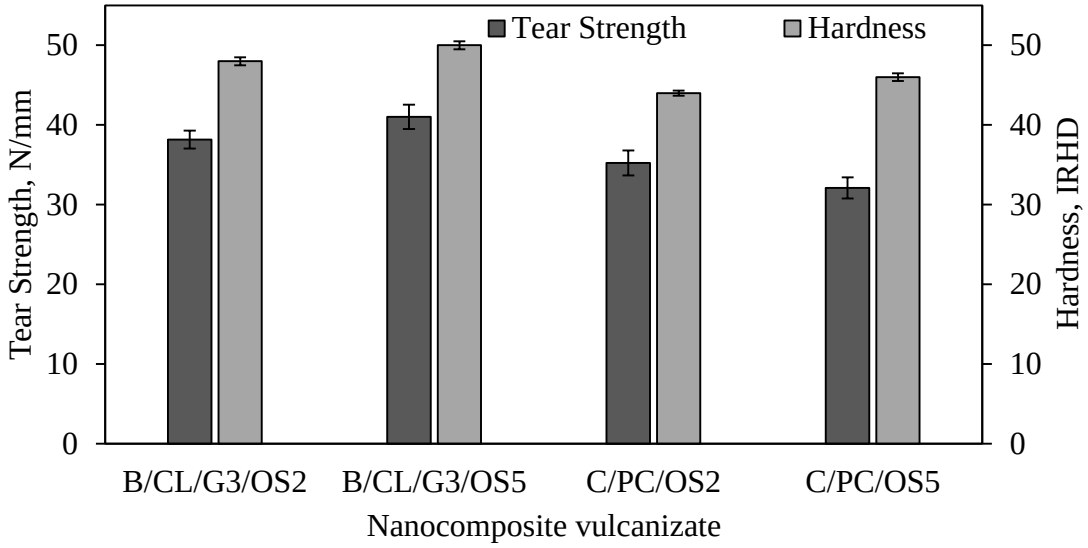

Figure 4. 73 Tear strength and hardness of B/CL/G3 and C/PC nanocomposite vulcanizates

Elongation at break of B/CL/G3/OS2 and C/PC/OS2 nanocomposite vulcanizates are higher than that of B/CL/G3/OS5 and C/PC/OS5 nanocomposite vulcanizates, whereas mod 300% of B/CL/G3/OS2 and C/PC/OS2 nanocomposite

vulcanizates are lower than that of B/CL/G3/OS5 and C/PC/OS5 nanocomposite vulcanizates. This evidence suggests that higher loading of OMMT-S increase the mod 300% without the influence of the processing methods. However, at the lower loading, B/CL/G3/OS2 nanocomposite vulcanizates show higher tensile strength by decreasing mod 300% without a reduction of elongation at break.

Tear strength and hardness of B/CL/G3/OS2 and B/CL/G3/OS5 nanocomposite vulcanizates (Figure 4.73) are higher than those of C/PC/OS2 and C/PC/OS5 nanocomposite vulcanizates. B/CL/G3/OS5 nanocomposite vulcanizate shows comparatively higher tear strength and hardness due to the dispersion of the higher number of smaller clay stacks in partially exfoliated OMMT-S clay layers by the effect of emulsion blending and use of higher surfactant content as the gelling agent.

4.3.3.5 Abrasion loss

The abrasion loss (Figure 4.74) of B/CL/G3/OS2 and B/CL/G3/OS5 nanocomposite vulcanizates are less than C/PC/OS2 and C/PC/OS5 nanocomposite vulcanizates due to better dispersion of OMMT-S in rubber with improved crosslink density.

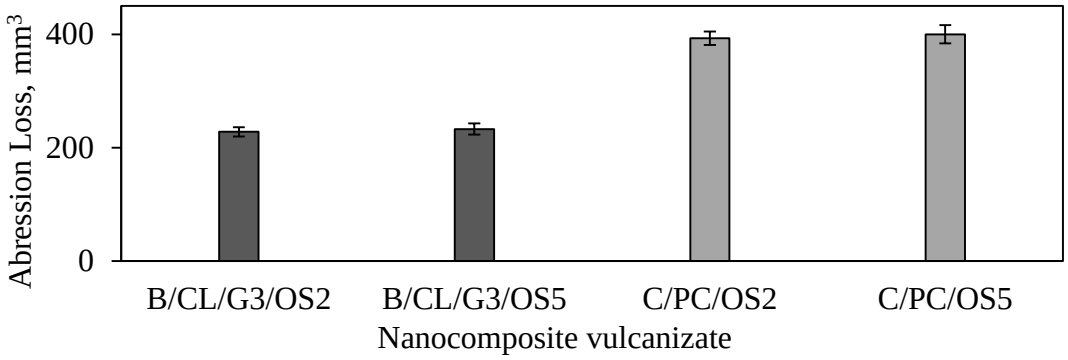

Figure 4. 74 Abrasion loss of B/CL/G3 and C/PC nanocomposite vulcanizates

The better dispersion of OMMT-S clay layers in NRL also contributes to decreasing the abrasion loss in B/CL/G3/OS2 and B/CL/G3/OS5 nanocomposite vulcanizates. A higher number of aggregated structures formed by direct addition of OMMT-S to C/PC/OS2 and C/PC/OS5 nanocomposite vulcanizates causes to have higher abrasion loss. Further, the improved crosslink density and rubber-clay

interaction in B/CL/G3/OS2 and B/CL/G3/OS5 nanocomposite vulcanizates also decrease the abrasion loss.

4.3.3.6 Ageing properties

Figure 4.75 shows PRV of tensile strength, mod 300%, and elongation at break in B/CL/G3/O2, B/CL/G3/O5, C/PC/OS2, and C/PC/OS5 nanocomposite vulcanizates after thermal ageing. All nanocomposite vulcanizates show superior ageing resistant. This could be the reason for better dispersion of clay layers in B/CL/G3/OS2 and B/CL/G3/OS5 nanocomposite vulcanizates, and less non-rubber substances presence in C/PC/OS2 and C/PC/OS5 nanocomposite vulcanizates.

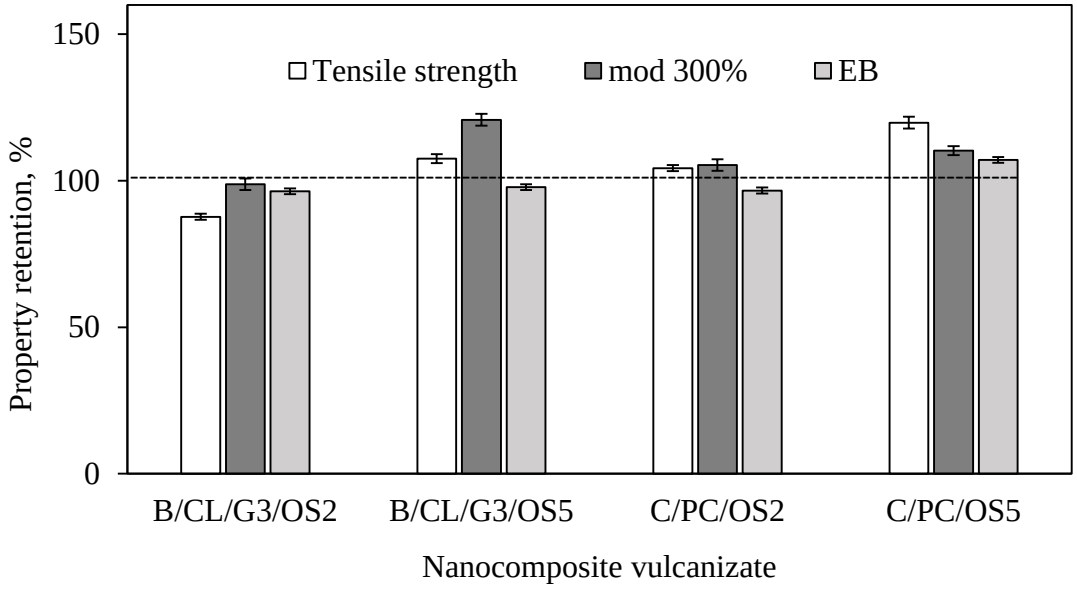

Figure 4. 75 Ageing properties of B/CL/G3 and C/PC nanocomposite vulcanizates

4.3.4 Characterization of modified NRL

It is very clear that modification of clay only by reducing its polarity is not necessary to disperse clay in NR. It needs higher rubber clay interactions to retain exfoliated clay structures in the rubber matrix. Hence, modification of NRL by grafting of the suitable polar group is aimed to develop in the current section. The new polar group named succinimide (SI) is grafted to NRL (Section 3.2.7.9) to increase the polarity and thereby improve the compatibility between polar rubber and polar

OMMT-S. Characterization of SI grafted NRL, and its grafting efficiency is discussed in this section.

4.3.4.1 Characterization of SI grafted NR

Figure 4.76 presents the FTIR spectra NR of as control (Table 3.6 in Section 3.2.7.8) and SI grafted NR as CT-B/gL/G3 (Table 3.7 in Section 3.2.7.9). CT-B/gL/G3 shows the peak at 1713 cm^{-1} due to the presence of succinimide grafted on NR. In literature, it was confirmed that the FTIR peak at 1713 cm^{-1} is assigned to the imide I functional group (Ishida & Ohbal., 2005).

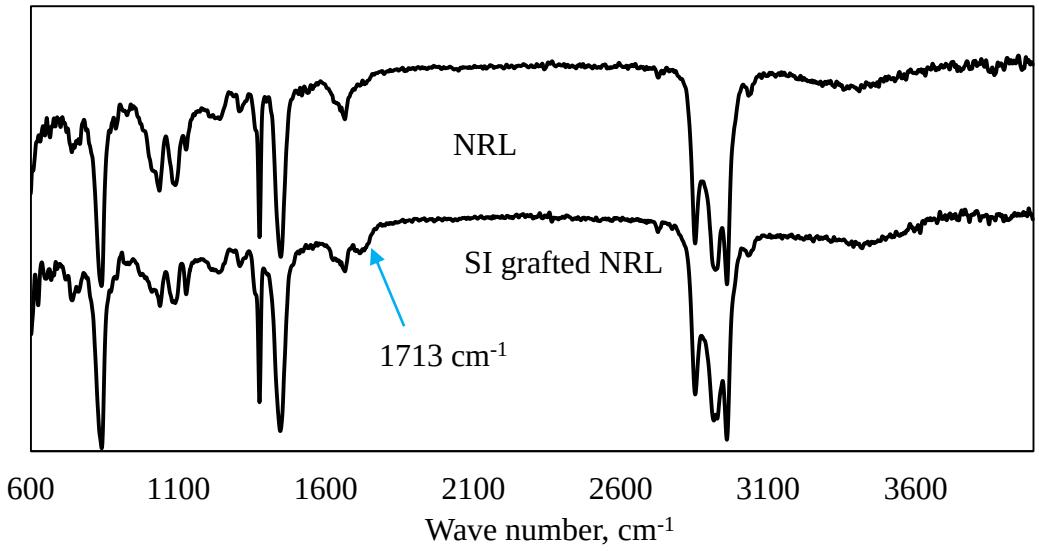

Figure 4. 76 FTIR spectra of NRL and SI modified NRL

In the presence of concentrated ammonia, the anhydride ring opens, and the maleamic acid (MA) is formed before the grafting process (Refer Figure 4.99 in Section 4.3.7). However MA is grafted into NR as succinamic acid (SA) which is the most stable grafting structure (refer Figure 4.100) described in the literature (Kannika & Beraheng., 2008). SA is then converted into SI after dehydration of the drying process in the raw rubber preparation stage (Refer Figure 4.102 in Section 4.3.7). The sharp peaks at 1668 cm^{-1} and 836 cm^{-1} assigned for C=CH stretching and deformation of NR are recorded in both CT-B/CL/G3 and CT-B/gL/G3. This confirmed that unsaturated bonds are not consumed while in the grafting and have no adverse effect on vulcanization. The broad and intense characteristic band at 1800 – 1775 cm^{-1} and

the weak absorption band at 1860-1850 cm^{-1} were not observed in the grafted rubber. Many researchers have found such bands corresponding to symmetric (strong) and asymmetric (weak) C=O stretching vibrations of succinic anhydride rings respectively (Ming et al., 2002; Nekason et al., 2003). The maleic anhydride after the modification with ammonia, MA is produced (refer 4.3.7) and it would fix to rubber in the form of a succinamic acid. Kannika & Beraheng also described similar grafting reaction that maleic anhydride is changed into succinic anhydride after grafting (Kannika & Beraheng., 2008). The un-grafted MA would give a peak at an extremely broad O-H absorption peak occurring in the region 3400-2400 cm^{-1} for carboxylic acid and 1690-1650 cm^{-1} for aliphatic amide. However those peaks are also not seen or prominent in the study.

The grafted SI functional groups on NRL interact with silanol and siloxane groups of clay, via hydrogen bond and dipole-dipole interactions. This study did not intend to create strong bonds between the grafted NR and clay; otherwise, such bonds would produce permanent structures and cause processing problems at compounding and molding stages. Further, it would hinder the formation of dominant sulphur crosslinks and thereby decreases the mechanical properties.

The grafting efficiency of SI grafted NR by the FTIR method is 41.4%. It is believed that unreacted MA and homopolymers produced from the reaction with MA are removed by washing the sample with a solvent. However, it is well-known that the unreacted MA would be further grafted during the vulcanization stage under higher temperature and pressure conditions, which is not counted by the grafting efficiency.

4.3.5 Effect of use of SI grafted NRL on properties of nanocomposites

Properties of B/gL/G3 nanocomposite vulcanizates prepared were compared to those of B/CL/G3 nanocomposites at respective OMMT-S loadings. The properties include cure characteristics (4.3.5.1), morphology (Section 4.3.5.2), XRD analysis (Section 4.3.5.3), bound rubber content (Section 4.3.5.4), crosslink density (Section 4.3.5.5), viscosity (Section 4.3.5.6), DMTA (Section 4.3.5.7), mechanical properties (Section 4.3.5.8), abrasion loss (Section 4.3.5.9), and ageing properties (Section 4.3.5.10) are discussed.

4.3.5.1 Cure characteristics

A decrease of t_{s2} and t_{90} and an increase of CRI are found in CT-B/gL/G3, B/gL/G3/OS2, and B/gL/G3/OS5 nanocomposite compounds compared to CT-B/CL/G3, B/CL/G3/OS2, and B/CL/G3/OS5 nanocomposite compounds, respectively (Figure 4.77). The grafted polar SI group on NR facilitates the dispersion of curatives in the rubber matrix, which causes lower t_{s2} and t_{90} together with a comparatively higher CRI. The imide is also reported as powerful activators for vulcanization reaction in the literature (Lawrence, 1979). Further, a higher number of zinc ammine complexes soluble in polar rubber decrease t_{s2} and t_{90}, thereby increase the CRI.

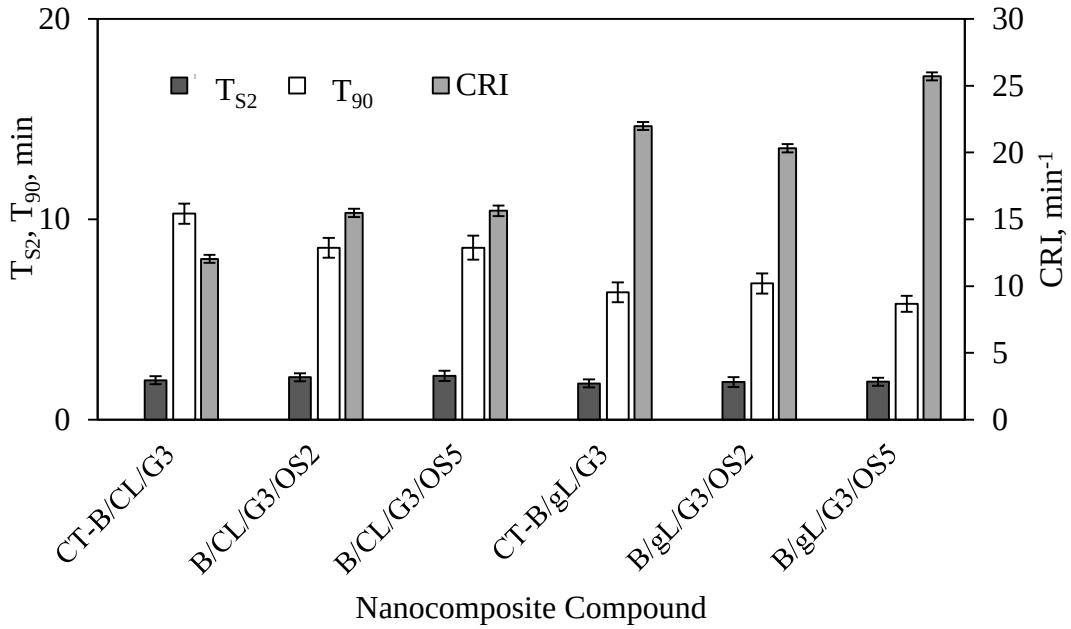

Figure 4. 77 t_{s2}, t_{90} and CRI of B/CL/G3 and B/gL/G3 nanocomposite compounds

The activation energy of CT-B/CL/G3, B/CL/G3/OS2, and B/CL/G3/OS5 nanocomposite compounds are higher than that of CT-B/gL/G3, B/gL/G3/OS2, and B/gL/G3/OS5 nanocomposite compounds (Figure 4.78) in a similar behavior corresponding to t_{s2}.

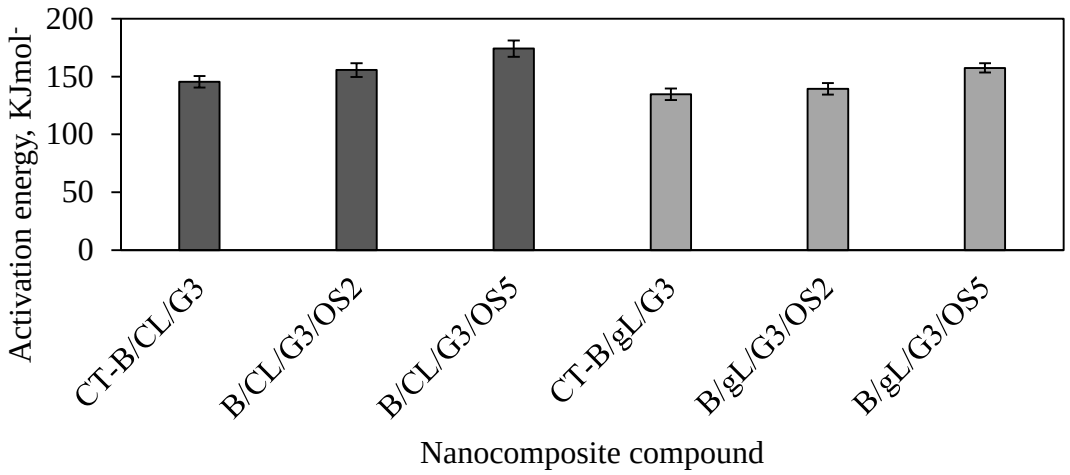

Figure 4. 78 Activation energy of B/CL/G3 and B/gL/G3 nanocomposite compounds

The higher polar nature of CT-B/gL/G3, B/gL/G3/OS2, and B/GL/G3/OS5 nanocomposite compounds facilitate the increase of solubility of the zinc ammine complexes and thereby decrease the activation energy.

M_H-M_L of CT-B/gL/G3, B/gL/G3/OS2, and B/gL/G3/OS5 nanocomposite compounds show comparatively lower values to CT-B/CL/G3, B/CL/G3/OS2, and B/CL/G3/OS5 nanocomposite compounds given in Figure 4.79.

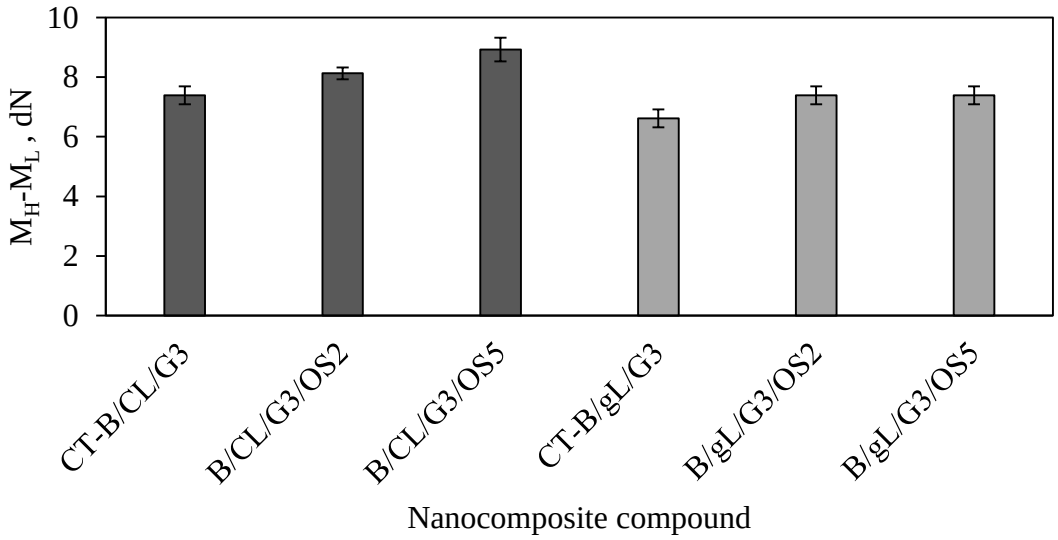

Figure 4. 79 M_H-M_L of B/CL/G3 and B/gL/G3 nanocomposite compounds

This may be due to the higher loading of surfactants added to stabilize NRL during de-proteinization and grafting before preparing B/gL/G3 nanocomposites. Hence the amount of surfactant in B/gL/G3 is higher than in B/CL/G3 nanocomposites which decreases M_H-M_L nanocomposites. The amount of surfactant added in B/gL/G3 nanocomposites is higher than B/CL/G3 nanocomposite to stabilize the latex while preparation of de-proteinized and grafting NRL. The surfactant would act as a plasticizing agent especially at higher temperatures and thereby reducing the rigidity of rubber resulting in lower M_H-M_L. Sulphur crosslink is the dominant influencing on the increase of M_H-M_L but the plasticizing effect of B/gL/G3 nanocomposite plays a vital role to reduce M_H-M_L significantly.

4.3.5.2 Morphology

SEM images of B/gL/G3/OS2 and B/gL/G3/OS5 nanocomposite vulcanizates are shown in Figure 4.79 and 4.80 respectively.

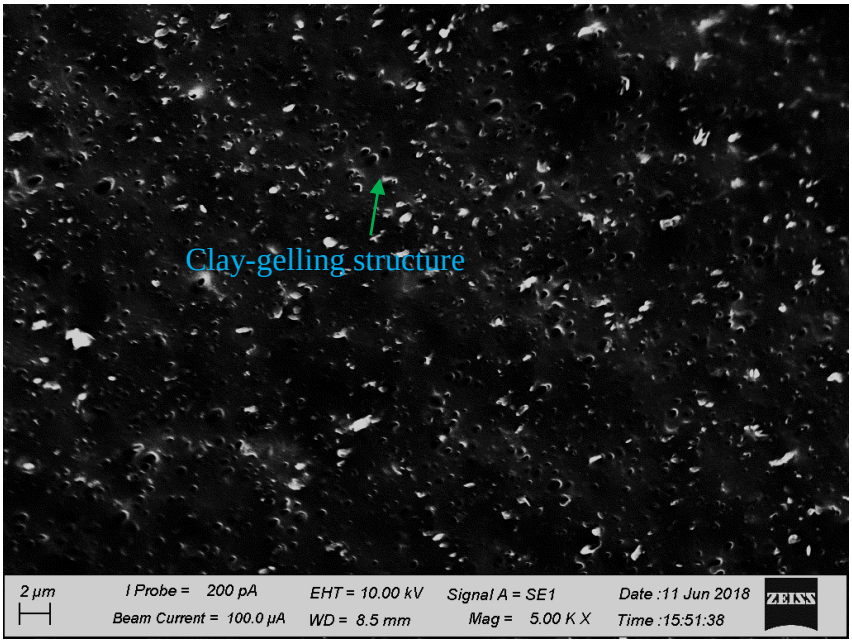

Figure 4. 80 SEM image of B/gL/G3/OS2 nanocomposite vulcanizate

Observation of SEM images of B/CL/G3/OS2 (Figure 4.56) and B/CL/G3/OS5 nanocomposite vulcanizates (Figure 4.57) are given in Table 4.15 and B/gL/G3 nanocomposites are given in Table 4.16. B/gL/G3 nanocomposite vulcanizate show lower number of aggregated clay structures compared to B/CL/G3 nanocomposite

vulcanizate due to better dispersion of OMMT-S in polar rubber. This may show that OMMT-S are exfoliated in the rubber matrix. Randomly distributed exfoliated clay structures in B/gL/G3 nanocomposite vulcanizate may disturb the formation of properly arranged gelling clusters and clay-gelling structures due to that polar head of surfactants, it will not only interact with exfoliated OMMT layers, also with polar SI modified NR as well.

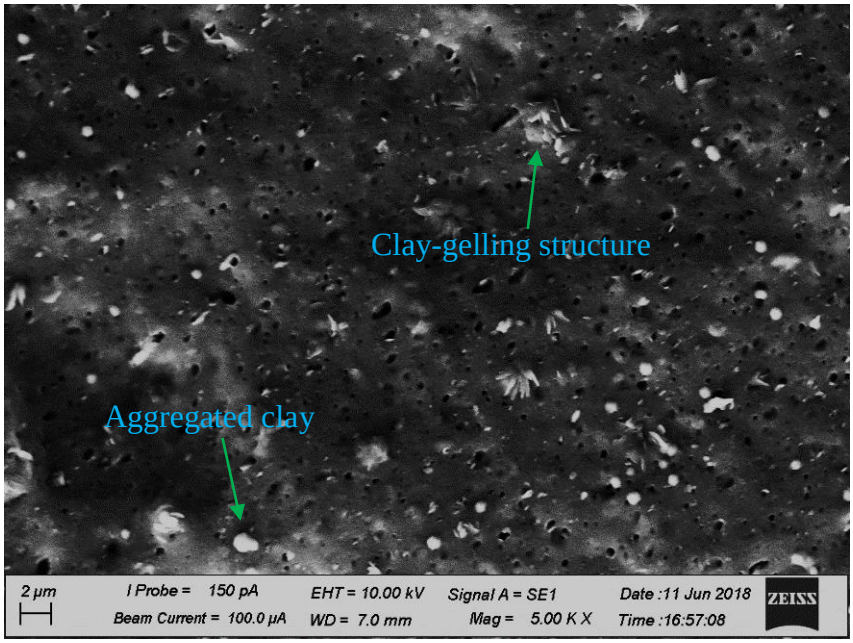

Figure 4. 81 SEM image of B/gL/G3/OS5 nanocomposite vulcanizate

Table 4. 16 Evaluation of SEM images of B/gL/G3 nanocomposite vulcanizates

Nanocomposite	**Appearance**
B/gL/G3/OS2	• Presence very few number of smaller aggregated clay structures • Presence of exfoliated clay layers
B/gL/G3/OS5	• Presence few number of smaller aggregated clay structures • Presence of higher number of exfoliated clay layers

4.3.5.3 XRD analysis

Figure 4.82 presents the XRD diffractograms of B/CL/G3 and B/gL/G3 nanocomposite vulcanizates. The lower number of clay structures could not disturb the arrangement of crystalline structures of gelling clusters and clay-gelling clusters. Instead, a higher number of better dispersed clay structures may disturb the crystalline structures and aggregated clay structures in B/CL/G3/OS5 nanocomposite vulcanizate.

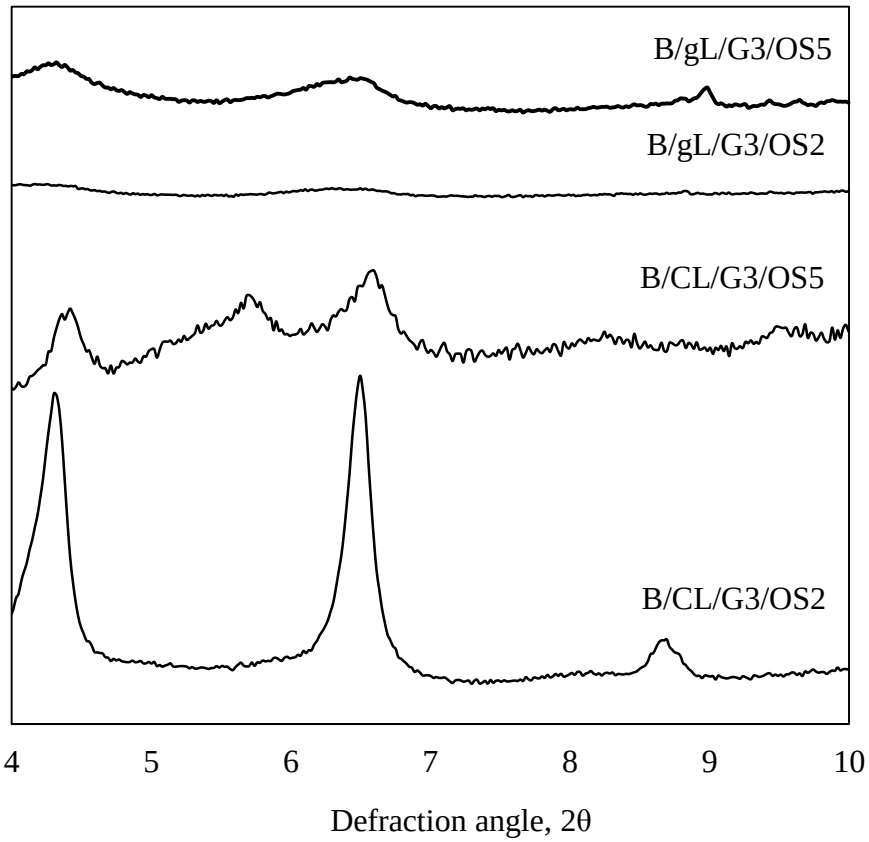

Figure 4. 82 XRD diffractograms of B/CL/G3 and B/gL/G3 nanocomposite vulcanizate

The higher polar SI grafted rubber in B/gL/G3 would cause a higher number of exfoliated clay layers get distributed randomly in rubber matrix and disturb crystalline structures even at 2 phr OMMT-S loading. Those individual clay layers dispersed in smaller structures are observed in SEM images (Figure 4.80 and Figure 4.81) and produce randomly distributed exfoliated clay structures. The proposed

structure of B/gL/G3/OS2 and B/gL/G3/OS5 nanocomposite vulcanizates is given in Figure 4.96 in section 4.4.

4.3.5.4 Bound rubber content

The bound rubber content of B/CL/G3 and B/gL/G3 nanocomposites and the crosslink density of their respective nanocomposite vulcanizates are presented in Figure 4.83. Bound rubber content of B/gL/G3/OS2 and B/gL/G3/OS5 nanocomposites show higher values than that of B/CL/G3/OS2 and B/CL/G3/OS5 nanocomposites. The improved hydrogen bonds and dipole-dipole interactions occurred between silanol groups in OMMT-S, and the grafted SI, in B/gL/G3/OS2 and B/gL/G3/OS5 nanocomposites cause better dispersion of clay in the rubber matrix and increase the bound rubber content with OMMT-S loading.

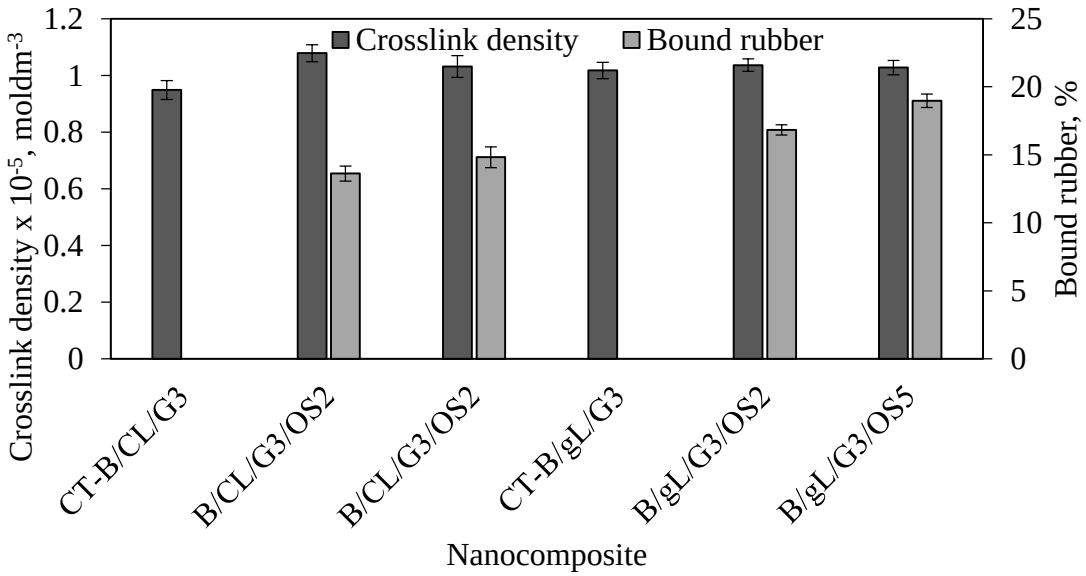

Figure 4. 83 Bound rubber content and crosslink density of B/CL/G3 and B/gL/G3 nanocomposite

4.3.5.5 Crosslink density

The crosslink density of B/gL/G3/OS2 and B/gL/G3/OS5 nanocomposite vulcanizates are almost similar to that of B/CL/G3/OS2 and B/CL/G3/OS5 nanocomposite vulcanizates (Figure 4.83). The crosslink density of nanocomposite vulcanizates mainly depends on sulphur crosslinks; the improved rubber-clay interactions of B/gL/OS nanocomposite vulcanizates do not effect much on increasing

the crosslink density due to the presence of higher plasticizers. However, the crosslink density of CT-B/gL/G3 vulcanizate is higher than that of CT-B/CL/G3 vulcanizate due to the effect of SI grafted NR. Imide group affects increasing the crosslink density reported by literature (Lawrence, 1976), however, the increased surfactant acted as plasticizers in the presence of clay would reduce the crosslink density of B/gL/G3 nanocomposites due to dissolution of the higher amount of sol.

4.3.5.6 Viscosity

Figure 4.84 illustrates the viscosity of B/gL/G3/OS5 nanocomposite as compared with that of B/CL/G3/O5 nanocomposite together with their Controls.

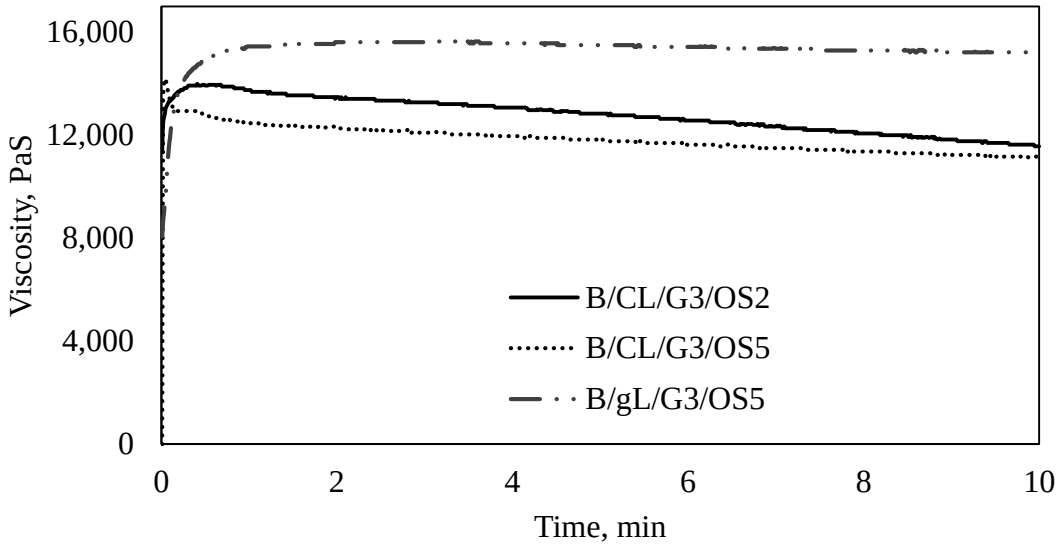

Figure 4. 84 Variation of Viscosity of B/CL/G3 and B/gL/G3 nanocomposites with time

The viscosity of CT-B/gL/G3 is lower than that of CT-B/CL/G3 due to the presence of higher surfactant content in CT-B/gL/G3. Interestingly, at the same OMMT-S loading, the B/gL/G3/OS5 nanocomposite shows a considerable increase of viscosity than the B/CL/G3/OS5 nanocomposite due to presence of rubber-clay interactions in different materials and is agreeable with results of bound rubber content. This further indicates that flow properties of B/gL/G3/OS5 nanocomposite are restricted by improved hydrogen bonds and dipole-dipole interactions when OMMT-S is introduced.

4.3.5.7 DMTA study

Figure 4.85 depicts tan δ verses temperature curves of B/CL/G3 and B/gL/G3 nanocomposite vulcanizates. According to that, the B/gL/G3/OS5 and B/CL/G3/OS5 nanocomposite vulcanizates have lower than B/CL/G3/OS2, and B/gL/G3/OS2 nanocomposite vulcanizates due to an increase of reinforcement by higher OMMT-S loading and lower in B/gL/G3/OS5 nanocomposite vulcanizate due to improved rubber-clay interactions. However, T_g of all nanocomposite vulcanizates in Figure 4.85 show a similar value and is mainly dependent on the excess amount of the gelling agents and its plasticizing effect rather than rubber-clay interactions. The reduction of tan δ without change of T_g in B/gL/G3/OS5 show that reinforcement is improved without reduction of flexibility.

In the present investigation, the secondary relaxation peaks at 42.9 ˚C and 81.5 ˚C appeared in B/gL/G3/OS2 and B/gL/G3/OS5 nanocomposite vulcanizates, respectively, at the rubbery state may be due to improved rubber-clay interactions.

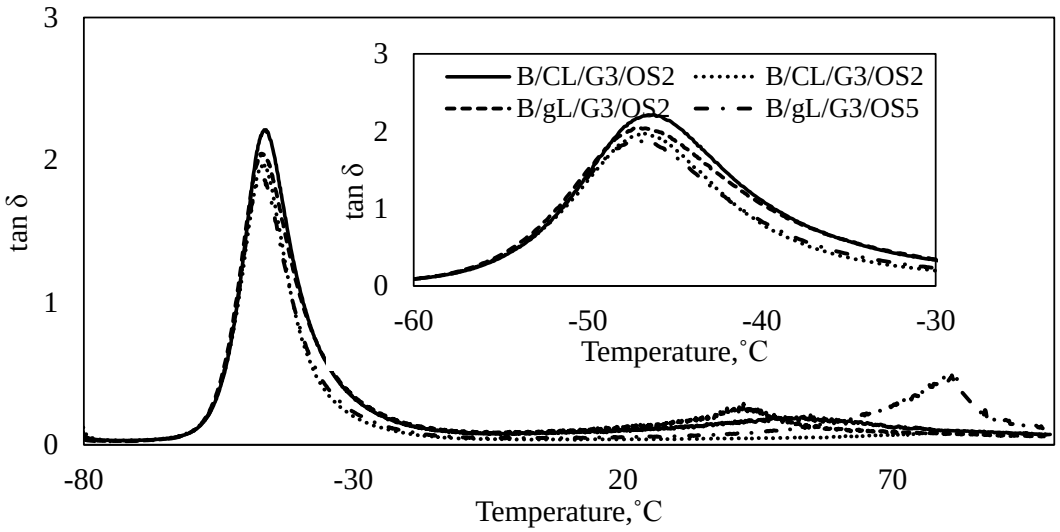

Figure 4. 85 tan δ of B/CL/G3 and B/gL/G3 nanocomposite vulcanizates

4.3.5.8 Mechanical properties

Figure 4.86 shows a stress-strain curve of B/CL/G3 and B/gL/G3 nanocomposite vulcanizates. The strain-induced crystallization of B/gL/G3/OS2 and B/gL/G3/OS5 nanocomposite vulcanizates is greater than that of B/CL/G3/OS2 and B/CL/G3/OS5 nanocomposite vulcanizates. It may be due to the presence of an

increased number of exfoliated OMMT-S clay layers with improved rubber-clay interactions. The combined effect of rubber-clay interactions and together with the presence of a higher number of exfoliated clay layers in B/gL/G3/OS5 nanocomposite vulcanizate shows higher strain-induced crystallization than B/gL/G3/OS2 nanocomposite vulcanizate. A study stated that (Fathurrohman et al., 2015), the exfoliated clay structures reduces strain-induced crystallization of rubber. B/gL/G3 nanocomposite vulcanizates achieve better strain-induced crystallization possibly due to the presence of exfoliated structures having stronger rubber-clay interactions between SI grafted NR and OMMT-S. In general, when strain-induced crystallization is increased, elongation at break is reduced. Most interestingly, B/gL/G3 nanocomposite vulcanizates claimed an increase of strain-induced crystallization without reduction of elongation at break.

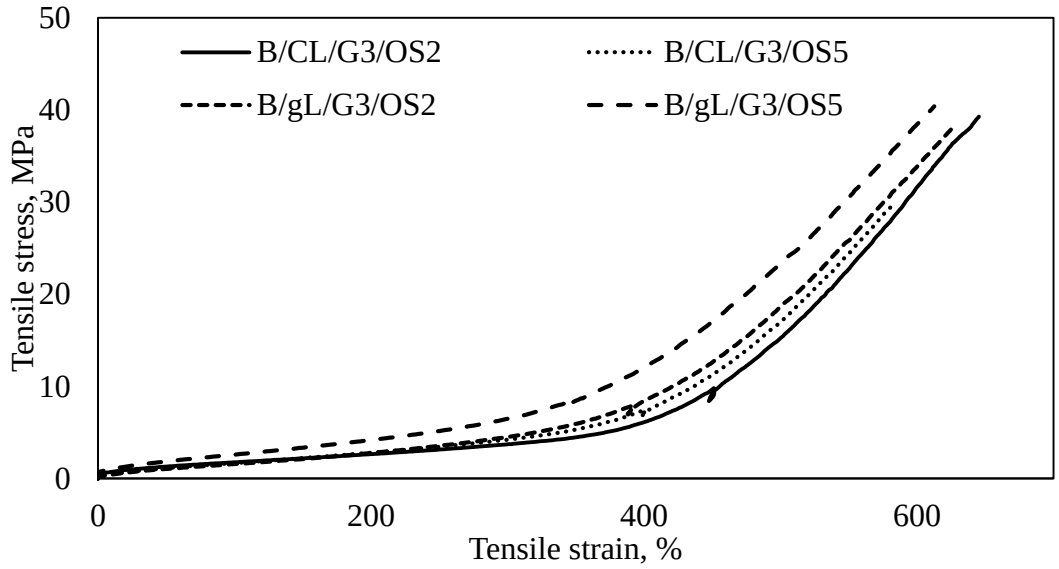

Figure 4. 86 Stress strain curves of B/CL/G3 and B/gL/G3 nanocomposite vulcanizates

The tensile strength, mod 300%, and elongation-at-break of CT-B/gL/G3 vulcanizate are greater than those of CT-B/CL/G3 vulcanizate by 150%, 24%, and 16% respectively (Figure 4.87). The presence of gelling clusters on reducing the tensile properties is improved by grafting the SI on NRL. With the addition of 2 phr OMMT-S loading, B/gL/G3 nanocomposite vulcanizate exhibit better mechanical properties; B/gL/G3/OS5 nanocomposite vulcanizate shows remarkably increased

tensile strength (41 MPa), mod 300% (6 MPa), and elongation at break (630%). Elongation at break of CT-B/gL/G3 and B/gL/G3/OS5 nanocomposite vulcanizates are almost the same, but the tensile strength and mod 300% of B/CL/G3/O5 nanocomposite vulcanizates are higher than that of CT-B/gL/G3 vulcanizate by 7.6% and 35% due to higher degree of exfoliation together with improved rubber-clay interactions. The slippery action of plasticizers would make it possible for the highly strained molecular chains to relieve the tension caused by stretching; hence, they will not break permanently, resulting in a higher strain at break and strength (Wu et al., 2004).

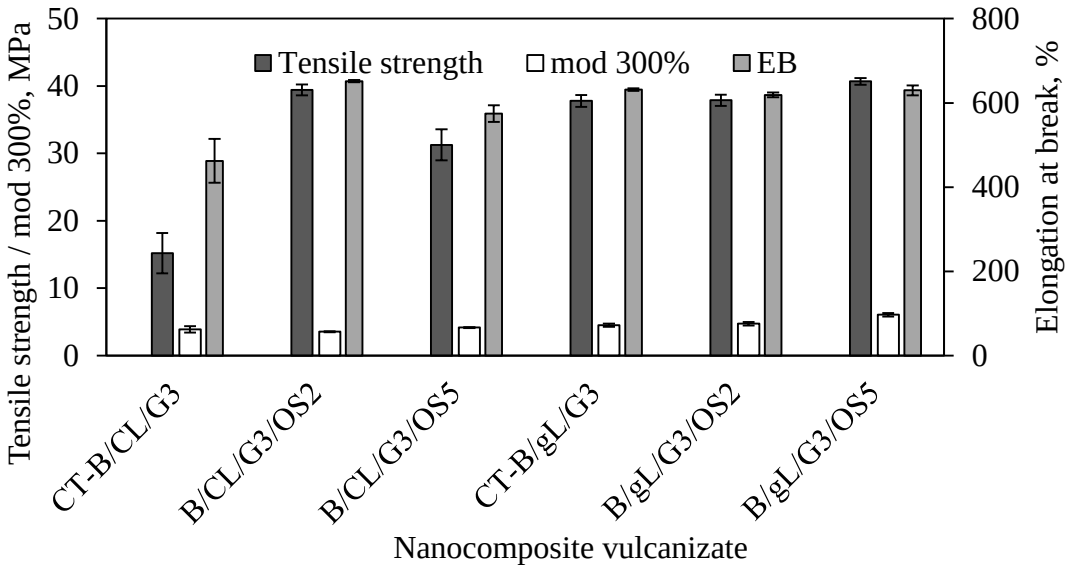

Figure 4. 87 Tensile properties of B/CL/G3 and B/gL/G3 nanocomposite vulcanizates

The tear strength and hardness of B/GL/G3/OS2 and B/GL/G3/OS5 nanocomposite vulcanizates are greater than those of B/CL/G3/OS2 and B/CL/G3/OS5 nanocomposite vulcanizates due to the improved rubber-clay interaction and a higher degree of clay exfoliation (Figure 4.88)

The B/gL/G3/OS5 nanocomposite vulcanizate shows the highest tear strength (48.6 N/mm) and hardness (55 IRHD) which values are greater than those in series A/FL/M to B/CL/G3 nanocomposite vulcanizate in the study. However, tear strength and hardness of CT-B/gL/G3 vulcanizate are greater than those of CT-B/CL/G3 vulcanizate due to an increase of the crosslink density of CT-B/gL/G3 vulcanizate.

4.3.5.9 Abrasion loss

The abrasion loss of CT-B/gL/G3 vulcanizate is almost similar to CT-B/CL/G3 (Figure 4.89) vulcanizate because of gelling agent and absence of improved rubber-clay interaction in both controls equally increased the abrasion loss. B/GL/G3/OS5 nanocomposite vulcanizate shows superior abrasion resistance with minimum abrasion loss (190 mm^3) compared to all other nanocomposite vulcanizates. This shows that both modifications of the rubber phase and incorporation of modified clay are vital to increasing the abrasion resistance. The better dispersion OMMT-S with improved rubber-clay interactions increases the abrasion resistance in the nanocomposite vulcanizates.

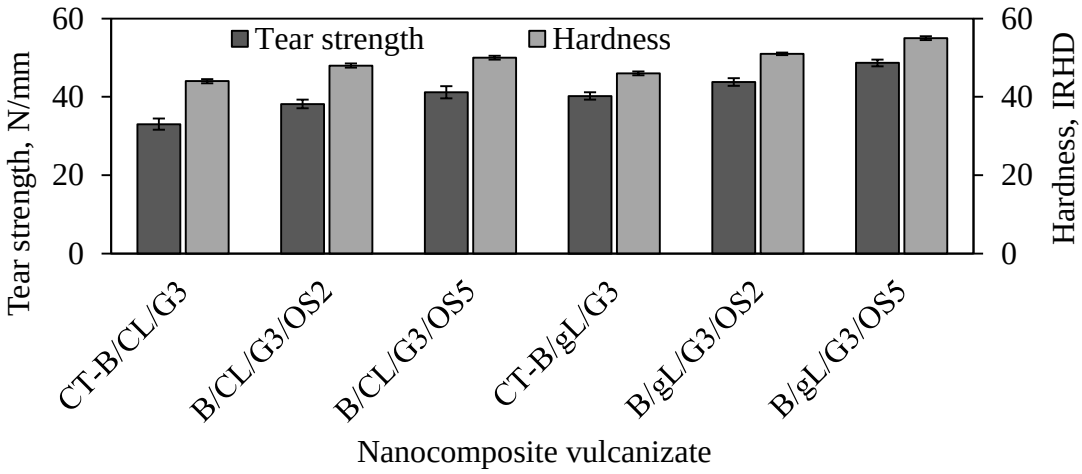

Figure 4. 88 Tear strength and hardness of B/CL/G3 and B/gL/G3 nanocomposite vulcanizates

4.3.5.10 Ageing properties

Figure 4.90 illustrates the PRV of tensile strength, mod 300%, and elongation at break, in B/CL/G3/OS2, B/CL/G3/OS5, B/gL/G3/OS2, and B/gL/G3/OS5 nanocomposite vulcanizates after thermal ageing. In B/gL/G3/OS5 nanocomposite vulcanizate, tensile properties are reduced by the deterioration of improved rubber-clay interaction by thermal ageing. The rubber-clay interaction such as hydrogen bond and dipole-dipole interactions are believed to be more vulnerable to rupture at higher temperatures for an extended period. Although the tensile properties are reduced by thermal ageing, the tensile strength (35.8 MPa), mod at 300% (4.8 MPa), and

elongation-at-break (600%) of B/GL/G3/OS5 nanocomposite vulcanizate are still higher than most of the tensile properties reported in previous sections.

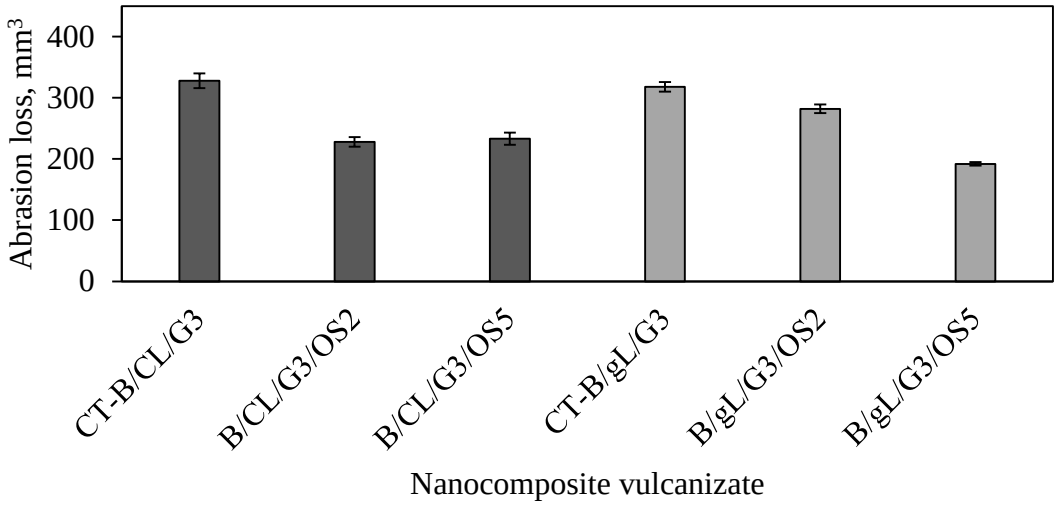

Figure 4. 89 Abrasion loss of B/CL/G3 and B/GL/G3 nanocomposite vulcanizate

4.3.5.11 TGA study

It is necessary to check the remaining amount of clay at the stage of the nanocomposite. Clay would be lost at each stage of latex blending, drying, and milling while preparation of nanocomposite. A small change of nanoclay lost may affect the properties of nanocomposite and give wrong information. TGA could be used to determine the percentage of remaining clay in the nanocomposites because clay as an inorganic substance, does not decompose at around 500°C but other organic substances in NR are pyrolysed at elevated temperature in an inert environment. The percentages of the remaining weight of CT-B/gL/G3, and B/gL/G3/OS5 nanocomposites are 7.6% and 10.4% (w/w) respectively at 500°C (Figure 4.91). The actual weight percentage of OMMT-S in B/gL/G3/OS5 (MB-F2) is 4.76%. The percentage un-decomposed weight of OMMT-S at 500°C was 68.6% (w/w). Therefore, the remaining weight after decomposition should be 3.2%. The difference between CT-B/gL/G3 and B/gL/G3/OS5 was 2.8% (w/w) corresponded to the percentage weight of undecomposed OMMT-S. This shows that 0.8% (w/w) of reduction of OMMT-S from the initial content, which may be mainly due to sedimentation of OMMT-S in OMMT-NRL mix. This means 99.2 % (w/w) OMMT-S remained in the final nanocomposite

stage after all processing methods. The sedimentation of OMMT-S could not be prevented comprehensively due to the suspension behavior of OMMT-S but could be minimized with a quick gelation process.

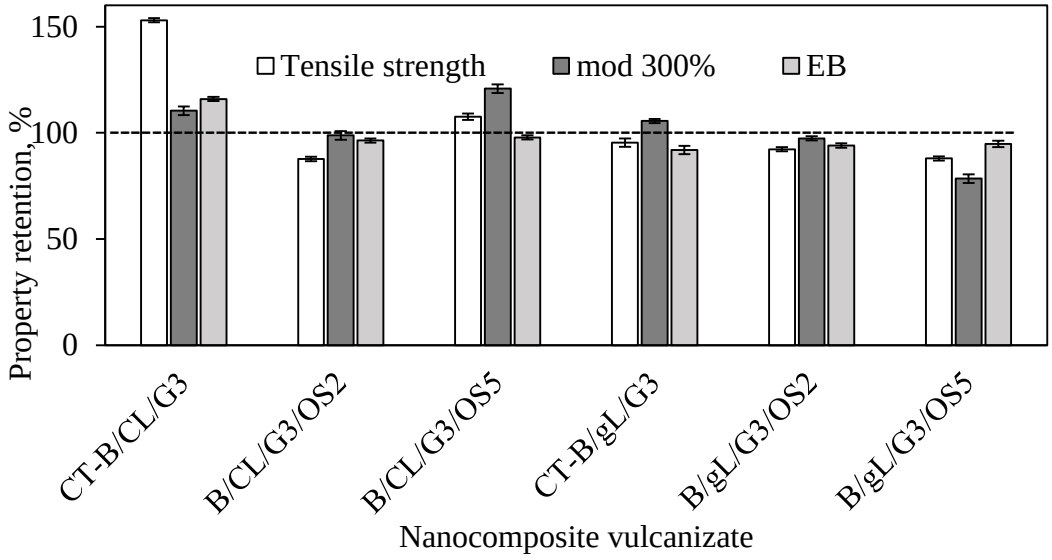

Figure 4. 90 Ageing properties of B/CL/G3 and B/gL/G3 nanocomposite vulcanizates

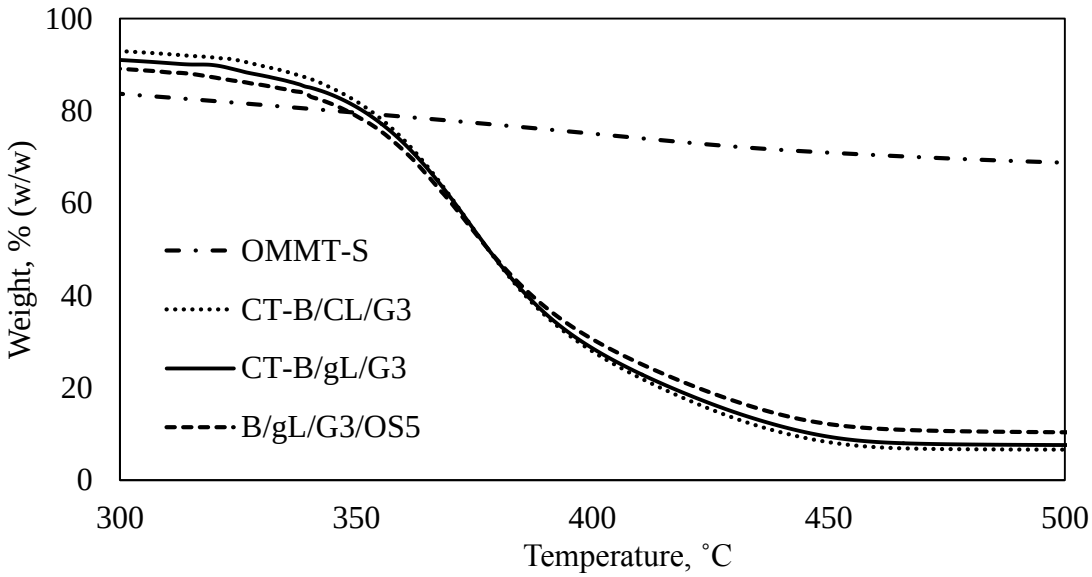

Figure 4. 91 Percentage of weight lost in nanocomposite by TGA study

4.4. Proposed structures of NR-clay nanocomposites

Figure 4.92, Figure 4.93, Figure 4.94, Figure 4.95 and Figure 4.96 propose the possible structures of CT-B/CL/G3 vulcanizate, B/CL/G3/O2 nanocomposite vulcanizate, B/CL/G3/O5 nanocomposite vulcanizate, B/CL/G3/OS series nanocomposite vulcanizates and B/gL/G3/OS series nanocomposite vulcanizates respectively. In CT-B/CL/G3 vulcanizate, the gelling clusters are distributed throughout the rubber matrix without disturbance of clay as presented in Figure 4.92.

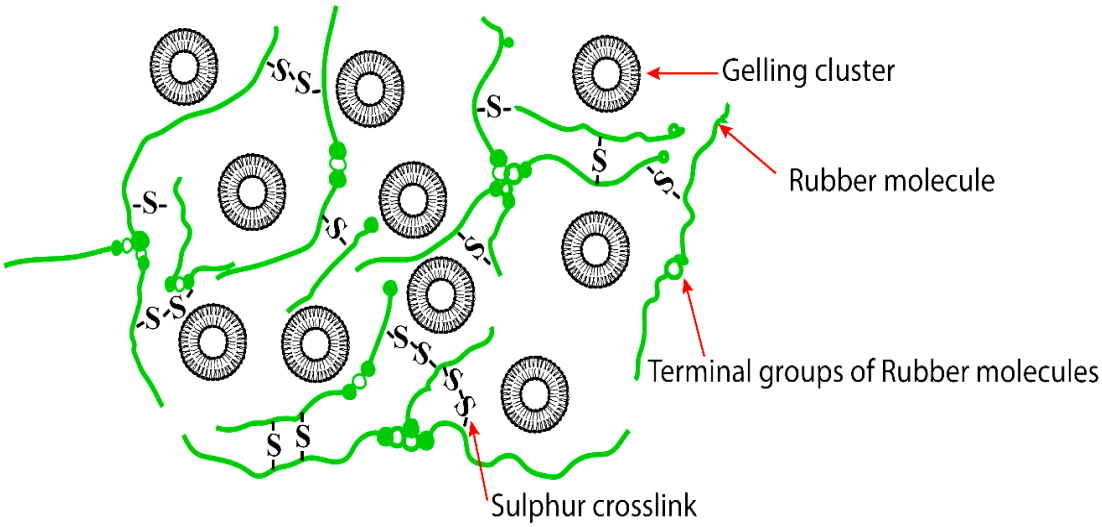

Figure 4. 92 Proposed structure of CT-B/CL/G3 vulcanizate

XRD plots in Figure 4.42 confirm the presence of crystalline structures in amorphous rubber. This may be due to the presence of properly dispersed well-ordered gelling clusters in the rubber matrix. When OMMT is added into rubber, the weak interphase in gelling clusters are reinforced by clay layers. The few smaller size clay stacks distribute in the rubber phase and such clay structures do not disturb the arrangement of crystalline structures of gelling clusters, hence a large number of gelling clusters are dominant in B/CL/G3/O2 nanocomposite vulcanizate shown in Figure 4.93.

At OMMT loading of 5 phr, in the B/CL/G3/O5 nanocomposite vulcanizate, the arrangement of crystalline structures of gelling clusters are disturbed by clay aggregates. However those clusters are arranged between clay stacks as seen in Figure

4.94. The presence of higher number of aggregated structures in Figure 4.94 is the main difference compared to Figure 4.93.

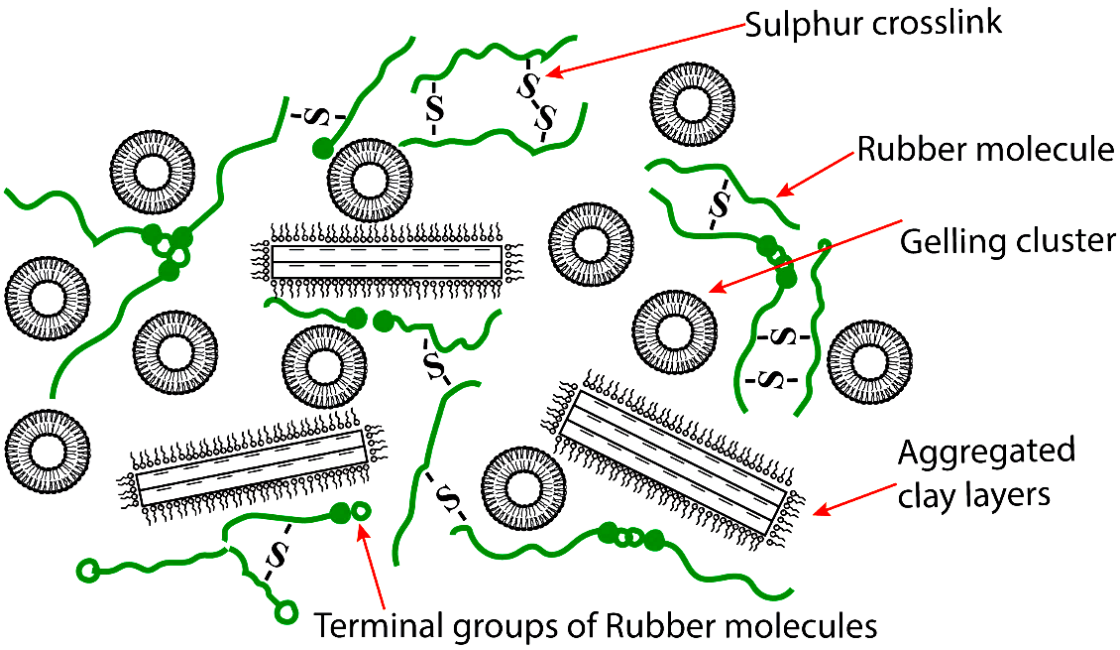

Figure 4. 93 Proposed structure for B/CL/G3 nanocomposite vulcanizate with 2 phr loading of OMMT

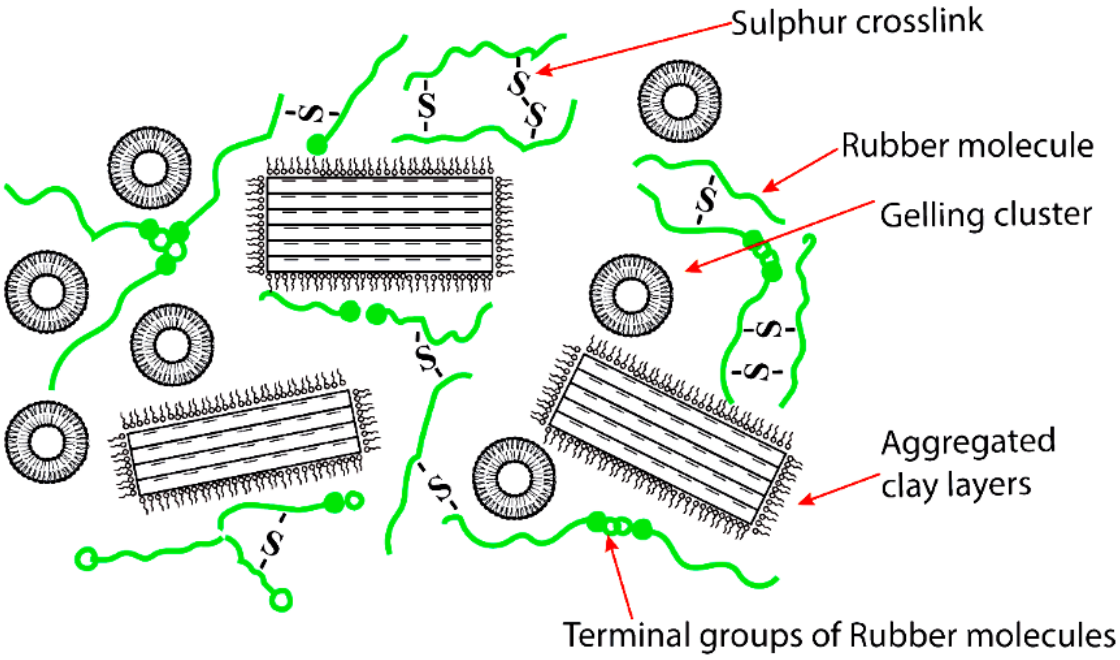

Figure 4. 94 Proposed structure for B/CL/G3 nanocomposite vulcanizates with 5 phr loading of OMMT

In B/gL/G3/OS2 and B/gL/G3/OS5 nanocomposite vulcanizates, as in Figure 4.96, OMMT-S is dispersed properly in polar rubber shows a higher degree of clay exfoliation. The addition of 2phr loading of OMMT-S is enough to disturb the crystalline arrangement gelling clusters and clay-gelling structures. With the addition of OMMT-S at 5 phr in B/GL/G3/OS5 nanocomposite vulcanizate, a higher number of exfoliated OMMT-S layers further disturb the crystalline structures and give a similar effect as B/GL/G3/OS2 nanocomposite vulcanizate.

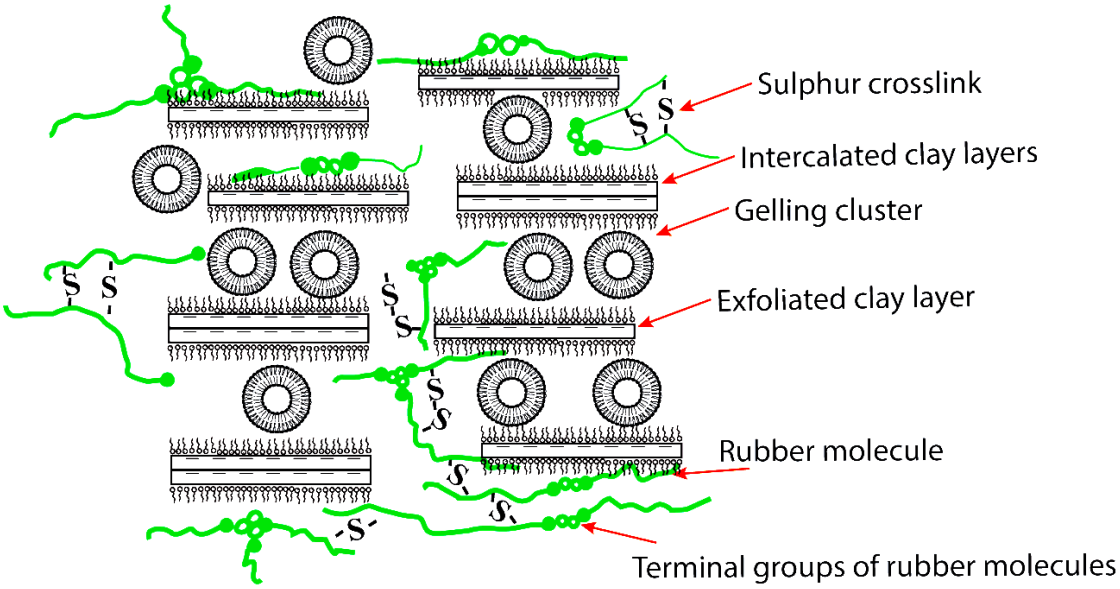

Figure 4. 95 Proposed structure for B/CL/G3/OS2 and B/CL/G3/OS5 nanocomposite vulcanizates

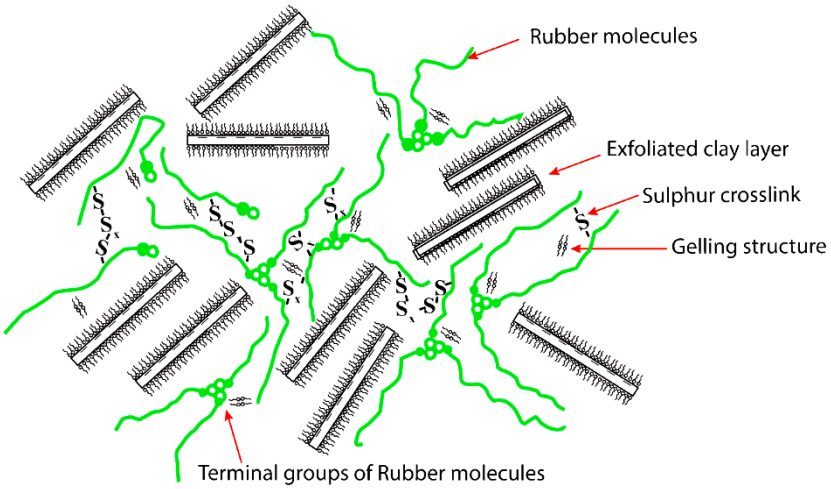

Figure 4. 96 Proposed structure for B/GL/G3 nanocomposite vulcanizate

4.5 Proposed reaction mechanisms for modification of NR and clay

MMT is first intercalated by CTAB to increase the interlayer-gallery space and improve the hydrophobic nature to be compatible with NR. Hence, the prepared organically modified (OMMT) clay is dispersed in the rubber matrix with considerably less aggregation with a restriction for phase separation.

OMMT is then grafted with the TESPT coupling agent to produce OMMT-S. TESPT is introduced to clay in ethyl alcohol medium in the absence of water; otherwise, TESPT is hydrolyzed by water and globules like TESPT particles would prevent grafting reaction with OMMT. A siloxane network is formed around OMMT by hydrolyzed TESPT and is illustrated in Figure 4.97.

In hydrated condition, a grafted reaction occurs between the silanol group of hydrolyzed TESPT and the silanol group of OMMT-S by creating hydrogen bonds. The ethoxy groups attached to adjacent TESPT molecules form siloxane bonds by condensation and dehydration reaction while heating at a higher temperature and finally produce a siloxane network. Figure 4.98 presents the grafted siloxane network around clay layers by dehydration.

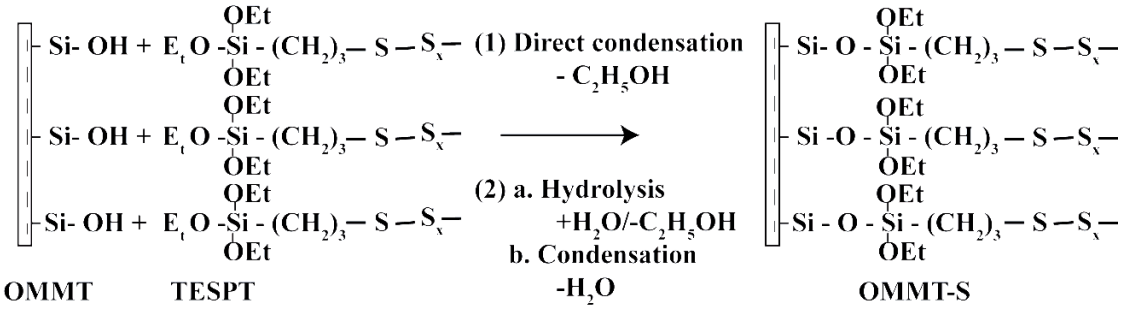

Figure 4. 97 The formation of grafted TESPT in OMMT-S

OMMT-S imparts two reactive sites, the alkoxy site by which it already grafted into clay, and the sulphidic site, which form sulphur crosslinks with rubber at later vulcanization stages. The interaction of OMMT-S with rubber and clay is depicted in Figure 4.99.

The developed rubber-clay interactions are responsible for having more distribution of clay with lowering surface energy. However, it needs reactive sites grafted on rubber

to interact with the clay to enhance rubber-clay interactions. Hence, rubber is also grafted by succinimide (SI) which is the derivative of maleic anhydride (MAH), specially produced by a series of reactions. MAH could not be directly added into NR due to its high reactivity since highly acidic MAH causes coagulation of rubber at the latex stage. MAH replaced by its less acidic derivative maleamic acid (MA) prevents coagulation and grafts into the rubber at the latex stage as SI, which was confirmed by FTIR analysis of dry NR (Section 4.3.4.1).

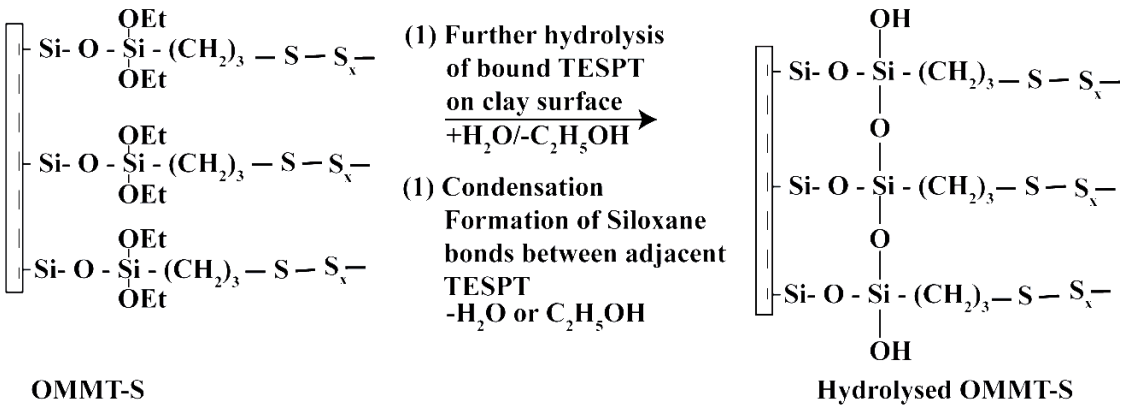

Figure 4. 98 The formation of grafted siloxane network TESPT grafted on clay

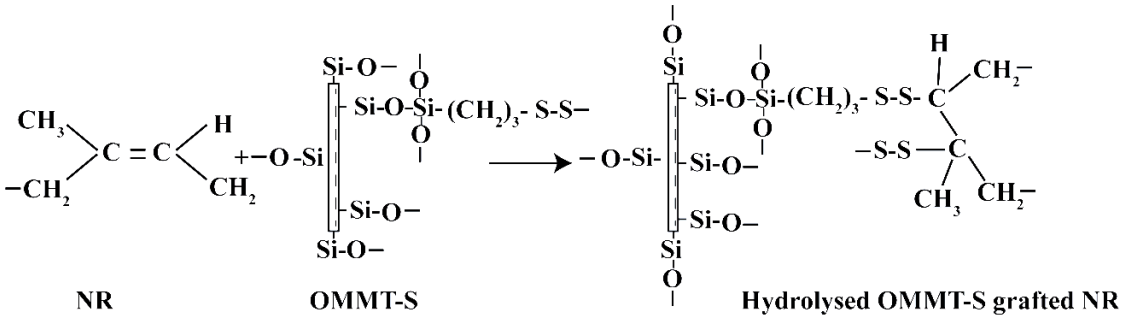

Figure 4. 99 The structure of OMMT-S clay grafted on NRL

Initially, MA was prepared by the reaction of concentrated ammonia with MAH during the reaction, the MAH ring is opened, and MA is produced by nucleophilic addition reaction (Figure 4.100).

It is expected that the MA would rearrange into succinamic acid (SA) after grafting into NRL. Many studies also proposed that the conversion of maleic form into succinic form is possible due to structural stability of succinic form with rubber

(Kannika and Beraheng., 2008). Figure 4.101 shows the grafted SA on NRL in latex medium before drying.

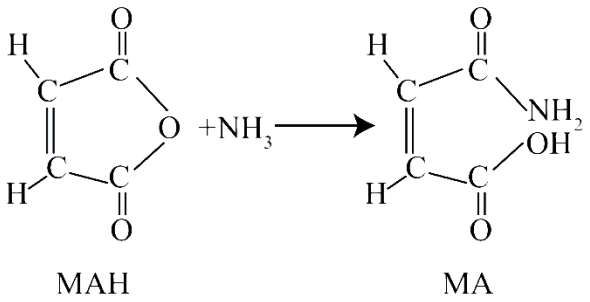

Figure 4. 100 Reaction between MAH and ammonia

With the addition of OMMT into NRL, the hydrogen bond and dipole-dipole interactions occurred between silanol groups of the clay surface and SA grafted group of on NRL which improves the compatibility between rubber and clay in latex medium as shown in the Figure 4.102.

However, SA graft on NRL is converted into succinimide (SI) after the dehydration reaction during drying in the preparation of dry raw rubber according to the reaction given by Figure 4.103. Kita & Kishino (1998) also prepared imide from different reactions similarly by dehydration in different fields of research.

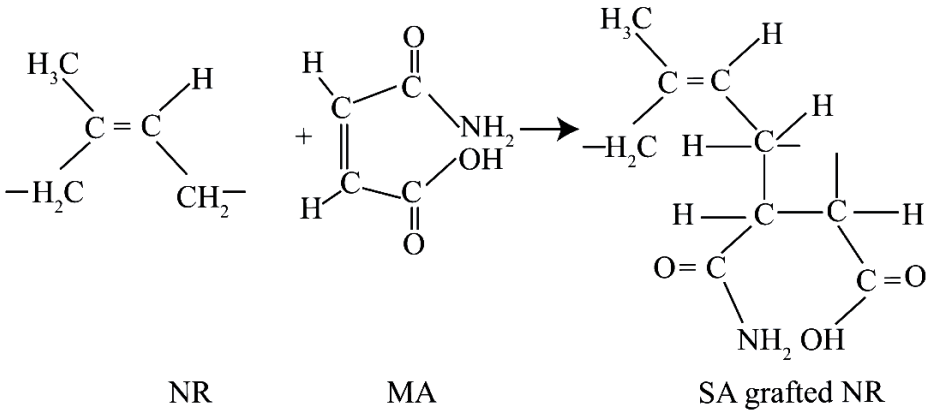

Figure 4. 101 The formation of SA grafted NRL before drying

SI graft NRL consist of hydrogen bond, and dipole-dipole interactions which increase the compatibility of clay and rubber. Creating such rubber-clay interactions before the formation of final sulphur crosslinks is crucial for better dispersion of exfoliated structure, otherwise surface active nanoclay forms aggregated structures easily. The

multifunctional coupling system (Figure 4.104) introduced in the study prevents such undesirable effects successfully. The coupling system consists of two reactive sites to interact with rubber and clay.

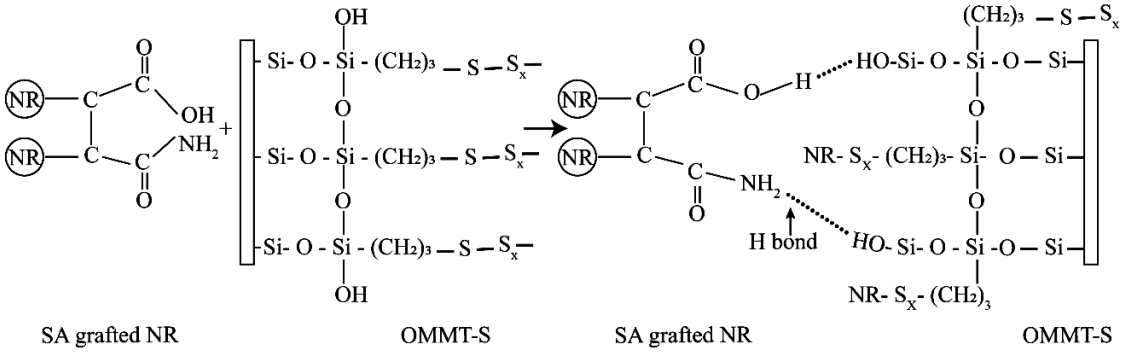

Figure 4. 102 The formation of SA grafted NRL and OMMT-S before dehydration

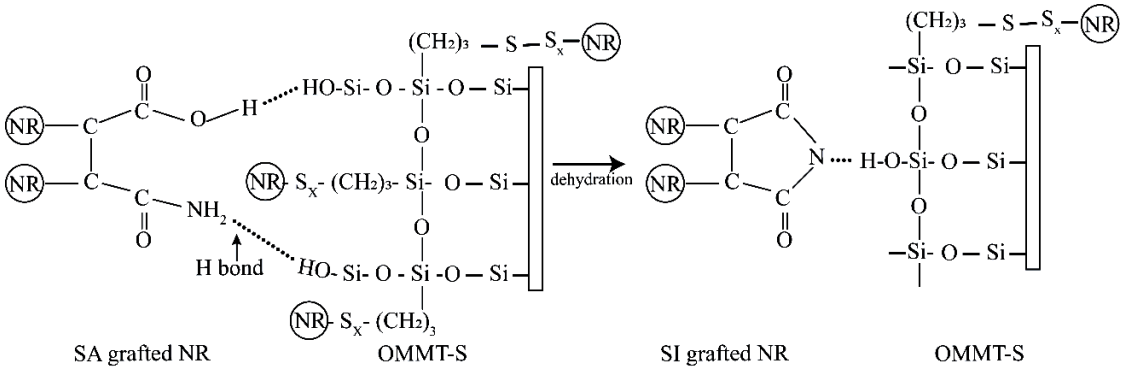

Figure 4. 103 The Structure of SI grafted NR and OMMT-S after dehydration

The grafted SI group in rubber forms hydrogen bonds and dipole-dipole interactions with both the silanol group and the siloxane group of clay. Further, sulphur crosslinks created between TESPT grafted clay and rubber, increase the rubber-clay interactions. The polar and non-polar balance between rubber and clay is maintained by the modification of both rubber and clay by a novel coupling system. The surface activity of clay is reduced by replacing the silanol group by siloxane network. The non-polar nature of clay is improved by the intercalation of organophilic CTAB. The polar nature of rubber is increased by grafting the SI group on non-polar rubber. Such modification would decrease the surface energy of clay and increase the surface energy of NR, hence aggregation of clay is minimum. As a result of that clay stacks with few clay layers are also separated into exfoliated clay layers. The electrostatic interaction

between CTAB and SDS in gelling agent G3 is also compatible with this novel coupling system and further enhance the properties.

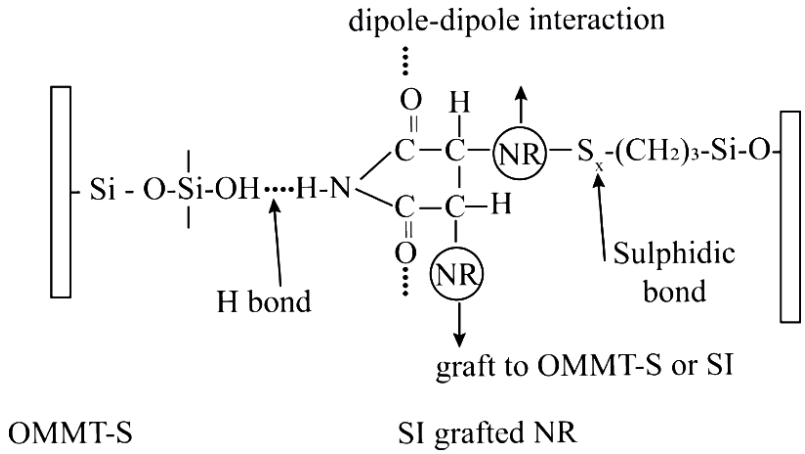

Figure 4. 104 The structure of the proposed multifunctional coupling system

The selected mechanical properties of nanocomposite at similar effective clay loading (5 phr) are shown in Table 4.17, and enhancement of the properties is clearly increased by the modification in the study.

Table 4. 17 Mechanical properties of different nanocomposite at 5 phr clay loading and percentage as compared to B/FL/M5 nanocomposite vulcanizate

	Tensile strength, MPa	**%**	**EB, %**	**%**	**Mod 300%, MPa**	**%**	**Hardness, IRHD**	**%**	**Tear strength**	**%**
B/FL/M5	31.3	-	485	-	5.1	-	40	-	20.6	-
A/FL/M5	13.8	-56	483	0	4.3	-18	37	8	18.4	12
C/PC/O5	25.0	-20	606	25	4.2	-18	44	9	35.6	73
B/FL/G1/M5	23.7	-24	587	21	3.9	-23	42	5	32.6	58
B/CL/O6	32.6	4	597	23	4.0	-22	47	18	34.4	67
B/CL/G3/O5	37.5	20	650	34	3.6	-29	49	22	42.8	108
B/CL/G3/OS5	31.3	0	574	18	4.1	-20	50	25	41.2	100
C/PC/OS5	29.7	5	589	21	4.2	-18	46	15	32.1	59
B/gL/G3/OS5	40.7	30	630	30	6.0	18	55	38	48.7	136

These properties show that the novel coupling system is responsible to have maximum values of all mechanical properties in B/GL/G3/OS5 nanocomposites, whereas other nanocomposites show that only some mechanical properties attain the maximum values.

CHAPTER 5

5. CONCLUSIONS AND RECOMMENDATIONS FOR FUTURE WORKS

5.1 Conclusions

The NR-clay nanocomposite vulcanizates at different compositions were successfully prepared from NRL and MMT or modified-MMT dispersions, using the novel Acid-free co-coagulation (AFCC) method, and the conventional acid co-coagulation (ACC) method followed by mechanical mixing. Nanocomposite vulcanizates prepared using AFCC method, compared to those prepared using ACC method, exhibited retaining of more exfoliated clay structures in the NR matrix, and superior physico-mechanical and chemical properties, concluding that the AFCC method is more suitable in the preparation of NR-clay nanocomposites.

The drawback of the slow drying stage of the AFCC method was overcome by introducing three different gelling agents, namely SSF (G1), CTAB (G2), and the novel combined gelling agent of CTAB and SDS (G3). The nanocomposites prepared with the gelling agent G3 had a few aggregated clay structures compared to the other two gelling agents and the gelling agent G3 was proven as the most effective gelling agent.

The nanocomposites prepared from pale crepe rubber and clay, using the conventional mechanical mixing method exhibited aggregated clay structures in the NR matrix, and poor physico-mechanical properties, deducing that the exfoliated clay structures would not be developed in the NR matrix when mechanical mixing method was used.

The XRD and SEM analysis of the nanocomposites and the nanocomposite vulcanizates prepared with MMT and modified-MMT (OMMT and OMMT-S) revealed that the exfoliated clay structures would be developed when modified-MMT was used. Further the SEM images of the nanocomposite vulcanizates prepared with OMMT-S, compared to those with OMMT, showed better distribution of clay layers with minimum clay aggregation. Therefore, it can be concluded that the enhanced mechanical properties along with fine morphology could be obtained when MMT was

organically modified with CTAB, and further treated with TESPT. Further enhancements in the dispersion of modified-MMT in NR matrix via polar non-polar balance, NR-clay interactions and degree of exfoliation were obtained by grafting of NR with SI, and therefore it could be concluded that the remarkable mechanical properties could be achieved when both NRL and MMT were modified and is the novel coupling system developed under this study.

The mechanical properties of the rubber vulcanizates were enhanced with the addition of MMT or OMMT or OMMT-S into NR. Further, the mechanical properties of the nanocomposite vulcanizates were increased initially with the increase of MMT/OMMT/OMMT-S loading and then decreased passing through an optimum loading. Best-balanced properties of the nanocomposite prepared with MMT and NRL using ACC method was obtained at the MMT loading of 12 phr, while that using AFCC method was obtained at the MMT loading of 8 phr. The nanocomposite vulcanizates prepared with OMMT and NRL using AFCC method showed best-balanced properties at a lower MMT loading of 2 phr and all the properties were greater compared to those prepared with MMT at the same loading. The nanocomposite vulcanizates prepared with OMMT and NRL in the presence of the combined gelling agent-G3 exhibited better properties at every clay loading studied and the best-balanced properties were obtained at the OMMT loading of 5 phr. Further enhancement in properties was recorded when OMMT-S was replaced by OMMT and the best balance properties were obtained at the OMMT-S loading of 2 phr. The highest improvement in overall properties was shown by the nanocomposite vulcanizate prepared with OMMT-S and SI grafted-NRL at the OMMT-S loading of 5 phr. The improvements of the tensile strength (40.7 MPa), elongation at break (630%), mod 300% (6 MPa), hardness (55 IRHD) and tear strength (38 N/mm) over those of the nanocomposite vulcanizate prepared using AFCC method with MMT and NRL at its optimum loading were 30%, 30%, 18%, 30%, and 136%, respectively. These property increments compared to those of the nanocomposite vulcanizate prepared using mechanical mixing with MMT and pale crepe rubber at the MMT loading of 5 phr were 63%, 4%, 43%, 25%, and 33%, respectively.

Considering the high strength with flexibility and improved compatibility between NR and clay resulted in the nanocomposite vulcanizate prepared with SI grafted-NRL and OMMT-S, a mechanism for the development of NR-clay interactions was proposed assuming that the different bonds/interactions would form between NR and clay. The imide groups of SI grafted-NRL interact with silanol/siloxane groups in OMMT-S and form hydrogen bonds while the sulphur atoms in OMMT-S form sulphidic links with NR. The dipole-dipole interactions occur between carbonyl groups in SI grafted-NRL and siloxane network/silanol around OMMT-S. Further, the sulphidic links would form between carbon-carbon double bonds in succinimide and NR.

5.2 Recommendations for future work

In the present study, the nanocomposites were prepared with clay and NRL using AFCC method in which destabilizing was occurred due to evaporation of high amount of water during oven drying. Due to high energy requirement, oven drying will not be a practical method to produce nanocomposites in a commercial scale. Therefore, a suitable drying technique; either solar drying or smoke drying is to be experimentally identified in the future.

The selection of a highly suitable surfactant and/or a modifier would minimize time and energy associated with the modification of MMT, which was carried out in two stages at the present study. Polymer network in general is more effective in the dispersion of negatively charged nanoclay in NRL, and in creating and retaining of exfoliated clay structures. Therefore, further studies could be focused on replacing CTAB, a monomeric cationic surfactant used to modify MMT, with a polymeric cationic surfactant such as poly(diallyldimethylammonium chloride). Alternatively, a cationic monomer could be incorporated into the NRL-MMT mix for in-situ polymerization. Polymers such as poly(glycidyl methacrylate) could also be grafted onto MMT by atomic transfer radical polymerization. Dimeric surfactant referred to as a Gemini surfactant is considered as a new generation of surfactant and it is made up of two identical amphiphilic moieties connected by a spacer near the head group. Lower critical micelle concentration, reduction of oil-water tension, and unusual aggregation morphology, better wetting, and solubilizing behavior are the main

advantages of Gemini surfactants over conventional surfactants. Therefore, the application of the Gemini surfactant as a gelling agent would be a better option to consider for future studies.

A variety of silane coupling agents with several functional groups such as epoxy groups, amino groups, vinyl groups, isocyanate groups, and mercapto groups are available for industrial use. Therefore, the applicability of silane coupling agents with multi-functional groups in treating of OMMT would also be an alternative option to enhance rubber-clay interactions and thereby to enhance mechanical properties of the nanocomposite vulcanizates.

Kaolin, though it has a nano layered structure, is used in rubber compounds as a non-reinforcing filler. Kaolin is a widely available inexpensive material and hence its use in the preparation of rubber-clay nanocomposites would be an economical advantage. The development of exfoliated clay structures and improvement of mechanical properties of the nanocomposite vulcanizates thereby would be a great challenge. Therefore, future studies could be conducted to use kaolin as an alternative to MMT.

REFERENCES

1. Abdollahi, M., Rahmatpour, A., Aalaie, J., Khanbabae, G., (2008). Preparation and evaluation of the microstructure and properties of natural rubber/ sodium montmorillonite nanocomposites, *Iranian Polymer Journal*, 17(7), pp. 519-529.

2. Adams, J.M., (1987). Synthetic organic chemistry using pillered cation exchange and acid treated montmorillonite ctalysts- a review. *Applied Clay Science, 2*(4), pp. 309-342.

3. AGM, Sri Lanka association of manufactors and exports of rubber product, Cinamon Grand Colombo, 21 January 2019, Avalable at http:/Slamerp.lk/news/SriLanka

4. Alex, R., Nah, C., (2006). Preparation and characterization of organoclay-rubber nanocomposites via a new route with skim natural rubber latex, *Journal of Apllied Polymer Science, 102*(4). pp. 3277-3285.

5. Alexandre, M., Dubois, P., (2000). Polymer-layered nanocomposites: preparation, properties and uses of a new class of materials, *Materials Science and Engineering, 28*(1-2), PP 1-63.

6. Alkadsi, N.A.N, (2008). Comparative studies on the effect of titanate coupling agent on the mechanical properties of zinc oxide- filled chlorprene and natural rubber, *International Polymer Science and Tecnology, 35*(7), pp. 226-230.

7. Alwis, G.M.C., Ratnayaka, U.N., Kottegoda, N., (2013). Reinforcement and curing characteristics of organoclay filled natural rubber nanocomposites, *Journal of Rubber Research Institute of Sri Lanka,* 93, pp. 89-103.

8. Amarasiri, A., Ratnayake, U.N., Silva, U.K., Walpalage, S., Siriwardena, S., (2013)., Natural rubber latex-clay nanocomposites: use of montmorillonite clay as an alternative for conventional $CaCO_3$, *Journal of the National Science Foundation of Sri Lanka, 41*(4), pp. 293-302.

9. Ames, K., Gibala, D., and Hamed, G.R., (1996). Styrene-Butadiene Rubber filled with fluorinated Carbon Black: part II. Effect of curative level. *Rubber Chemistry and technology, 69*(2), pp. 273-276.

10. Amnuaypornsri, S., Sakadapipanich, J., Toki, S., Hsiao, B.S., Ichikawa, N., Tanaka, Y., (2008). Strain-induced crystallization of natural rubber: effect of proteins and phospholipids, *Rubber Chemistry and Technology, 81*(5), pp. 753-766.

11. Aranda, P., Ruiz-Hitzky, E., (1992). Poly(ethylene oxide)- silicate intercalation materials, *Chemistry of Materials*, *4*(6), pp. 1395-1403.

12. Arrighi, V., McEwen, I.J., Qian, H., Prieto, M.B.S., (2003). The glass transition and interfacial layer in styrene-butadiene rubber containing silica nanofiller, *Polymer*, *44*(20), pp. 6259-6266.

13. Arroyo, M., Lopez-manchado, M.A., Herrero, B., (2003). Organo-montmorillonite as subtitute of carbon black in natural rubber compounds, *Polymer, 44*(8), pp. 2247-2453.

14. Ashraf, S.M., Ahmad, S., Riaz, U., (2009). *A laboratotory manual of polymers*, PP. 35. L.K Publishing house pvt(Ltd). New Delhi

15. Avalos, F., Ortiz, J.C, Zitzumbo, R., Lopez-Manchado M.A., Verdejo, R., Arroyo, M., (2008). Effect of montmorillonite intercalant structure on the cure parameters of natural rubber, *Europhian Polymer Journal, 44*(10), pp. 3108-3115.

16. Bala, P., Samantaray, B.K., Srivastavas, K., Nando, G.B., (2004). Organomodified montmorillonite as filler in natural and synthetic rubber, *Applied Polymer Sience, 92*(6), pp. 3583-3592.

17. BaO, Y., LiGong, T.J (2010). *Testing and evaluation of inorganic materials*, Trans Tec Publications Ltd, Switzerland.

18. Beall, G.W., Goss, M., (2009). Self assembly of organic molecules on montmorillonite. *Applied Clay Science*, *27*(3), pp. 179-186.

19. Belton, D.B., Deschaume, O., Perry, C.C., (2012). An overview of the fundermentals of the chemistry of silica with relavance to biosilicification and tecnological avances, *FEBS Journal*, *279*, pp. 1710-1720.

20. Bharadwaj, R.K., Mehrabi, A.R., Hamilton, C., Trujillo, C., Murga, M., Fun, R., Chavira, A., Thompson, A.K., (2002). Structure-property relationships in cross-linked polyester-clay nanocomposites, *Polymer*, *43*(13), pp 3699-3705.

21. Bharadwaj, P., Singh, P., Panday, K.N, Verma, V., Srivastava S.K., (2013). Structure and properties of styrene buitadiene rubber/ modified hectorite clay nanocomposite, Applied Polymer Composites, *1*(4), pp. 207-224.

22. Bhattacharya, M., Maiti, M., Bhowmick, A.K., (2008). Influence of different nanofillers and their dispersion methods on the properties of natural rubber nanocomposites, *Rubber Chemistry and Technology*, *81*(5), pp. 782-808.

23. Bhowmick, A.K., Bhattacharya, M., Mitra, S., (2010). Exfoliation of nanolayer assemblies for improved natural rubber properties: methods and theory, *Journal of Elastomers and Plastics*, *42*(6), pp. 517-537.

24. Biswas, M., Ray, S.S., (2000). Water –dispersible nanoomposites of poly aniline and montmorillonite, *Journal of Applied Polymer Science*, *77*(13), pp. 2948-2956.

25. Blacklley D.C. (1997a). Types of lattices, *Polymer lattices science and Technology*, Volume 2, 2nd edition, pp.72-97. Chapmann & Hall, London, UK.

26. Blacklley D.C. (1997b). Applications of latices, *Polymer lattices science and Technology*, Volume 3, 2nd edition, pp.271-272. Chapmann & Hall, London, UK.

27. Blacklley D.C. (1997c). Fundamental principles, *Polymer lattices science and Technology*, Volume 1, 2nd edition, pp.351-355. Chapmann & Hall, London, UK.

28. Blow, C.M (ed)., (1971). *Rubber Technology and Manufacture*, Buttenvorths, London, P 227.

29. Blow S (ed)., (1998). *Handbook of Rubber technology*, Galcotia Publication Ltd, New Delhi, p 483.

30. Bottcher, H., Hallensleban, M.L, Wurm, H., Bauer, J., Behrens, P., (2002). Organic/ inorganic hybrids by living/ controlled ATRP grafting from layered silicates, *Journal of Material Chemistry*, *12*(5), pp. 1351-1354.

31. Brown, P.S., Tinker, A.J., (1990). Crosslink distribution in vulcanized blends of NR and EPDM, *J.nat.Rubb.Res.*, *5*(3), pp. 157-162.

32. Burnside, S.D., Giannelis, E.P., (2000). Nanostructure and properties of poly siloxane-layered silicate nanocomposites, *Journal of Polymer Science Part B Polymer Physics*, *38*(12), pp. 1595-1604.

33. Camargo, P.H.C., Satyanarayana, K.G., Wypych, F., (2009). Nanocomposites: synthesis, properties and new application opportunities, *Material Research*, *12*(1), pp. 1-39.

34. Carli, L.N., Roncato, C.R., Zanchet, A., Mauler, R.S., Giovanela, M., Brandalise, R.N., Crespo, J.S., (2011). Characterization of natural rubber nanocomposites filled with organoclay as a substitute for silica obtained by the conventional two-roll mill method, *Applied Clay Science*, *52*(1-2), pp. 56-61.

35. Carretero-Gonzalez, J., Valentin, J.L., Arroyo, M., Saalawachter, K., Lopez-Manchado, M.A., (2008). Natural rubber/clay nanocomposites: Influence of poly(ethylene glycol) on the silicate dispersion and local order of rubber network, *Europhean Polymer Journal*, *44*(11), pp. 3493-3500.

36. Carter, L., Hendricks, J.G., Bolley, D.S & The national lead Co 1950, Elastomer reinforced with a modifie clay, US Patentent 2531396150.

37. Chakraborty, A., Basak, S., (2008). Effect of surfactants on casein structure: a spectroscopic study, *Biointerphases*, *63*(1), 83-90.

38. Chattopadhyay, P.K., Basuli, U., Chattopadhyay, S., (2010). Studies on navel dual filler based exfoliated natural rubber nanocomposites, *Polymer Composites*, *31*(5) pp. 835-846.

39. Chazeau, L., Cavaille J.Y., Canava, G., Dendievel, R., Boutherin, B., (1999). Viscoelasic properties of plastcized pvc reinforced with cellulose whiskers, *Applied Polymer Science*, *71*(11), pp. 1797-1808.

40. Chen, C.W., Higashi, M., Naito, T., Akashi, M. (2001). Size-selective synthesis of CdS nanoarticles on polyethylene films. *Chemistry Letters*, *20*(9), pp.870-871.

41. Choi, Y.S., Chung, I.J., (2008). Comprehending polymr-clay nanocomposites and their future works, *Korean Chemical Engineering Research*, *46*(1), pp. 23-36.

42. Chou, C.C., Chang, Y.C., Chiang, M.L., Lin, J.J., (2004). Conformational change of trifunctional poly (Oxypropylene) amines intercalated with a layered silicates confinement, *Maromolecules*, *37*(2), pp. 473-477.

43. Chow, W.S., Neoh, S.S., (2009). Dynamic mechanical thermal and morphological properties of silane treated montmorillonite reinforced polycarbonate nanocomposites, *Journal of Applied Polymer Science*, *114*(6), pp. 3967-3975.

44. Cornish K., Castillon J., Scott D.J. (2000). Rubber molecular weight regulation, in vitro, in plant species that produce high and low molecular weights in vivo. *Biomacromolecules*, *1*(4). pp. 632-641.

45. Cornish K., Wood D.F., Windle J.J. (1999). Rubber particles from four different species, examined by transmission electron microscopy and electron-paramanatic-resonance spin labeling, are found to consist of a homogeneous rubber core enclosed by a contiguous, monolayer biomembrane. *Planta, 210*(1): 85-96.

46. Dannenberb E.M. (1975). The effect of surfacce chemical interactions on the properties of filler-reainforced rubbers, *Rubber Chemistry and Technology, 48*(3): 410-444.

47. Das, A., Werner, K., Jurk, R., Jehnichen, D., Henrich, G., (2011). A general approch to rubber-montmorillonite nanocomposites: intercalation of stearic acid, *Applied Clay Science, 51*(1-2), pp. 117-125.

48. Datta, R.N., (2001). *Rubber curing system*, Rapra review reports, Rapra Technology Ltd, volume 12, pp. 3-26.

49. Deller, M., Kong, L., Rupp, B., (2016). Protein Stability: a crystallographer's perspective, *Acta Crystallographica, 72*(2), pp. 72-95.

50. Dietsche, F., Thomann, Y., Thomann, R., Mulhaupt, R.J., (2000). Translucent acrylic nanocomposites containing anisotropic laminated nanoparticles derived from intercalated layered silicates, *Applied Polymer Science, 75*(3), pp. 396-405.

51. Dresselhaus, M.S., Endo, M., (2001). In: Relation of carbon tubes to other carban materials, Dresslhaus, M.S., Dresselhaus, G., Avouris, P., (eds). Carbon nanotubes: synthesis, structute, prperties and applications, *Topics of Applied Physics,* vol 80, Springer-Verlag, Heidelberg, pp. 11-28.

52. Duy N.Q., Bich N.N. (2009). Nanocomposite from natural rubber latex and organoclay by dipersion destabilization. *Nanocomposite of natural rubber and organoclay*. Rubber research institute of Vietnam. pp. 1-5.

53. Ehabe E.J., Bonfils F. (2014). Novel insight into the gel phase of hevea natural rubber. *Journal of rubber research*, 14(1), pp, 1-10.

54. Ellis, B., Welding, G.N., (1964). Estimation from swelling of the structural contribution of chemical reactions to the vulcanization of natural rubber II. Estimation of equlibrium degree of swelling, *Rubber Chemistry and Technology*, *37*(2), pp. 571-575.

55. Ewulonu, C.M., Obele, C.M., Arukalam, I.O., Odera, S.R., (2015). Effect of local clay incorporation technique on the mechanical properties of natural rubber vulcanizates, *International Journal of Applied Sciences and Engineering Research*, *4*(3), pp. 307-320.

56. Fathurrohman, M.I., Soegijono, B., Budianto, E., Rohman, S., Ramadhan, A., (2015). The effect of organoclay on curing characteristics, mechanical properties, swelling and morphology of natural rubber/ organoclay nanocomposites, *Macrpmolecular Symposia*, *353*(1), pp. 62-69.

57. Fathurrohman, M.T., Rugmis, S., Hayeemasae, N., Sahakaro, K., (2019). Dispersion and properties of natural rubber-montmorillonites nanocomposites fabricated by novel in situ organo modified and latex compounding method, *Polymer Engineering and Science, 59*, pp. 1830-1839.

58. Favier, V., Gavaille, J.Y., Canova, G.R., Shirivastava, S.C., (1997). Mechanical percolation in cellulose whisker nanocomposites, *Polymer Engineering and Science*, *37*(10), pp. 1732-1739.

59. Finocchio, E., Baccini, I., Cristiani, C., Dotell, G., Stampino, P.G., Zampori, L., (2011). Hybrid organo-inorganic clay with nonionic interlayers. Mid and near IR spectroscopic, *The Journal of Physical Chemistry A*, *115*(26), pp. 7484-7493.

60. Flory P.J, Rehner, J.R., (1943). Statistical mechanics of cross-linked polymer networks II. Swelling. *Journal of Chemical Physics*, *11*(11), pp. 521-526.

61. Fox, D.M., Maupin, P.H., Harris, R.H., Gliman, J.W., Eldred D.V., Katsoulis, D., Trulove, P.C., Delong, H.C., (2007). Use of a polyhedral oligomeric sisesquioxane (Poss) imizazolium cation as organic modifier for montmorillonite, *Langmuir*, *23*(14), pp. 7707- 7014.

62. Fukushima, Y., Okada, A., Kawasumi, M., Karauchi, T., (1988). Swelling behaviour of montmorillonite by poly-6-amide, *Clay Minerals*, *23*(1), pp 27-34.

63. Galimberti, M., Senatore, S., Lostritto, A., Giannini, L., Conzatti, L., Costa, G., Guerra, G., (2009). Reinforcement of diene elastomers by organically modified layered silicates, *e-Polymer*, *9*(1). pp. 1-16.

64. Galimberti, M., (2011). *Rubber-clay nanocomposites; science, technology and applications*, John Wiley and Sons Inc, New York, PP. 28-36.

65. Ganter, M., Gronski, W., Reichert, P., Mulhaupt, R., (2001). Rubber nanocomposites: Morphology and mechanical properties of BR and SBR vulcanizates reinforced by organophilic layered silicates, *Rubber Chemistry and Technology*, *74*(2), pp. 221-235.

66. Gardolinski, J.E., Carrera, L.C.M., Canto, M.P., Wypych, F., (2000). Layered polymer-kanlinite nanocomposite, *Journal of Material Science*, *35*(2), pp. 3113-3119.

67. Ghari, H.S., Jalali-Arani, A., (2016). Nanocomposites based on natural rubber, organoclay and nano-calcium carbonate: Study on the structure, cure behaviour, static and dynamic-mechanical properties, *Applied Clay Science*, *119*(2), pp. 348-357.

68. Giannelis, E.P., (1996). Polymer layered silicates nanocomposites, *Advanced Materials*, *8*(1), pp. 29-35.

69. Giger, G., Liponski, M., (1957). Melanges-maitres de caoutchouc et dArgile, *Revue Generale du cautchouc*, *34*, pp. 473-477.

70. Glosh, P., Katare, S., Patkar, P., Caruthers, J.M., Venkatessubramanian, V., (2003). Sulphur vulcanization of NR for benzothiazole accelerated formulations: from reaction mechanism to rational kinetic model, *Rubber Chemistry and Technology*, *76*(3), pp. 592-693.

71. Goerl, U., Hunsche, A., Muller, A., Koban, H.G., (1997). Investigation into the silica/ silane reaction system, *Rubber Chemistry and Technology*, *70*(4), pp. 608-623.

72. Goh, S.H., Phang, K.W., (1978). Thermoanalytical studies of rubber oxidation catalysed by metallic ions, *Thermochemica Acta*, *25*(1), pp 109-115.

73. Gu, Z., Song, G., Liu W., GaO, P., Li H., Hu X. (2009). Preparation and properties of styrene butadiene rubber/natural rubber/organo-bentonite nanocomposites prepared from latex dispersions. *Applied clay science*, *46*(3). pp. 241-244.

74. Guegan, R., (2010). Intercalation of nonionic surfactant ($C_{10}E_3$) bilayer into a Na-montmorillonite clay, *Langmuir*, *26*(24), pp. 19175-19180.

75. Guggenheim, G., (n.d). *Introduction to the properties of clay materials*, [online] Avalable from: http:// minsocam.org/msa/monographs [Accessed 26th may 2019].

76. Guo, F., Aryana, S., Han, Y., Jiao, Y., (2018). A review of the synthesis and applications of polymer-nanoclay composites, *Applied Sciences*, *8*(9), pp. 1696-1725.

77. Gunister, E., Isci, S., Alemdar, A., Gungor, N., (2004). Effect of sodium dodecyl sulfate on flow and electrokinetic properties of Na-activated bentonite dispersions, *Bulletin of materials science*, *27*(3), pp. 317-322.

78. Hakim, R.N., Ismail, H., (2009). Compositon of the effect of organoclay loading on curing and mechanical properties of organoclay-filled epoxidsed

natural rubber nanocomposites and organoclay-filled natural rubber nanocomposites, *Journal of Physical Science*, *20*(2), pp. 37-39.

79. Harahap, H., Surya, E., Surya, I., Ismail, H., Azahari, B., (2014). Effect of leaching treatment on mechanical properties of natural rubber latex products filled modified kaolin, *Applied Mechanics and Materials*, *548-549*, pp. 90-95.

80. Hasma, H., Othman, A.B., (1990). Role of some non-rubber constituents on thermal oxidative ageing of natural rubber, *J.nat.Rubb.Res*, *5*(1), pp. 1-8

81. Heideman, G., Datta, R.N., Noordermeer, J.W.N., Baarle, B.N., (2004). Activators in accelerated sulphur vulcanization, *Rubber Chemistry and Technology*, *77*(3), pp. 512-541.

82. Ho, C.C., Kondo T., Muramatsu N., Ohshima H. (1996). Surface strucure of natural rubber latex particles from electophoretic mobility data. *Journal of Colloidal interface science*,*178*(2): 442-445.

83. Hofman W. (1989). *Rubber Technology Handbook*, Hanser Publishers, Munich, P 284.

84. Hrachova, J., Komadel, P., Jochec-Moskova, D., Krajci, J., Janogova, I., Slouf, M., Chodak, I., (2013). Properties of organoclay natural rubber nanocomposites: Effect of organophillic modifiers, *Journal of Applied Polymer Science*, *127*(5), pp. 3447-3455.

85. Huskic, M., Zagar, E., Zigon, M., Brnardic, I., Macan, J., Ivankovic, M. (2009). Modification of montmorillonite by cationic polyester, *Applied Clay Science*, *43*(3-4), pp. 420-424.

86. Hwang, W.G., Wei, K.H., Wu, C.M., (2004). Preparation and mechanical properties of nitrile butadiene rubber/ silicate nanocomposite", *Polymer*, *45*(16), pp. 5729-5734, 2004.

87. Ishiaku, U., Chong, C., Ismail, H., (2000). Cure characteristics and vulcanizate properties of a natural rubber compound extended with convoluted rubber powder, *Polymer Testing*., *19*(5), pp 507-521.

88. Ishida, H., Ohba, S., (2005). Synthesis and characterization of maleimide and nobornene functionalized of maleimide and nobornene functionalized benzoxazines, *Polymer*, *46*(15), pp. 5588-5595.

89. Ishikawa, W., (2011). Systematic review of tire technology, *National Museum of Nature Science*, *16*, pp. 131

90. Ismail, N.I.N., Veerasamy, D., (2011). Value-added natural rubber skim latex concentrate/ montmorillonite as envirnmentally frendly nanocomposite materials, *Journal of Rubber Research*, *14*(4). Pp. 216-219.

91. Jacob, A., Kurian, P., Aprem, A.S., (2007). Cure characteristics and mechanical properties of natural rubber layered clay nanocomposites, *International Journal of polymeric materials and polymeric bomaterials*, *56*(6), pp. 593-604.

92. Jang, K.H., Kim, E., Jeon, Y.H., Yoon, J., (2012). Clay modification with silane compounds and characteristion of the silicon rubber/ clay composites, *Journal of Polymer Engineering*, *32*(8-9), pp.493-502.

93 Jelinska, A., Zagozdzon, A., Gorecki, M., Wisniewska, A., Frelek, J., Holyst, R., (2017). Denaturation of proteins by surfactants studied by taylor dispersion analysis, *PLOSONE*, 12(4), pp. 1-11.

94. Jeon, H.S., Rameshwaram, J.K., Kim, G., Weinkaul, D.H., (2003). Characterization of polyisoprene-clay nanocomposites prepared by solution blending, *Polymer*, *44*(19), pp. 5749-5758.

95. Joly, S., Garnaud, G., Ollitrault, R., Bokobza, I., Mark J.E., (2008). Organically modified layered silicates as reinforcing fillers for natural rubber, *Chemistry of Materials*, *14*(10), pp. 4202-4208.

96. Juntuek, P., Rukakulpiwat, C., Chumsamrong, P., Ruksapulpiwat, Y., (2012). Effect of glycidyl methacrylate-grafted natural rubber on physical properties of polylactic acid and natural rubber blends, *Applied Polymer Science*, *125*(1), pp. 745-754.

97. Jurkowska, B., Jurkowski, B., Oczkowski, M., Presetskii, S.S., Koval, V., Olkhov, Y.A., (2007). Properties of montmorillonite-containing natural rubber, *Journal of Applied Polymer Science*, *106*(1), pp. 360-371.

98. Kaewkumay, C., Jarukumjorn, K., Suppakarn, N., (2010). Effect of surfactant content and clay content on propertes of NR nanocomposites, *Advance Materials Research*, *123-125*, pp. 55-58.

99. Kaewkumay, C., Jarukumijorn, K., Wittayakun, J., Suppakarn, N., (2012). Influences of surfactant content and type on physical properties of natural rubber/organoclay nanocomposites, *Journal of polymer reserarch*, *19*(7), pp. 1-9.

100. Kaewsakul, W., Sahakaro, K., Dierkers, W.K, Noordermeers, J.W.M., (2015). Mechanical aspects of silane coupling agent with different functionalities on reinforcement of silica-filled NR compounds, *Polymer Engineering and Science*, *55*(4), pp.836-842.

101. Kajima, Y., Usuki, A., Kawasumi, M., Okada, A., Fukushima, Y. (1993a). Mechanical properties of nylon 6-clay hybrid. *Journal of Material Research*. *8*(5), PP.1185-1189.

102. Kajima, Y., Usuki, A., Kawasumi, M., Okada, A., Karauchi, T., Kamigaito, O., (1993b). Sorption of water in nylon 6-clay hybrid, *Journal of Applied Polymer Science*, *49*(7), pp. 1259-1264.

103. Karger-Kocsis, J., Wu, C.M., (2004). Thermoset rubber/ layered silicate nanocomposites. status and future trends, *Polymer Engineering and Science*, *44*(6), pp. 1083-1093.

104. Kannika, S., Beraheng, S., (2008). Reinforcement of maleated natural rubber by precipitated silica, *Journal of Applied Polymer Science*, *109*(6), pp. 3839-3848.

105. Kawasumi, M., Hasegawa, N., Kato, M., Usuki, A., Okada, A., (1997). Preparation and mechanical properties polypropylene clay hybrids, *Macromolecules*, *30*(20), pp. 6333-6338.

106. Khalid, M., Walvekar, R., Ketabchi, M.R., Siddiqui, H., Hoque, M.E., (2016). Rubber/ nanoclay composites: towards advanced functional materials, *Nanoclay reinforced polymer composites*, Singapore, Springer, PP. 209-224.

107. Kim C., Beuve J.S, Guilbert S., Bonfils F. (2009). Study of chain branching in natural rubber using size-exclusion chromatograpy coupled with a multi-angle light scattering detector (SEC-MALS). *Europhian Polymer Journal* 45(8): 2249-2259.

108. Kim, E., Kim, E.J., Lee, T.H., Yoon, J., (2011). Clay modification and its effect on the physical properties of silicon rubber/ clay composites, *Journal of Applied Polymer Science*, *125*(S1), pp. 298-30.

109. Kim, W., Kim, S.K., Kang, J., Choe, Y., (2006). Structure and properties of the organoclay filled NR/BR nanocomposites, *Macromolecular Research*, *14*(2), pp. 187-193.

110. Kim, W.S., Paik, H.J., Base, J.W., Kim, W. (2011). Effect of polyethylene glycol on the properties of styrene-butadiene rubber/organo clay nanocomposites filled with silica and carbon black. *Journal of Applied Polymer Science*, *122*(3), pp. 1766-1777.

111. Kita, Y., Kishino, K., (1998). New process for manufacturing maleimides, *Catalysis survays from Japan*, PP 187-198.

112. Kornmann, X., Berglund, L.A., Sterte, J., (1998). Nnocomposites based on montmorillonite and unsaturated polyester, *Polymer Engineering and Science*, *38*(8), pp. 1351-1358.

113. Lagaly, G., Ogawa, M., Dekany, I., (2013). Clay mineral-organic interactions. in *Development in clay science*, vol.5, pp. 435-505.

114. Lan, T., Padmananda, D., Kaviatne, D., Pinavaia, T.G., (1994). On the nature of polyimide-clay hybrid composites, *Chemistry of Materials*, *6*(5), pp. 573-575.

115. Lapattananon, N., Jitkalong, D., Seadan, M., (2011). Hybridized reinforcement of natural rubber with silane modified short cellulose fibers and silica, *Journal of Applied Polymer Science*, *120*(6), pp. 3242-3254.

116. Lebrun, J.J, Porte, H., *Comprehensive polymer science and supplements* (1989). Geoffrey, A., Bevington, J.C.,(eds), Elsevier Ltd, vol 5, PP. 593-609.

117. Lee, C.W., Hwang, T., Nam, G., Hong, J.P., Lee D.A., Ohj, S., Kwak, S.B., Lee, S.H., Lee, W.S., Yang, K.M., Park, J.M., Lee, Y.S., Chung, K.H., Lee, Y., Choi, H.R., Nam, J.D., (2011). A novel synthetic route to natural rubber/ montmorillonite nanocomposite using colloid stabilation-destabilization method, *Composites: Part A*, *42*(11), pp. 1826-1832.

118. Lent, L., Vanasupa, L., Tong, P., (1998). Whey protein edible film structures determined by atomic force microscope, *Journal of Food Science*, *63*(5), pp. 824-827.

119. Li, P., Wang, L., Song, G., Yin, L., Qi, F., Sun, L., (2008). Characterization of high-performance exfoliated natural rubber/ organoclay nanocomposites, *Journal of Applied Polymer*, *109*(6), pp. 3831-3838.

120. Liao, Y.L., Chiu, C.W., Lin, J.J., (2010). General intercalation of poly(oxyalkylene)-amidoacids for anionic and cationic layered clays, *Industrial & Engineering Chemistry Research*, *49*(10), pp. 5001-5005.

121. Lin, J.J., Chang, Y.C., Chang, I.J., (2004). Novel mechanism for layered silicate clay intercalation by poly(polypropylene oxide)-segmented carboxylic acid, *Macromolecular Rapid Communications*, *25*(3), pp. 508-512.

122. Ling, Y., Long, J., Huang C., (2016). Preparation and modification of polythiophene – organic montmorillonite composite, Polymer Composites, 37(8), PP. 2503-2510.

123. Liu, L., Luo, Y., Jia, D., Fu, W., Guo, B., (2006). Structure and properties prepared of natural rubber organoclay nanocomposites prepared by grafting and intercalating method in latex, *Journal of Elastomers and Plastics*, *38*(), pp. 147-161.

124. Liu, Y., Li, L., Wang, Q., (2010). Effect of carbon black/ nanoclay hybrid filler on the dynamic properties of natural rubber vulcanizates, *Journal of Applied Polymer Science*, *118*(2), pp. 1111-1120.

125. Lopez-Manchado, M.A., Arroyo, M., Herrero, B., Biagiotti, J., (2003). Vulcanization kintics of natural rubber-organo clay nanocomposites, *Journal of Applied Polymer Science*, *89*(1), pp. 1-15.

126. Lopez-Manchado, M., Herrero, B., Arroyo, M., (2004). Organoclay-natural rubber nanocomposites synthesized by mechanical and solution mixing method, *Polymer International*, *53*(11), pp. 1766-1772.

127. Lorenz, O., Parks, C.R., (1961). The crossliking efficiency of some vulcanizing agents in natural rubber, *Journal of Polymer science*, *50*(154), pp. 299-312.

128. Lorenz, J.P., (1976). N-(aminothio)imide cure modifiers, *Rubber Chemistry and Technology*, *49*(2), pp. 333-340.

129. Luginsland, H.D., (2000). Reactivity of the sulphur chains of tetra sulfane silane si69 and the disulfane silane TESPD, *Kautschuk and Gummi Kunststoffe*, *53*, pp. 10-23.

130. Madhusoodanan, K.N., Verghese, S., (2006). Technological and processing properties of natural rubber layered silicate-nanocomposites by melt intercalation process, *Journal of Applied Polymer Science*, *102*(3), pp. 2537-2543.

131. Magaraphan, R., Thaijaroen, W., Lim-Ochakun, R., (2003). Structure and properties of natural rubber and modified montmorillonite nanocomposites, *Rubber Chemistry and Technology*, *76*(2), pp. 406-415.

132. Manzur, A., Rubio., L., (1997). Strain-induced crystallization in cis and trans polyisoprene blends: Effect of molecular weight of trans PI, *Journal of macromolecular science Part B, 36*(1), pp.

133. Mao, L., Xiang, G., Zhange, M., Jin, R., (2006). Polycarbonate/ polypropylene/ fibrillar silicates ternary nanocomposites via two-step blending process: degradation and morphology, *Chinese Journal of Chemical Engineering, 14*(2), pp. 248-252.

134. Marini, J., Bretas, R.E.S., (2013). Influnce of shape and surface modification of nanoparticle on the rheological and dynamic-mechanical properties of polyamide 6 nanocomposites, *Polymer Engineering and Science*, *53*(7), pp. 1512-1528.

135. Mark, J.E., (1996). Ceramic-reinforced polymers and polymer-modified cersmics, *Polymer Engineering and Science*, *36*(24), pp. 2905-2920.

136. Martin, G., Davey, W.S., (1934). Rubber from latex coagulated with sulphric acid, *Journal of rubber reserch institute of Malaysia*, 5(3), pp. 282-294.

137. Matayabas, J., Turners, S., In Pinnavaia, Beall, G., (Eds). (2001). *Polymerclay nanocomposites*. John Wiley and Son, New york, P.207.

138. Nicholas, A., Matwiyoff, N.A., Drago, R.S., (1965). Donor and acceptor properties of some trisubstituted oxy compounds of the group IV elements, Journal of organometallic chemistry,3(5), pp. 393-399.

139. Maslowski, M., Miedzianowska, J., Strzeleck, K., (2019). Natural rubber composites filled with crop residues as an alternative to vulcanizates with common fillers, Polymers, 11(6), 972

140. Medalia A.I., Kraus G. (1994). *Science and Technology of Rubber*. Eds. Mark B., Erman B., Enrich R.F, Acadamic Press, New York, p 387.

141. Messersmith, P.B., Giannelis, E.P., (1994). Synthesis and characterization of layered silicate-epoxy nanocomposites. *Chemistry of Materials*, *6*(10), pp. 1719-1725.

142. Messersmith, P.B., Giannelis, E.P., (1995). Synthesis and barrier properties of poly(Ɛ- caprolactane)- layered silicate nanocomposites, *Journal of Polymer Science Part B Polymer Physics*, *33*(7), pp. 1047-1057.

143. Ming, H., Chen, H., Shen, Z., Lin, S., (2002). Preparation and characterization of maleic anhydride-functionlized syndiotactic polystyrene, *Polymer*, *43*(20), pp. 5455-5461.

144. Miranda-Trevino, J.C., Coles, C.A., (2003). Kaolinte properties, structure and influence of metal retention on pH, *Applied Clay Science*, 23(1-4), pp. 133-139.

145. Moczo, J., Punanszky, B., (2008). Polymer micro and nanocomposites: *Journal of industrial and Engineering Chemistry*, *14*(5), pp. 535-563.

146. Mohan, T.P., Kuriakose, J., Kanny, K., (2011). Effect of nanoclay reinforcement on structure, thermal and mechanical propeties of natural rubber-styrene butadiene rubber (NR-SBR), *Journal of Industrial and Engineering Chemistry*, *17*(2), pp. 264-270.

147. Morrison, N.J., (1984). Reactions of crosslink precursors, *Rubber Chemistry and Technology*, *57*(1), pp. 86-96.

148. Mousa, A., Kager-Kocsis, J., (2001). Rheological and thermodynamical behaviour of styrene/ buitadiene rubber-organoclay nanocomposites, *Macromolecular materials and Enginering*, *284*(4), pp. 260-266.

149. Nah, C., Ryu, H.J., Han S.H., Rhee J.M, Lee, M., (2001). Fracture behaviour of acrylonitrile-butadiene rubber/clay nanocomposites, *Polymer International*, *20*(11), pp. 1265-1268.

150. Nakason, C., Kaesaman, A., Supasanthitikul, P., (2003). The grafting of maleic anhydride onto natural rubber, *Polymer Testing*, *23*(1), pp. 35-41.

151. Nakason C., Sookyung U., Vennemann N., Thaijaroen.W. (2015). *Acid free preparation of natural rubber/ clay nanocomposite*. Society of plastic Engineering. Avalable at http:/w.w.w.4spepro.org, Accessed 23 April 2016.

152. Nawamawat K., Sakdapipanich T.T., Ho C.C., Ma Y., Song J. (2011). Surface nanostructure of Havea brasiliensis, natural rubber latex particles. *Colloids Surfaces A*, 390 (1-3): 157-166.

153. Nematollahi, M., Jalali-Arani, A., Golzark, K., (2014). Organoclay maleated natural rubber nanocomposite. prdiction of a abresion and mechanical properties by artificial neural network and adaptive neuro-fuzzy inference, *Applied Clay Science*, *97-98*, pp. 187-199.

154. Okada, A., Usuki, A., Kurauchi, T., Kaminggaito, O., in *hybrid organic-inorganic composites* (1995). Mark, J.E., Lee, C.Y.C, Bianconi, P.A., (eds), ACS symposium Series, American Chemical Society, Washington, vol 585, PP. 55-65.

155. Okada, A., Usuki, A., (1995). The chemistry of polymer-clay hybrids, *Material Science and Engineering:C*, *3*(2), pp. 109-115.

156. Paiva, L.B., Morales, A.R., Francisco, R., Diaz, V., (2008). Organoclay: properties, preparations and applications, *Applied Clay Science*, *42*(1-2), pp. 8-24.

157. Park, J., Lee, Y.S., Lee, C.W., Yang, Y., Lee, J., Nam G., Lee, S., Lee, Y.S., Lee, Y., Nam, D., (2012). Montmorillonite reinforced natural rubber nanocomposites through emulsion stabilization destabilization method, *Rubber Chemistry and Technology*, *85*(2), pp-165-179.

158. Pinnavaia, T.J., Beall, G.W., (2001). Polymer-Clay nanocomposites, John Wiley and Sons Ltd, New York, pp. 3-9.

159. Pongnara, P., Poonsawat, C., Amnuaypanich, S., (2008). Adsorption study of surfactant on natural rubber latex particles, *Asia-Pacfic Journal of Science and Technology*, *13*(6), pp. 694-700.

160. Premachandra, J., Kumudinie, C., Zhao,W., Mark, J.E., Dang, T.D., Chen, J.P., Arnold F.E., (1996). Polymer-silica hybrid materials prepared from some functionlized polybenzoxazoles and polybenzobisthiazoles, *Journal of Sol-Gel Science and Technology*, *7*(3), pp. 163-175.

161. Pramanik, M., Srivastava, S.K., Samantaray, B.K., Blowmick, A.K., (2003). Rubber-Clay nanocomposites by solution blending, *Applied Polymer Science*., *87*(14), pp. 2216-2220.

162. Qu, L., Huang, G., Liu, Z., Zhange, P., Weng, G., Nie, Y., (2009). Remarkable reinforcement of natural rubber by deformation-induced crystallization in the presence of organophilic montmorillonite, *Acta Materialia*, *57*(17), pp. 5053-5060.

163. Qureshi, M.N., Qammar, H., (2010). Mill processing and properties of rubber-clay nanocomposites, *Material Science and Engineering:C*, *30*(4), pp. 590-596.

164. Rajasekar, R., Heinrich, G., SI, A., SI, C.K., (2009). Development of SBR-Nanoclay composites with epoxidized natural rubber as compatibilizer, *Research Letters in Nanotechnology*, *405153*, pp. 1-5.

165. Ratnayake, U.N., (2003a). Ribbed smoked sheet, In Tilakeratne, L.M.R., Nugawela, A., Seneviratne, W.M.G., (eds.). *Hand book of rubber*, Rubber Research Institute of Sri Lanka, Darton field, Agalawatta, pp. 15-32.

166. Ratnayake, U.N., (2003b). Water used in raw rubber manufacture In Tilakeratne, L.M.R., Nugawela, A., Seneviratne, W.M.G., (eds.). *Hand book of rubber*, Rubber Research Institute of Sri Lanka, Darton field, Agalawatta, pp. 134-139.

167. Ratnayake U.N., Kumara P.H.S., Siriwardena T.A.S., Prasad A.K.D.W., Rohanadeepa, V.C., (2011). Effect of iron in processing water in quality of crepe rubber rubber, *Journal of Rubber Research Institute of Sri Lanka, 91*, pp. 1-14.

168. Ratnayake, U.N., Premathunga, D.E., Peris, C., Karunaratne, V., Amarathunga, G.A., (2015). Polyethylene glucol-intercalated organoclay on vulcanization characteristics and reinforcement of natural rubber nanocomposites, *Journal of Elastomer and Plastics*, *48*(8), pp. 711-727.

169. Rattanasom, N., Thammasiripong, U., Suchiva, K. (2005). Mechanical properties natural rubber in comparision with synthetic cis-1,4 polyisoprene vulcanizates: Gum and blacked-filled vulcanizates. *Journal of Applied Polymer Science*, 97(3): 1139-1144.

170. Rattanasom S., Prasertsri S & Ruangritnumchai T. (2009). Comparison of the mechanical properties at similar hardness level of natural rubber filled with various reinforcing-fillers. *Polymer Testing* 28(1). pp. 8–12.

171. Ray, S.S., Yamada, K., Okamoto, M., Fugimoto, Y., Ogami, A., Ueda, K., (2003 a). New polylactide/ layered silicate nanocomposites.5. Designing of materials with desired properties, *Polymer*, *44*, pp. 6633-6646.

172. Ray, S.S., Okamoto, K., Okamoto, M., (2003 b). Structure-property relationship in biodegradable poly(butylene succinate)/ layered silicate nanocoposites, *Macromolecules*, *36*(7), pp. 2355-2367.

173. Ray, S.S., Okamoto, M., (2003). Polymer/ layered silicates nanocomposites: a riview fom preparation to processing, *Progress in Polymer Science*, *28*(11), pp. 1539-1641.

174. Reichert, P., Kressler, J., Thomann, R., Mulhaupt, R., Stoppelman, G., (1998). Nanocomposites based on a synthetc layer silicate and polyamide-12, *Acta Polymerica*, *49*(2-3), pp. 116-123.

175. Reuvekam, L.A.E.M., Brinke, J.W.T., Swaaij, P.J., Noordermeer, J.W.M., (2002). Effect of time and temperature on the reaction of TESPT silane coupling agent during mixing with silica filler and tire rubber, *Rubber Chemistry and Technology*, *75*(2), pp. 187-198.

176. Rezende, C.A., Braganca, F.C., Doi, T.R., Lee, L., Galebeck, F., Baue, F., (2010). Natural rubber clay nanocomposites: mechanical and structural properties, *Polymer Journal*, *51*(16), pp. 3644-3652.

177. Rippel, M.M., Leite, C.A.P., Galembeck, F., (2002). Elemental mapping in natural rubber latex films by electron energy loss spectroscopy associated with transmission electron mocroscopy, *Analytical Chemistry*, *74*, pp. 2541-2548.

178. Rippel, M.M., Lee, L.T., Leite, C.A.P., Galembeck, F., (2003). Skim and cream natural rubber particles: colloidal properties, coalescence and film formation, *Journal Collioid Interface Science*, *268*, pp. 330-340.

179. Rodriguez, J., Hamed, G.R., (1993). Styrene-Buitadiene Rubber filled with fluorinated Carbon black. *Rubber Chemistry and Technology*, *66*(2), pp. 286-294.

180. Rooj, S., SI, A., Stockelhuber, K.W., Mukhopardhyay, N., Bhattacharyya, A.R., Jehnichen, D., Heinrich, G., (2012). Pre-intercalation of long chain fatty acid in the interlayer space of layered silicates and preparation of montmorillonite/ natural rubber nanocomposites, *Applied Clay Science*, *67-68*, pp. 50-56.

181. Sadhu, S.D, Blowmick, A.K., (2004). Preparation and properties of styrene-butadiene rubber based nanocomposites: the influence of the structural and processing parameters, *Journal of Applied Polymer Science*, *92*(2), pp. 698-709.

182. Sadhu,S.D, Rajeev R.S., Bhowmick, A.K., (2008). Thermal degradation of elastomer based nanocomposites, *Polymer & Polymer Composites*, *16*(5), pp. 283-293.

183. Saelao, J., Phinyocheep, P., (2005). Influence of stryrene on grafting efficiency of maleic anhydride on to natural rubber, *Journal of Applied Polymer Science, 95*(1), pp. 28-38.

184. Sae-oui, P., Sirisinha, C., Hattahapanit, K., Thessuwan, U., (2005). Comparision of reinforcing efficiency between si-69 and si-264 in an efficient vulcanization system, *Polymer Testing 24*(4), pp. 439-446.

185. Sae-oui, P., Sirisinha, C., Thepsuwan, U., Hatthapanit, K., (2006). Roles of silane coupling agents on properties of silica coupling agents on properties of silica-filled polychloreprene, *European Polymer Journal*, *42*(2), pp. 479-486.

186. Saha, D., Ray, D., Kohlbrecher, J., Aswal, V.K., (2018). Unfolding and refolding of protein by a combination of ionic and non ionic surfactants, *ACS Omega*, *3*, pp. 8260-8270.

187. Sakdapipanich J.T., (2007). Structural characterization of natural rubber based on recent evidence from selective enzymatic tratments, *Journal of bioscience and bioengineering,103*(4), pp. 287-292.

188. Santipanuscopon.S., Riyajan.S., (2009). Effect of field natural rubber latex with different ammonia contents and storage period on physical properties of latex concentrate, stability of skim latex and dipped film, *Physics Procedia*, *2*, pp. 127-134

189. Sarkawi, S.S., Dierkes, W.K., Noordermeer, J.W.M., (2013). The influence of non-rubber constituents on performance of silica reinforced natural rubber compounds, *European Polymer Journal*, *49*(10), pp. 3199-3209

190. Selleh, M.Y.B., (2010). The effect of carbon black loading on tensile strength of rubber vulcanizates, Degree of Bachelor of Chemical Engineering, University Malaysia Pahang, Available at https://core.ac.uk/download/pdf/157179161pdf

191. Seneviratne, W.M.G., Kumara, P.H.S., (2003). Centrifuged latex In Tilakeratne, L.M.R., Nugawela, A., Seneviratne, W.M.G., (eds.). *Hand book of rubber*, Rubber Research Institute of Sri Lanka, Darton field, Agalawatta, pp. 80-82.

192. Sengloyluan, K., Sahakaro, K., Dierkes, W.K., Noordermeer J.W.N., (2017). Silane grafted natural rubber and its compatibilization effect on silica-reinforced rubber tire compounds, *EXPRESS Polym. Lett*, *11*(12), pp. 1003-1022.

193. Sharif, J., Yunus, W.M.Z.W., HJ, K.Z., Dhhlan, M., Ahmad, M.H., (2005). Preparation and properties of radiation crosslinked natural rubber/ clay nanocomosites, *Polymer Testing*, *24*(2), pp. 211-217.

194. Sharif-Pakdaman, A., Morshedian, J., Jahani, Y., (2013). Effect of organoclay and silane grafting of polyethylene on morphology barrierity and rheological properties of HDPE/ PA 6 Blends, *Journal of Applied Polymer Science*, *127*(2), pp. 1211-1220.

195. Sharma, P.K., Upadhyaya, P., Chand, N., (2015). Effect of heat aging on mechanical performance of MMT clay reinforced thermplastic polyurethane (TPU)/ EPDM rubber blends based on nano composite, *Europhean Journal of advances in Engineering and Technology*, *2*(5), pp 23-26.

196. Singla. P., Mehta, R., Upadhyay, S.N., (2012). Clay modification by use of cations, *Green and Sustainable Chemistry*,*2*, pp. 21-25.

197. Sookyung, U., Nakason, C., Thijaroen, W., Vennemann, N., (2014). Influence of modifying agent of organoclay on properties of nanocomposites based on natural rubber, *Polymer Testing*, *33*(3), pp. 48-56.

198. Son, P.N., Andrews, K.E., Schooley, A.T., (1972). Kinetics and mechanism of the reaction of z-mercapto benzothiazole with N-(cyclohexylthio) phthalimide and related compounds, *Rubber chemistry and technology*, *45*(6), pp. 1513-1531.

199. Strawhecker, K.E., Manias, E., (2000). Structure and properties of poly (vinyl alcohol) / Na^+ montmorillonite nanocomposites, *Chemistry of materials*, *12*(10), pp.2943-2949.

200. Subramani, S., Choi. S.W., Lee, J.Y., Kim, J.H., (2007). Aqueous dispersion of novel silylated (polyurethane-acrylic hybrid/ clay) nanocomposite, *Polymer*, *48*(16), pp. 4671-4703.

201. Sukumar, R., Menon, A.R.R., (2008). Organomodified kaolin as a reinforcing filler for natural rubber, *Journal of Applied Polymer Science*, *107*(6), pp. 3476-3483.

202. Sun, Y., Luo, Y., Jia, D., (2008). Preparation and properties of natural rubber nanocomposites with solid-state organomodified montmorillonite, *Journal of Applied Polymer Science*, *107*(5), pp. 2786-2792.

203. Tan, J., Wang, X., Luo, Y., Jia, D., (2012). Rubber/ clay nanocomposites by combined latex compounding and melt mixing: A nanocomposite process, *Material and Design*, *34*, pp. 825-831.

204. Tan, J., Wang, X., Liu, Y., LuO, Y., Jia, D., Liu, Y., Xiong, Y., Wang, W., (2016). Effect of epoxidized natural rubber as compatibilizer on latex compounded natural rubber-clay nanocomposites, *Journal of Polymer Engineering*, *31*(1), pp. 43-52.

205. Tanaka Y., Sato H., Kageyu A. (1983). Structure and biosynthesis mechanism of natural Cis-Polyisoprene from goldenrod. *Rubber Chemistry and Technology* 56(2):299-303.

206. Tanaka Y., Mori M., Ute K., Hatada K. (1990). Structure and biosynthesis mechanism of rubber from fungi, *Rubber chemistry and Technology*, *63*(1):1-7.

207. Tangpakdee J., Tanaka Y. (1997) Purification of natural rubber. *Journal of Natural Rubber Research*, *12*(2), pp.112-119.

208. Tangpakdee J., Tanaka Y. (1998) Long-chain polyprenols and rubber in young leaves of hevea brasiliensis, *Phytochemistry*,*48*(3), pp. 447-450.

209. Tarachiwin L., Sakadapipanich J., Ute K., Kitayama T., Bamba T., (2005). Structural characterization of alpha-terminal group of natural rubber.2.Decomposition of branch-point by phosphatase and chemical treatments. *Biomacromolecules*, *6*(4), pp.1858-1863.

210. Tasban, N., Wirasates, S ., Suchiva, K., (2010). Abresion behaviour of layered siliate reinforced natural rubber, *Wear*, *269*(5-6), pp. 394-404.

211. Teh, P.L., Ishak, Z.A.M., Hashim, A.S., Karger-Kocsis, J., Ishiaku, U.S., (2004). On the potential of organoclay with resprct to convenctional fillers (carbon black, silica) for exfoliated natural rubber compatibilized natural rubber vulcanizates, *Journal of Applied Polymer Science*, *94*(6), pp. 2438-2445.

212. Teh, P.L., Ishak, Z.A.M., Hashim, A.S., Karger-kocsis, J., Ishiaku, U.S., (2005). Physical properties of natural rubber/ organoclay nanocomposites compatibilized with epoxidized natural rubber, *Journal of Applied Polymer Science*, *100*(2), pp. 1083-1092.

213. Theng, B.K.G., (1979). *Formation and properties of clay-polymer composites*, Elsevier, Amsterdam.

214. Theng, B.K.G., Bureau, S., Hutt, L., (1982). Clay-polymer interactions summary and perspectives, *Clay and Clay Minerals*, *30*(1), pp. 1-10.

215. Thomas, S., Stephen R., (2010)., *Rubber nanocomposites preparation, properties and applications*, John wiley and sons. Inc, New York, pp. 46-220.

216. Thongpin, C., Tangchantra, N., Kaewpetch, P., Dejkun, J., Chartsiriwattana, A., (2008). The effect of organic modifiction method on to montmorillonite on mechanical properties of natural rubber, *Advnced Material Research*, *55-57*, pp 341-344.

217. Tjong, S.C., (2006). Structural and mechanical properties of polymer nanocomposites, *Mater.Sci.Eng*, *53* (3-4), pp 73-197.

218. Tuampoemsab, S., Skadapipanich, J., (2007). Role of naturally occurring lipids and proteins on thermal ageing behavior of purified natural rubber, *KGK Rubber Point*, 60(12), pp. 678-684.

219. Tosaka, M., Farutani, M., Tsuji, M., Ikeda, Y., Kohjiya, S., Wititsuwannakul, G., Wititsuwannakul., D., Nagayama, K., Danev, R., (2009). Strain induced crystallization of fractionated natural rubber from fresh latex, *Journal of Society of Material Science Japan*, *58*(1), pp. 5-10.

220. Uddin, F., (2008). Nano clay, and montmorillonite minerals, *Metallurgical and Materials Transactions A*, *39*(12), pp 2804-2814.

221. Uddin, F., (2018). Montmorillonite: an introduction to properties and utilization, In Zoveidavianpoor, M., (eds.). *The current tropics in utilization of clay in industrial and midicinal application*, Intehopen.77987.

222. Unalan, I.U., Gerri, C., Marcuzzo, E., Cozzolino, C.A., Farris, S., (2014). Nanocomposites films and coatings using inorganic nanobuilding blocks (NBB): Current applications and future opportunities in food packaging sector, *RSC.Adv*, *4*, pp. 29393-29428.

223. Usuki, A., Koiwai, A., Kojima, Y., Kawasumi, M., Okada, A., Karauchi, T., Kamigaito, O., (1995). Interaction of nylon 6-clay surface and mechanical properties of nylon 6-clay hybrid, *Journal of Applied Polymer Science*, *55*(1), pp. 119-123.

224. Valadares, L.F., Leite, C.A.P, Galembeck, F., (2006). Preparation of natural rubber-momtmorillonite nanocomposite in aqeous medium: evidence for polymer platlet adhesion, *Polymer*, *47*(2), pp. 672-678.

225. Vaia, R.A., Ishil, H., Giannelis, E.P., (1993). Synthesis and properties of two dimentional nanostrutures by direct interaction of polymer melts in layered silicates, *Chemistry of Materials*, *5*(12), pp. 1694-1696.

226. Vaia, R.A, Price, R., Ruth, P., Nguyen, H., Lichtenhan. J., (1999). Polymer/ layered silicate nanocomposites as high performance ablative materials. *Applied Clay Science*, *15*(1-2), pp. 67-92.

227. Varghese, S., Karger-Kocsis, J., Gatos, K.G., (2003 a). Melt compound epoxidized natural rubber layered siicate nanocomposites: structure-properties relationships, *Polymer*, *44*(14), pp. 3977-3983.

228. Varghese, S., Karger-kocsis, J., (2003 b). Natural rubber-based nanocomposites by latex compounding with layered nanocomposites by latex compounding with layered silicates, *Polymer*, *44*(17), pp. 4921-4927.

229. Viana, R.B., Silva, A.B.F., Pimentel, A.S., (2012). Infrared spectroscopic of anionic, cationic, and Zwitterionic surfactants, *Advance in Physical Chemistry, 903272*, pp. 1-14.

230. Vieira, M.G.A., Silva, A., Santos, L.O.D., Beppu M.M., (2011). Natural – based plasticizers and biopolymer films: A review, *European Polymer Journal*, *47*(3), pp. 254-263.

231. Viet, C.X., Ismail, H., Rashid, A.A., Takeichi, T., Thao, V.H., (2008). Organoclay filled natural rubber nanocomposite: the effect of filler loading, *Polymer-Plastic Technology and Engineering*, *47*(11), pp. 1090-1096.

232. Vijayalekshmi, V., George, K.E., Pavithra, C., (2010). Studies on maleated natural rubber/ organoclay nanocomposites, *Progress in Rubber Plastic and RecyclingTechnology*, *26*(4), pp. 183-198.

233. Vu, Y.T., Mark, J.E., Pham, L.H., Engelhard, T.M., (2001). Clay nanolayer reinforcement of cis-1,4-polyisoprene and epoxidized natural rubber, *Journal of Applied Polymer Science*, *82*(6), pp. 1391-1403.

234. Wagner, M.P., (1976). Rainforcing silicas and silicates. *Rubber Chemistry Technology*, *49*(3). PP. 703-774.

235. Walter D. (2013). Primary particles-Agglomerates-Aggregates, Eds Deutshe Willey on line libry http:doi.org/10.1002/9783527673919.

236. Wang, M.S., Pinnavaia, T.J., (1998). Nanolayer reinforcement of elastomeric polyurethane, *Chemistry of Materials*, *10*(12), pp. 3769-3721.

237. Wang, Y., Zhang, L., Tang, C., Yu, D., (2000). Preparation and characterization of rubber clay nanocomposites, *Journal of Applied Polymer Science, 78*(11), pp. 1879-1883.

238. Wang, K.H., Xu, M., Choi, Y.S., Chung, I.J., (2001). Effect of aspect ratio of clay on melt extensional process of maleated polyehylene/clay nanocomposite. *Polymer Bulletin*, *46*(6), pp. 499-505.

239. Wang, Y., Zhang, H., Wu, Y., Yang, J., Zhang, L., (2005 a). Preparation and properties of natural rubber/ rectorite nanocomposites, *European Polymer Journal*, *41*(11), pp. 2776-2783.

240. Wang, J., Lu, D., Lin, Y., Liu, Z., (2005 b). How CTAB assists the refolding of native and recombinant lysozyme, *Biochemical Engineering Journal*, *24*(3), pp. 269-277.

241. Wen, J., Wikes, G.L., (1996). Organic/ inorganic hybrid network materals by sol-gel approach, *Chemistry of materials*, *8*(8), pp. 1667-1681.

242. Werne, T.V., Pattern, T.E., (1999). Preparation of structurally well-defined polymer-nanoparticle hybride with controlled/ living radical polymerizations, *Journal of american Chemical Society*, *121*(32) pp. 7409-7410.

243. Wloch, M., Ostaszewska, U., Datta, J., (2019). The effect of polyurethane glycolysate on the structure and properties of natural rubber/ carbon black composites, *Journal of polymers and the envirnment*, *27*(6), pp. 1367-1378.

244. Wolff S., Wang M.J., Tan E.H. (1993). Filler – elatomer interactions. Part VII. Study on bound rubber. *Rubber Chemistry and Technology*, *66*(2), pp.167-177.

245. Wren W.G. (1942). Application of the langmuir trough to the study of rubber latex. *Rubber Chemistry and Technology*,*15*(1): 107-114.

246. Wu, Y., MA, Y., Wang, Y., Zhang, L., (2004). Effect of characteristics of rubber, mixing and vulcanization on the structure and properties of rubber/ clay nanocomposites by melt melting, *Macromolecular Materials and Engineering*, *289*(10). pp. 890-894.

247. Wu Y.P., Wang Y.Q., Zhang H.F., Wang Y.Z., Yu D.S., Zhang L.Q & Yang, J. (2005). Rubber-pristine clay nanocomposites prepared by co-coagulating rubber latex and clay aqueous suspension. *Composites Science and Technology*, *65*(7), pp.1195–1202.

248. Wu J., Qu W., Huang G., Wang S., Liu H. (2017). Super-resolution fluorescence imageing of spatical organization of protein and lipids in natural rubber. *Biomacromolecules*,*18*(6): 1705-1712.

249. Wong, A., Wijannds S.F.L., Kubokit, T., Park C,B., (2013). Mechanisms of nanoclay-enhanced plastic forming processes: effects of nanoclay intercalation and exfoliation, *Journal of Nanoparticle Research*,*15*(8), pp. 1815.

250. Wongthong, P., Nakason, C., Pan, Q., Rempel., G.L., Kiatkamjornwong., (2013). Modification of deproteinized natural rubber via grafting polymerzation with maleic anhydride, *European Polymer Journal*, *49*, pp. 4035-4046.

251. Xu, Y., Guo, Z., Fang, Z., Peng, M., Shen, L., (2013) Combination of double-modified clay and polypropylene-graft maleic anhydride for the smultaneously improved thermal and mechanical properties of polypropylene, *Journal of Applied Polymer Science*, *128*(1), pp. 283-291.

252. Yahaya, L.E., Adebowale, K.O., Menon, A.R.R., (2009). Mechanical properties of organo modified Kaolin/natural rubber vulcanizates, *Applied Clay Science*, *46*(3), pp.283-288.

253. Yahaya, L.E., Adebowale, K.O., Menon, A.R.R., Rugmini, S., Olu-Owolabi, B.I., Chameswary, J., (2010). Natural rubber/ organoclay nanocomposites: Effect of filler dosage on the physico mechanical properties of vulcanizates, *African Journal of Pure and Applied Chemistry*, *4*(9), pp. 198-205.

254. Yanchan W., Zhang H., Longmei W., Jin L., Liao S., (2017). a review on characterization of molecular structure of natural rubber. *MOJ Polymer Science*, 1(6). pp.197-199.

255. Yangchuan, K., Chefen, L., Zongneng, Q., (1997). Crystallization properties and crystal and nanoscale morphology of PET-clay nanocomposite, *Journal of Applied Polymer Science*, *71*(7), pp. 1139-1146.

256. Yano, K., Usuki, A., Okada, A., Kurauchi, T., Kamigaito, O., (1993). Synthesis and properties of polyimide-clay hybrid. Journal of Polymer Science Part A: Polymer Chemistry, 31(10), pp. 2493-2498.

257. Yano, K., Usuki, A., Okada, A., (2000). Synthesis and properties of polyimide-clay hybrid films. *Journal of polymer science part A: Polymer Chemistry*, *35*(11), PP. 2289-2294.

258. Zhang, L., Wang, Y., Sui, Y., Yu, D., (2000). Morphology and mechanical properties of clay/ SBR nanocomposites, *Journal of Applied Polymer Science*, *78*(11), pp. 1873-1878.

259. Zhang, X., Loo, L.S., (2008). Morphology and mechanical properties of a novel amorphous polyamide/ nanoclay nanocomposite, *Journal of Polymer Science Part B Polymer Physics*, *46*(23), pp. 2605-2617.

260. Zhang, C., Wang, J., (2018). Natural rubber/ Dendrimer modified montmorillonite nanocomposites; mechanical and flame retardant properties, *Materials, 11*(1), pp. 1-17.

261. Zhong, J., Li, C., Li, S., Kong, L., Yang, L., Liao, S., She, X., (2009). Study on properties natural rubber during maturation, *Journal of Polymer Materials*, 26(3), pp. 351-360.

262. Zhou, W., Mark, J.E., Unroe, M.R., Arnold, F.E.J., (2001). Some clay nanocomposites based on a high-temperature, high-perfomance polymer, *Macromolecular Science Part A Pure and Applied Chemistry*, *38*(1), pp. 1-9.

263. Zilg, C., Thomann, R., Mulhaupt, R., Finter, J., (1999). Morphology and toughness/ stiffness balance of nanocomposites based upon anhydride-cured epoxy resin and layered silicates, *Macromolecule Chemistry and Physics*, *200*(3), pp. 661-670.

APPENDIX-A

Specification of high ammonia centrifuged latex by ISO 2004-2017

Property	Requirement
Total Solid Content (%), min	61.5
Dry Rubber Content (%), min	60.0
Non Rubber Solids (%), max	2.0
Ammonia (%), min	0.6
Mechanical Stability (%), min	650
Volatile fatty acid	Not to exceed 0.2
KOH number	Not to exceed 1.0

APPENDIX-B

Specification of Field latex

Property	Requirement
pH	9 - 10
Dry Rubber Content (%), min	30-35
Mg content	Less than 50 ppm

APPENDIX – C

Average raw rubber specification for crepe rubber by RRISL

Property	Specification
Dirt content % (w/w)	0.020 (max.)
Volatile matter content % (w/w)	0.5 (max.)
Ash content % (w/w)	0.20 (max.)
Initial plasticity number (Wallace units)	30 (min)
Plasticity retention index (PRI)	60 (min)
Nitrogen content% (w/w)	0.35 (max)
Mooney viscosity ML 1+ 4 @ 100°C	75-85

APPENDIX-D

Mechanical Properties and Crosslink density of nanocomposite vulcanizates

	Crosslink Density, 10^{-5} molg^{-1}	**Tensile Strength, MPa**	**EB, %**	**mod 300%, MPa**	**Hardness, IRHD**	**Tear Strength, N/mm**
CT-A/FL	16.7	18.0	472	3.2	34	19.3
A/FL/M2	16.5	14.9	480	4.1	35	18.6
A/FL/M5	18.1	13.8	483	4.3	37	18.4
A/FL/M8	19.0	18.5	480	5.8	46	20.8
A/FL/M12	18.3	22.6	452	7.3	42	15.1
A/FL/M 20	17.1	19.0	420	7.9	46	13.9
CT-B/FL	24.4	26.2	495	4.3	37	19.3
B/FL/M2	22.5	26.3	489	4.5	38	20.7
B/FL/M5	23.4	31.3	485	5.1	40	20.6
B/FL/M8	23.5	34.5	491	6.3	44	21.3
B/FL/M12	22.9	32.1	479	7.6	42	21.0
B/FL/M20	20.8	27.7	440	8.7	46	21.0
CT-B/FL/G1	16.3	29.0	701	2.5	-	30.1
B/FL/G1/M2	15.4	29.4	676	3.6	-	28.5
B/FL/G1/M5	11.5	23.7	587	3.9	41	32.6
B/FL/G1/M8	9.82	21.9	589	2.2	-	27.5
B/FL/G2/M2	-	15.8	492	3.9	-	29.2
B/CL/G2/M2	-	28.5	579	4.2	-	33.8
B/CL/G3/M2	-	32.7	597	4.0	-	36.3
CT-B/CL	19.6	30.5	711	2.4	42	29.5
B/CL/O2	23.3	37.1	632	3.8	48	35.0
B/CL/O4	22.7	33.6	605	4.0	46	34.8
B/CL/O6	20.4	32.6	597	4.0	47	34.4
B/CL/O8	19.9	32.1	585	4.3	49	28.4
CT-B/CL/G3	19.8	15.2	462	3.9	44	33.0
B/CL/G3/O2	20.6	35.8	649	3.1	47	39.6
B/CL/G3/O5	20.9	37.5	650	3.6	49	42.8
B/CL/G3/OS2	22.5	39.4	651	3.5	48	38.2
B/CL/G3/OS5	21.5	31.3	574	4.1	50	41.2
CT-B/gL/G3	21.2	37.8	631	4.5	46	40.2
B/gL/G3/OS2	21.6	37.9	618	4.7	51	43.7
B/gL/G3/OS5	21.4	40.7	630	6.0	55	48.7
CT-C/PC	11.2	24.7	703	1.9	39	24.0
C/PC/O2	17.1	29.4	626	3.5	43	31.4
C/PC/O5	16.9	25.0	606	4.2	44	35.6
C/PC/OS2	17.5	30.4	659	3.0	44	35.2
C/PC/OS5	18.4	29.7	590	4.1	46	32.1

APPENDIX-E

Cure Properties of nanocomposite compounds

	t_{s2}, min	**t_{90}, min**	**M_H-M_L, dN**	**CRI, min^{-}**	**Activation energy, KJmol^{-1}**
CT-A/FL	12.7	41.6	16.4	3.5	-
A/FL/M2	10.3	49.7	15.4	2.5	-
A/FL/M5	8.8	44.8	15.1	2.8	-
A/FL/M8	7.8	41.2	18.2	3.0	-
A/FL/M12	8.0	36.1	18.0	3.0	-
A/FL/M20	7.6	36.3	16.9	3.5	-
CT-B/FL	2.0	11.2	16.75	10.0	-
B/FL/M2	2.9	12.5	14.5	10.4	-
B/FL/M5	3.2	12.3	18.7	11.0	-
B/FL/M8	2.2	11.0	19.3	11.4	-
B/FL/M12	2.5	12.1	18.3	10.4	-
B/FL/M20	3.2	13.8	17.0	9.4	-
CT-B/CL	10.7	28.6	8.3	5.6	-
B/CL/O2	4.4	14.9	11.3	9.6	-
B/CL/O4	4.7	14.2	10.9	10.5	-
B/CL/O6	4.8	14.1	12.1	10.9	-
B/CL/O8	5.0	13.6	12.5	11.7	-
CT-B/CL/G3	2.0	10.3	7.4	12.0	145
B/CL/G3/O2	2.0	8.8	7.6	14.8	131
B/CL/G3/O5	2.0	8.8	8.1	14.8	143
B/CL/G3/OS2	2.1	8.6	8.1	15.5	155
B/CL/G3/OS5	2.2	8.6	8.9	15.6	174
CT-B/gL/G3	1.8	6.4	6.6	21.9	135
B/gL/G3/OS2	1.9	6.8	7.4	20.3	139
B/gL/G3/OS5	1.9	5.8	7.4	25.7	157
CT-C/PC	25.7	32.4	4.1	15.0	299
C/PC/O2	4.1	8.9	7.4	20.8	290
C/PC/O5	3.2	7.8	7.9	21.9	221
C/PC/OS2	6.2	12.9	6.7	14.8	-
C/PC/OS5	5.6	12.3	6.3	15.0	-

APPENDIX-F

Abrasion Loss of nanocomposite vulcanizates

	Abrasion Loss, mm^3
CT-B/CL/G3	328
B/CL/G3/O2	395
B/CL/G3/O5	324
B/CL/G3/OS2	228
B/CL/G3/OS5	233
CT-B/gL/G3	318
B/gL/G3/OS2	282
B/gL/G3/OS5	192
CT-C/PC	430
C/PC/O2	248
C/PC/O5	346
C/PC/OS2	393
C/PC/OS5	400

APPENDIX-G

Journal publications

1. Jayaraj S, Egodage S.M, Walpalage S (2017) Incorporation of nanoclay into field latex to develop nanoclay filled dry rubber compounds, Journal of National Science Foundation 45(2): 121-132.

2. Jayaraj S, Egodage S.M, Walpalage S (2018) New approach for preparation of dry rubber nanocomposites through acid-free co-coagulation: Effect of organoclay content, Journal of Applied Polymer Science, 135, 46502.

3. Jayaraj S, Egodage S.M, Walpalage S (2020) Preparation of natural rubber-OMMT nanocomposites using mechanical mixing and acid free co-coagulation methods: effect of processing method on mechanical properties, Biointerface Research in Applied Chemistry, 10(3), 5640-5647.

4. Jayaraj S, Egodage S.M, Walpalage S (2020*)* Enhanced mechanical properties natural rubber-clay nanocomposites prepared with silane grafted organoclay by acid free co-coagulation method with the effect of gelling agent. e-Polymers 20: 144–153.

APPENDIX-H

Conference publications

1.Jayaraj S, Egodage S.M, Walpalage S (2015) Review on development of natural rubber/ nanoclay nanocomposites. The MERCon 2015 International Conference: 07 April 2015, University of Moratuwa, Sri Lanka.

2. Jayaraj S, Egodage S.M, Walpalage S (2019) Preparation of natural rubber-OMMT nanocomposites using mechanical mixing and acid free co-coagulation methods: effect of processing method on mechanical properties, International Conference on Materials Engineering and Nanotechnology ICMEN 2019, 02-05 December 2019, Kuala Lumpur, Malaysia.